AD-A034 201 ARMY MISSILE RESEARCH DEVELOPMENT AND ENGINEERING LAB--ETC F/G 19/7
A STUDY OF VARIOUS SLENDER AND NON-SLENDER FIN-BODY COMBINATION--ETC(U)
NOV 76 N UCHIYAMA, J M WU

UNCLASSIFIED RD-CR-76-5 NL

1 OF 2
AD-A
034 201

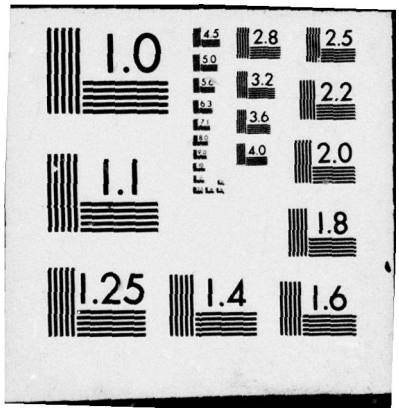
1.0
1.1
1.25
1.4
1.6
1.8
2.0
2.2
2.5
2.8
3.2
3.6
4.0
4.5
5.0
5.6

U.S. DEPARTMENT OF COMMERCE
National Technical Information Service

AD-A034 201

A STUDY OF VARIOUS SLENDER AND NON-SLENDER FIN-BODY COMBINATIONS OF MISSILE CONFIGURATIONS

ARMY MISSILE RESEARCH, DEVELOPMENT AND
ENGINEERING LABORATORY
REDSTONE ARSENAL, ALABAMA

12 NOVEMBER 1976

013024

ADA034201

TECHNICAL REPORT RD-CR-76-5

A STUDY OF VARIOUS SLENDER AND NON-SLENDER FIN-BODY COMBINATIONS OF MISSILE CONFIGURATIONS

N. Uchiyama and J. M. Wu
The University of Tennessee Space Institute
Tullahoma, Tennessee

12 November 1976

APPROVED FOR PUBLIC RELEASE; DISTRIBUTION UNLIMITED.

U.S. ARMY MISSILE COMMAND
Redstone Arsenal, Alabama 35809

Prepared for:

Aeroballistics Directorate
US Army Missile Research, Development and Engineering Laboratory
US Army Missile Command
Redstone Arsenal, Alabama 35809

REPRODUCED BY
NATIONAL TECHNICAL INFORMATION SERVICE
U. S. DEPARTMENT OF COMMERCE
SPRINGFIELD, VA. 22161

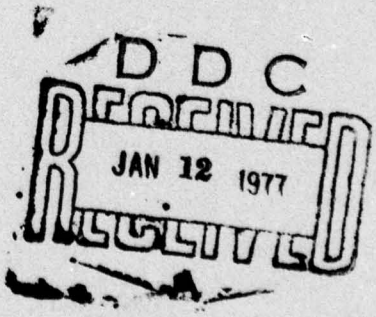

Copy available to DDC does not permit fully legible reproduction

ARM 1021, 1 MAR 66 REPLACES AMSMI 1021 WHICH MAY BE USED

DISPOSITION INSTRUCTIONS

DESTROY THIS REPORT WHEN IT IS NO LONGER NEEDED. DO NOT RETURN IT TO THE ORIGINATOR.

DISCLAIMER

THE FINDINGS IN THIS REPORT ARE NOT TO BE CONSTRUED AS AN OFFICIAL DEPARTMENT OF THE ARMY POSITION UNLESS SO DESIGNATED BY OTHER AUTHORIZED DOCUMENTS.

TRADE NAMES

USE OF TRADE NAMES OR MANUFACTURERS IN THIS REPORT DOES NOT CONSTITUTE AN OFFICIAL INDORSEMENT OR APPROVAL OF THE USE OF SUCH COMMERCIAL HARDWARE OR SOFTWARE.

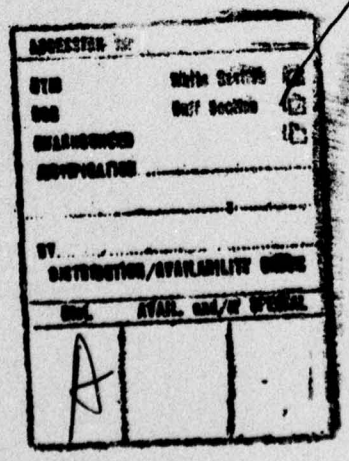

REPORT DOCUMENTATION PAGE

READ INSTRUCTIONS BEFORE COMPLETING FORM

1. REPORT NUMBER: RD-CR-76-5	2. GOVT ACCESSION NO.
3. RECIPIENT'S CATALOG NUMBER	
4. TITLE (and Subtitle): A STUDY OF VARIOUS SLENDER AND NON-SLENDER FIN-BODY COMBINATIONS OF MISSILE CONFIGURATIONS	5. TYPE OF REPORT & PERIOD COVERED: Technical Report
	6. PERFORMING ORG. REPORT NUMBER
7. AUTHOR(s): N. Uchiyama and J. M. Wu	8. CONTRACT OR GRANT NUMBER(s)
9. PERFORMING ORGANIZATION NAME AND ADDRESS: Commander, US Army Missile Command, Attn: DRSMI-RD, Redstone Arsenal, Alabama 35809	10. PROGRAM ELEMENT, PROJECT, TASK AREA & WORK UNIT NUMBERS
11. CONTROLLING OFFICE NAME AND ADDRESS: Commander, US Army Missile Command, Attn: DRSMI-RPR, Redstone Arsenal, Alabama 35809	12. REPORT DATE: 12 November 1976
	13. NUMBER OF PAGES: 194
14. MONITORING AGENCY NAME & ADDRESS (if different from Controlling Office)	15. SECURITY CLASS. (of this report): Unclassified
	15a. DECLASSIFICATION/DOWNGRADING SCHEDULE

16. DISTRIBUTION STATEMENT (of this Report)

Approved for public release; distribution unlimited

17. DISTRIBUTION STATEMENT (of the abstract entered in Block 20, if different from Report)

18. SUPPLEMENTARY NOTES

Reproduced from best available copy.

19. KEY WORDS (Continue on reverse side if necessary and identify by block number)

Rectangular and Constant Chord Sweptback Fins
Clipped Delta Fin
Slender Fin-Body Combination
Singularity Method

20. ABSTRACT (Continue on reverse side if necessary and identify by block number)

The aerodynamic loading on a number of rocket body-control surface combinations has been calculated using methods developed at the University of Tennessee Space Institute over the past five years. Variations in control surface planform, roll angle, control surface deflection or incorporation of elevons, are included. Compressibility is accounted for. Details of the digital computer program are included.

CONTENTS

		Page
SECTION I.	INTRODUCTION	1
SECTION II.	BASIC ANALYSIS	2
	1. Basic Consideration	2
	2. Basic Equations and Coordinates	5
SECTION III.	RESULTS AND DISCUSSIONS ON VARIOUS FINS	15
	1. Rectangular and Constant Chord Sweptback Fins	15
	2. Compressibility Effect on Pressure Coefficient of Rectangular Fins	18
	3. Clipped Delta Fin	18
SECTION IV.	RESULTS AND DISCUSSIONS ON VARIOUS FIN-BODY COMBINATIONS	24
	1. Rectangular Fin-Body Combination	24
	2. Constant Chord Sweptback Fin-Body Combination	28
	3. Tapered, Sweptback Fin-Body Combination	32
	4. Cruciform, Slender Delta Fin-Body Combination	32
	5. Discussions on Compressible Effect of Fin-Body Combination	37
	6. Effect of Small Control Fin on Slender Fin-Body Combination	42
SECTION V.	KOERNER'S APPROACH COMPARED WITH OTHER METHODS AND DATA	44
	1. Comparison with Slender-Body Theory	44
	2. Comparisons with FLEXSTAB Singularity Distribution Method and Data	48
SECTION VI.	COMPARISONS OF POTENTIAL FLOW THEORIES WITH DATA ON SLENDER CRUCIFORM CLIPPED DELTA FIN-BODY WITH ELEVON DEFLECTION	70
	1. Results and Discussions on Various Effects of the Elevon Deflection on Fin-Body Combination	70
	2. Comparison with Experimental Data	85

Page

3. Variation of Surface Pressure and Lift Coefficient with Free Stream Mach Number..... 92

SECTION VII. CONCLUSIONS AND RECOMMENDATIONS.. 95

REFERENCES..... 96

APPENDICES..... 98

1. Determining Aerodynamic Matrices..... 98

2. Computer Program for Determining Pressure Distribution on Fin-Body Combination..... 108

LIST OF SYMBOLS

a	Body radius, location of the fin corner in x-direction (see Figure 2).
AR	Aspect ratio of fin extended into the body.
b	Fin span, location of the fin corner in y-direction (see Figure 2).
c	Local chord.
$\bar{c}$	Reference chord $\left(= \frac{1}{S} \int_{-s}^{s} c^2(y)dy \right)$.
C_L	Lift coefficient based on S.
$C_{L\alpha}$	Derivative of lift coefficient $\left(\text{lift curve slope; } = \left(\frac{\partial C_L}{\partial \alpha}\right)_{\alpha = 0}\right)$ based on S.
C_N	Normal force coefficient based on S.
C_n	Spanwise normal force distribution (see Figure 34).
$C_{N\alpha}$	Derivative of normal coefficient $\left(\text{normal force slope; } = \left(\frac{\partial C_N}{\partial \alpha}\right)_{\alpha = 0}\right)$ based on S.
C_p	Surface pressure coefficient.
ΔC_p	Surface pressure difference $\left(= (C_p)_{\text{lower}} - (C_p)_{\text{upper}} \right)$
d	Fractional location of local panel in x-direction (see Figure 2).
D	Body diameter.
e	Location of local panel in y-direction (see Figure 2).
h	Half width of local fin panel (see Figure 3).
l(y)	Local chord at y.
LPC	Local panel chord (see Figure 3).
M	Number of half body panels.
M_∞	Free stream Mach number.
n	Total number of half fin panels.

p	Total number of panels on fin-body combination (= 2n + 2M) .
$\bar{p}$	Aerodynamic matrix (= u/U_∞ per unit γ) .
$\Delta p/q$	Load distribution (= ΔC_p) .
q	Strength of source per unit body surface area.
$\bar{Q}$	Aerodynamic matrix (v/U_∞ per unit γ).
r	Distance between two points.
$\bar{R}$	Aerodynamic matrix (w/U_∞ per unit γ).
s	Fin semi span.
S	Fin surface area extended into body.
ΔS	Local panel area.
u	Perturbation velocity component in x-direction.
U_∞	Free stream velocity.
v	Perturbation velocity component in y-direction.
w	Perturbation velocity component in z-direction.
$\vec{W}$	Velocity vector.
x	Body fixed x-coordinate parallel to free stream, positive downstream.
y	Body fixed y-coordinate in the spanwise direction of a fin, positive in right hand side direction facing forward.
z	Body fixed z-coordinate, positive upward.
Z_o	Fin location in z-direction mounted on the body.
α	Angle of attack.
β	Prandtl-Glauert parameter (= $\sqrt{1-M_\infty^2}$) .
γ	Circulation strength of fin vortex.

Γ Circulation of fin vortex.

δ Cant angle of fin, deflection angle of flap or elevon.

θ Azimuth angle of body, positive counterclockwise facing forward (see Figure 4)

$\bar{\theta}$ Azimuth angle of body, positive clockwise facing forward (see Figure 13b).

λ Gradient of bound vortex, (see Figure 3), taper ratio.

Λ Sweptback angle at specified chordwise position.

ω Apparent angle of attack.

ρ^* Distance between two points.

Subscripts

b Body

B Due to bound vortex (see Appendix 1).

D Control point on panel (see Figure 3).

e Elevon.

f Fin.

F Flap.

i,j,k, l,m,q, ν,μ Local panel name.

n Normal to body surface.

P Due to port side vortex (see Appendix 1).

S Due to starboard side vortex (see Appendix 1).

t Tangential to body surface.

V Bound vortex (see Figure 3).

SECTION I. INTRODUCTION

Aerodynamic performance of various kinds of fin-body combinations in inviscid, subsonic flow at small angles of attack can be analyzed by the "singularity method" (Refs. 1 and 5). Koerner's approach (Ref. 1) is followed in this analysis. In general, the singularity method has an advantage over the slender body theory in the sense of less restriction in the fin shape. By means of a modern high speed electronic computer, the pressure coefficient can be calculated rather simply.

The surface pressure distribution on the rectangular, the sweptback, and the tapered sweptback fins and fin-body combinations have been analyzed. The effect of compressibility is taken into account by Goethert's rule which showed very satisfactory with the experimental data up to a high subsonic free stream Mach number. For all of these no shock waves on fins and fin-body combinations are treated.

The present analysis has been extended to include the slender, cruciform, canted delta fin and fin-body combination and also includes the case of slender, cruciform, clipped delta fin-body combination geometry with a deflected small control fin. The results have been compared with the slender body theory (Ref. 2) and other singularity methods (Refs. 5 and 8).

The present method, with slight modification, can be applied also to a fin-body combination geometry of a fin with twist, camber, thickness, and arbitrary plan form. From the analytical study, it is also clear that a viscous flow study is needed in estimating the more accurate pressure distribution in the region of the fin-body junction as well as the fin tip, even at small angles of attack.

For more condensed contents of the present report and its interaction to the exhaust jet plume, see Ref. (12).

SECTION II. BASIC ANALYSIS

In estimating the aerodynamic performance on a fin-body combination geometry, the method based on slender body theory has been developed and easily applied. Very reasonable results have been obtained (see Ref. 2). The practical difficulty in applying the slender body theory is in its limitation to the very slender fin configuration (e.g., one needs to assume that $AR << 1$ theoretically, or $AR \tilde{<} 1$ even for a practical application to be held. On the other hand, the Prandtl's well-known "lifting line theory" has approximated very well the lift distribution for a rectangular fin with very large aspect ratio. The application to the other fin configurations (such as a finite AR fin) seems not that good as far as the accuracy is concerned for the surface pressure distribution. To overcome this deficiency, Lawrence (Ref. 4) has developed the approximate solution of the lifting line theory for low aspect ratio wings(including the rectangular shape) and delta fins with the aspect ratio from zero to four. However, the application of this technique to the fin-body combinations with the other fin configurations seems to be still in difficulty. A "singularity method" is a method of numerical analysis. From the study of literature, it can be said that such a numerical approach will provide the best estimation of the pressure distribution in nearly all the fin-body configurations with a good accuracy.

1. Basic Consideration

For simplicity, the following assumptions were made in this analysis, i.e.,

(i) A steady, inviscid, uniform, subsonic free stream.

(ii) A flat fin with a straight leading and trailing edge, and a streamwise fin tip.

(iii) Fins are attached to a circular cylindrical body.

(iv) A small angle of attack.

Based on the singularity method, constant strength vortex singularities are used to replace a lifting fin on a horizontal

plane. The image vortices are placed inside the body with respect to the body surface in order to compensate the body displacement effect. To obtain a good aerodynamic interaction for a fin-body geometry, the source-sink singularities are distributed on a body surface and the doublet singularities are distributed along the body axis. The doublet distribution gives the effect of a body inclination to a free stream. The iteration scheme is used so that all the simulated lifting surfaces can eventually satisfy the flow boundary conditions everywhere on the surface of the fin-body combination.

Figure 1 shows a schematic model of a basic fin-body combination for this analysis. A fin (or wing) has been divided to many panels and each one has been replaced by a horseshoe-type vortex which consists of three vortices (i.e., one bound vortex and two free vortices). The body has been divided also into many panels, each of which consists of a correct part of a body, and it has been replaced by a source or a sink at its surface. (Also, see Figure 51 in Appendix 1).

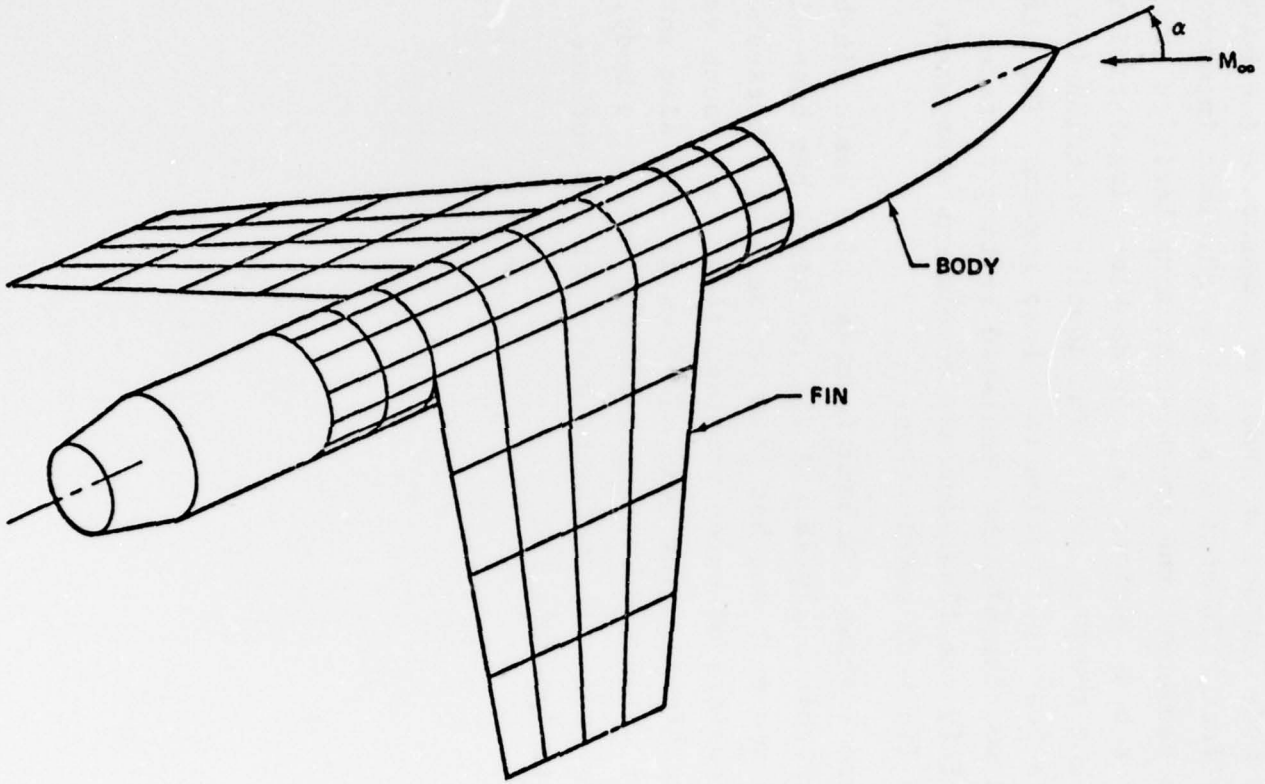

Figure 1. Schematic model of fin-body combination in present analysis.

2. Basic Equations and Coordinates

Figure 2 shows the coordinate of a fin part, which is divided by a number of trapezoidal panels which have the sides parallel to a free stream. Each panel has three vortices with a constant strength, i.e., one bound vortex, which is located at one quarter local panel chord length, and two free vortices which are located at local panel edges, parallel to the free stream.

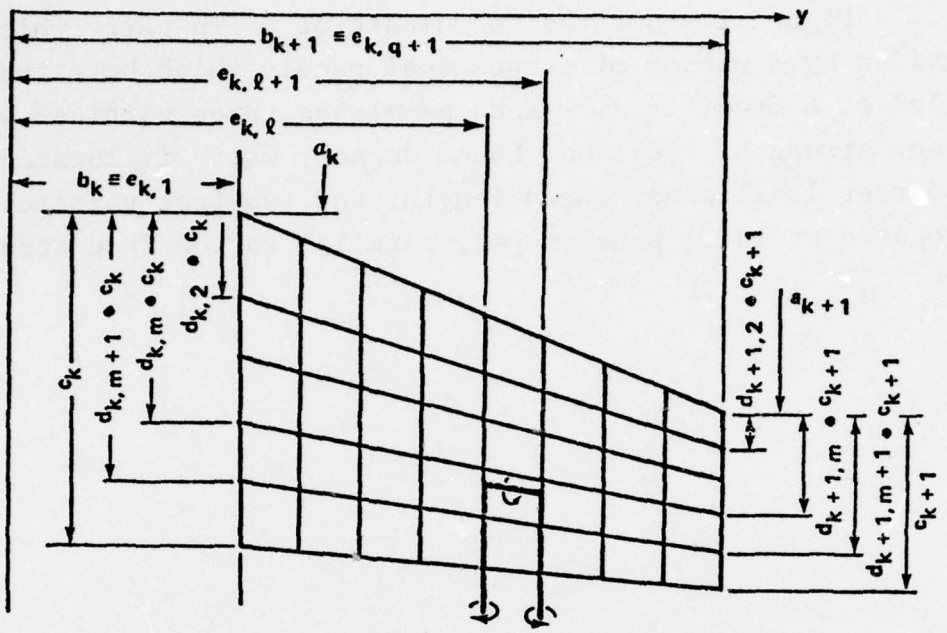

Figure 2. Fin panels [7]

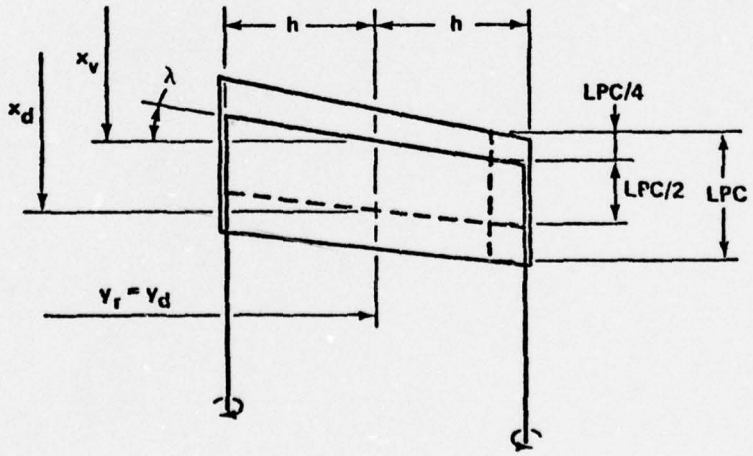

Figure 3. Location of horseshoe vortex and control point on panel [7].

The location of a control point at which the boundary condition will be satisfied is assumed at three-quarters of a local panel chord length in the center line of a local panel as shown in Figure 3. In addition to this, the Goethert compressible similarity rule has been employed to the present analysis, i.e., the coordinates normal to a free stream have been multiplied by Prandtl-Glauert Parameter β.

The following five steps are essential to the analysis. The steps were established by Ref. 1.

(i) Determining circulation distribution (γ_i) on a fin.

Normalized perturbation velocity components at any control point on panel i induced by any panel j which makes four discrete horseshoe vortices (two are from a pair of fins themselves, and two are from their body images) can be written as,

$$\left.\begin{aligned} \frac{u_i}{U_\infty} &= \sum_{j=1}^{n} \bar{P}_{ij}\, \gamma_j \\ \frac{v_i}{U_\infty} &= \sum_{j=1}^{n} \bar{Q}_{ij}\, \gamma_j \\ \frac{w_i}{U_\infty} &= \sum_{j=1}^{n} \bar{R}_{ij}\, \gamma_j \qquad i = 1, n \end{aligned}\right\} \quad (1)$$

where: u_i, v_i, w_i are perturbation velocity components and $\bar{P}_{ij}$, $\bar{Q}_{ij}$ and $\bar{R}_{ij}$ are the aerodynamic matrices given in Appendix 1.

The third equation as stated above is used for satisfying the boundary conditions of any panel, i.e.,

$$-\beta\omega_i = \frac{w_i}{U_\infty} = \sum_{j=1}^{n} \bar{R}_{ij}\, \gamma_j \qquad i = 1, n \qquad (2)$$

where $\omega_i = \alpha_{fi}$. Equation 2 is n simultaneous linear equations with n x n constant coefficients. The γ_j can be solved by Gaussian elimination technique.

(ii) Determining Source Distribution (q_ν) on the Body.

Induced velocity components at any point on panel ν on the body surface due to the fin and its image vortices on the control point of panel j is expressible as,

$$\vec{W}_\nu = \begin{pmatrix} u_{b\nu} \\ v_{b\nu} \\ w_{b\nu} \end{pmatrix} = \sum_{j=1}^{n} \begin{pmatrix} \bar{P}_{b\nu_j} \\ \bar{Q}_{b\nu_j} \\ \bar{R}_{b\nu_j} \end{pmatrix} \gamma_j \qquad (3)$$

$$\nu = 1, 2M$$

where $\bar{P}_b$, $\bar{Q}_b$, and $\bar{R}_b$ are the same aerodynamic matrices as those in Equation (1), except taking the control points on the body, which are located at the center of local panels (see Figure 51 in Appendix 1), in the former case.

In cylindrical coordinates,

$$\begin{aligned} v_{n1} &= v_b \cos\theta + w_b \sin\theta \\ v_t &= -v_b \sin\theta + w_b \cos\theta \end{aligned} \qquad (4)$$

Geometrical relationships are illustrated in Figures 4 and 5.

The resultant velocity component normal to the body surface due to the fin vortices and the sources must be varnished, i.e.,

$$v_{n1} + v_{n2} = 0 \qquad (5)$$

where v_{n2} is the velocity component normal to the body surface due to the sources distributed on it, v_{n2} can be written as,

$$v_{n2} = \frac{q(x,\theta)}{2} + \int_{-\infty}^{\infty} \frac{q(x',\theta')}{4\pi} \frac{\{1 - \cos(\theta-\theta')\}\, a^2}{\rho^{*3}} \, d\theta' \, dx' \qquad (6)$$

in incompressible flow, where

$$\rho^* = (x - x')^2 + (y - y')^2 + (z - z')^2 \qquad (7)$$

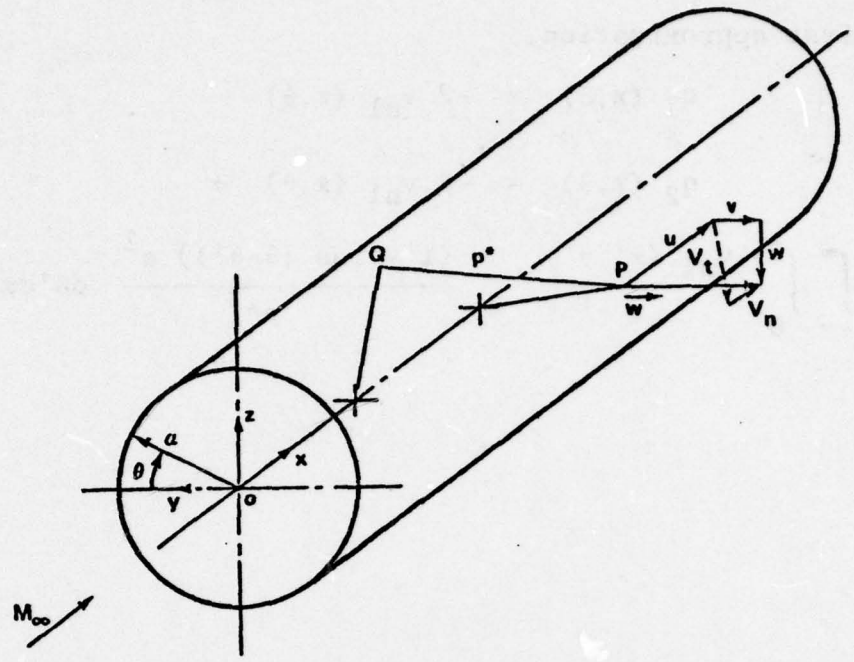

Figure 4. Induced velocity at P by a source Q [1].

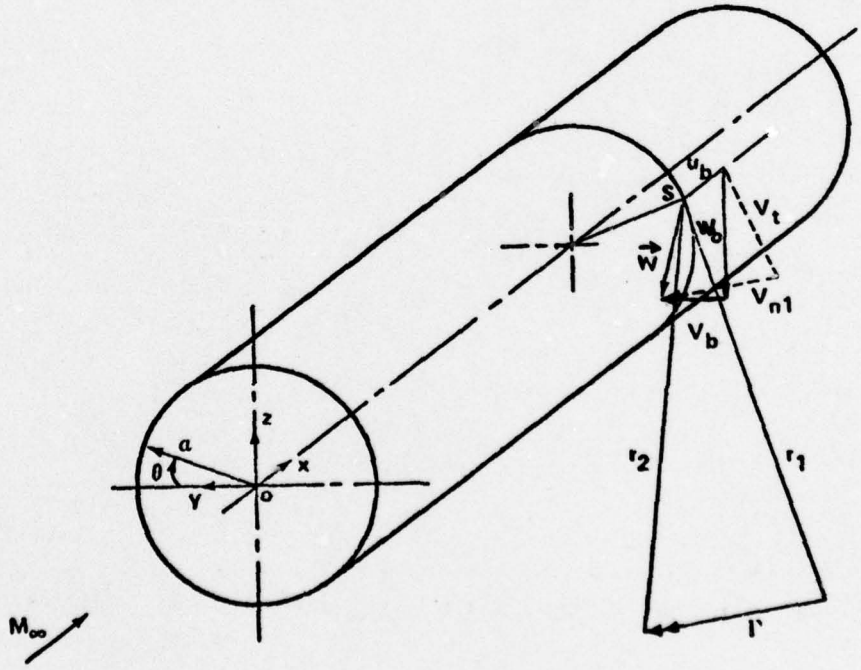

Figure 5. Induced velocity at S by a line vortex element Γ [1].

The integral equation (6) can be solved by the iteration scheme; For the first approximation,

$$q_1(x,\theta) = -2\, v_{n1}(x,\theta) \tag{8}$$

or,

$$q_2(x,\theta) = -2\, v_{n1}(x,\theta) + \int_{-\infty}^{\infty}\int_{0}^{2\pi} \frac{v_{n1}(x',\theta')}{\pi} \quad \frac{\{1-\cos(\theta-\theta')\}\, a^2}{\rho^{*3}}\, d\theta' dx' \tag{9}$$

The m^{th} approximation of the source strength q_ν at a point ν on a body surface which cancels the induced velocity v_{n1} in Equation (4) normal to a body surface can be written as

$$q_{m\mu} = -2\,(v_{n1})_{m\mu} - \sum_{\substack{\nu=1 \\ \nu\neq\mu}}^{2M} \frac{q_{(m-1)\nu}}{2\pi} \frac{\{1-\cos(\theta_\mu-\theta_\nu)\}\,\beta\,a\,\Delta S_\nu}{\left[(x_\mu-x_\nu)^2 + \beta^2\{1-\cos(\theta_\mu-\theta_\nu)\}\,a^2\right]^{3/2}} \tag{10}$$

and,

$$\Delta S_\nu = \beta\,a\,\Delta\theta\;\Delta x_\nu \tag{11}$$

(iii) Determining Downwash ($w_{b\mu}$) on Fin Due to Sources Distributed on the Body Surface

The downwash on panel μ due to source on panel ν can be written as,

$$W_{b\mu} = \sum_{\substack{\nu=1 \\ \nu\neq\mu}}^{2M} \frac{q_\nu}{4\pi} \frac{\beta(z_o-z_\nu)\,\Delta S_\nu}{\left[(x_\mu-x_\nu)^2+\beta^2\{(y_\mu-y_\nu)^2+(z_o-z_\nu)^2\}\right]^{3/2}} \tag{12}$$

(iv) Determining Circulation Distribution (γ_i) for Second Iteration

By the downwash obtained in Equation (12), the corresponding angle of attack is induced on a fin, which can be written as W_{bi}/U_∞. Then, this term should be added to the original, i.e., geometrical angle of attack in Equation (2), thus ω_i must be written as,

$$-\omega_i = -\alpha_{fi} + \frac{w_{bi}}{U_\infty} \qquad i = 1,n \tag{13}$$

After ω_i has been obtained on fin panels, the same procedure should be repeated until γ_i will not change greatly.

(v) In Case of Body with Angle of Attack.

Downwash on a fin due to the doublet along a body axis (as shown in Fig. 6) can be written as

$$\frac{w_f}{U_\infty} = \alpha_b a^2 \frac{y^2 - z_o^2}{(y^2 + z_o^2)^2} \tag{14}$$

This downwash has been assumed constant at any spanwise location, and it changes an apparent angle of attack (ω_i) as mentioned above. Thus, in this case, ω_i should be replaced by,

$$-\omega_i = -\alpha_{fi} + \frac{W_{bi}}{U_\infty} + \frac{W_{fi}}{U_\infty} \tag{15}$$

The aerodynamic performance coefficient can be computed in the usual manner for the pressure coefficient, C_p, on panel;

$$\left.\begin{aligned} C_{pj} &= \pm \frac{\Delta C_{pj}}{2} \quad \text{..... for fin,} \\ &= -\frac{2u_{bj}}{U_\infty} \quad \text{..... for body.} \end{aligned}\right\} \tag{16}$$

where "+" is for an upper surface of a fin and "-" is for a lower surface.

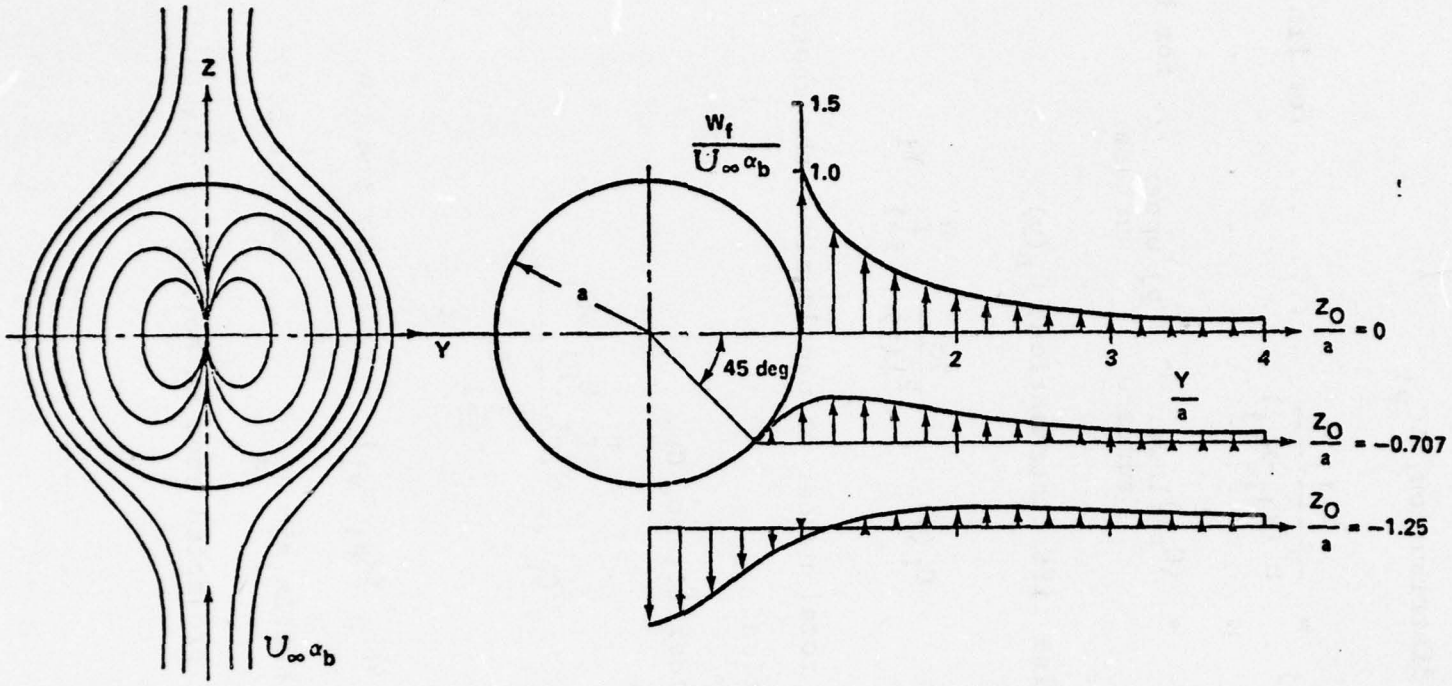

Figure 6. Velocity distribution on fin induced by the body angle of incidence [3].

For the load distribution, ΔC_p,

$$\left.\begin{aligned} \Delta C_{pj} &= \frac{b\,\gamma_j}{\beta^2(x_{dj}-x_{vj})} \quad \ldots\ldots\ldots\ldots \text{ for fin,} \\ &= (C_{pj})_{\substack{\text{lower}\\\text{surface}}} - (C_{pj})_{\substack{\text{upper}\\\text{surface}}} \ \ldots \text{ for body.} \end{aligned}\right\} \quad (17)$$

For the spanwise lift distribution, $C_L(y)$,

$$C_L(y) = \frac{2b}{\beta^2 l(y)} \sum_{i=1}^{n'} \gamma_i \qquad (18)$$

where n' is a total number of panels along the chord $l(y)$ at a fixed y station.

For the lift coefficient, C_L,

$$C_L = \frac{\sum_{j=1}^{p} C_{pj}\,\Delta S_j}{\sum_{j=1}^{p} \Delta S_j} \qquad (19)$$

$$\left.\begin{aligned} \text{where } \Delta S_j &= 4\beta h_j\,(x_{dj}-x_{vj}) \ \ldots\ldots\ldots \text{ for the fin,} \\ &= \beta a \Delta\theta \Delta x_j \sin\theta_j \ \ldots\ldots\ldots \text{ for the body.} \\ &\quad \text{(projected area on horizontal plane)} \end{aligned}\right\} \quad (20)$$

SECTION III. RESULTS AND DISCUSSIONS ON VARIOUS FINS.

1. Rectangular and Constant Chord Sweptback Fins.

As the first example by the singularity method, the spanwise lift distribution at $M_\infty = 0$ was computed for the fin with the three different leading edge sweptback angles, that is, zero (rectangular fin), 30 and 45 degrees. The aspect ratio of these fins is taken as all the same equals to six. The fin configuration and the computed results are shown in Fig. 7. This figure shows the spanwise lift distribution per unit angle of attack over the semi span of the fin. The half of the fin has been divided into the sixteen trapezoidal panels, i.e., four equidistantly in the chordwise direction, and four with cosine in the spanwise direction. The present calculations have been compared with those in Ref. (1), on which the present analysis was based. The results are shown in Fig. 7. It can be seen that there is little difference between them. As the ordinate in Fig. 7 is considered proportional to the circulation distribution per unit angle of attack over the semi-span of the fin (see curve A), i.e., the rectangular fin, is very close to the elliptics. With increasing the sweptback angles of a fin, the lift distribution around the center of the fin is decreasing, or the maximum point of the lift distribution moves to the fin tip, and thus the lift of the fin decreases accordingly. This means that the characteristics of the fin will be close to the one of the "delta" fin (compare it with Figs. 11 and 12).

The typical chordwise pressure distribution on a rectangular fin at the different spanwise positions is shown in Fig. 8. The same rectangular fin configuration as the one in Fig. 7 was used here. The pressure goes to infinity at the leading edge of the fin because of the "leading edge singularity" of the fin with zero thickness. It can be also been that the Kutta's conditions at subsonic speed are certainly satisfied at the trailing edge of the fin.

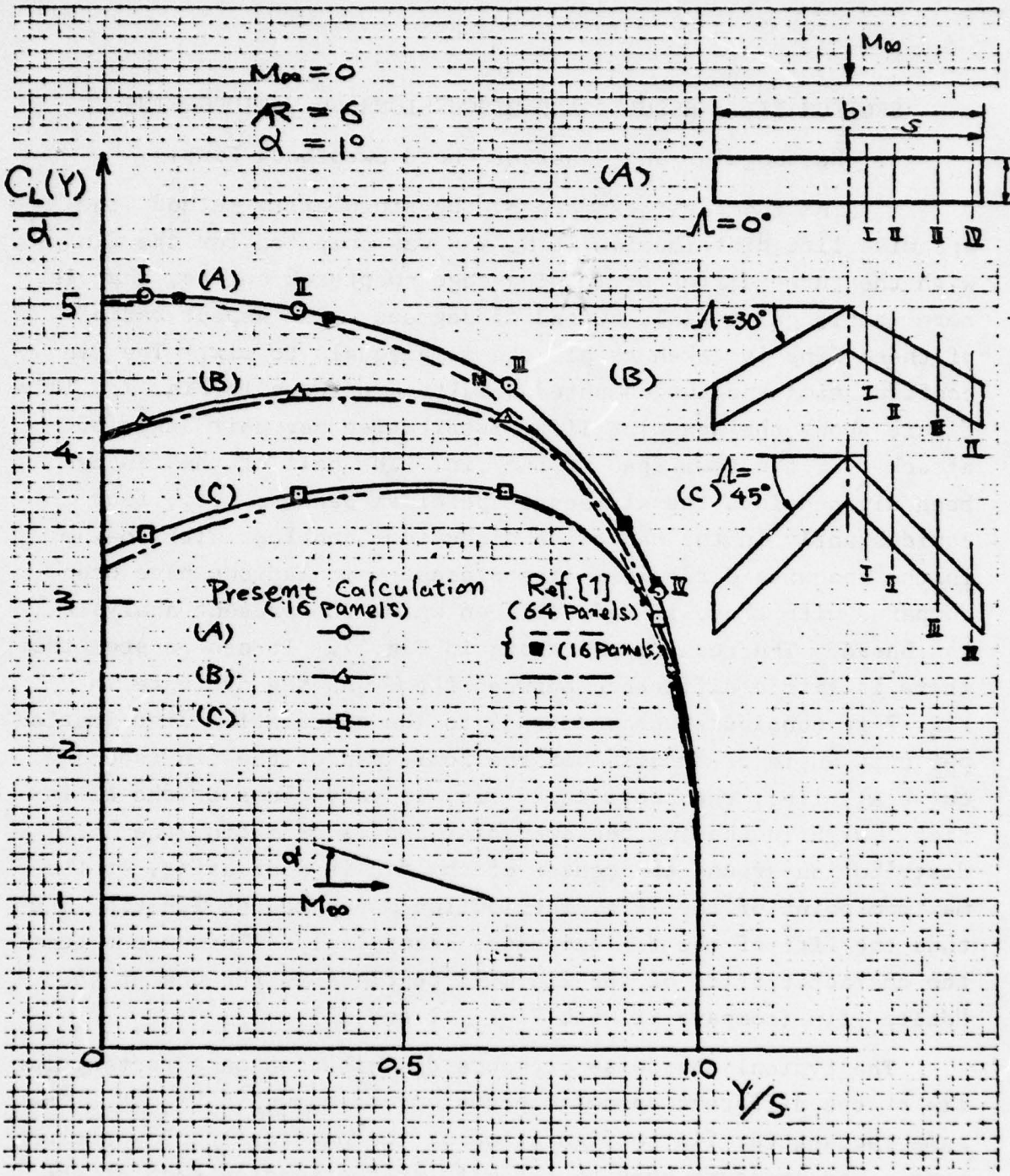

Figure 7. Spanwise lift distributions on constant chord sweptback fins.

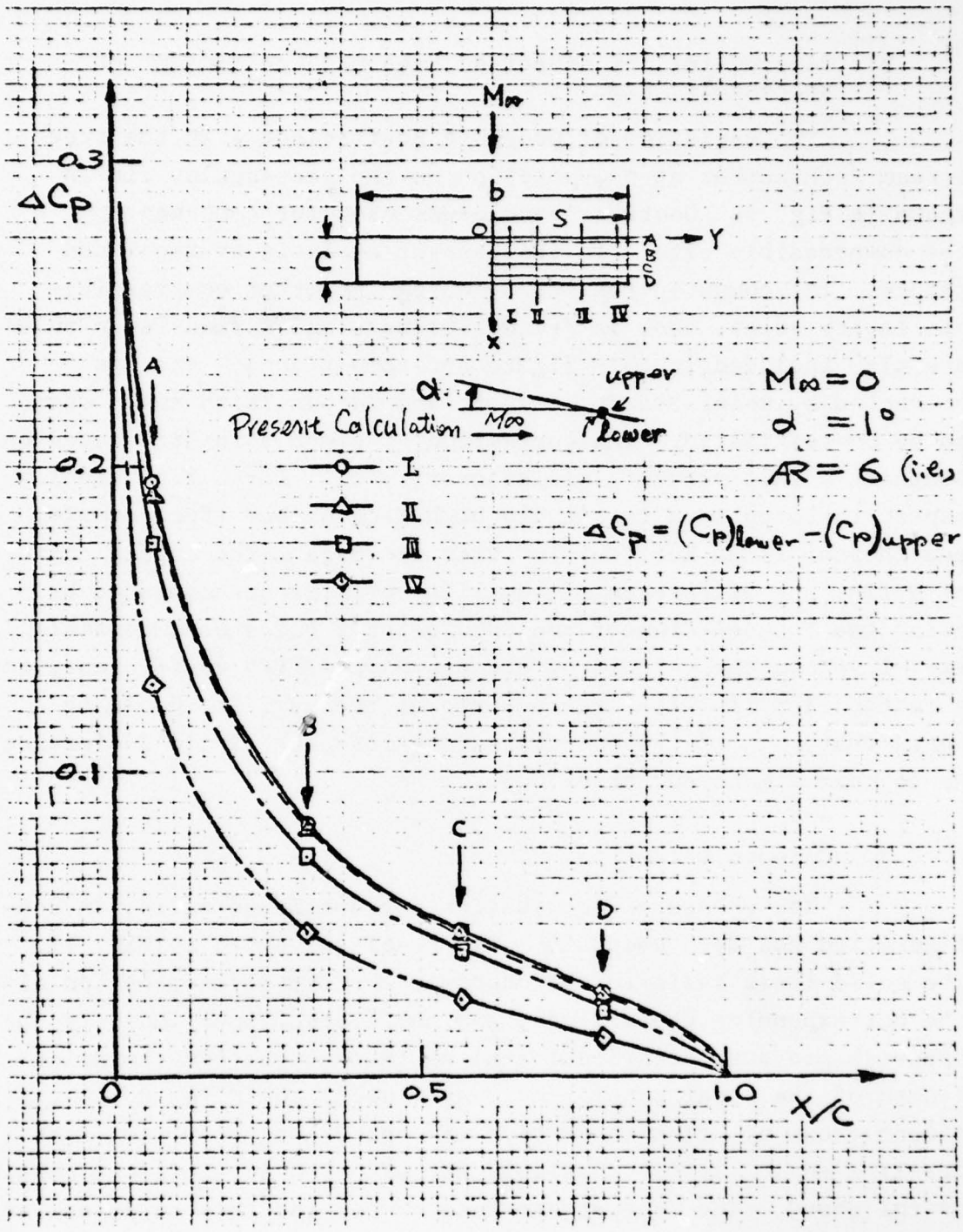

Figure 8. Chordwise pressure distribution on rectangular fin.

2. Compressibility Effect on Pressure Coefficient of Rectangular Fin.

The variation of pressure coefficient with the free stream Mach number at one position on the rectangular fin is shown in Fig. 9. Goethert's rule was used for compensating the compressible effect in the present analysis as mentioned before. The computed results by using the other compressible similarity rules, such as Prandtl-Glauert and Kármán-Tsien rules, are also included in this figure for comparisons. The Cps corrected by using Prandtl-Glauert and Kármán-Tsien rules seem to be overestimated. The correction of compressibility based on Goethert's rule predicts satisfactorily well for a fin with low-aspect ratio up to a relatively high Mach number (for example, see Chapter 13 in Ref.(10)). With increase in the aspect ratio of a fin, the difference of the lift coefficients computed by using the Prandtl-Glauert and the Goethert rules becomes small. Fig. 10 shows the calculated example on the lift coefficient, for a rectangular fin with aspect ratio of twenty. It should be noted that both of the calculated results have little difference up to near a Mach number of 0.8.

3. Clipped Delta Fin.

The pressure distribution for a clipped delta fin configuration has been computed. The result is shown in Fig. 11. The solid lines indicate the chordwise pressure distribution along the corresponding chord lines, and the dotted lines indicate the spanwise pressure distribution along the one-quarter chordwise length of the local panel. As can be seen, the clipped fin tip effect shows up after the entire mid chord length or toward the trailing edge. It is relatively not affected in the front portion of the chord. The free stream Mach number for this computed case is 0.7, the leading edge sweptback angle is 77.2°, and the angle of attack is taken as one degree. From this figure, it can be seen that the aerodynamic characteristics of the clipped delta fin has the one combined with those of the sweptback and

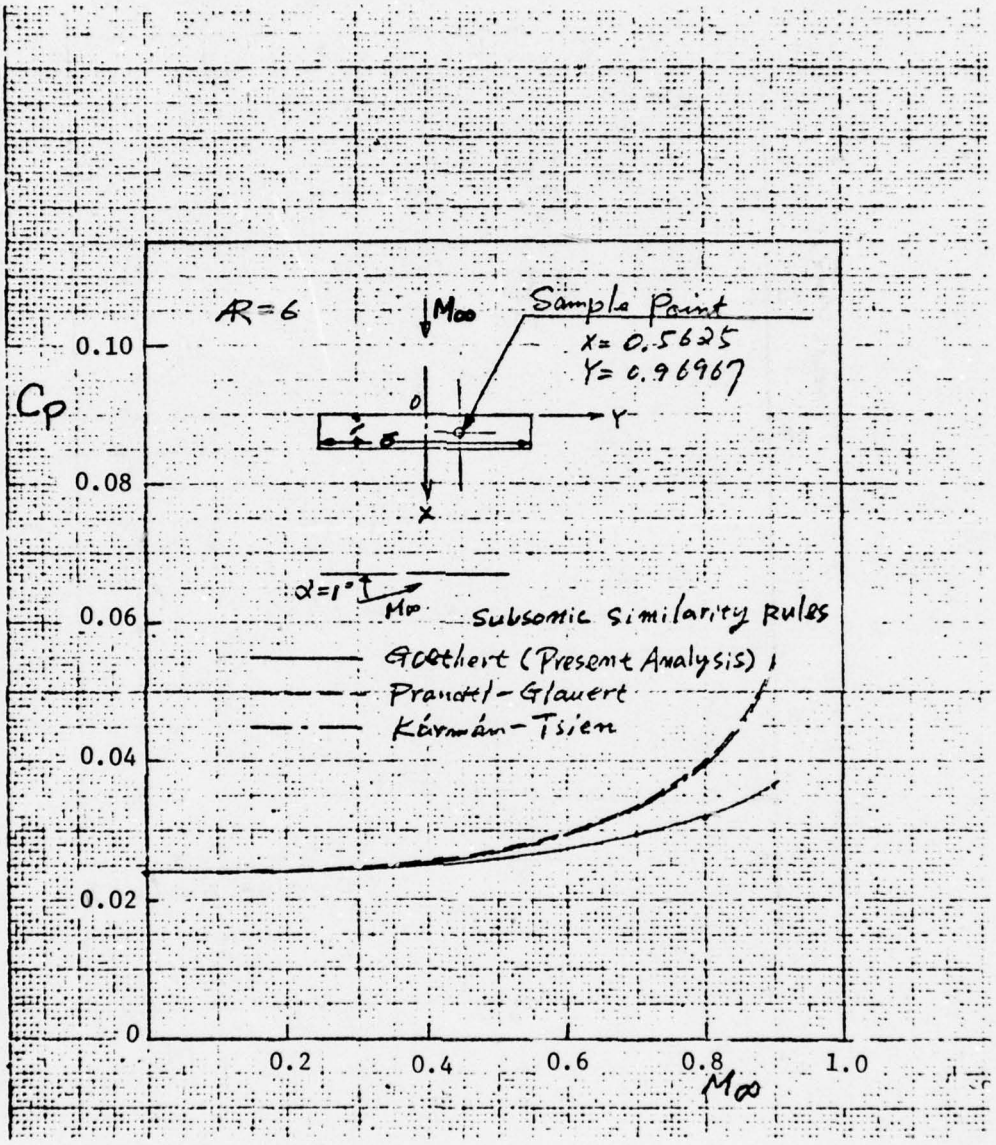

Figure 9. C_p at one point on rectangular fin changing with free stream Mach number computed by different subsonic compressible similarity rules.

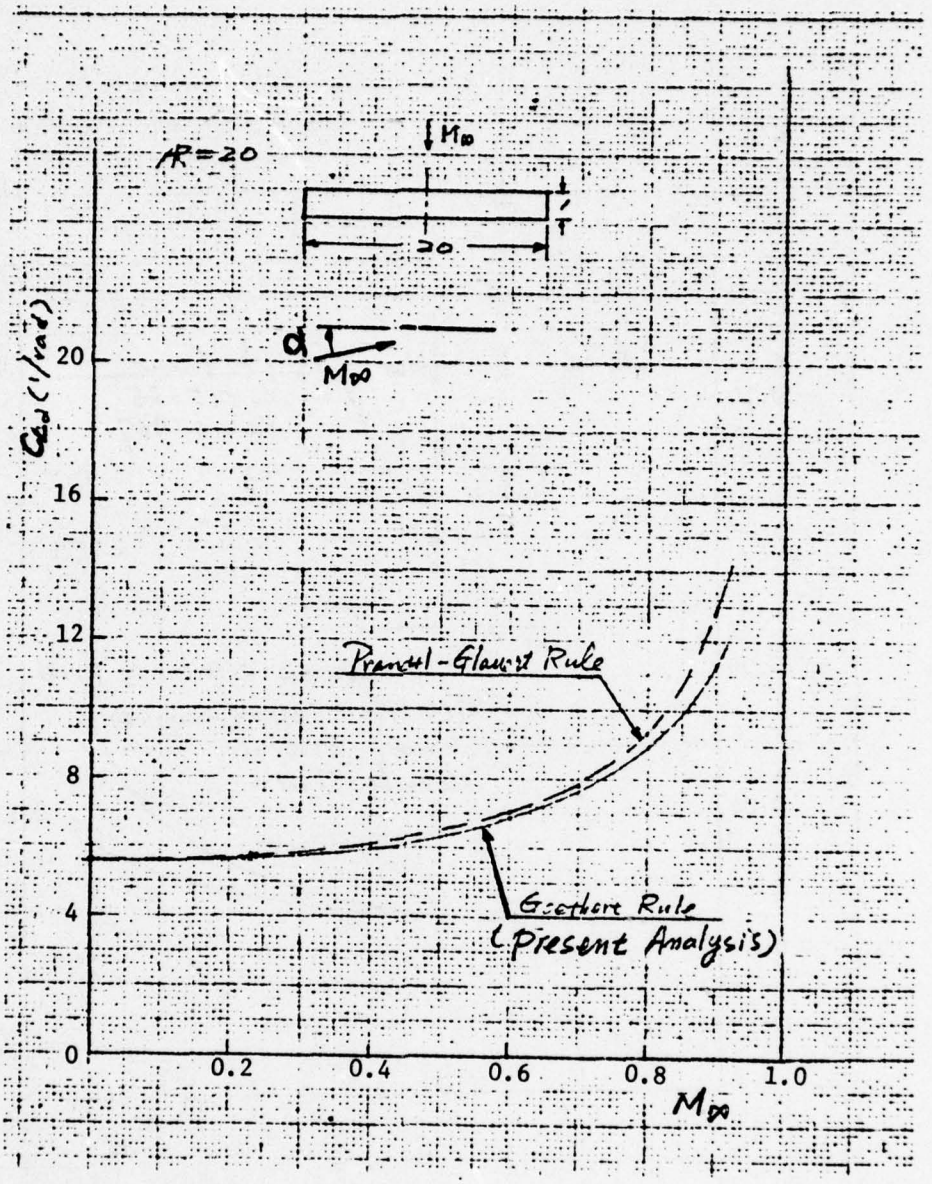

Figure 10. Comparison of lift coefficient of rectangular fin with large aspect ratio by two different similarity rules.

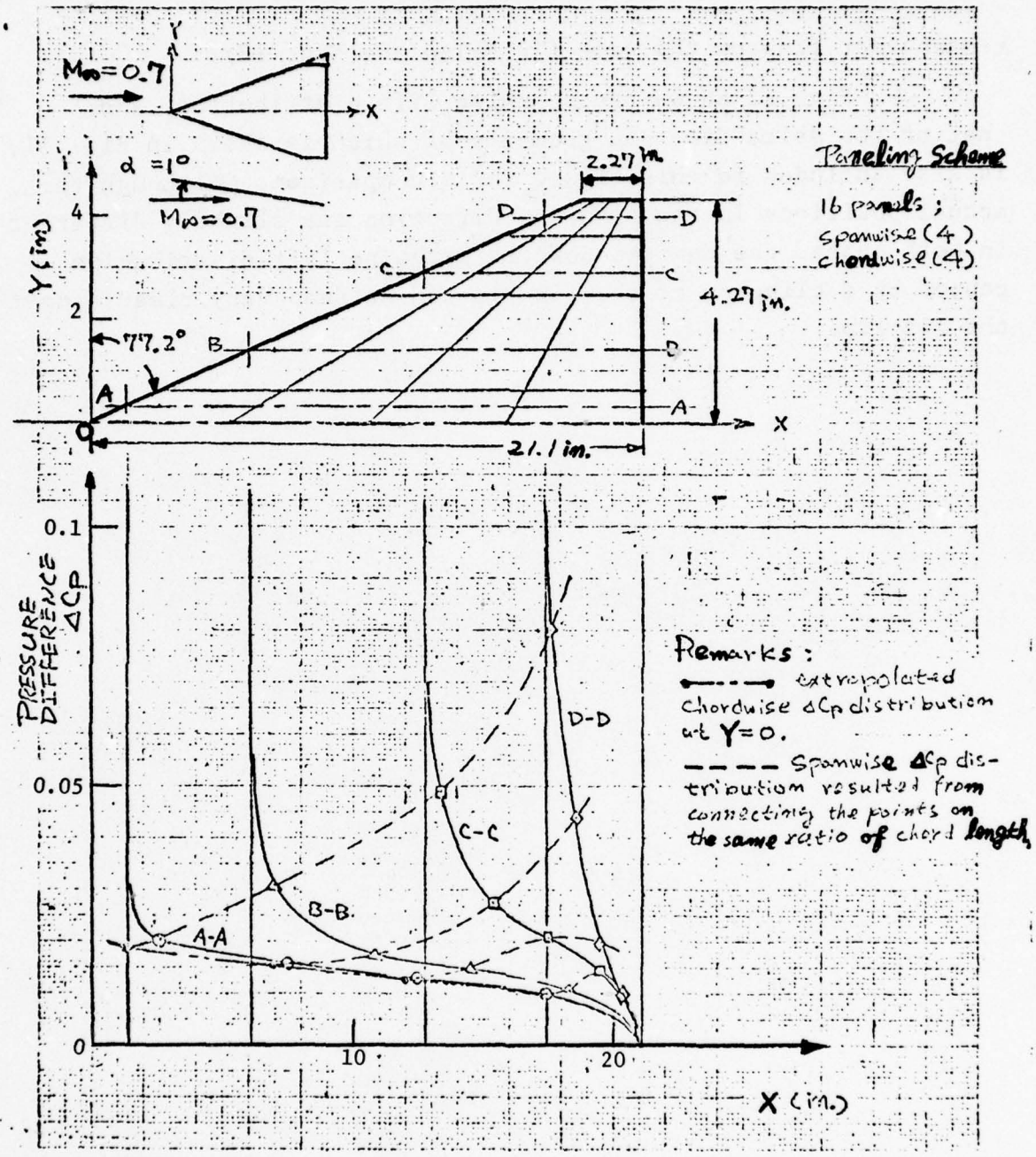

Figure 11. Pressure difference $\left(\Delta C_p = (C_p)_{lower} - (C_p)_{upper}\right)$ of clipped delta fin with angle of attack of one degree and free stream Mach number of 0.7.

rectangular fins on the same fin (also see Fig. 12).

Fig. 12 shows the spanwise lift distribution, and that of the delta fin, the geometry of which is shown in Fig. 11, is also included in this figure for a comparison. Although the actual positions in the spanwise direction are slightly different in both cases, the decrease of the spanwise lift distribution caused by a clipping of the fin tip can be seen very clearly near the fin tip.

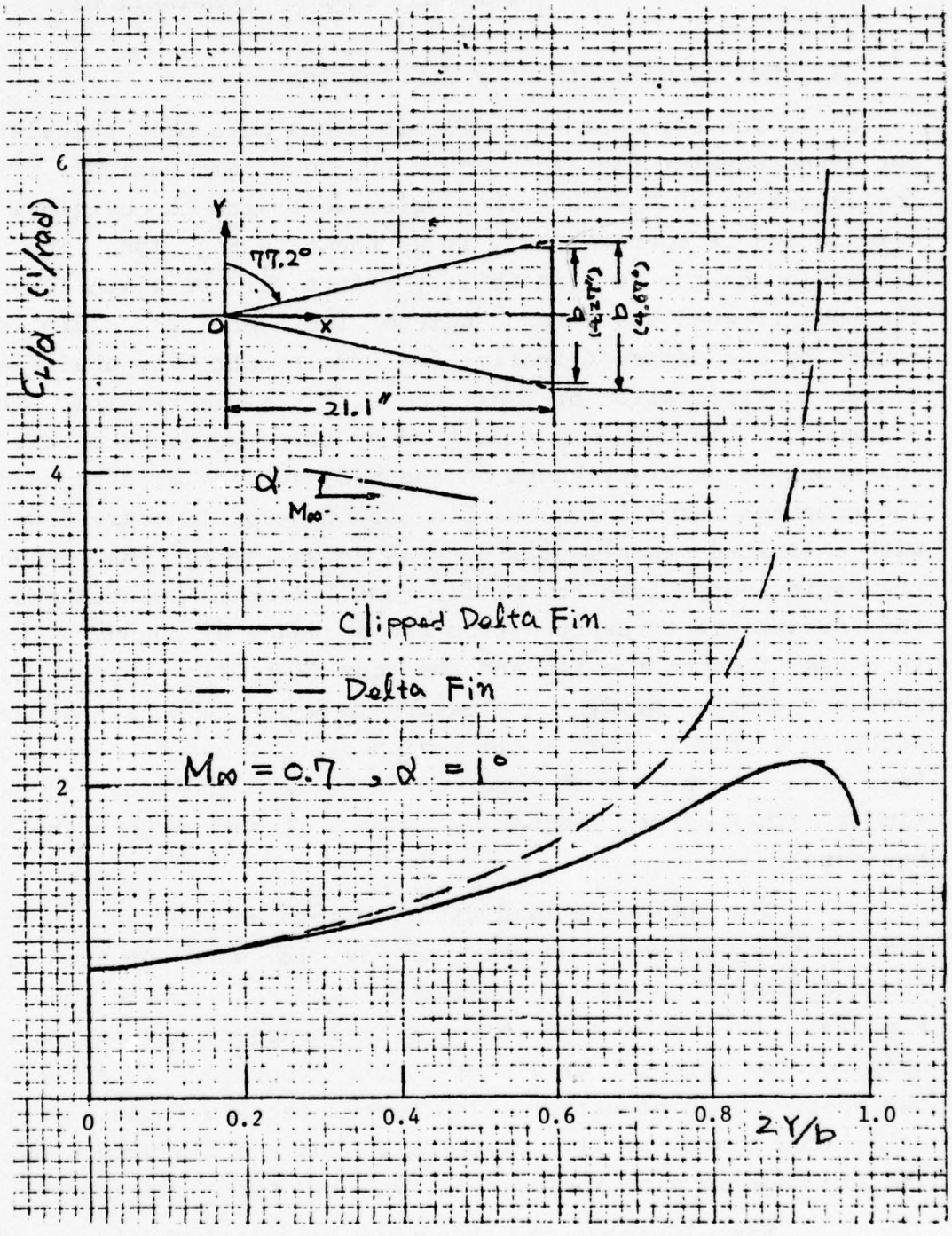

Figure 12. Spanwise lift distribution on clipped delta fin (M_∞ = 0.7, α = 1°; also, the delta fin's case is included).

SECTION IV. RESULTS AND DISCUSSIONS ON VARIOUS FIN-BODY COMBINATIONS.

1. Rectangular Fin-Body Combination.

The spanwise lift distributions have been calculated for a rectangular fin alone and a fin-body combination configuration at $M_\infty = 0$. They agree well with the original calculation of Koerner (Ref. 1) as shown in Fig. 13a. The discussion on the compressibility effect will be given later. The body treated has a zero angle of incidence, and a fin is canted by one degree (clearly, for a more cant fin, a simple linear multiplication of amplitude will yield a result). The presence of the body was simulated by image vortices of the fin and source-sink distributed on the body surface as discussed. The computed results for the fin-body interaction agreed well with a limited experimental data as shown in Fig. 13a, except in the region very close to the fin root. Koerner pointed out that this disagreement resulted from the presence of boundary layer in a real flow on the fin and the body (Ref. 1). This suggests that the viscous study is necessary in order to obtain a more accurate result in this small region. As it can be seen from Fig. 13a , the mutual interaction between the body and the fin is rather strong (comparing cases with and without the body presence).

The chordwise load distributions on the body in the same fin-body geometry as shown in Fig. 13a were computed at three different azimuthal positions. The results are shown in Fig. 13b. It can be seen that the influence of the fin on the body becomes stronger as closer to the fin root. It affects both the upstream and downstream flow beyond the fin location. The calculated chordwise lift distribution on the fin very close to the fin root is also included in Fig. 13b for a comparison.

Fig. 14 shows the chordwise load distribution on the rectangular fin-body combination, in which the fin is not canted,

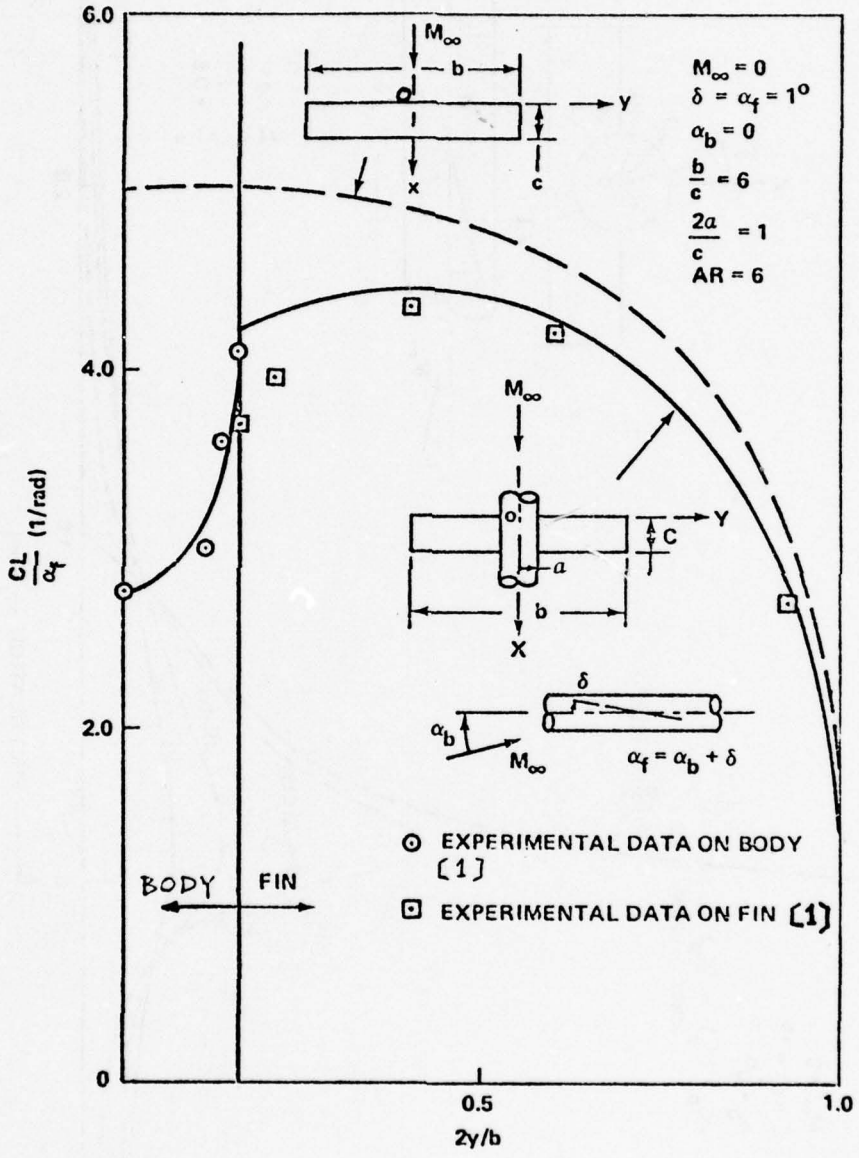

Figure 13a. Recalculated spanwise lift distribution of rectangular fin-body combination given by Korner [1].

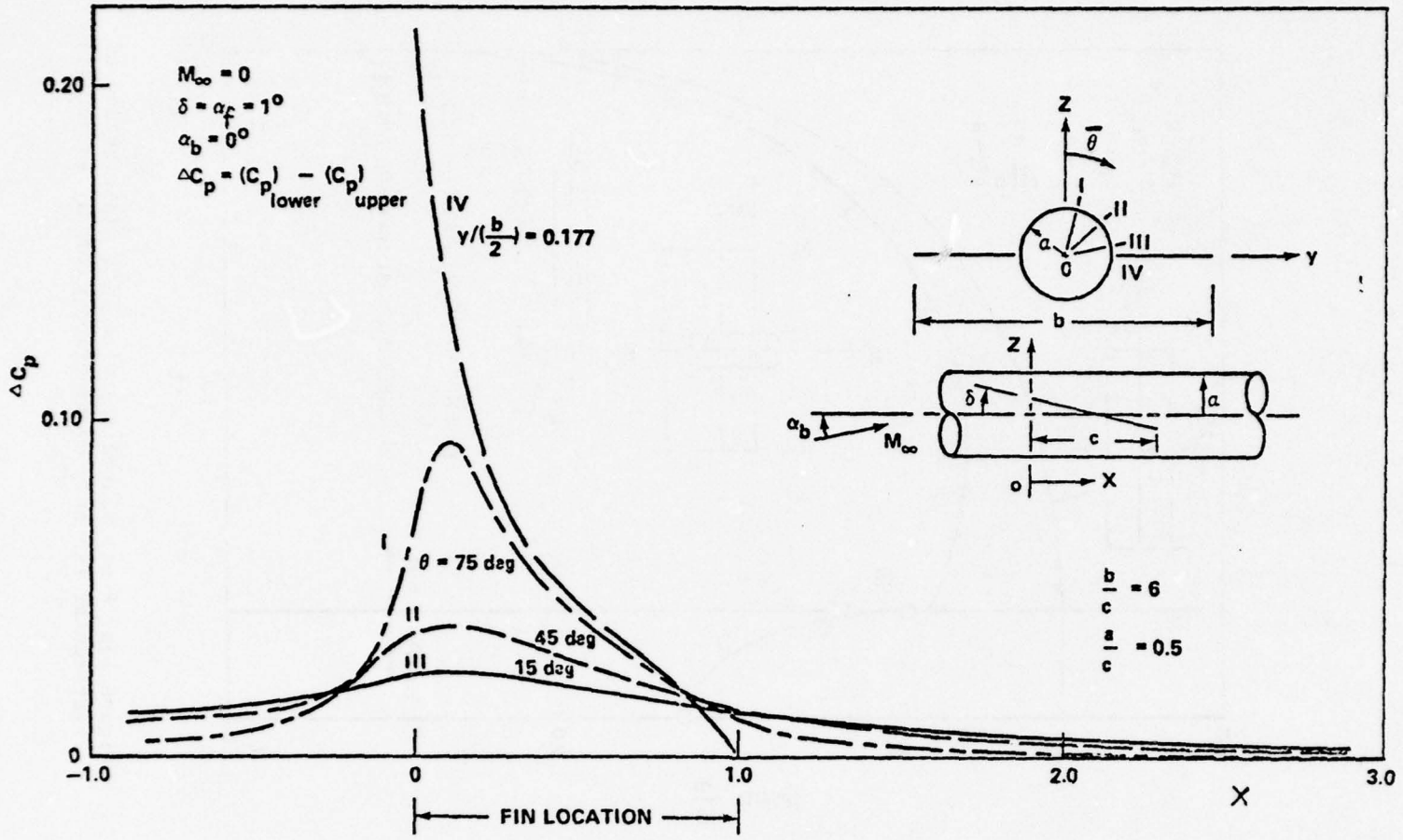

Figure 13b. Longitudinal pressure distribution of body with rectangular fin.

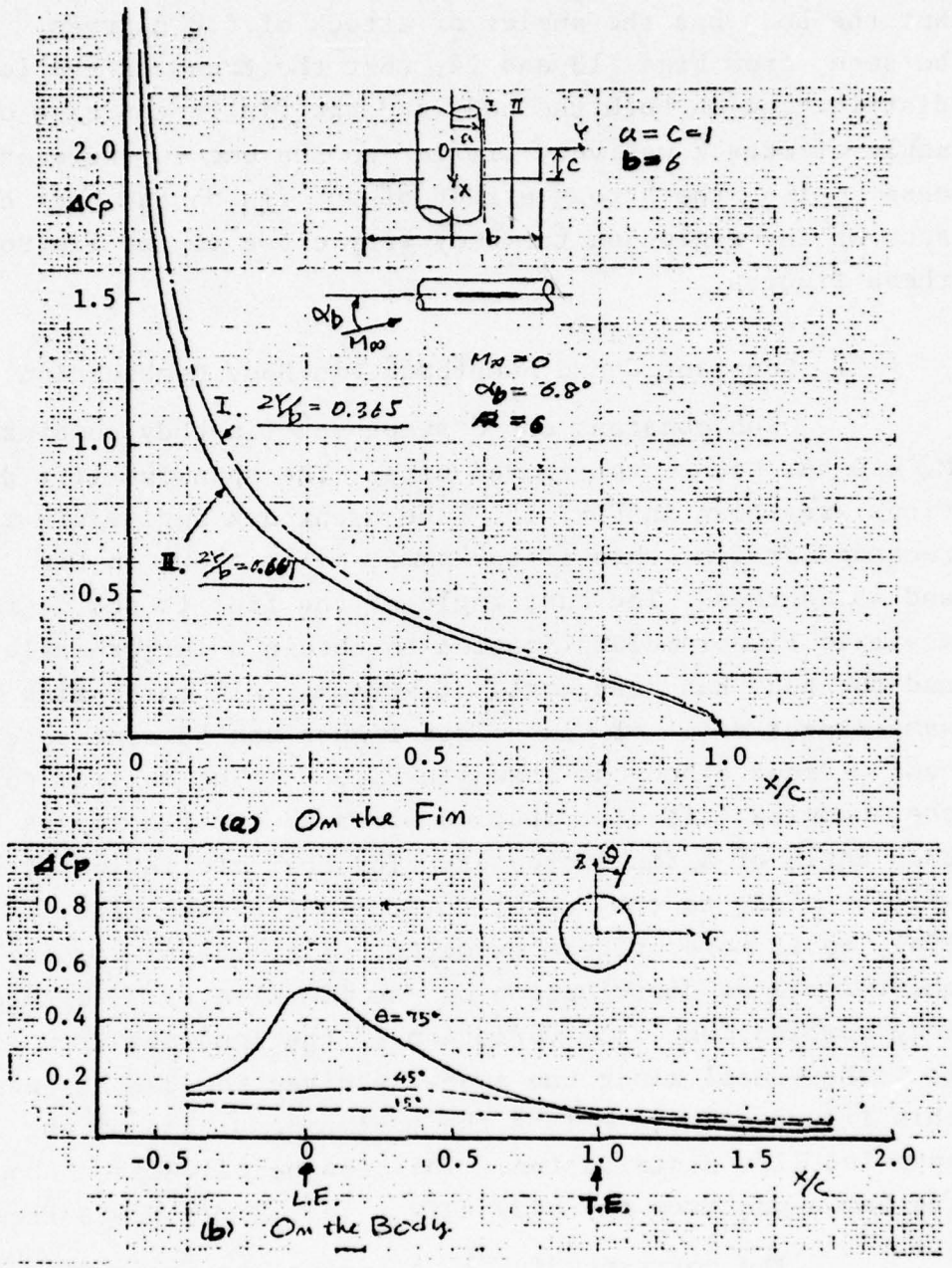

Figure 14. Longitudinal pressure distribution on rectangular fin-body combination (α_b = 6.8°, M_∞ = 0).

but the body has the angles of attack of 6.8 degrees. It can be seen, from Figs. 13 and 14, that the trend of the load distribution on both the body and the fin in the case of the angle of attack was very similar to the one in the cant fin case. Also, the strong effect of the fin on the body can be seen at the region on the body very close to the fin root from these figures.

2. Constant Chord Sweptback Fin-Body Combination.

The constant chord sweptback fin-body combination at $M_\infty = 0$ has been investigated here. The spanwise lift distributions are shown in Fig. 15. The sweptback angles are zero (i.e., rectangular fin, this is the same one as shown in Fig. 13), 30 and 45 degrees. The cant angle of the fins is one degree (again a simple linear multiplication to obtain a larger angle result) and the body has zero angle of attack. All three fins have the same aspect ratio of six. This figure can be contrasted to the case without a body as shown in Fig. 7. The maximum point of the spanwise lift distribution moves to the fin tip as the sweptback angle of a fin increases. The characteristics of a fin will be close to the one of the delta fin (see Figs. 17, 18, and 19a), as is more or less expected. Fig. 16a shows a calculated chordwise load distribution on the fin of a 45^o sweptback fin-body combination. The variation of the load distribution which is rather small along the spanwise direction can be seen from this figure. There exists the maximum position of the semi-spanwise lift distribution. This can be calculated about 60% of the semi-span from the body axis, i.e., $2\ y/b \simeq 0.6$ from Fig. 15.

The corresponding longitudinal pressure distribution on the body is shown in Fig. 16b. The gradient of the pressure distribution curve was not so steep as the one in the rectangular fin case, as shown in Fig. 13b.

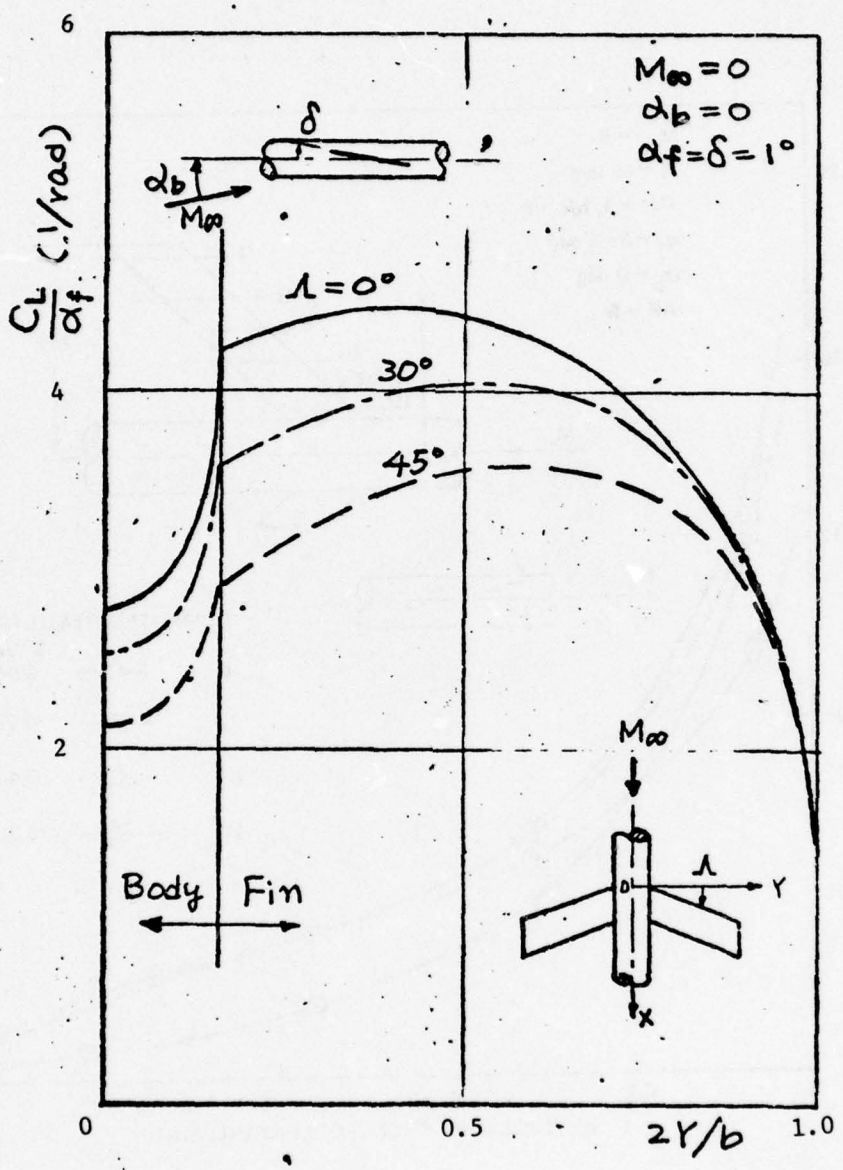

Figure 15. Spanwise lift distribution of constant chord sweptback fin-body combination.

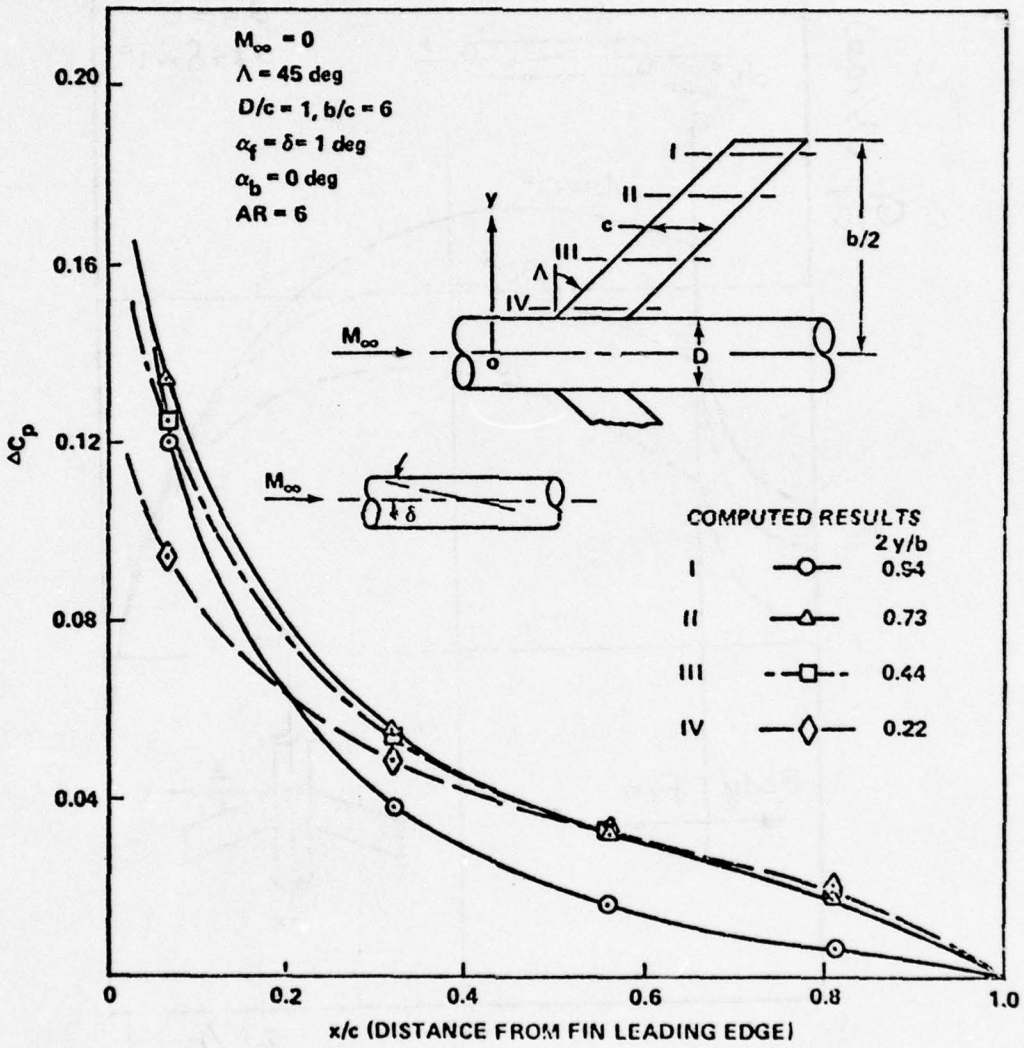

Figure 16a. Chordwise pressure distribution on 45° sweptback fin with body.

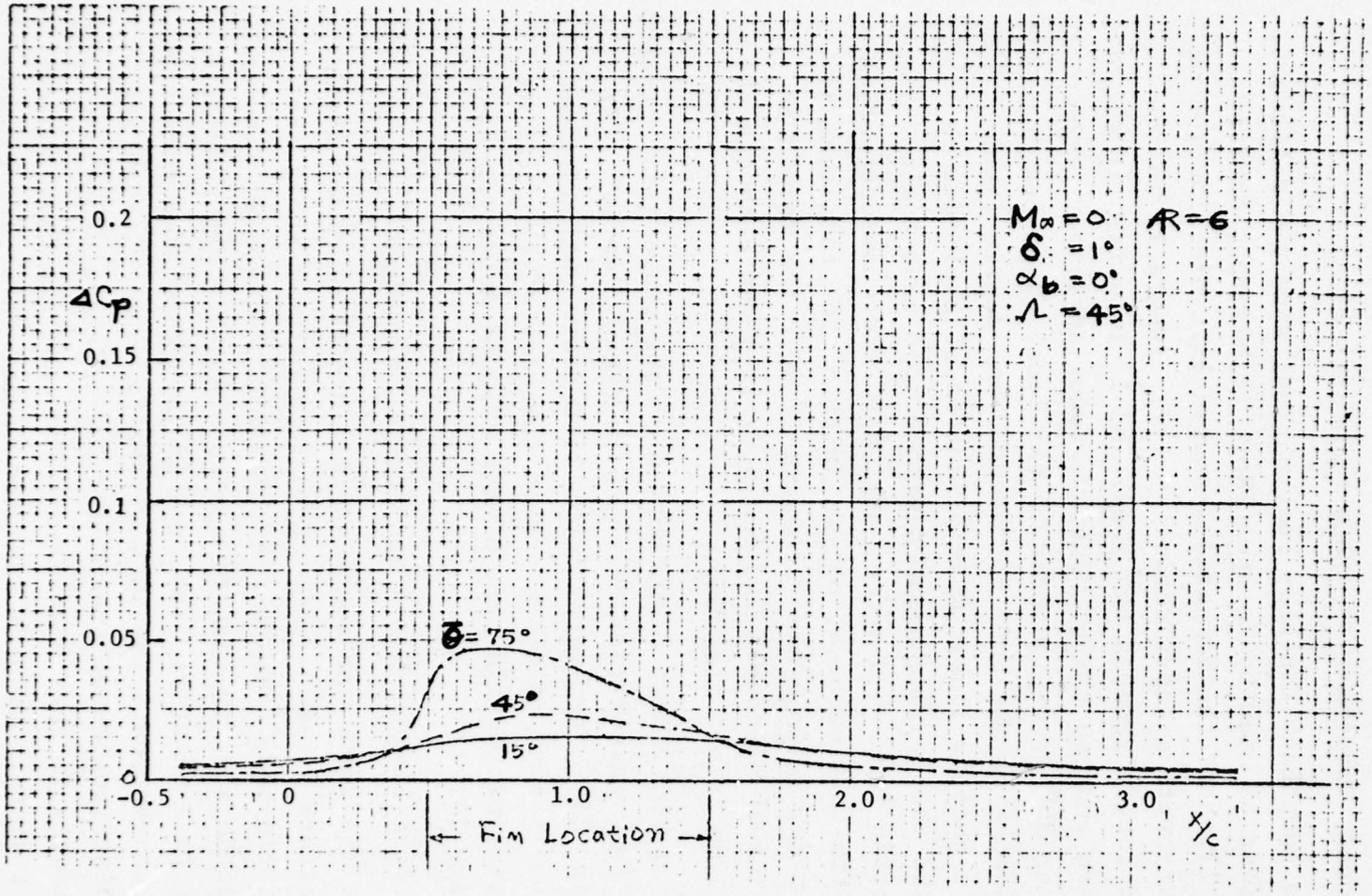

Figure 16b. Longitudinal pressure distribution on body.

3. Tapered, Sweptback Fin-Body Combination.

The sweptback fin-body combination, with two different taper ratio fins as used by Koerner (Ref. 1) has been investigated. Fig. 17 shows the computed spanwise lift distribution on such a geometry with a taper ratio $\lambda = l_a/l_i$ (where l_i is the maximum chord length through the body, and l_a is a fin tip chord length) of zero and one third. The sweptback angle for both cases was taken 30^o at one quarter of the local chord length. The angle of incidence of the body was assumed one degree (again, for a larger angle case, a linear multiplication of amplitude is sufficient) and the fin was assumed with a zero cant angle. The lift distribution for $\lambda = 0$ agrees well with the characteristics of the delta fin-body combination, in spite of the fact that it is not quite a delta fin. Also, compare it with the result in Fig. 19a, a case of slender delta fin-body is shown although the fin configuration is not the same.

The spanwise lift distribution of the trapezoidal fin-body combination, the configuration of which is taken from Ref. (7), is shown in Fig. 18. The trend of the lift distribution curve has not much difference with the one in the case of $\lambda = 1/3$ as mentioned before, or the fin part of the clipped delta fin case as shown in Fig. 12.

4. Cruciform Slender Delta Fin-Body Combination.

Fig. 19a shows the spanwise lift distribution on three different cruciform fin-body combinations. In the case of the cruciform cant fin-body combination, a pair of horizontal fins is canted by three degrees so that it can rotate about the body axis (i.e., x-axis) to a negative direction in the sense of a commonly-accepted sign convention. The case of the fin only yielded the largest lift distribution as expected. The effect of the body can be seen clearly in this case also. The cant fin case showed the lowest lift distribution as expected (about this, for example, see Ref. (2)).

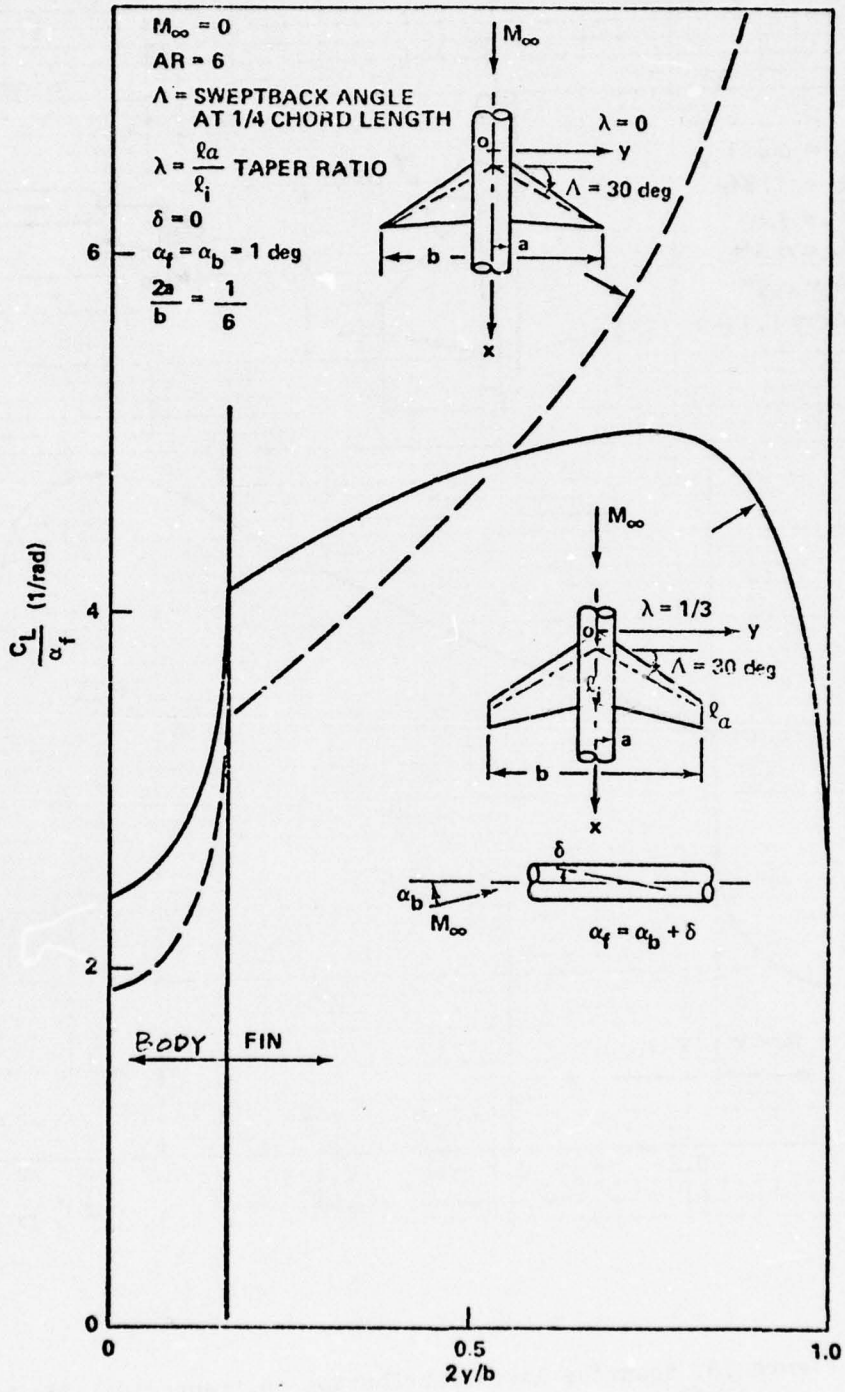

Figure 17. Recalculated spanwise lift distribution with different taper ratio fin given by Korner [3].

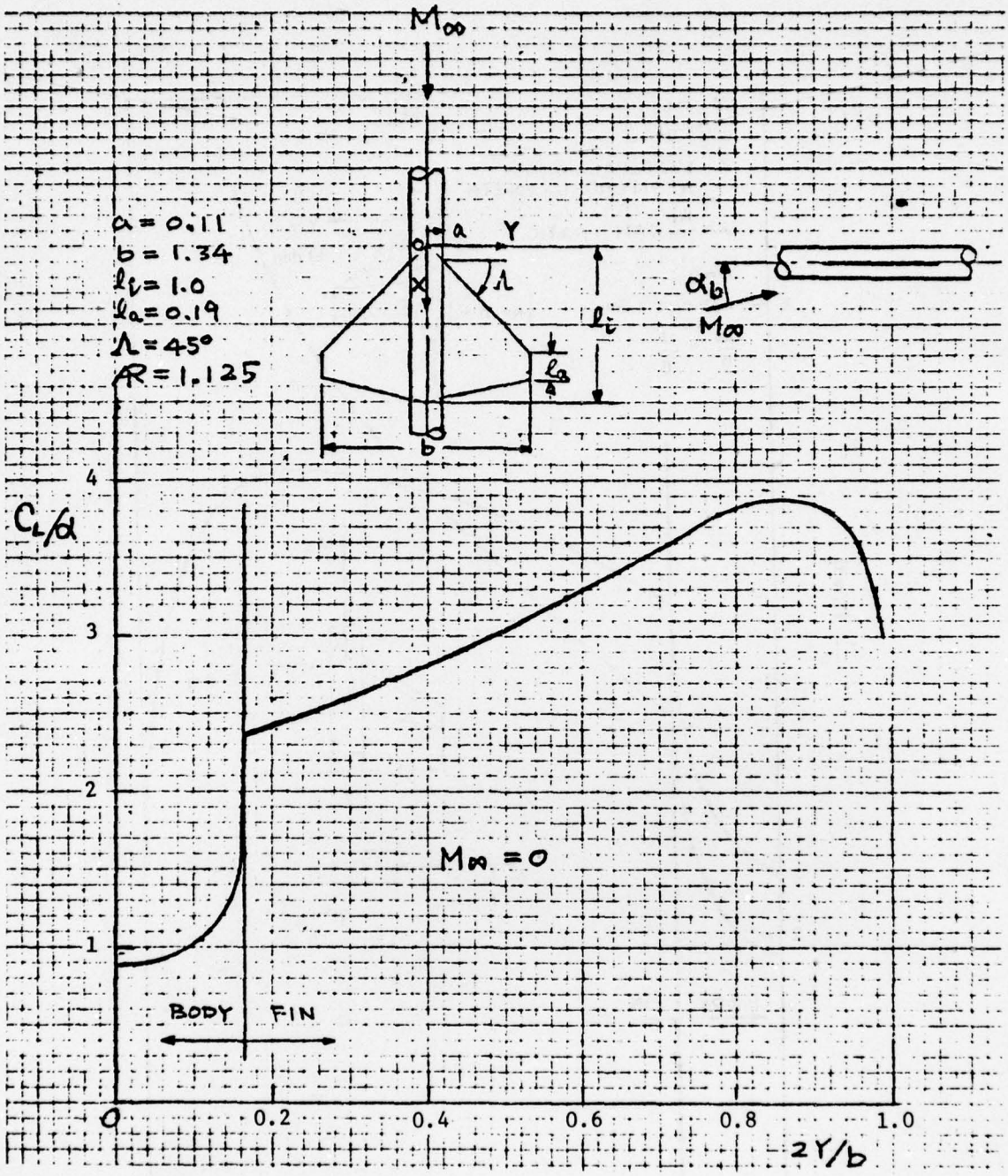

Figure 18. Spanwise lift distribution on trapezoidal fin-body combination.

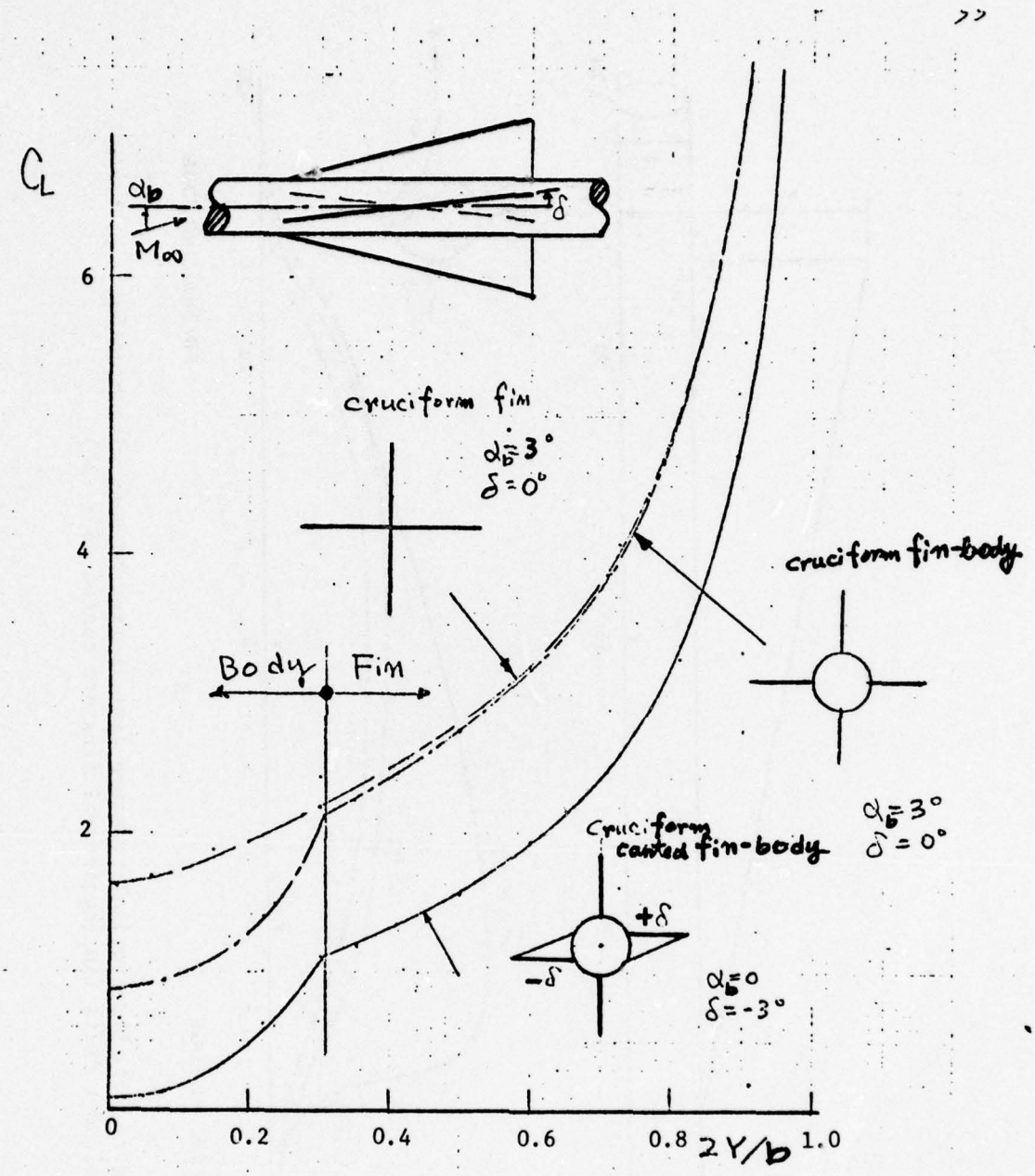

Figure 19a. Spanwise lift distribution on cruciform delta fin-body combination.

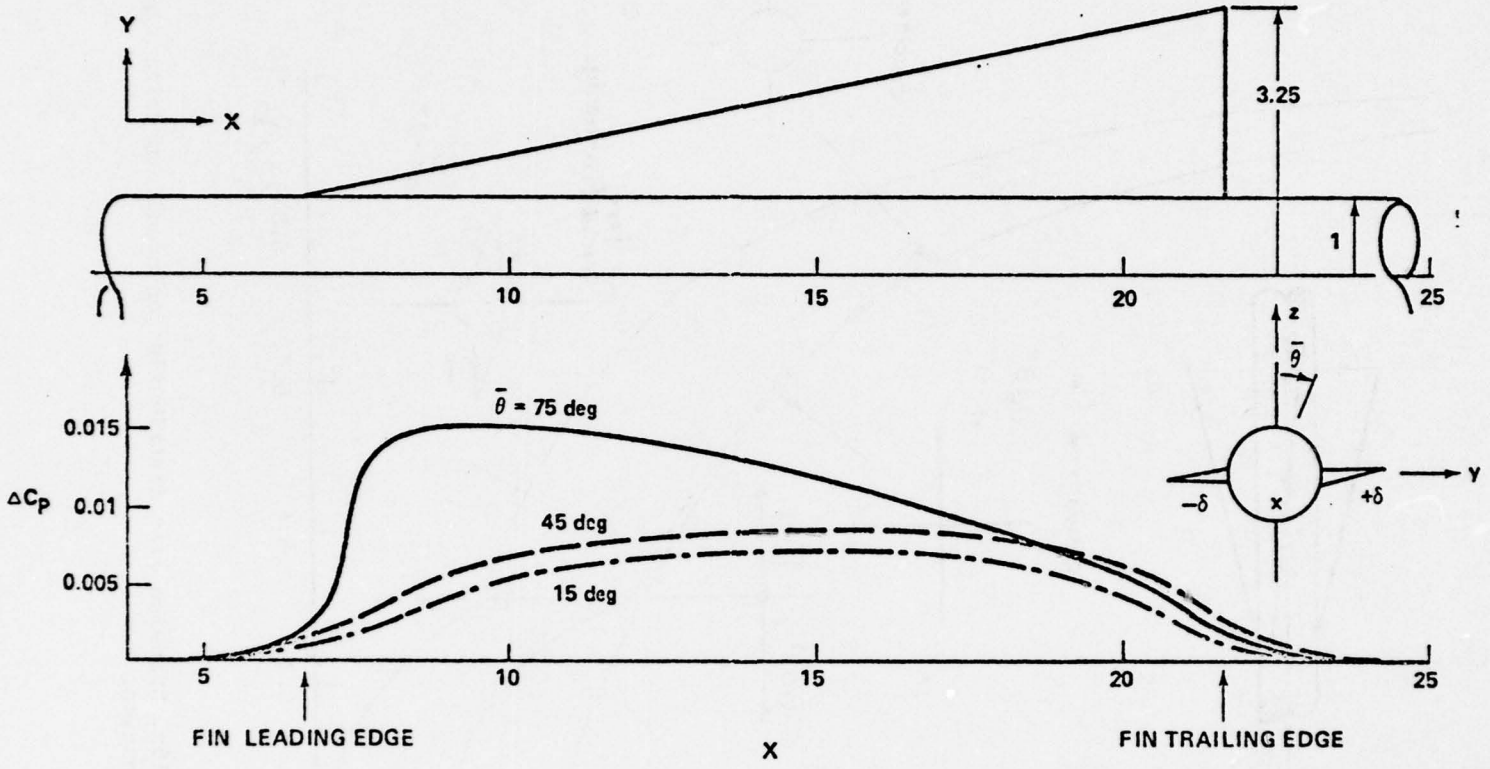

Figure 19b. Longitudinal pressure distribution on body with cruciform slender delta fin (horizontal fins are canted, $\delta = -3°$).

Fig. 19b shows the calculated longitudinal pressure distribution on the body. It should be noted that the rate of perturbation pressure change is very sharp at the leading and the trailing edges with lower magnitude pressure as compared with the large aspect ratio fin case (see Fig. 13b). This is expected because the fin is slender so the influence of the fin on the body should be small. This result agrees well with the concept of the slender-body theory which states that the aerodynamic disturbance influences only in the cross plane to the free stream (see Ref. (2)).

5. Discussions on Compressibility Effect on Fin-Body Combination.

The effect of the compressibility on a lift coefficient of a cruciform slender delta fin-body combination is shown in Fig. 20. (Only the angle of attack influence is considered here for the sake of discussion.) The fin area extended through the body as shown on a dotted line was used as a reference area for the lift coefficient computation. In general, as mentioned before, the Prandtl-Glauert rule resulted in an over correction for such a small aspect ratio fin configuration (see Fig. 20).

It is more appropriate to use the Goethert's rule to calculate the compressibility effect in a fin-body combination geometry. For a slender fin-body combination case, after using the Goethert rule correction, the result (see Fig. 20) agreed very well with the result computed by the slender body theory. In view of a wider range of Mach number applicability of the slender body theory, such an agreement is not totally surprising. In the same figure, a result by Nielsen's estimation (Ref. 11) is also included for a comparison. For a non-slender fin case, the result by using Goethert's rule correction is shown in Figs. 21 and 22.

Fig. 23 shows the lift coefficient varying with the freestream Mach number on the non-slender rectangular fin-body combination. The configuration is given in Fig. 22. As it

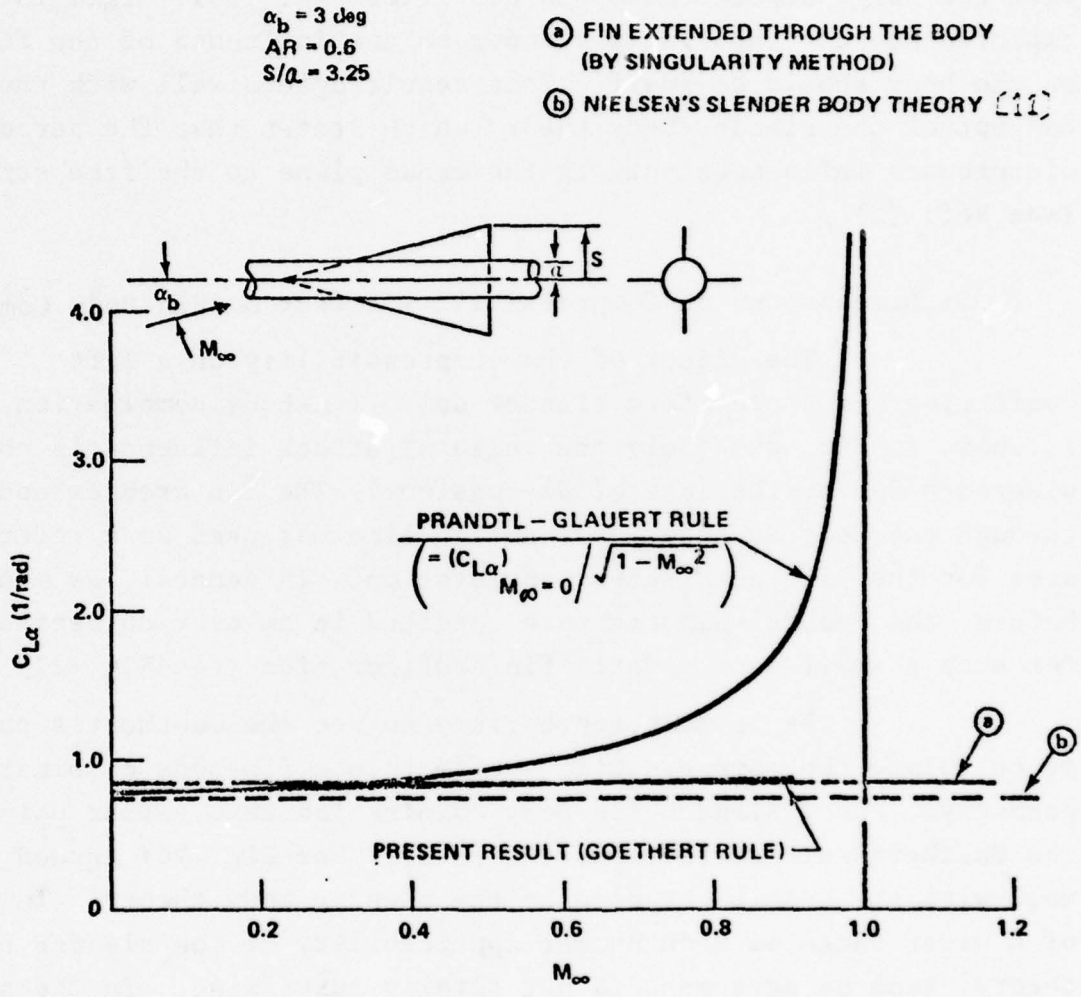

Figure 20. Comparison of subsonic similarity rules for cruciform slender delta fin-body combination at angle of incidence (also includes result from slender body theory).

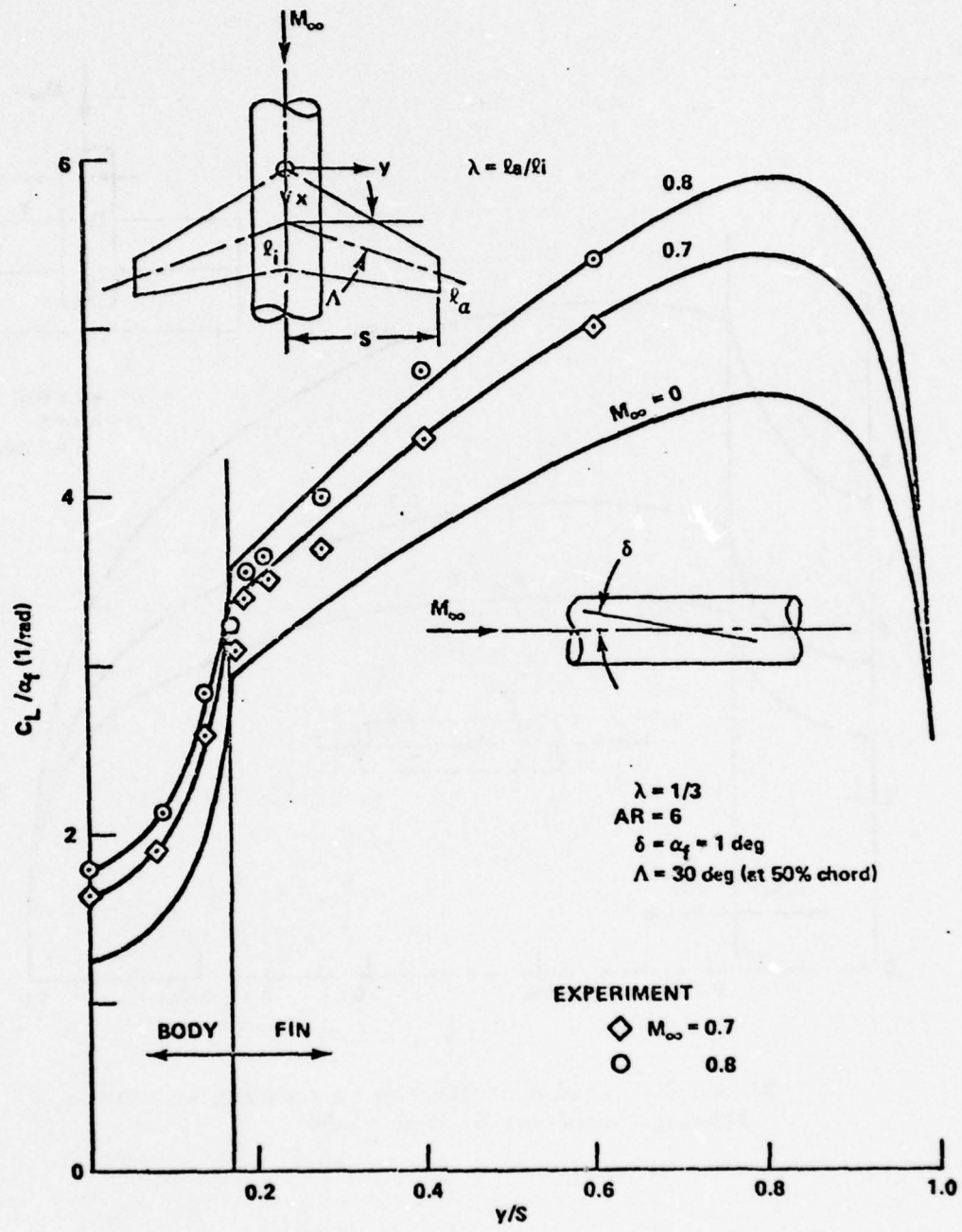

Figure 21. Local lift coefficient on fin body junction showing effect of Mach number change, -30° swept fin [43].

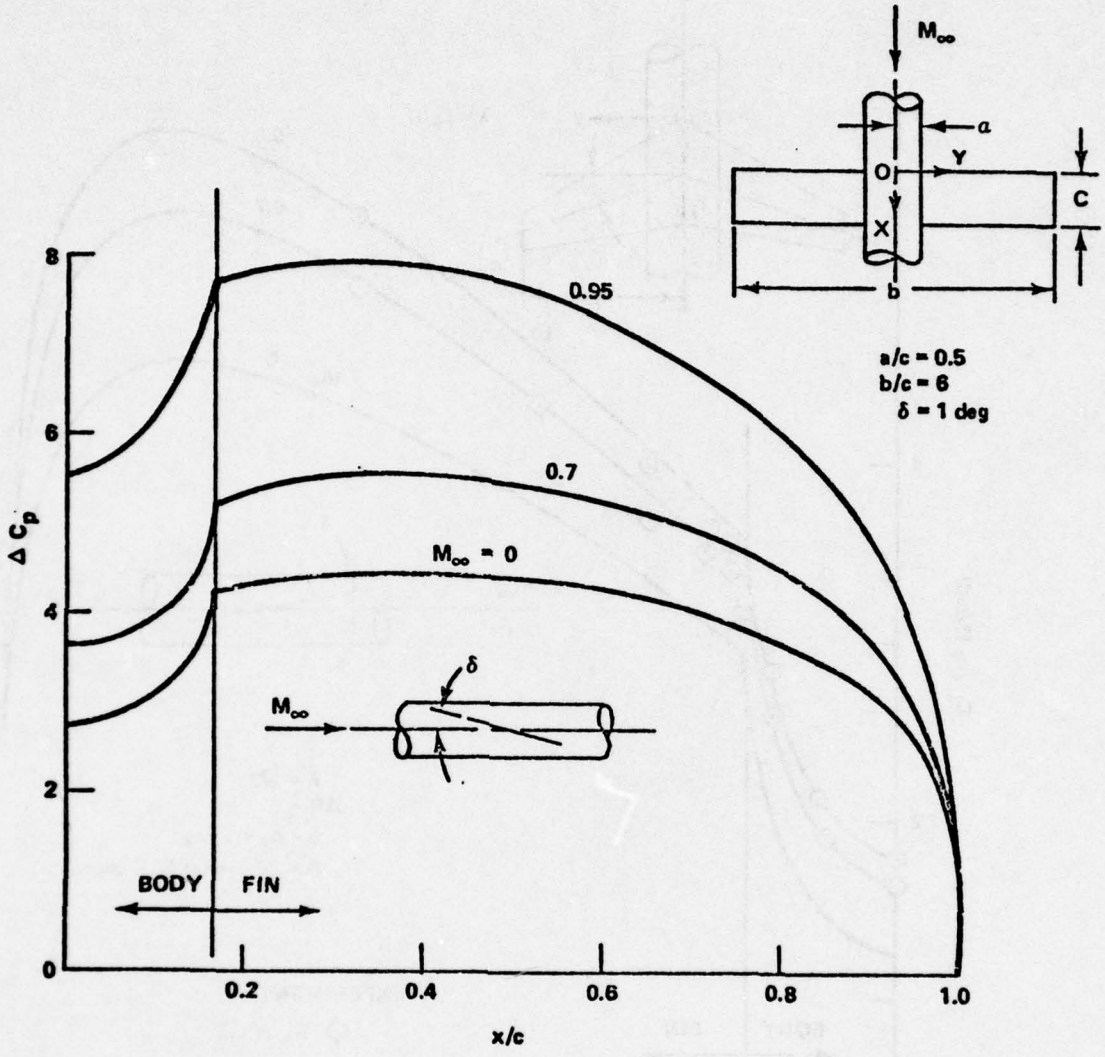

Figure 22. Load distribution on rectangular wing showing the effect of Mach number.

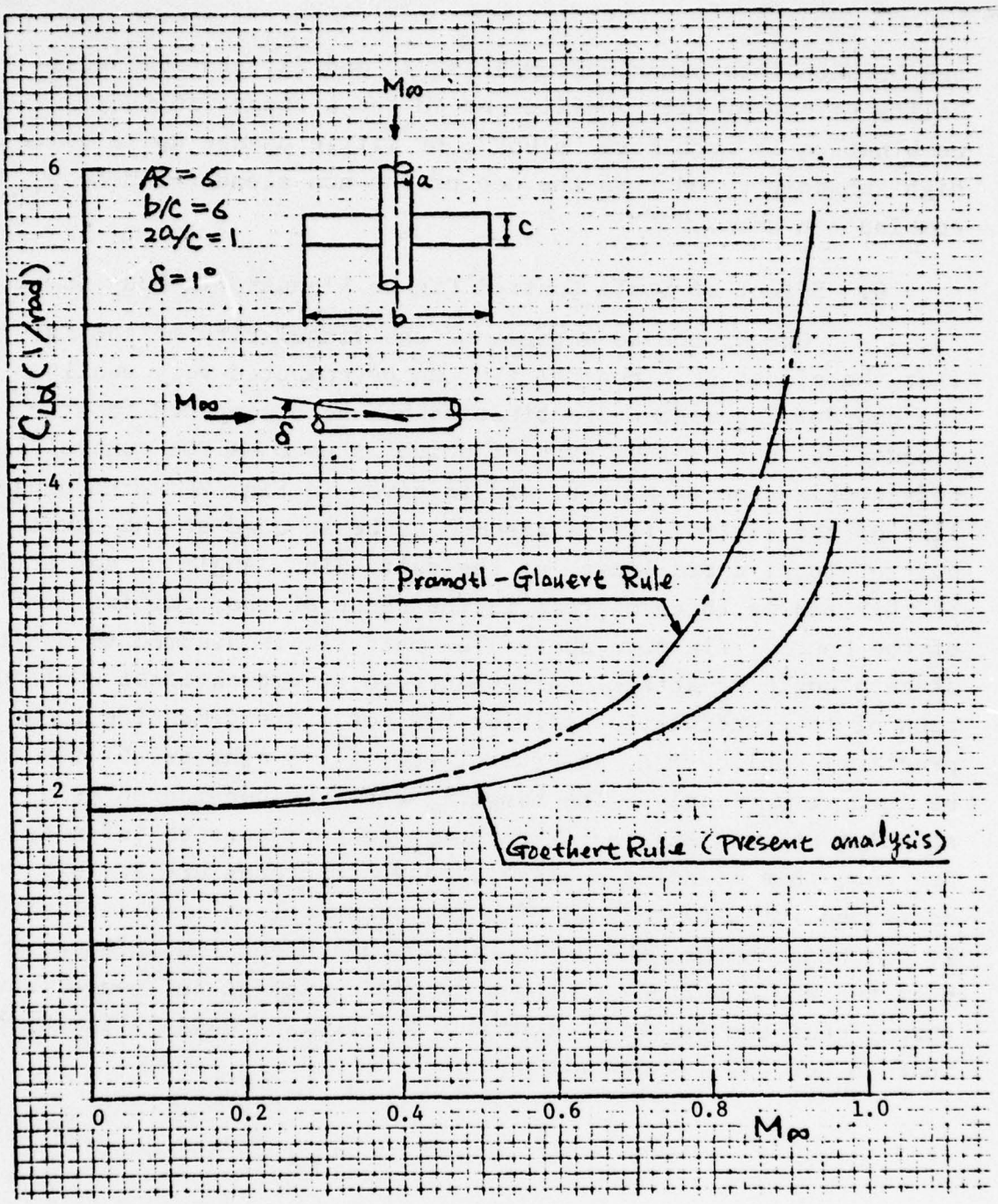

Figure 23. Comparison of subsonic similarity rules for non-slender rectangular fin-body combination.

can be seen very clearly from Figs. 20 and 23, the compressibility effect of lift coefficient on the slender fin-body combination is much more "blunt", or little change up to quite high subsonic speed than the one of the non-slender fin-body combination case.

6. Effect of Small Control Fin on Slender Fin-Body Combination.

One of the advantages of the singularity method is that the effect of a control fin can be computed very easily. The chordwise pressure distribution has been computed for the slender delta fin- (one part of which is used as the control fin) body combination at $M_\infty = 0$, and is given in Fig. 24. The hinge line of the control fin is assumed to be located at the three quarter local chord length of the delta fin. Angle of deflection of this fin is three degrees in the sense of the trailing edge of the control fin downwards. The main fin is assumed to position at zero angle of attack. Although such a computational configuration of the control fin position has not a great meaning in a practical application, yet the effect of its controllability can be seen very clearly. The hinge line can be considered as a singular point. And thus the local pressure goes to infinity. However, this is not a realistic case. The pressure at this point cannot be infinity because of the viscous effect in a real situation. It can be seen that the deflection of a control fin influences over the whole surface of the main fin. Such an influence is very strong near the fin tip. (Compare the present calculation with that in Ref. 9, for example.)

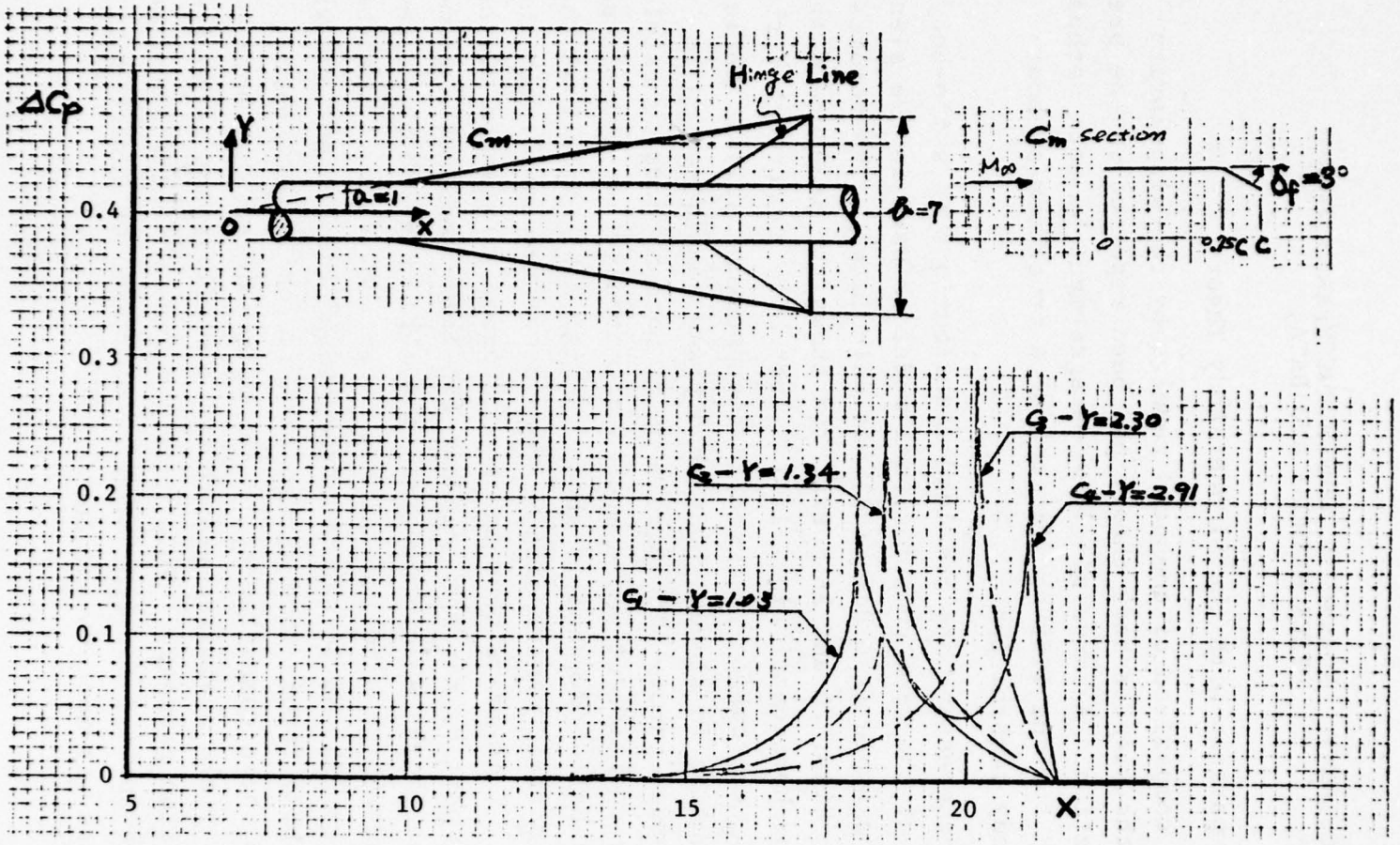

Figure 24. Chordwise pressure distribution due to small control fin ($M_\infty = 0$, $\delta_f = 3°$).

SECTION V. KOERNER'S APPROACH COMPARED WITH OTHER METHODS AND DATA.

1. Comparison with the Slender-Body Theory.

A comparison of computed results by the singularity method and the slender-body theory had been reported in the previous subsection. A surprisingly good agreement by both methods was obtained for the lift coefficient of a cruciform slender delta fin-body combination.

The pressure and the load distributions on a fin-body combination of the same computational model as used in the slender body theory example (see Ref. (2)) was calculated. The results are shown in Figs. 25 and 26. Fig. 25a shows the pressure distribution on one horizontal fin. It is worthwhile to note that the linearized C_p expression was used in the present analysis while the C_p expression in slender-body theory was considered up to the second order terms. The agreement of both methods is excellent. The pressure coefficient was computed azimuthally, at the six positions on the half body, and is shown in Fig. 25b. Note that the difference in the C_p expression is more sensitive on the fin than on the body. This means that the second order expression of the C_p is more important for such slender fin-body combination geometry even though its absolute value is small. Fig. 26 shows the load distribution on a horizontal and a vertical fin. It can be seen from Figs. 25 and 26 that the results of the present analysis and slender-body theory have agreed satisfactorily with each other. From these comparisons, it can be concluded that both methods will yield a similar result for a small aspect ratio fin-body combination geometry. This merely proves that the singularity method can be applied for fins with a wide range of aspect ratios and, therefore, is more versatile.

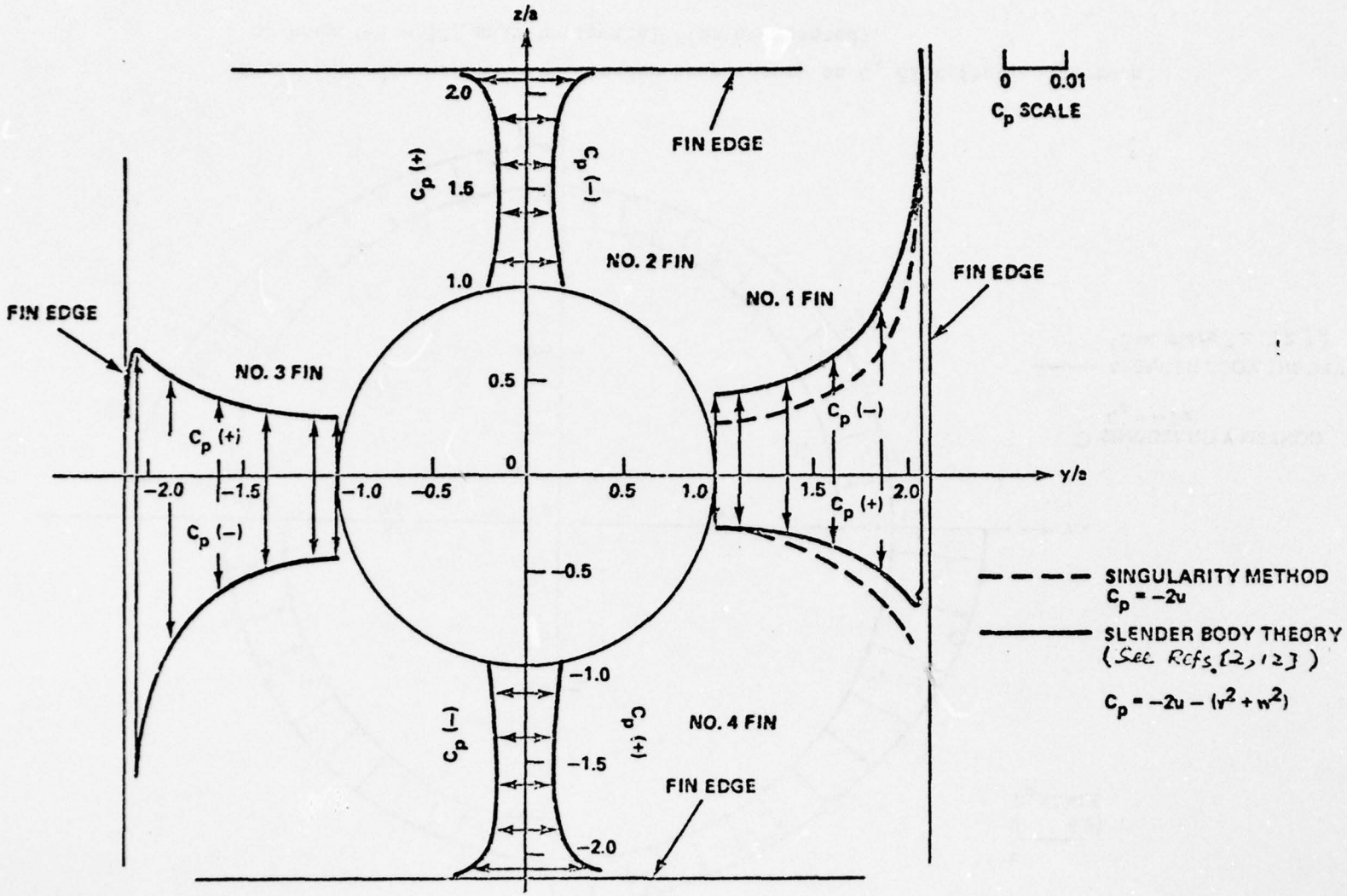

Figure 25a. Comparison with slender body theory, C_p distribution pattern. on fins ($-\delta = 3°$, only horizontal fins are canted).

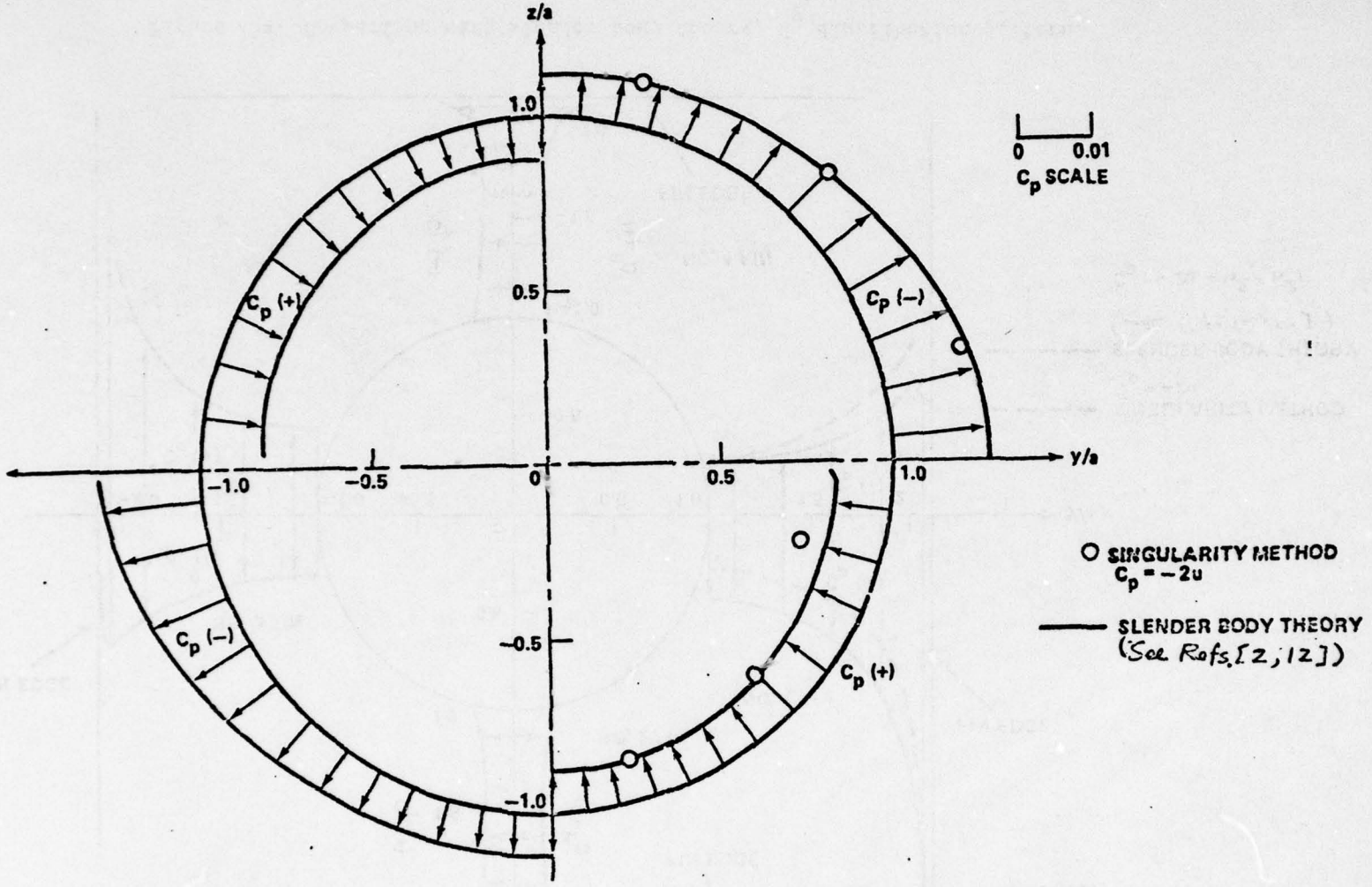

Figure 25b. Comparison with slender body theory on C_p distribution pattern on body ($-\delta = 3°$, only horizontal fins are canted).

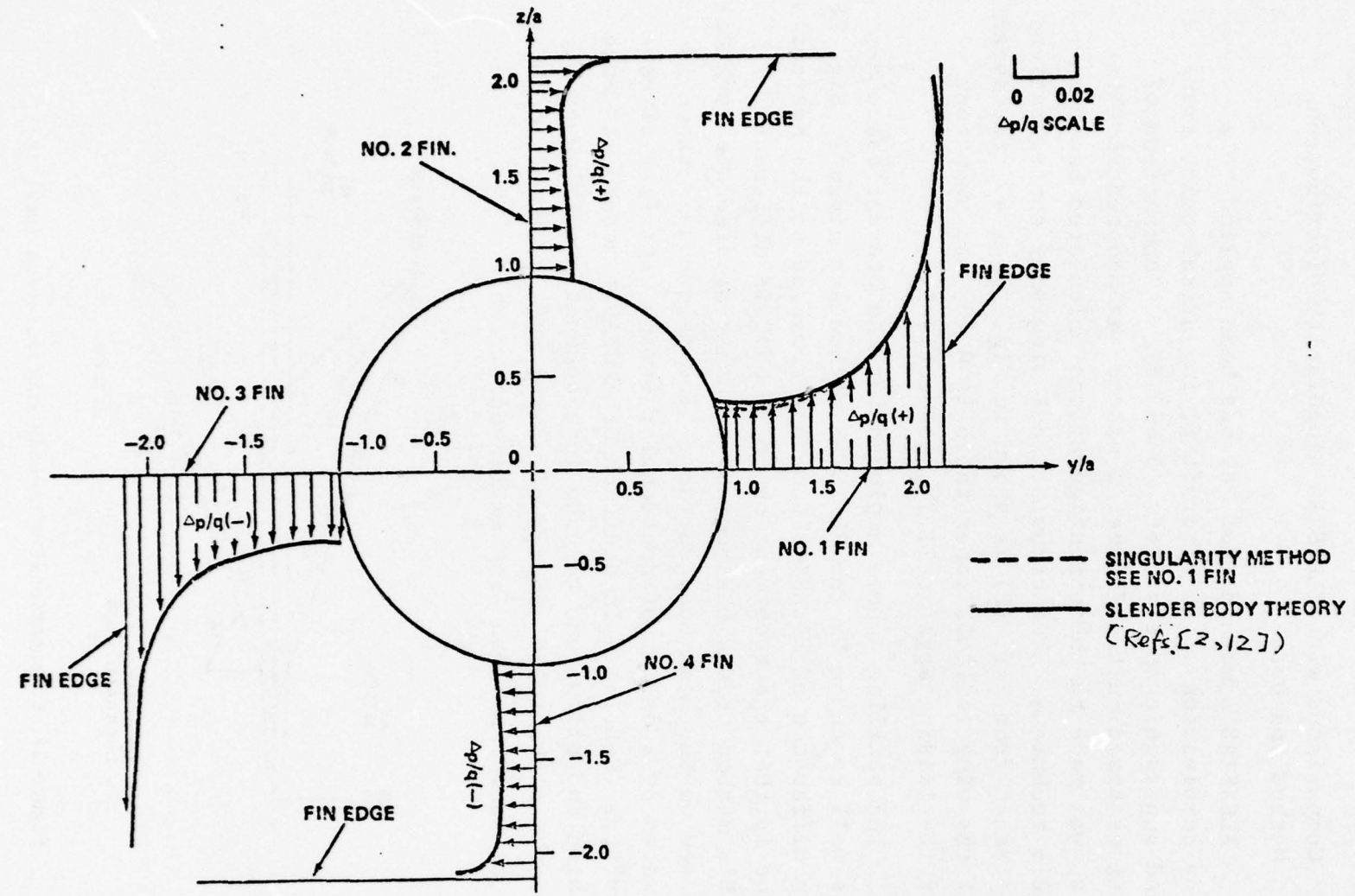

Figure 26. Comparison with slender body theory of load distribution pattern on fins ($-\delta = 3°$, only horizontal fins are canted).

2. Comparisons with FLEXSTAB Singularity Distribution Method and Data.

FLEXSTAB's method (Ref. 8) has been applied to a wing-body combination of an aircraft flying at subsonic, transonic and supersonic speeds (Refs. 5 and 8). A comparison of computations based on the Koerner's scheme, as adapted in this analysis, was made to those configurations calculated based on FLEXSTAB's technique. The computational wing-body configuration which is taken from Ref. (8) is shown in Fig. 27, i.e., the aspect ratio of the wing is 1.65, taper ratio is 0.10, and sweptback angle of the leading edge is 71.2°, respectively.

The paneling scheme employed for the present calculations as well as those by the FLEXSTAB method are given in Fig. 28. The main difference of FLEXSTAB's method compared to the Koerner's technique is that the treatment on the "body" is different. FLEXSTAB's method treats the body by a number of discrete vortices distributed on the mean body surface. The main body surface is approximated by a number of rectangular strips with free streamwise surfaces (Ref. 5). In addition, FLEXSTAB's method was more complicated and allows one to take into account the thickness, the camber and the twist effects of a wing by a distribution of additional source-sink and vortex singularities.

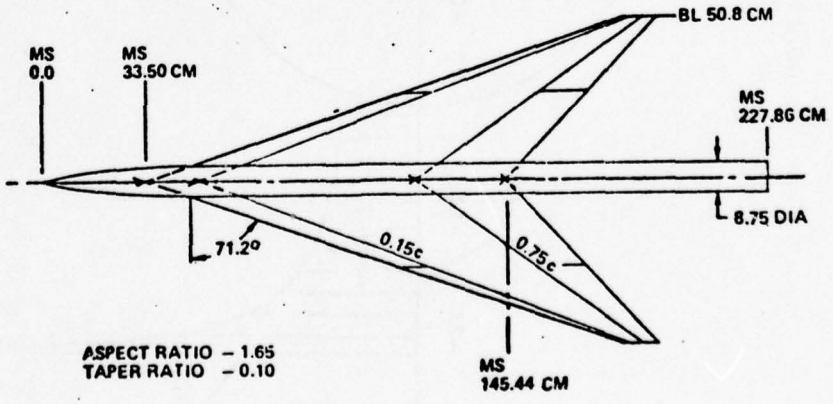

Figure 27. Computational wing-body configuration (Red. [8]).

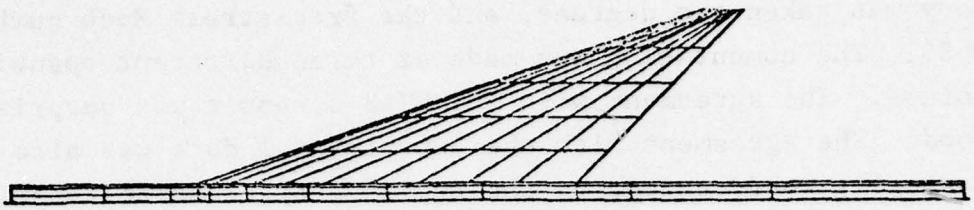

(a) PRESENT PANELING SCHEME (FOR ZERO DEFLECTED FLAP)

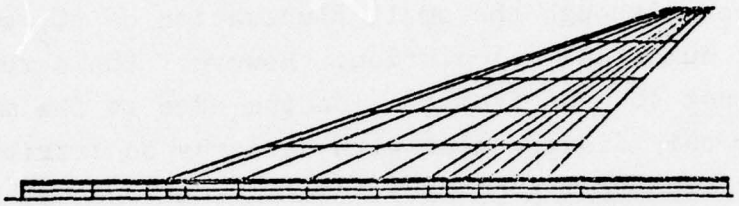

(b) PRESENT PANELING SCHEME (FOR A DEFLECTED FLAP)

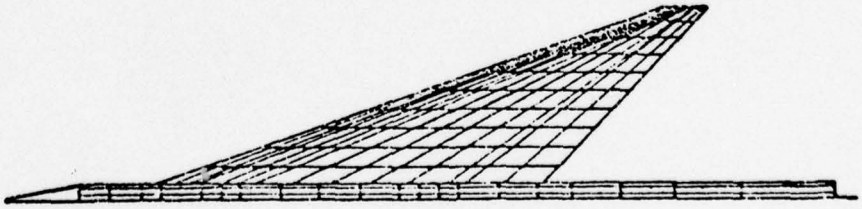

(c) FLEXSTAB PANELING SCHEME. (Ref. 8)

Figure 28. Paneling schemes.

2.1 Effect of Angles of Attack on Chordwise Pressure Distribution.

The calculated chordwise pressure distribution on the wing is shown in Fig. 29, in which the angle of incidence of the body was taken two degrees, and the free-stream Mach number was 0.85. The computation was made at three different spanwise points. The agreement with FLEXSTAB's result was surprisingly good. The agreement with the experimental data was also satisfactorily good, except in the region very close to the wing leading edge, where a sudden pressure drop can be seen because of the local flow separation. The case of the angle of incidence of eight degrees is shown in Fig. 30. The agreement with FLEXSTAB's method was very good in this case also. The agreement with the experimental data was still very good at the region very close to the wing root although the small fluctuation of ΔC_p was caused by the present numerical calculation. However, the agreement with data was not so good from the leading edge to the mid-chord. The reason for this disagreement with data may be attributed to the flow separation from the sharp leading edge because of a considerably higher angle of incidence. A further study on such a situation is needed.

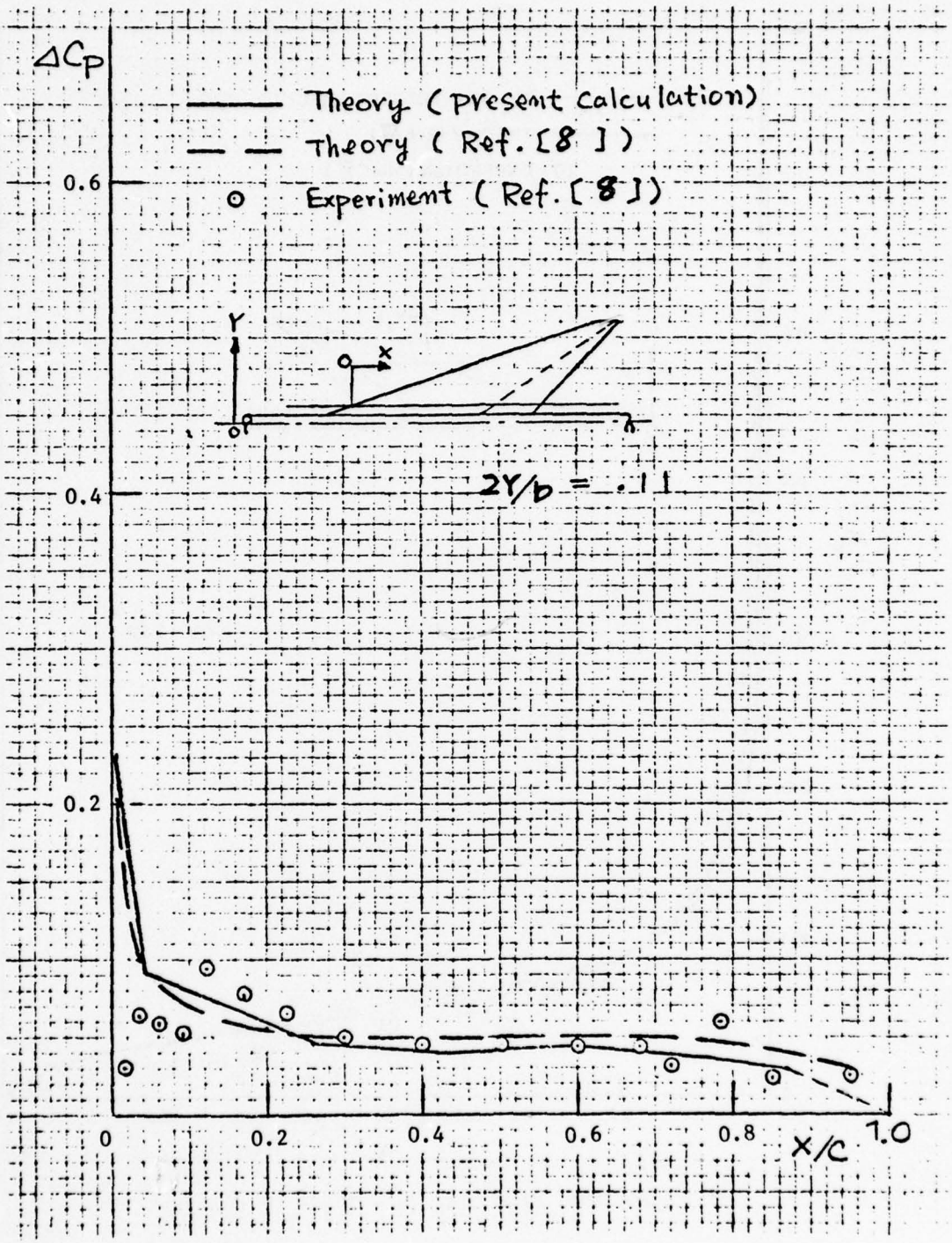

Figure 29a. Flat wing ($\alpha = 2°$, $M_\infty = 0.85$).

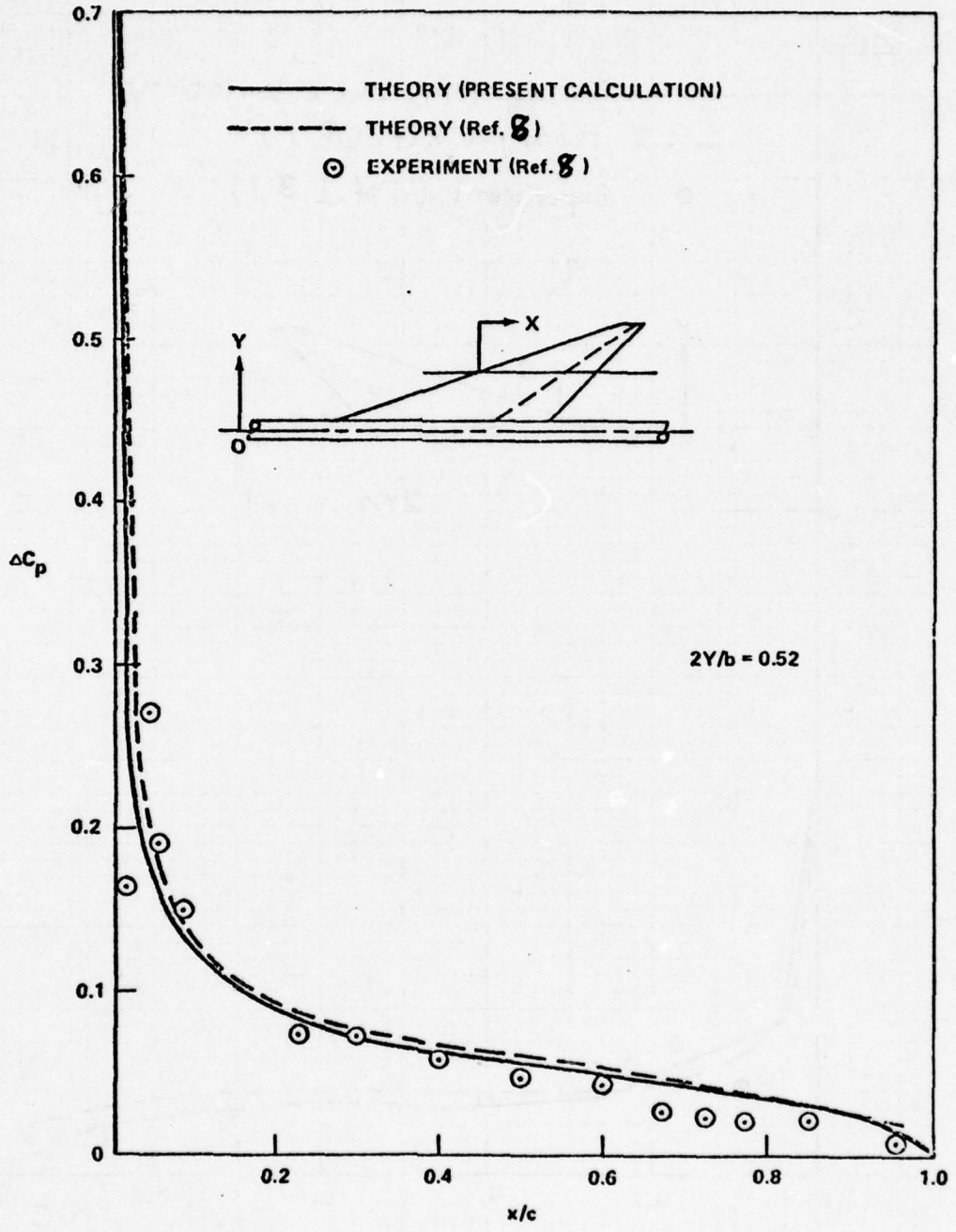

Figure 29b. Flat wing ($\alpha = 2°$, $M_\infty = 0.85$).

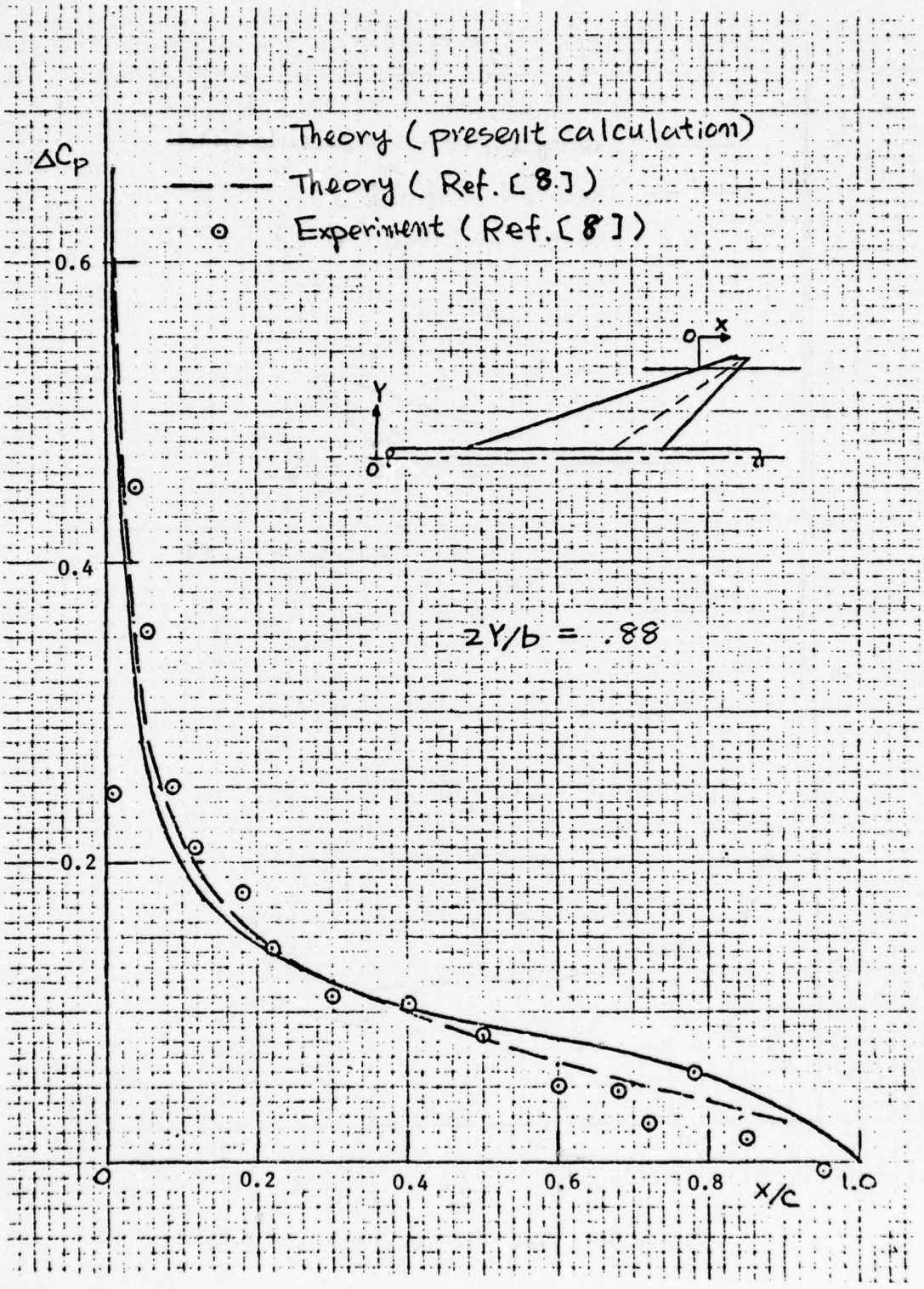

Figure 29c. Flat wing ($\alpha = 2°$, $M_\infty = 0.85$).

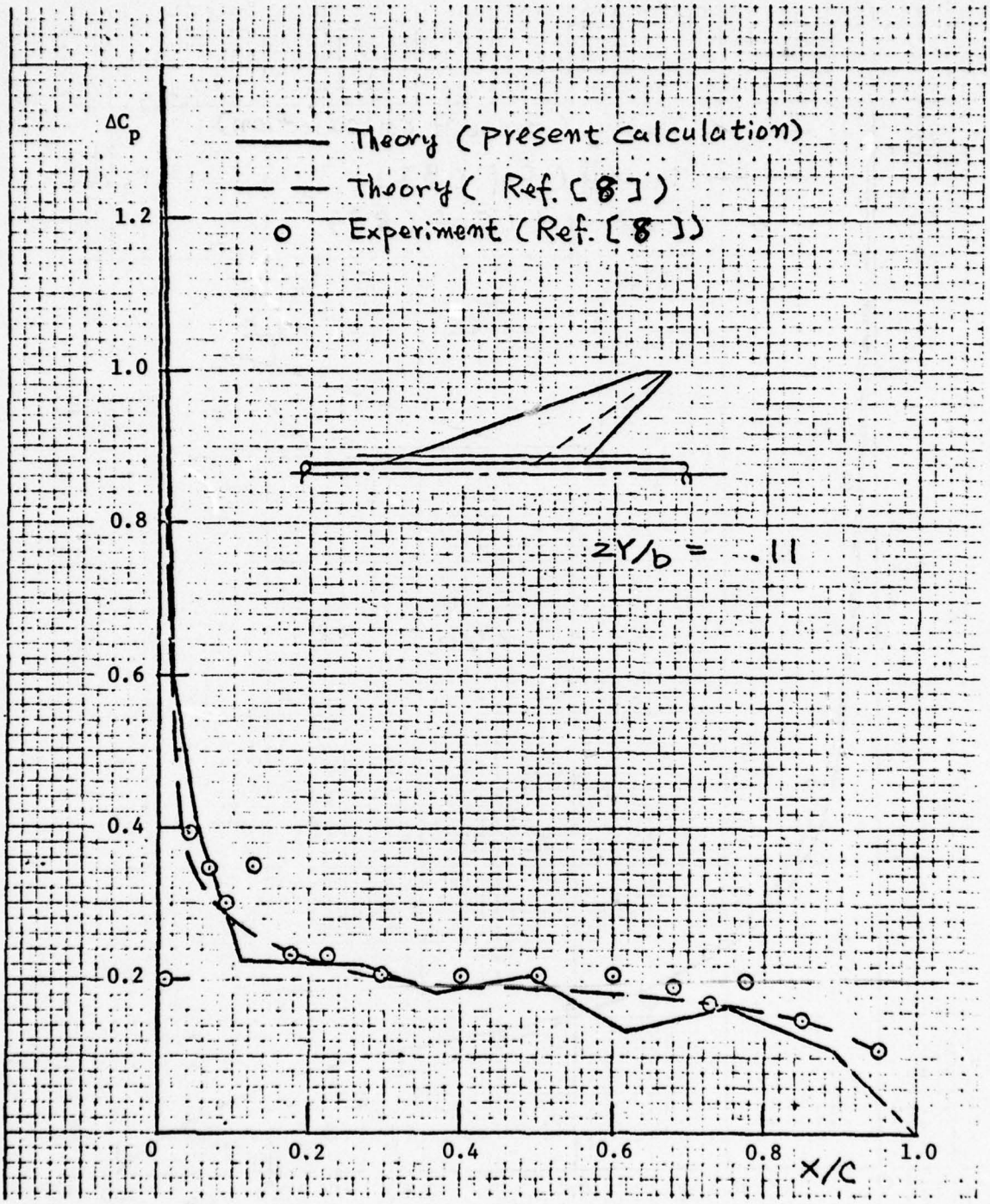

Figure 30a. Flat Plate ($\alpha = 8°$, $M_\infty = 0.85$).

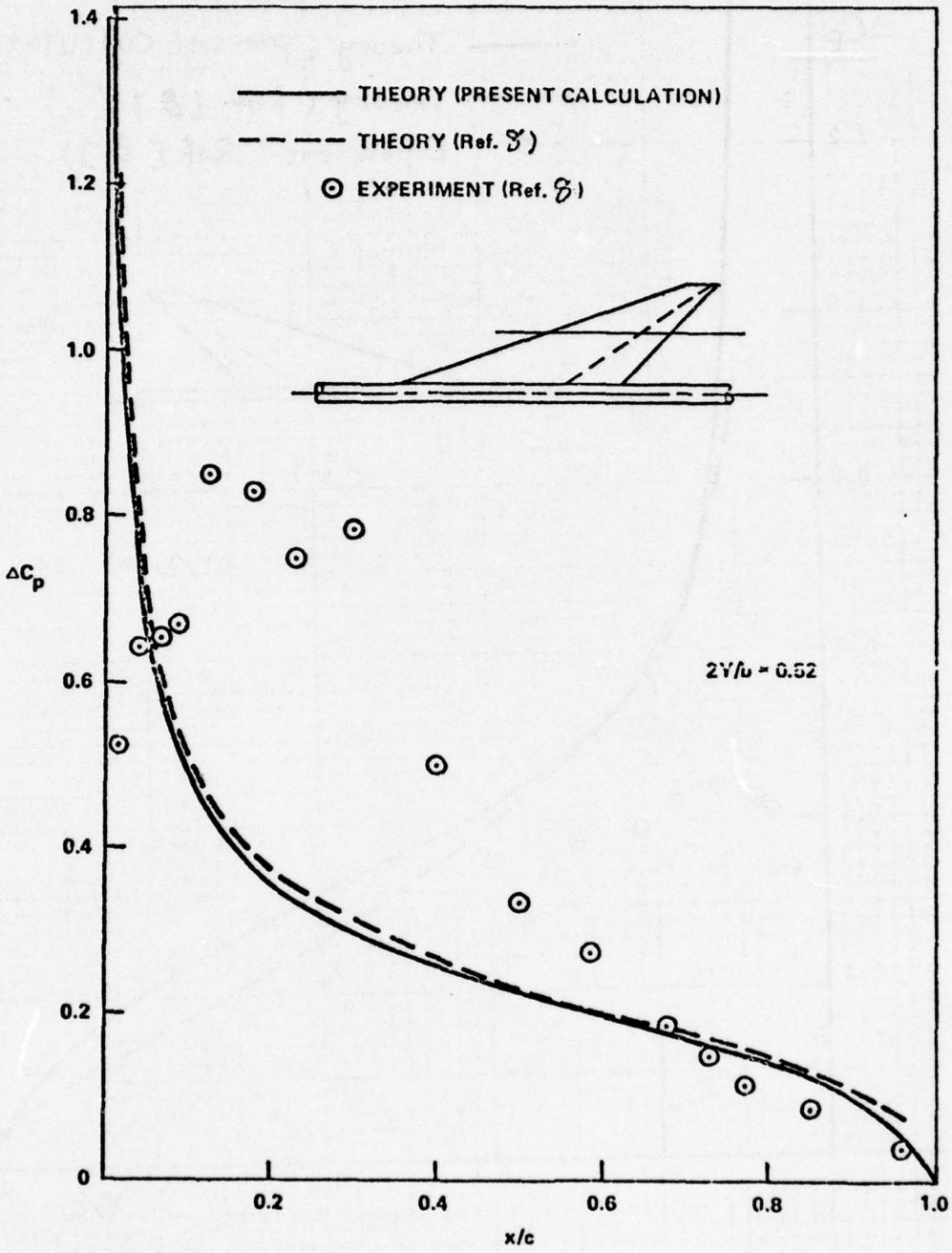

Figure 30b. Flat wing ($\alpha = 8°$, $M_\infty = 0.85$).

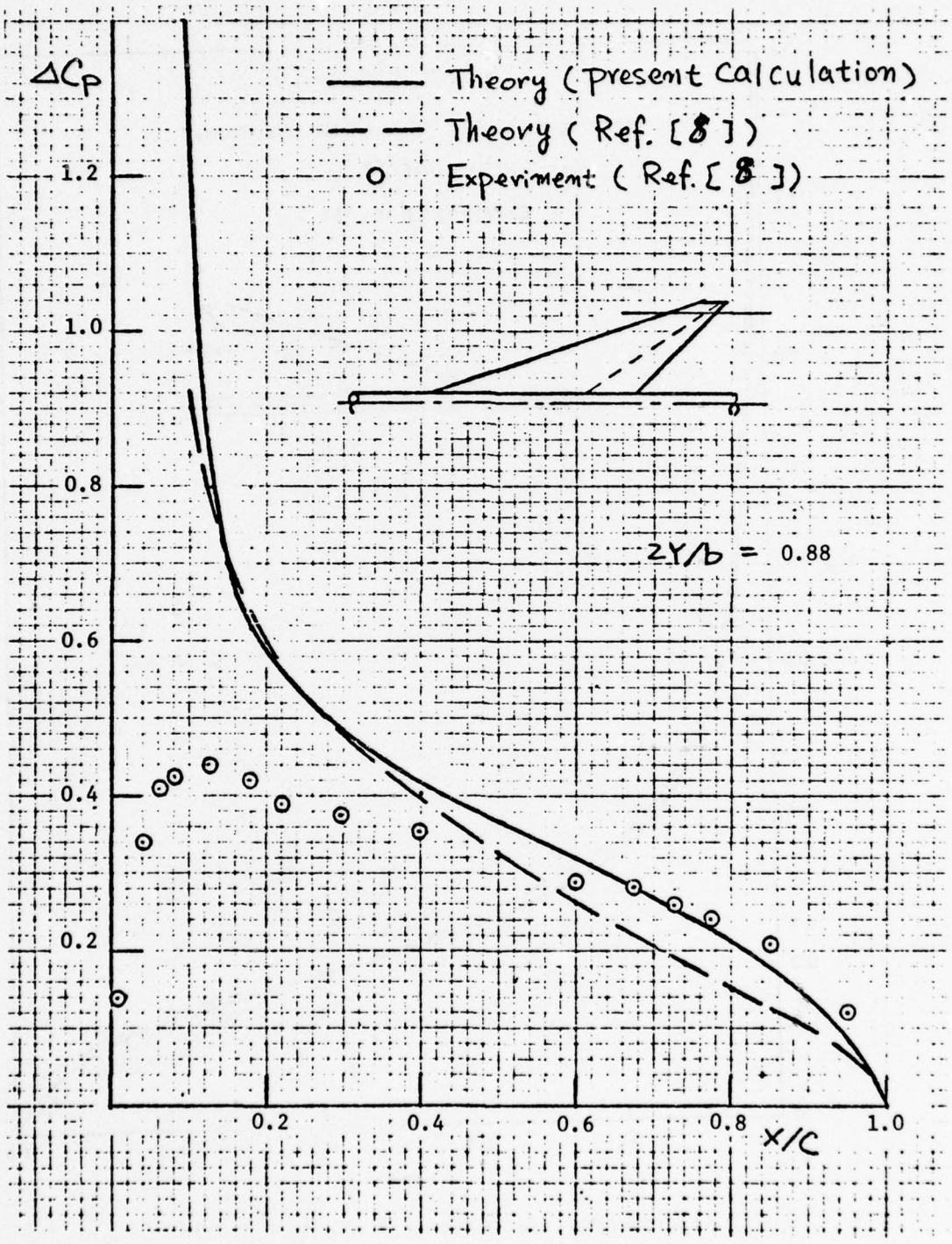

Figure 30c. Flat wing ($\alpha = 8°$, $M_\infty = 0.85$).

2.2 Flap Effect on Chordwise Pressure Distribution.

A further comparison with the FLEXSTAB method was made on the effect of the flap of the wing. The calculated chordwise pressure distributions, based on both methods, are given in Figs. 31 to 33. In these cases, it is assumed that the wing has zero angle of attack and the flap angle is 8.3^{o}. The following two examples (Figs. 31 and 32) show the chordwise C_p distribution on the upper and the lower surfaces of a wing and deflected flap at $M_\infty = 0.4$ and 0.85, respectively. The calculated position is near the mid span. $\Delta C_p/2$ was taken for C_p in the present calculation (see Eq. 16). Fig. 31 shows the chordwise C_p distribution at $M_\infty = 0.4$. No correction about the round leading edge of a flat wing was made in the present analysis. Therefore, the C_p close to the leading edge of the wing has resulted in a rather poor agreement with those of the FLEXSTAB and experimental data. Except for this region of the wing, the agreement of the C_p distribution calculated by the present analysis compared favorably with data. The poor agreement with data near the flap hinge line is attributed to the local flow separation on the wing because of a considerably higher flap angle.

Fig. 32 shows the chordwise C_p distribution at $M_\infty = 0.85$. In this case, the values of C_p from Ref. (8) were replotted for eliminating the influence of the round leading edge of the wing at $\delta_F = 0^{o}$ as shown in this figure. The agreement of the present calculation with that of the FLEXSTAB was good, in general, over the whole surface of the wing, and with the experimental data, except the regions very close to the wing leading edge and the flap hinge line. The poor agreement with data near the flap hinge line is a result from the same reason as mentioned before. The variation of C_p with the free stream Mach number was very small in this type of body configuration.

The calculated chordwise pressure (ΔC_p) distribution at three different spanwise positions at $M_\infty = 0.85$ is shown in Fig. 33.

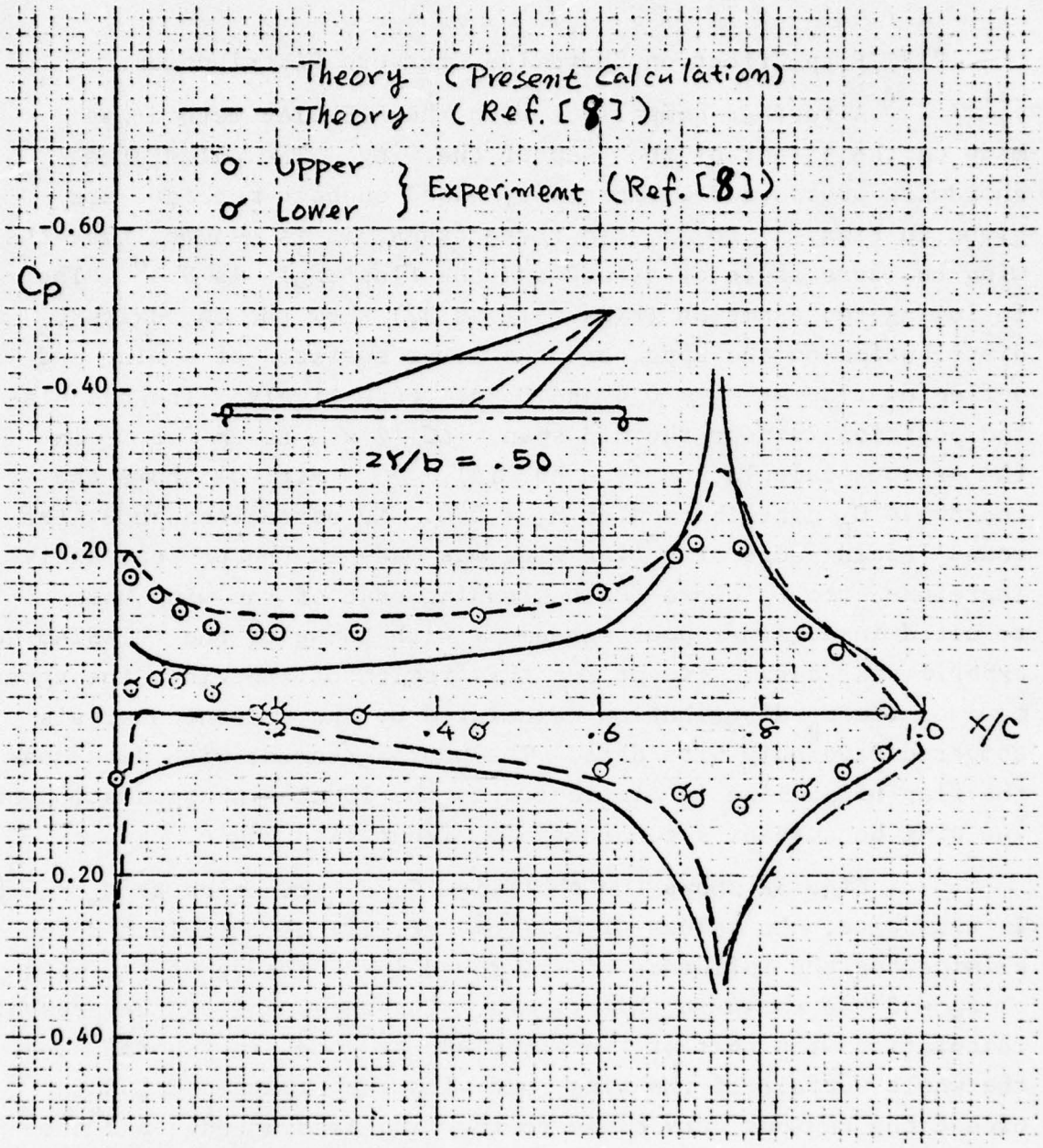

Figure 31. Surface pressure distribution of flat wing (trailing-edge $\delta_F = 8.3°$, $\alpha = 0$, $M_\infty = 0.4$)

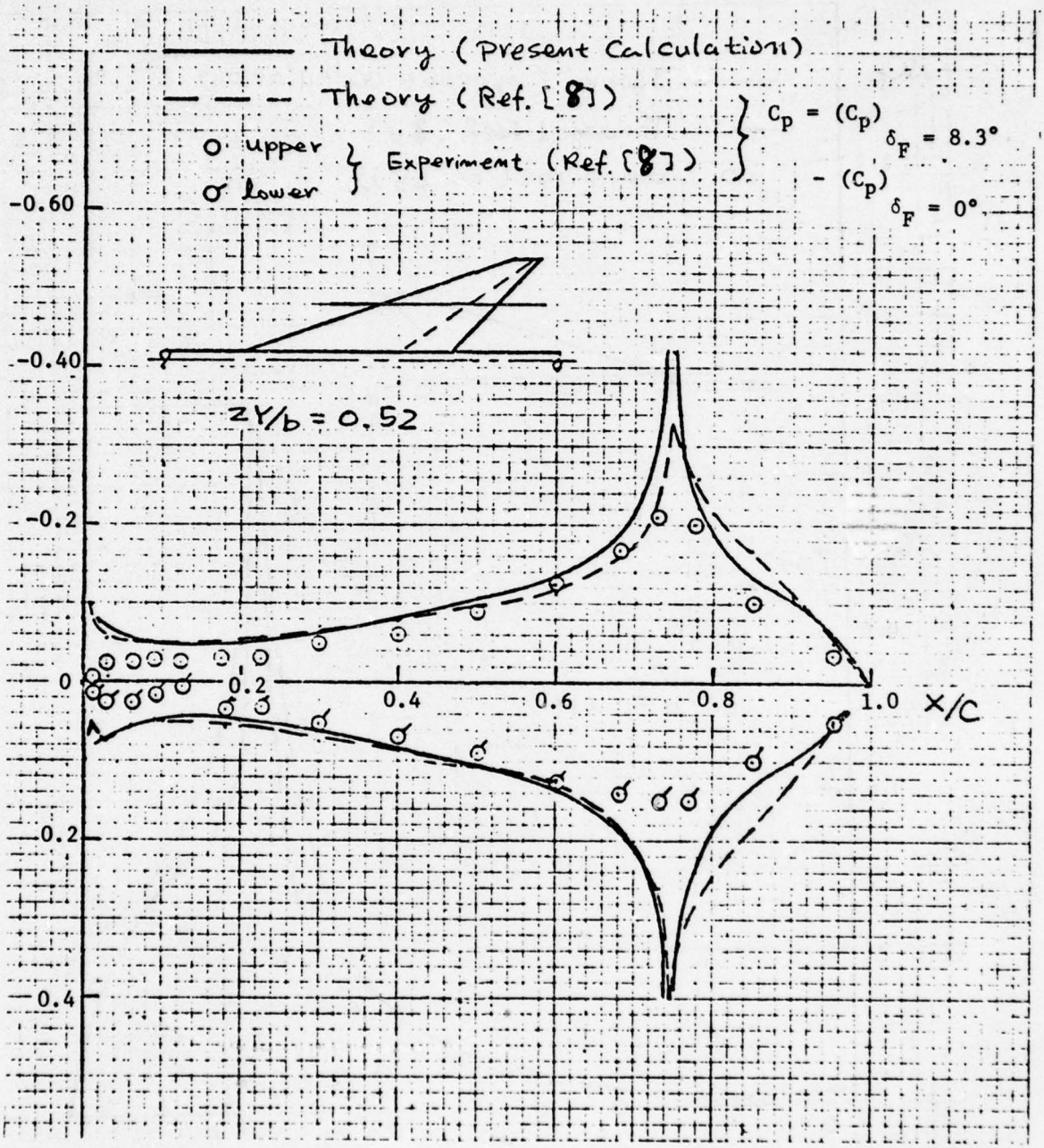

Figure 32. Surface pressure distribution of flat wing (trailing-edge $\delta_F = 8.3°$, $\alpha = 0$, $M_\infty = 0.85$).

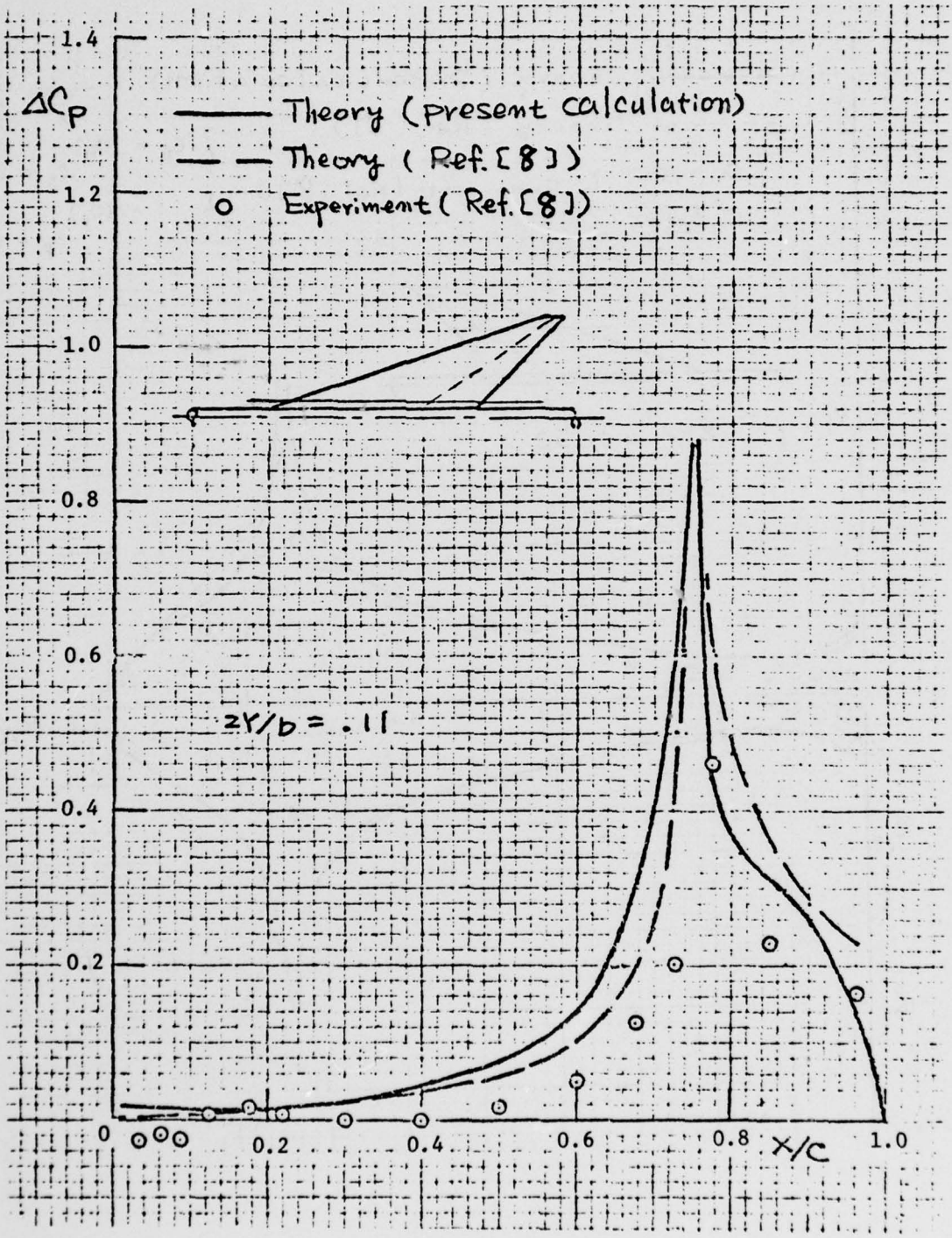

Figure 33a. Flat wing (trailing edge $\delta_F = 8.3°$, $\alpha = 0$, $M_\infty = 0.85$).

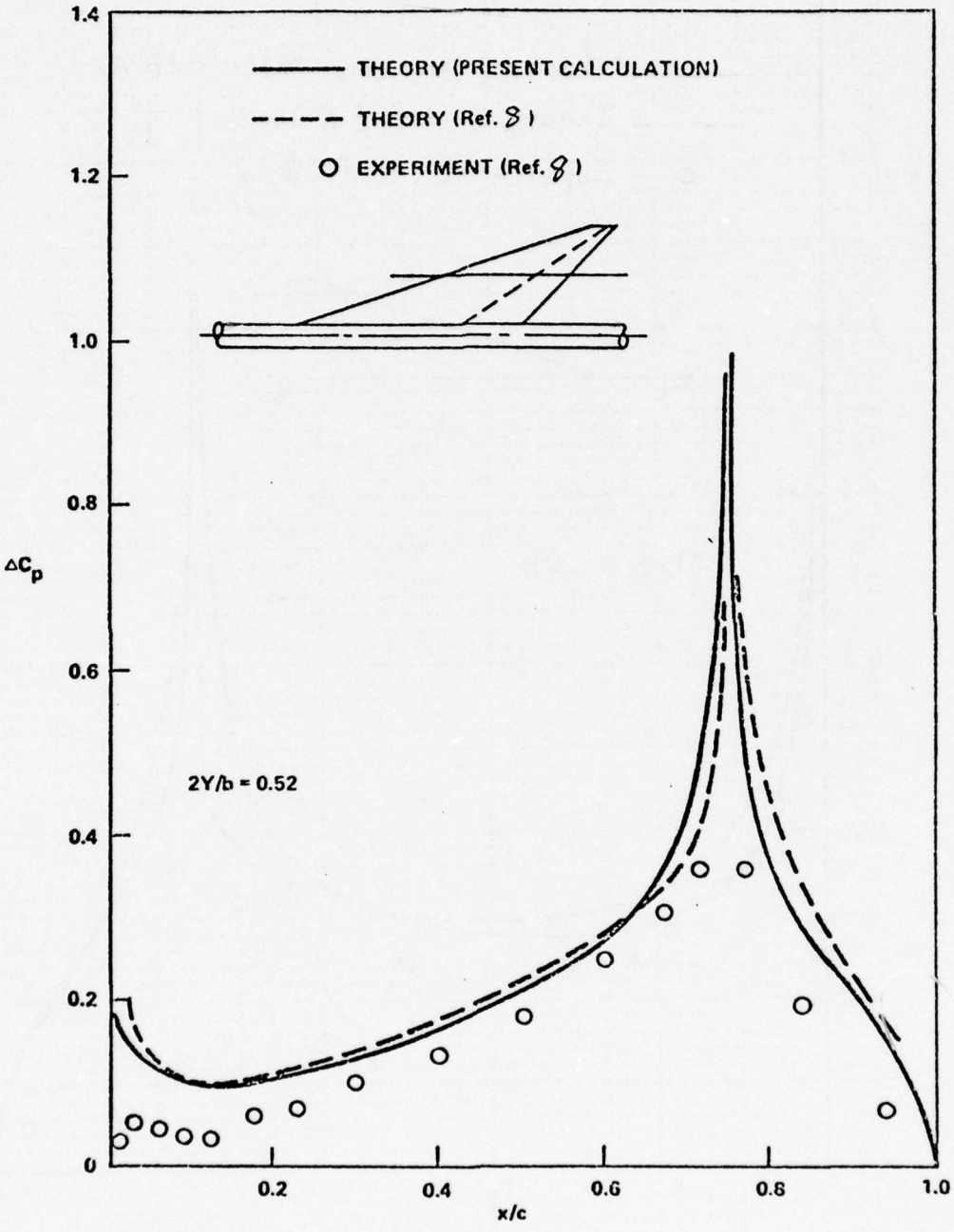

Figure 33b. Flat wing with deflected flap (trailing edge $\delta_F = 8.3°$, $\alpha = 0°$, $M_\infty = 0.85$).

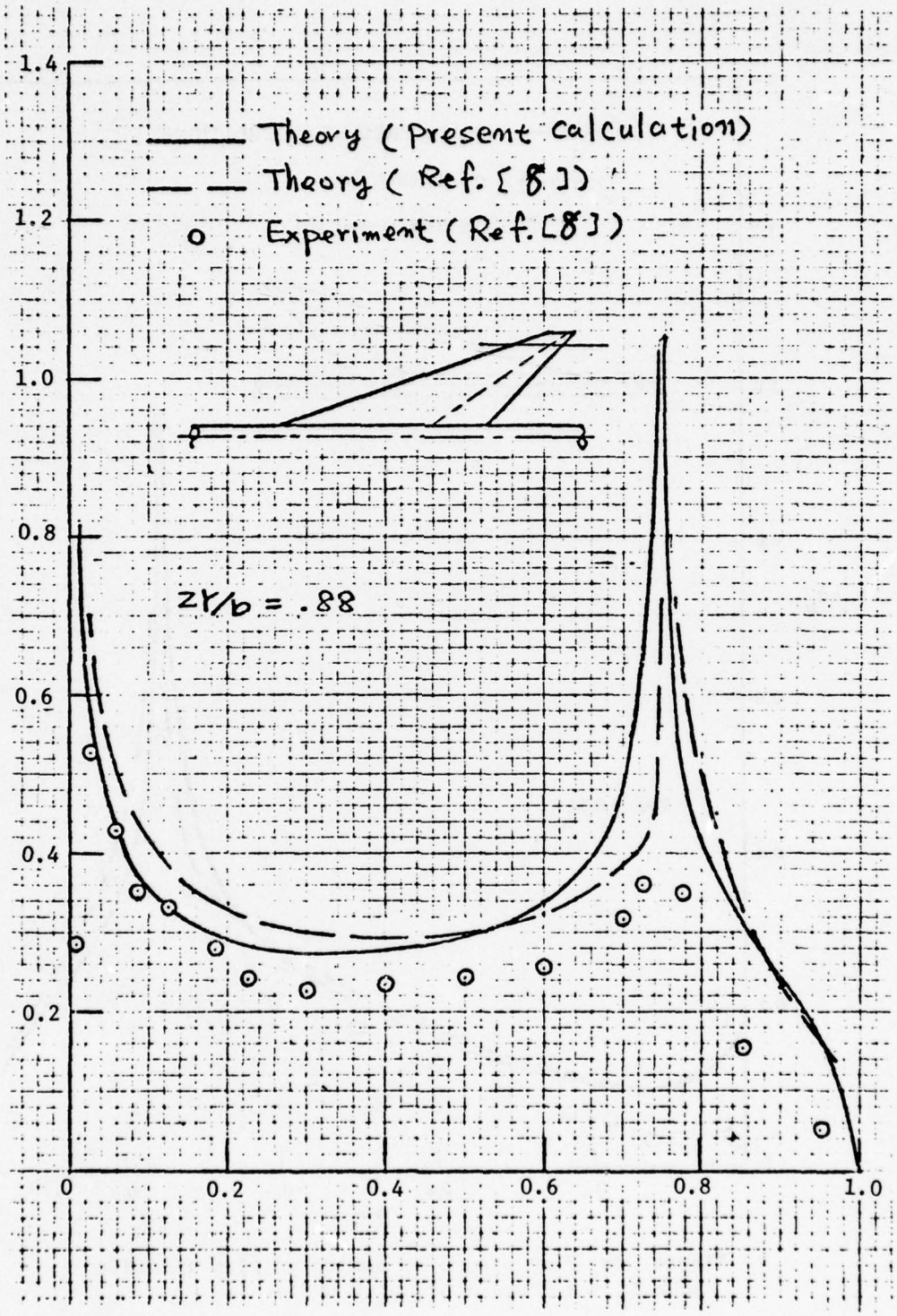

Figure 33c. Flat wing (trailing-edge $\delta_F = 8.3°$, $\alpha = 0$, $M_\infty = 0.85$)

The agreement on both methods is good, however, the inviscid flow theory predicts a larger pressure difference than data indicated over the flap surface. Again, such a disagreement is probably attributed to the flow separation on the upper wing because of a considerably higher flap angle given in this example.

2.3 Spanwise Load Distribution.

The spanwise load (directly related to the lift) distribution was computed for two different angles of attack cases. And then they were compared with the results by the FLEXSTAB method. They are shown in Fig. 34 (for the chordwise pressure distributions, see Figs. 29 and 30). It was assumed that there is little difference between the lift and the normal force in this case, or, it is assumed negligibly small. In the case of the angles of attack of two degrees, the agreement of the present calculation with both the FLEXSTAB and data is satisfactorily good; this is apparent from Figs. 29a to c. On the other hand, the poor agreement with the experimental data occurred in the region from the mid span to the wing tip at the angles of attack of eight degrees. This can be also understood by looking back at Figs. 30b and c. The satisfactorily good agreement can be seen at the region below the mid span.

Figs. 35 and 36 show the spanwise load distribution in the case of a deflected flap at Mach number 0.4 and 0.85, respectively. Nonetheless, even with the large flap deflections, both the theoretical calculations were in good agreement with the experimental data. This means that the flap deflection does not influence the spanwise load distribution so much in this case as the angle of attack case did (see the case at $\alpha = 8^{o}$ in Fig. 34), because the part of the flap is small as compared with the total wing surface area. Little difference in the compressibility influence can be seen in this wing-body configuration (also, see Fig. 37 for the compressible effect to the normal force slope).

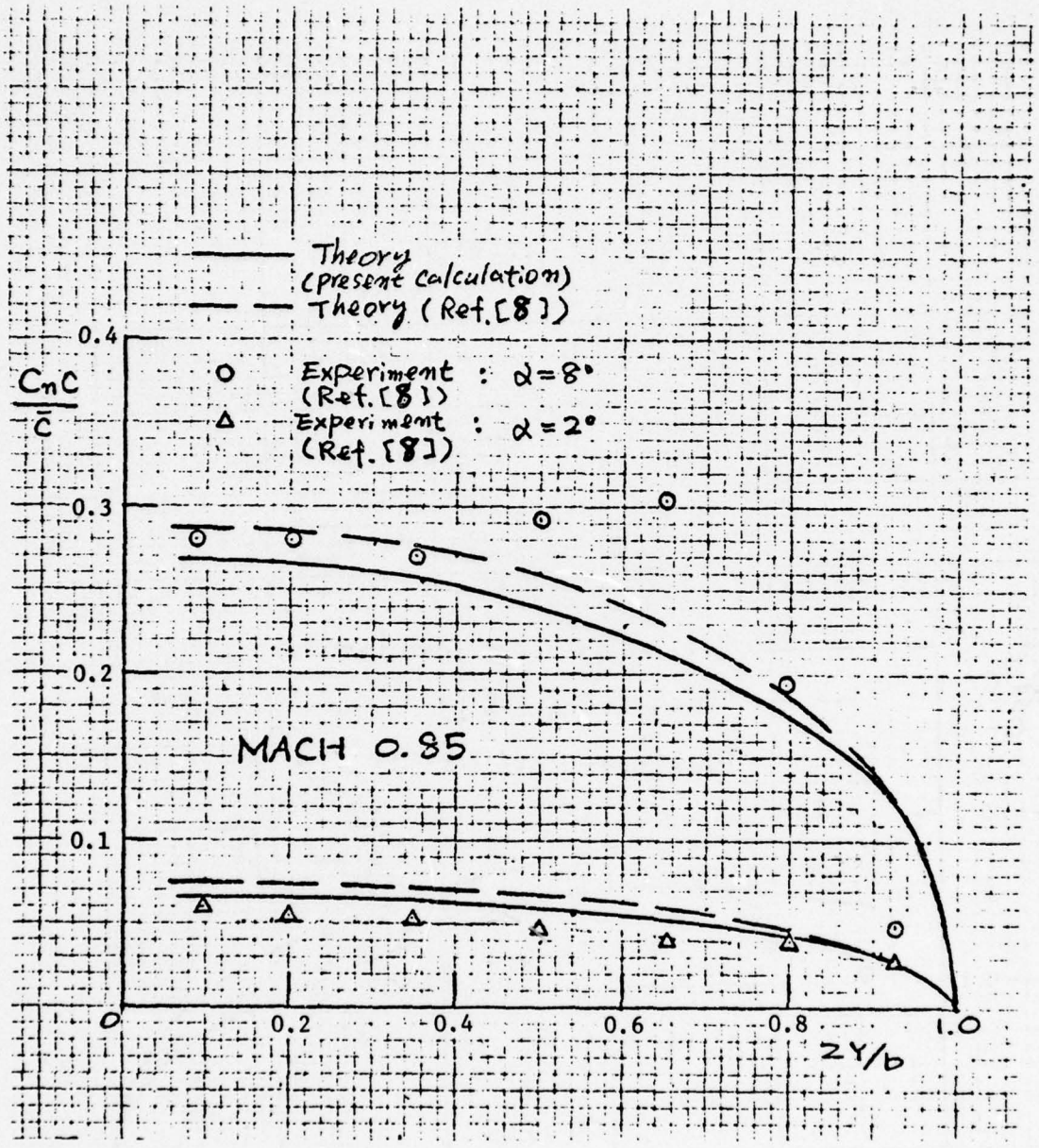

Figure 34. Spanwise load distribution (M_∞ = 0.85).

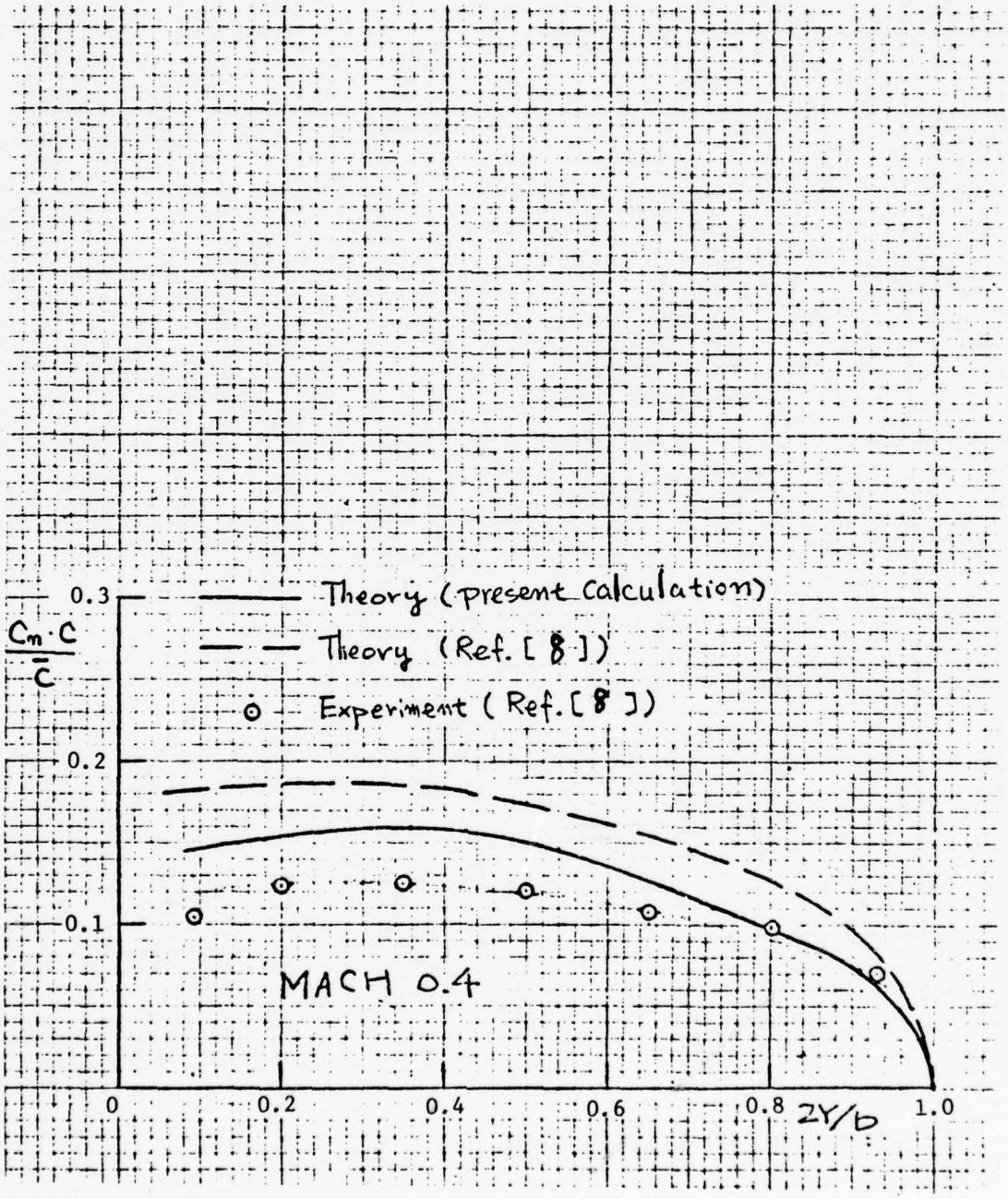

Figure 35. Spanwise load distribution (trailing-edge).

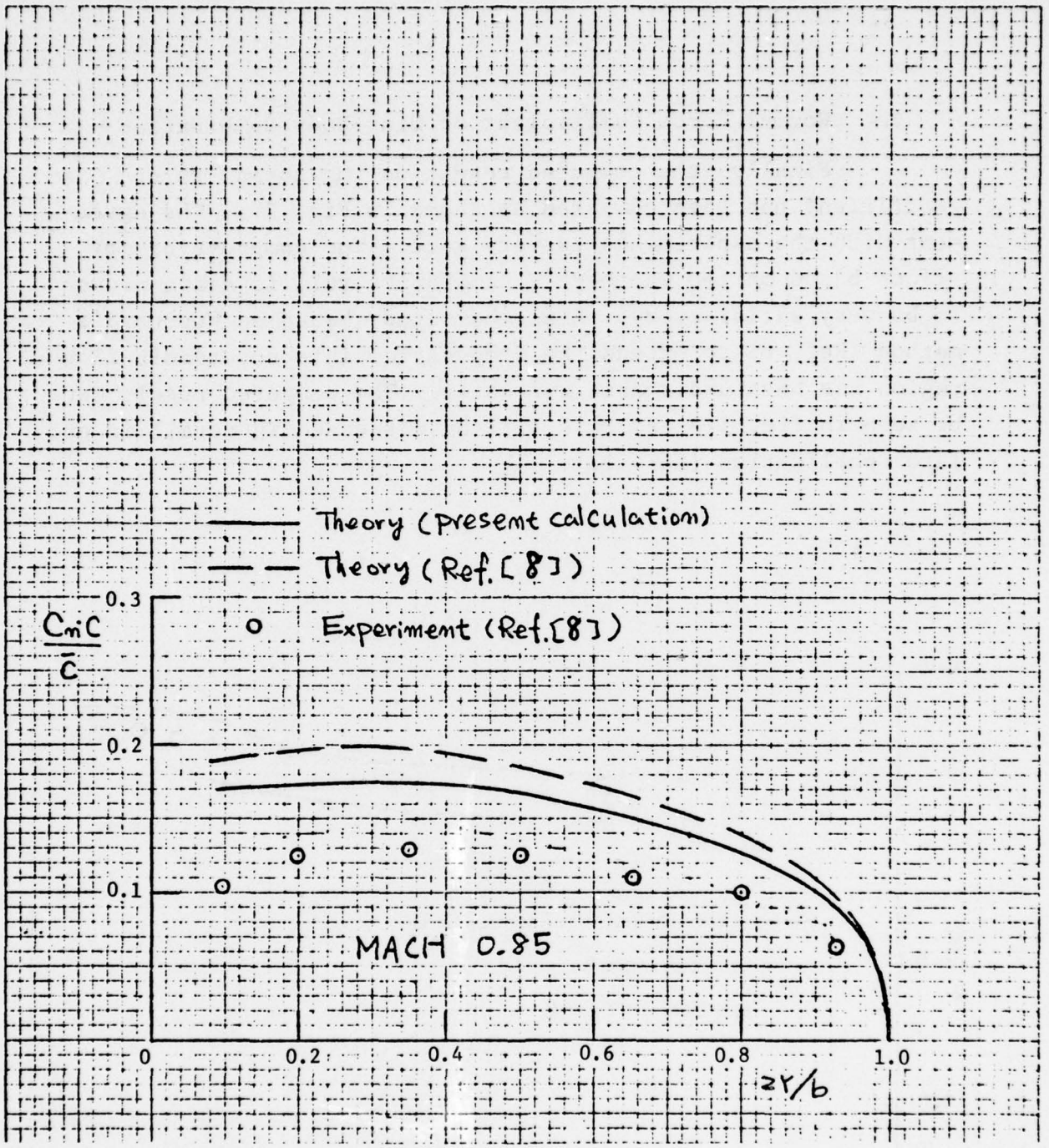

Figure 36. Spanwise lift distribution (trailing-edge δ_F = 8.3°, α = 0, M_∞ = 0.85).

2.4 Normal Force Coefficient of Wing-Body Combination.

Finally, the computed result on the normal force coefficient has been compared as shown in Fig. 37a. The agreement with the experiments is very good. The compressibility effect based on the Goethert's similarity rule is again proven to be very satisfactory. A further study based on Woodward's method (Ref. 6) to extend the computation into supersonic flow region has been undertaken currently. The computed result can be seen in Fig. 37b and this will be discussed in detail in our later publication (Ref. 13).

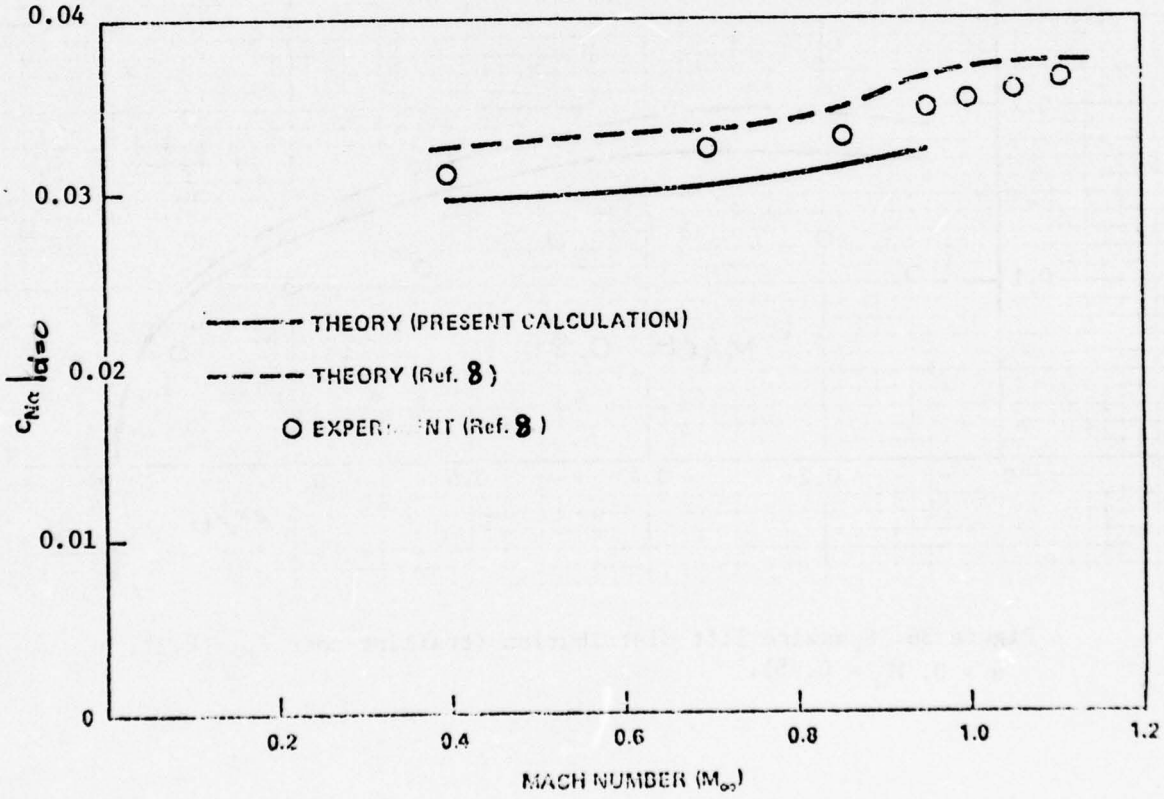

Figure 37a. Normal force coefficient.

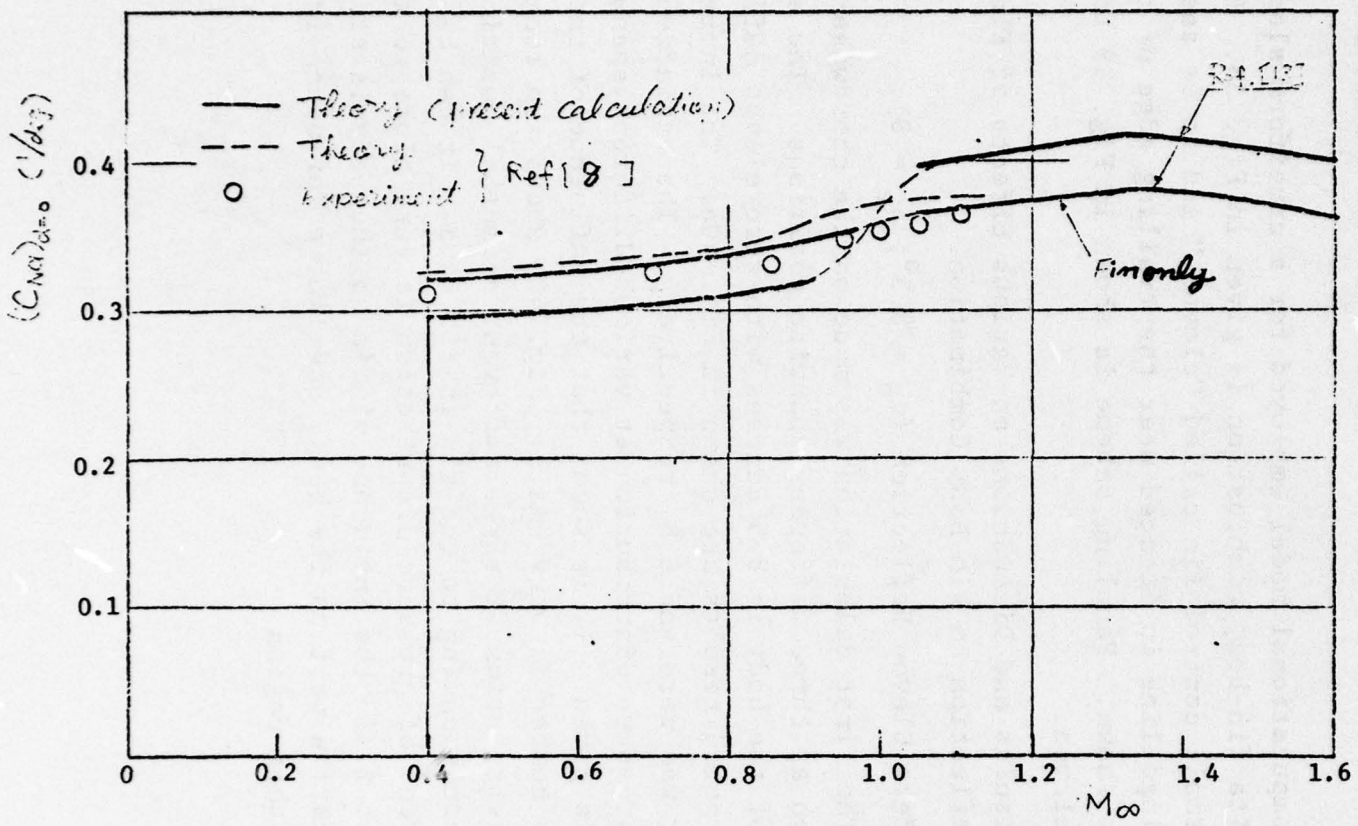

Figure 37b. Normal force slope of arrow fin-body combination.

SECTION VI. COMPARISONS OF POTENTIAL FLOW THEORIES WITH DATA ON CRUCIFORM SLENDER CLIPPED DELTA FIN-BODY COMBINATION WITH ELEVON DEFLECTION.

The computational model employed for a cruciform slender clipped delta fin-body combination is given in Fig. 38. Each fin has a small control fin called "eleven," and it is assumed that its hinge line is located near the trailing edge of the main fin as shown. Paneling scheme is shown in Fig. 39 for a deflected elevon.

1. Results and Discussions on Various Effects of Elevon Deflection on Fin-Body Combination.

1.1 Zero Elevon Deflection ($\alpha_b = 8.5^o$, $\delta_e = 0$).

The first calculation was made on the chordwise pressure distribution at three different spanwise positions. The angle of attack of the body is 8.5 degrees with zero elevon deflection, and the computed results are shown in Fig. 40a. The investigated Mach number was zero and 0.8, respectively. The variation of the chordwise pressure distribution at various different spanwise positions is given. It is found that the influence of the free stream Mach number is very small. Fig. 40b shows the longitudinal pressure distribution at three different azimuthal positions on the body corresponding to the fin in Fig. 40a. It can be seen that the trend of pressure distribution is very close to the one in Fig. 19b, i.e., the influence of fin on the body is strong in the fin location part on the body, and little influence from it outside of this region.

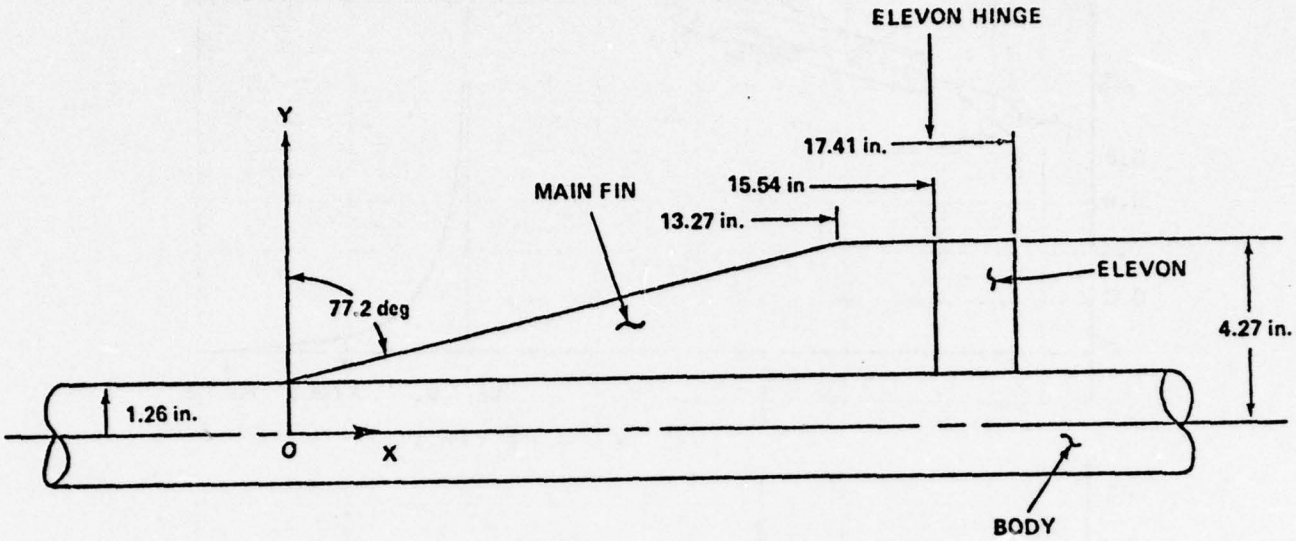

Figure 38. Fin-body geometry.

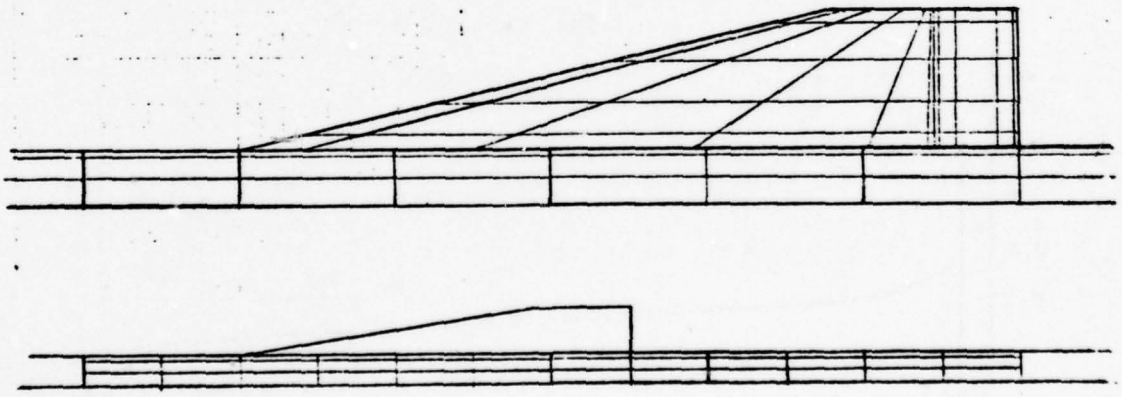

Figure 39. Paneling scheme.

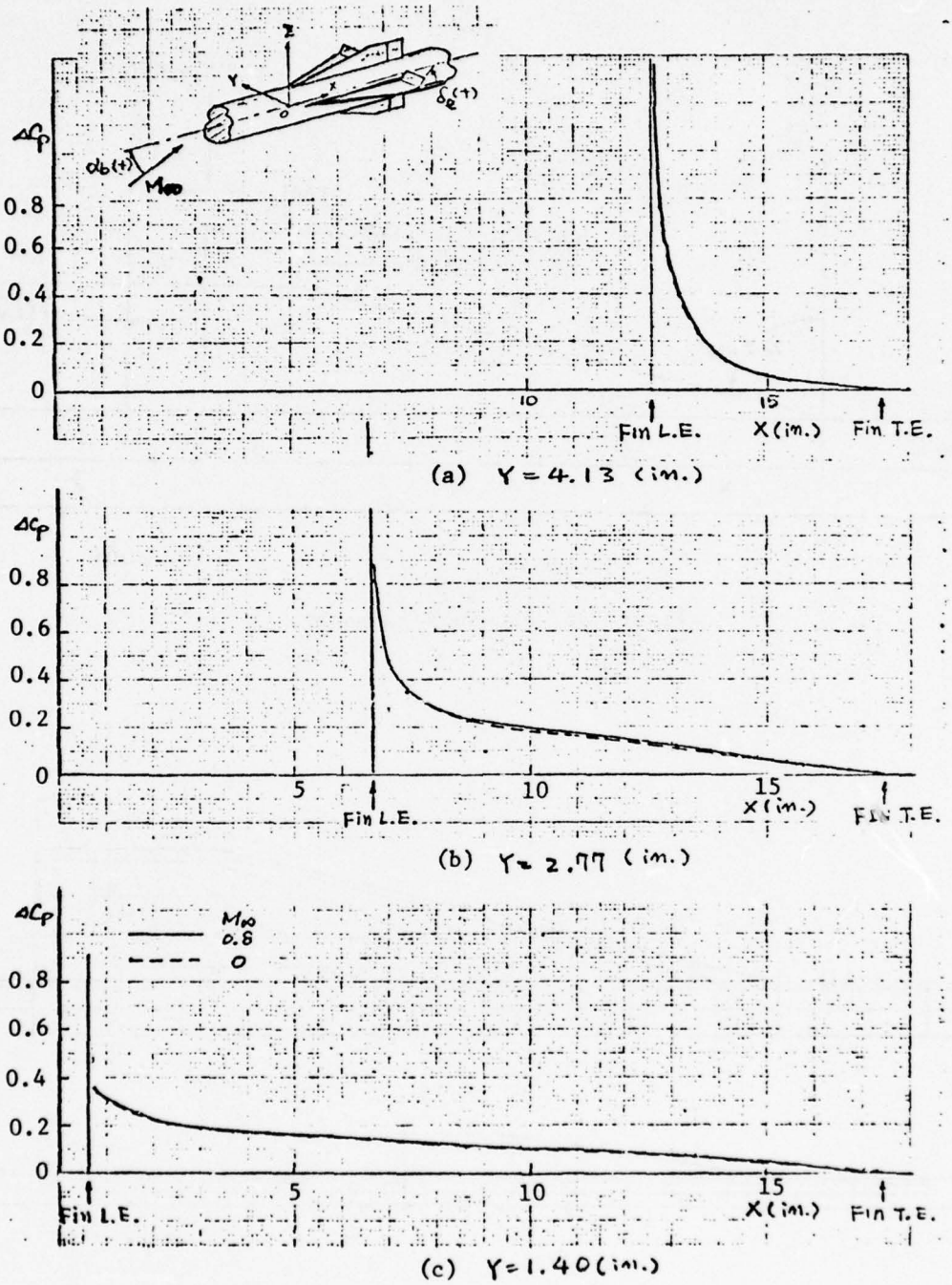

Figure 40a. Chordwise pressure distribution at three different spanwise positions on fin with zero deflected elevon of slender fin-body combination (α_b = 8.5°, δ_e = 0°, M_∞ = 0 and 0.8).

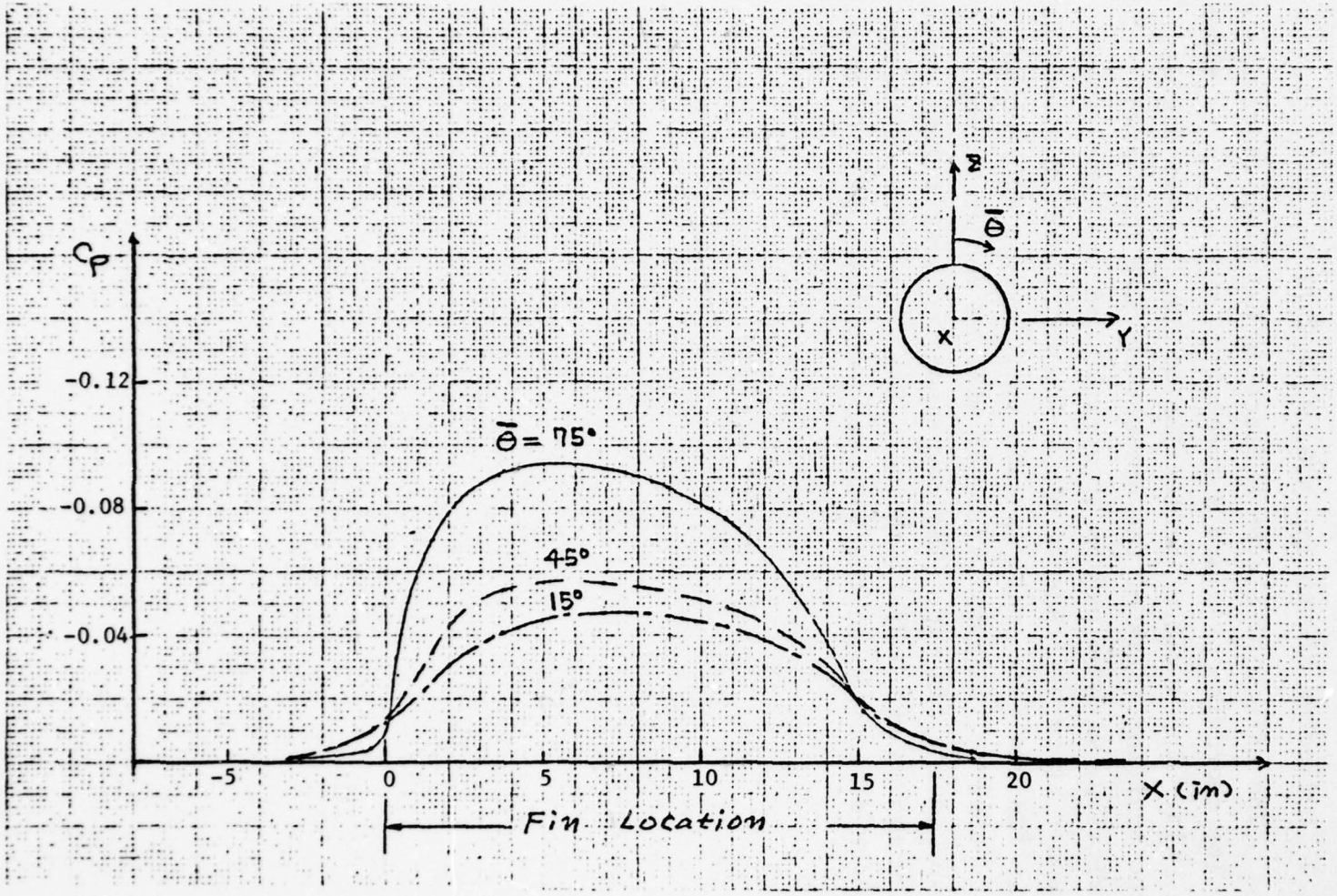

Figure 40b. Body longitudinal pressure distribution ($M_\infty = 0$, $\alpha_b = 8.5°$).

1.2 Deflected Elevon ($\alpha_b = 0$, $\delta_e = 2^o$).

The effect of elevon deflection has been investigated next. The chordwise pressure distribution on the fin is shown in Fig. 41a. The angle of deflection of flap is two degrees, with the trailing edges of the elevons on both fins down symmetrically, with no angles of attack, and the free stream Mach number is zero, respectively. The influence of elevon on the main fin was very small in such small elevon deflection angles. However, such an influence will be rather strong as it is closer to the fin tip. The corresponding longitudinal pressure distribution on the body is shown in Fig. 41b. The influence of the elevon deflection on the body was very small in this case.

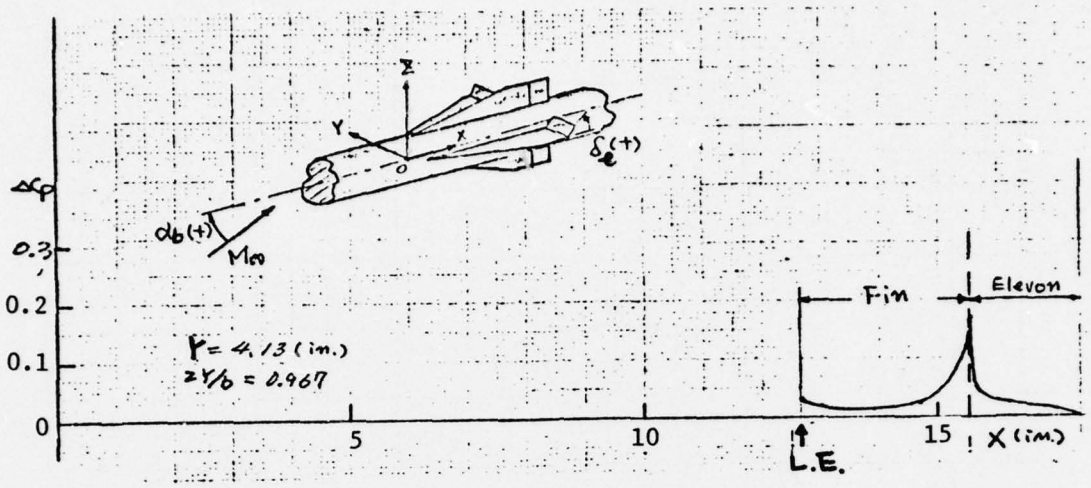

(a)

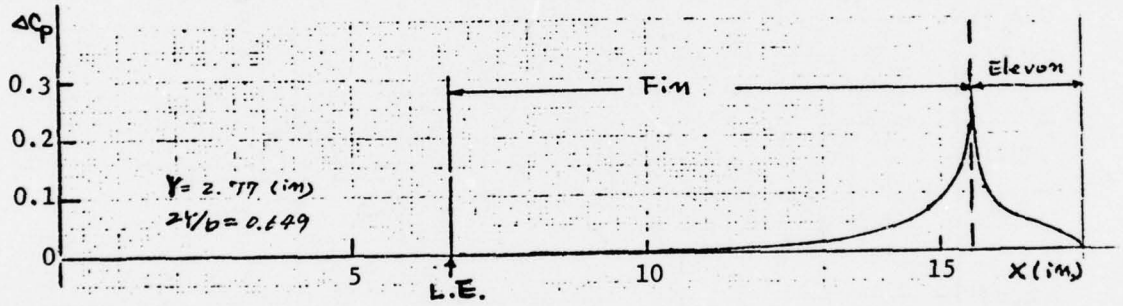

(b)

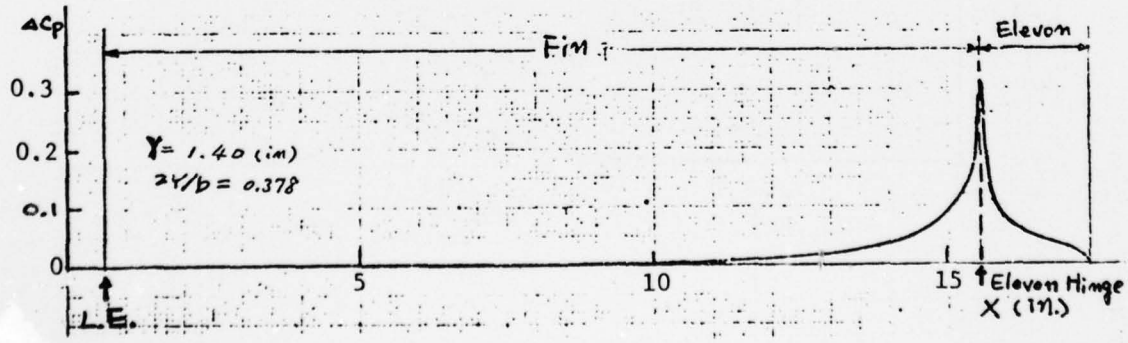

(c)

Figure 41a. Chordwise pressure distribution on fin with deflected elevon ($\delta_e = -2°$, $\delta_b = 0$, $M_\infty = 0$).

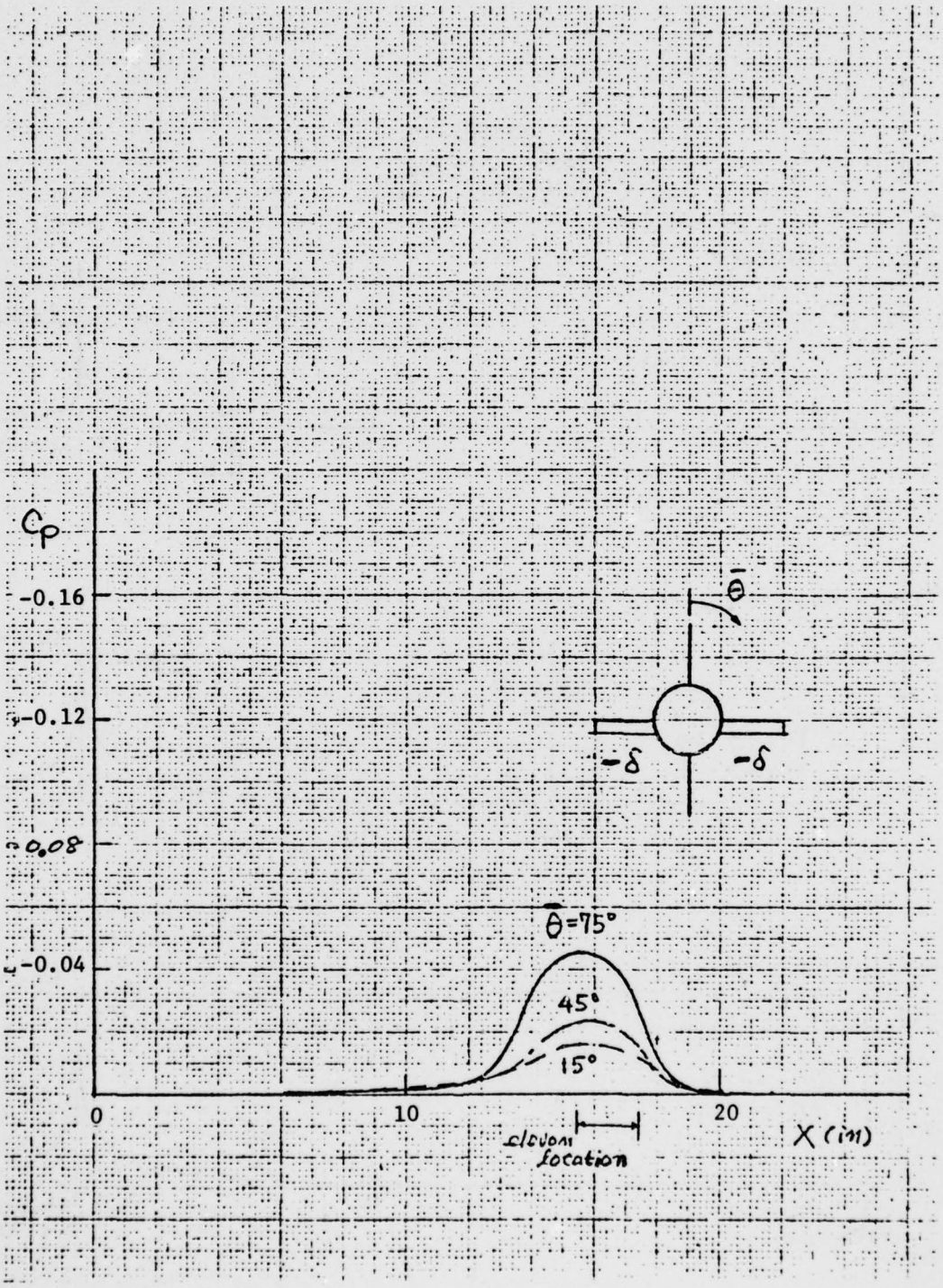

Figure 41b. Longitudinal pressure distribution on body ($\delta_e = 2°$, $\alpha_b = 0$, $M_\infty = 0$).

1.3 Combined Effects ($\alpha_b = 8.5^o$, $\delta_e = 2^o$).

Fig. 42a shows the chordwise pressure distribution on a fin at an angle of attack of the body of 8.5^o as well as the symmetrical elevon deflection of 2^o or -2^o, where the results of Figs. 40a and 41a were combined linearly. The corresponding longitudinal pressure distribution on the body is shown in Fig. 42b. This result was made also by the linear combination of the ones of Figs. 40b and 41b.

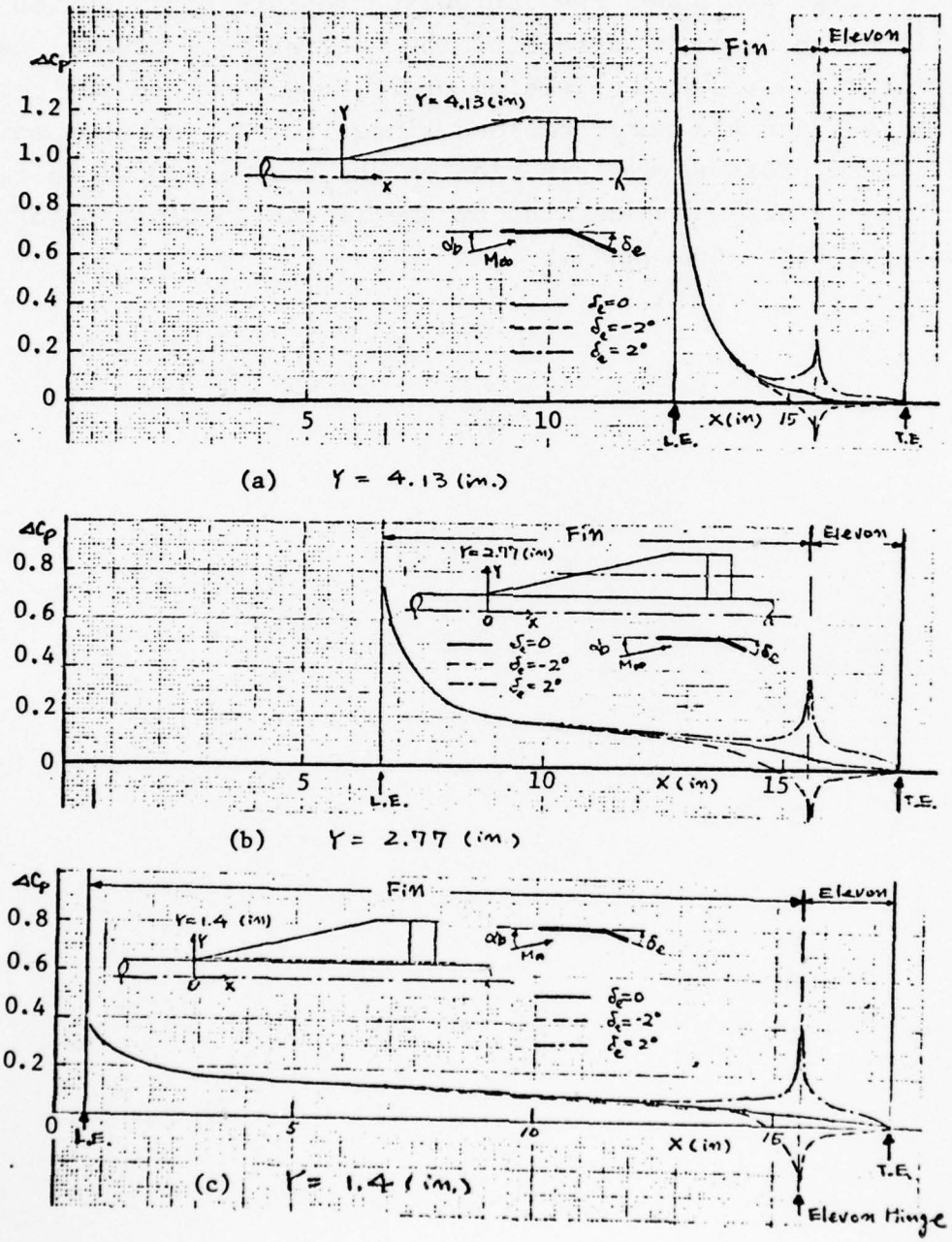

Figure 42a. Chordwise pressure distribution on fin with and without deflected elevon (δ_b = 8.5°, M_∞ = 0).

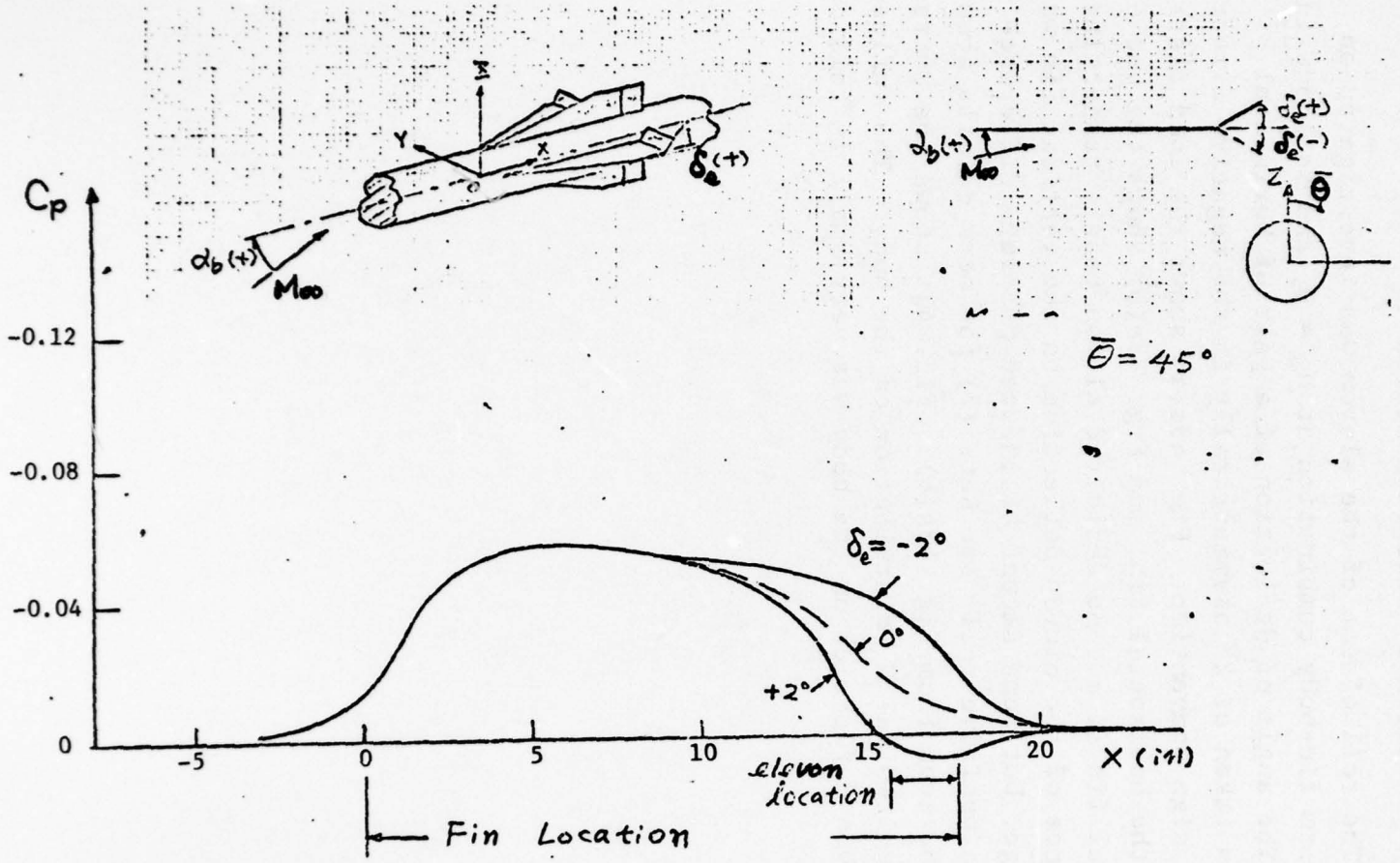

Figure 42b. Longitudinal body surface pressure distribution with and without elevon deflection ($M_\infty = 0, \alpha_b = 8.5°$).

1.4 Asymmetrically Deflected Elevon.

The roll effect of the elevon was investigated on the cruciform fin-body combination at $M_\infty = 0$, and is shown in Fig. 43. The angle of deflection of a pair of horizontal elevons was taken as 2^o asymmetrically in the negative direction of roll in sign convention. Fig. 43a(a) shows the load distribution on the horizontal fin, and Fig. 43a(b) shows the one on the vertical fin (i.e., no deflected elevon case), respectively. The influence of the elevon deflection on the vertical fin was not so large, but some amount of induced pressure difference (it acts as positive roll; see Ref. (2) for more details about this) can be seen from Fig. 43a(b). Fig. 43b shows the corresponding longitudinal C_p distribution on the body. The influence of the elevon deflection on the body was very small in this case.

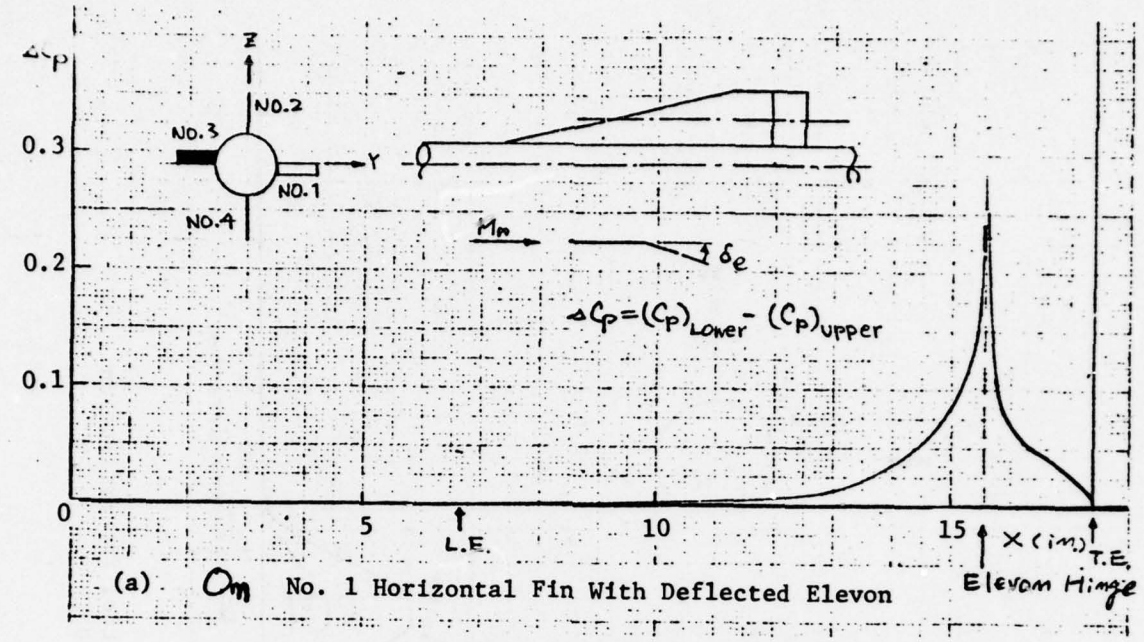

(a) C_m No. 1 Horizontal Fin With Deflected Elevon

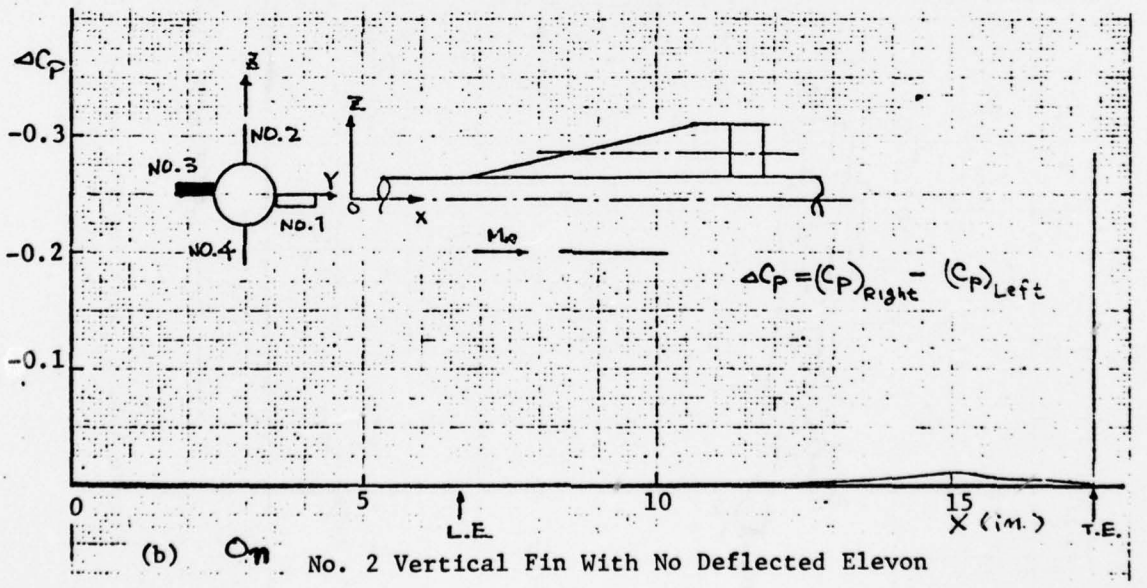

(b) C_n No. 2 Vertical Fin With No Deflected Elevon

Figure 43a. Effect of antisymmetrically deflected horizontal elevon on fins ($\delta_e = \pm 2°$, $M_\infty = 0$).

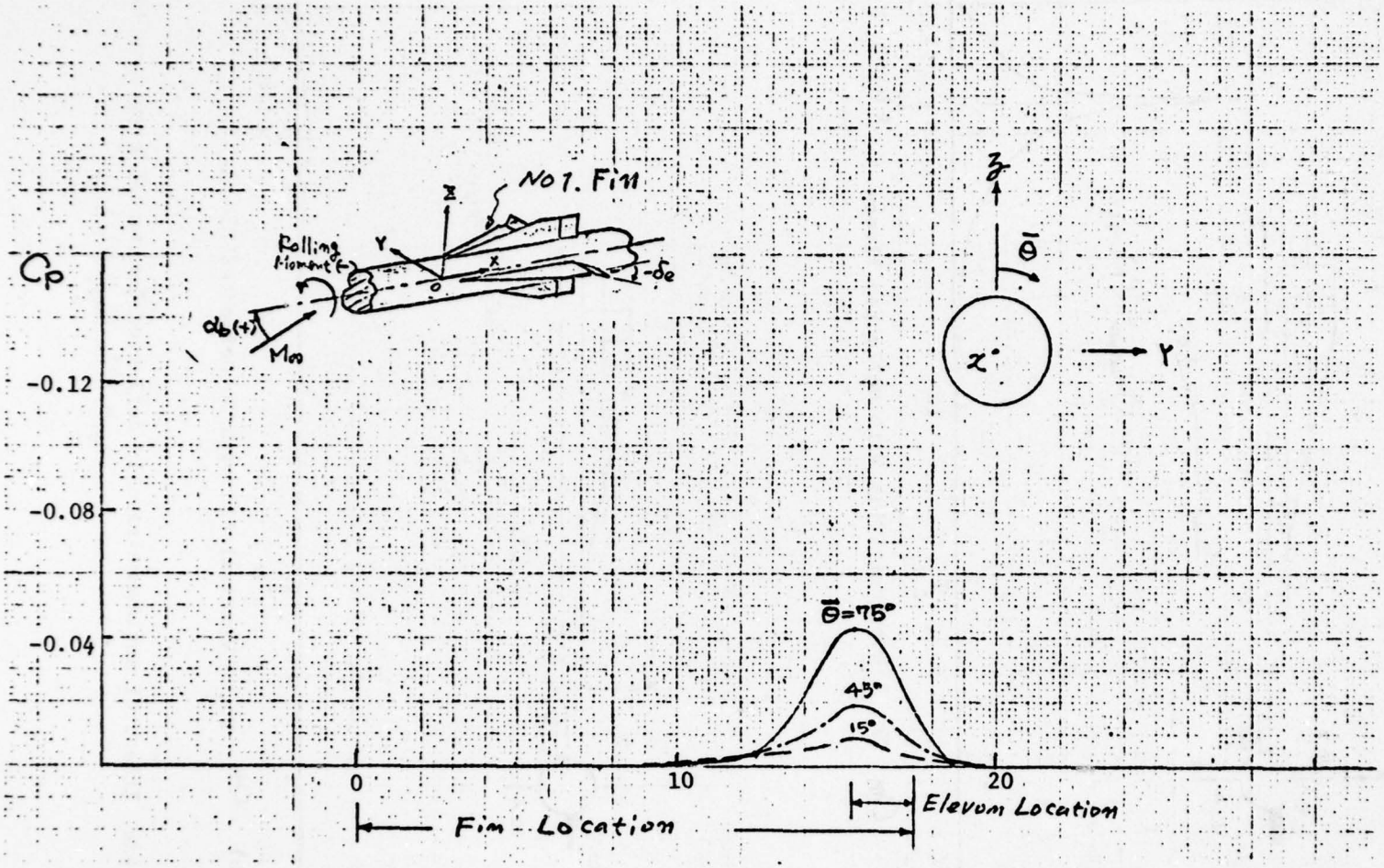

Figure 43b. C_p distribution on body with control fin deflection ($\delta_e = \pm 2°$, $\alpha_b = 0$, $M_\infty = 0$).

1.5 Fin-Body Combination with Angles of Attack and Yaw.

The pressure distribution on the body is shown in Fig. 44 for the fin-body combination at angles of incidence of 7.4^{o}. This result was obtained from the linear summation of the ones of angles of attack of 6.8^{o} and yaw angle of 2.8^{o} based on the linearity of the basic equations (see Ref. (2)).

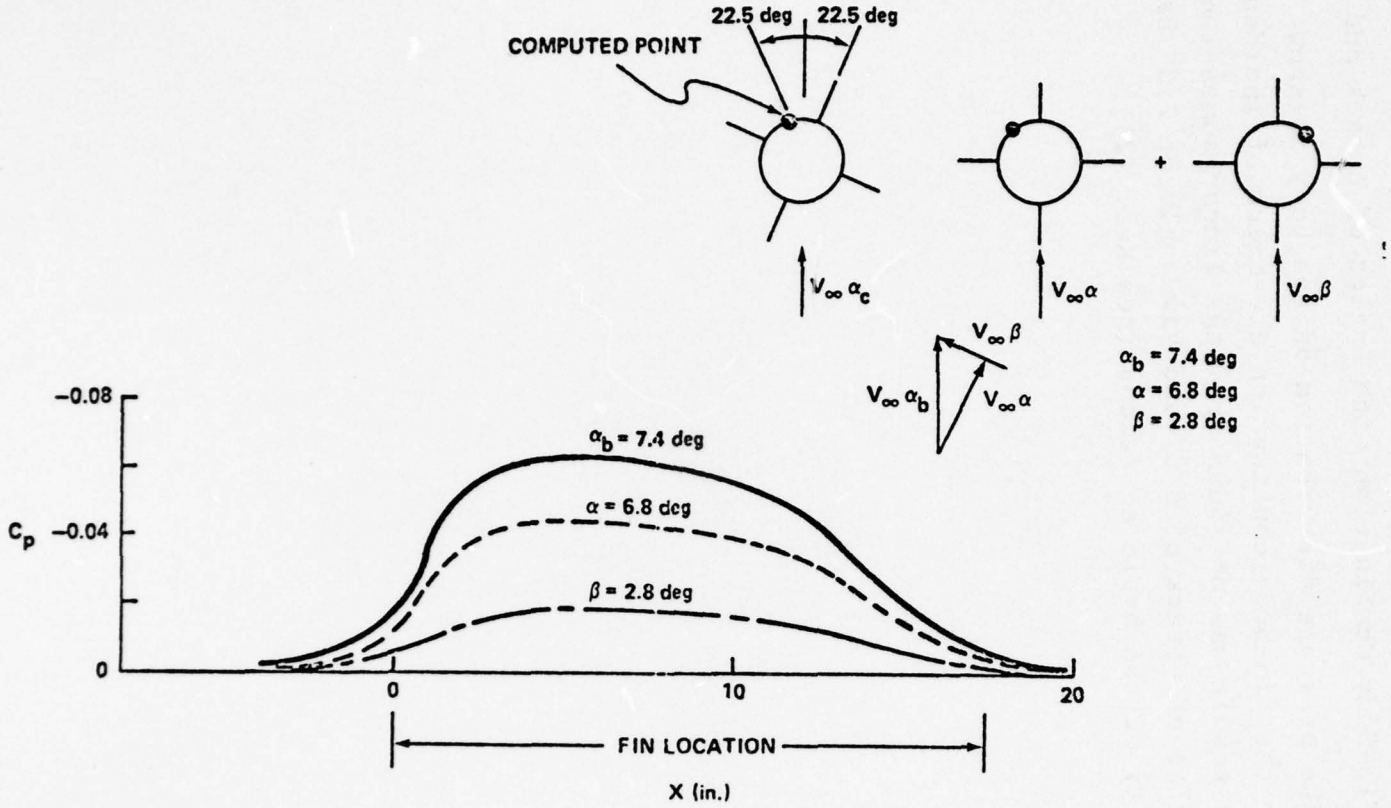

Figure 44. Longitudinal pressure distribution on body with angle of attack and yaw (0° elevon deflection angle).

2. Comparison with Experimental Data.

The angle of incidence of a body is taken at 8.54^{o} with an elevon deflection angle of $\pm 30^{o}$, with which the body generates a counterclockwise roll facing to the upstream direction. The free stream Mach number is 1.62. With a proper sweptback, as in this example calculation, the leading edge of the fin is submerged in a subsonic stream. Because of the slenderness of the fin and its subsonic leading edge, one expects that a better agreement may be resulted by employing a slender body theory than the singularity distribution method. After a comparison with data, it indicates indeed that this is true. (The analysis at supersonic speeds by using "Singularity Method" similar to that at subsonic speeds is currently under investigation. The method employed is mainly as given in Ref. (6).)

Figs. 45a to f show the chordwise pressure distribution computed by singularity distribution and slender body theories, at different spanwise positions together with experimental measurements (MICOM). The agreement of the singularities distribution method by Koerner with the data was not bad in general over a fin surface even though the flow is supersonic. The pressure distribution on the elevon surface could not be compared because of a lack of the data on this part.

As is expected, the computed result by slender-body theory showed a better agreement with the data over a fin. This is especially so on the lower surface of the fin, however, it cannot calculate the effect of the elevon deflection, and a clipped tip effect. The Koerner's method estimated a rather large pressure distribution on the fin close to the hinge line of the elevon because of a very large elevon deflection angle. The large pressure increase is again attributed to the flow separation. This can be seen more clearly on the upper surface of the fin near the hinge line. The tip effect caused by the leading point P of the tip Mach cone may cause the pressure to increase. However, no correction has been made in the present analysis.

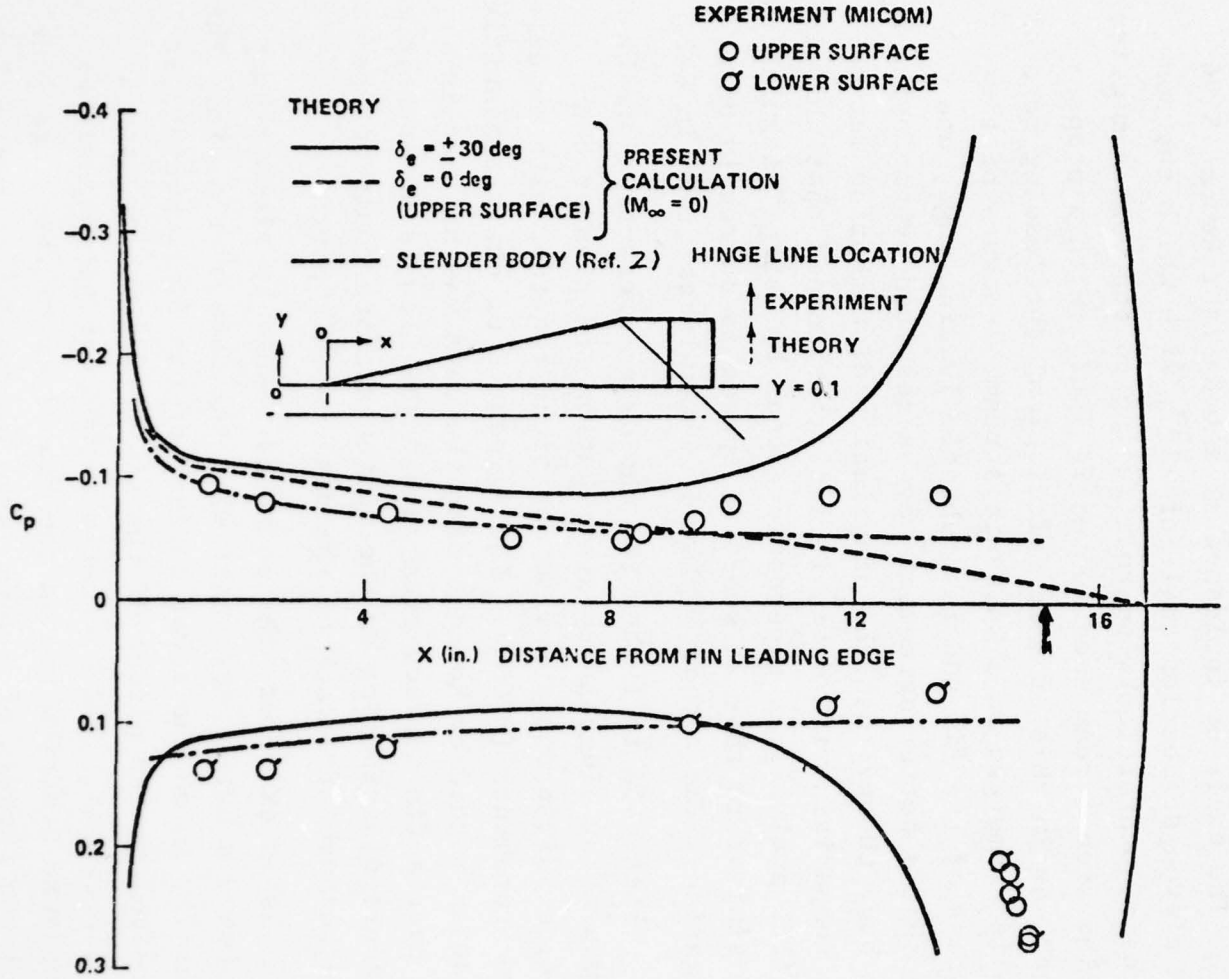

Figure 45a. Chordwise C_p distribution on fin: $M_\infty = 1.62$, $\alpha = 8.54°$, $\delta_e = \pm 30°$.

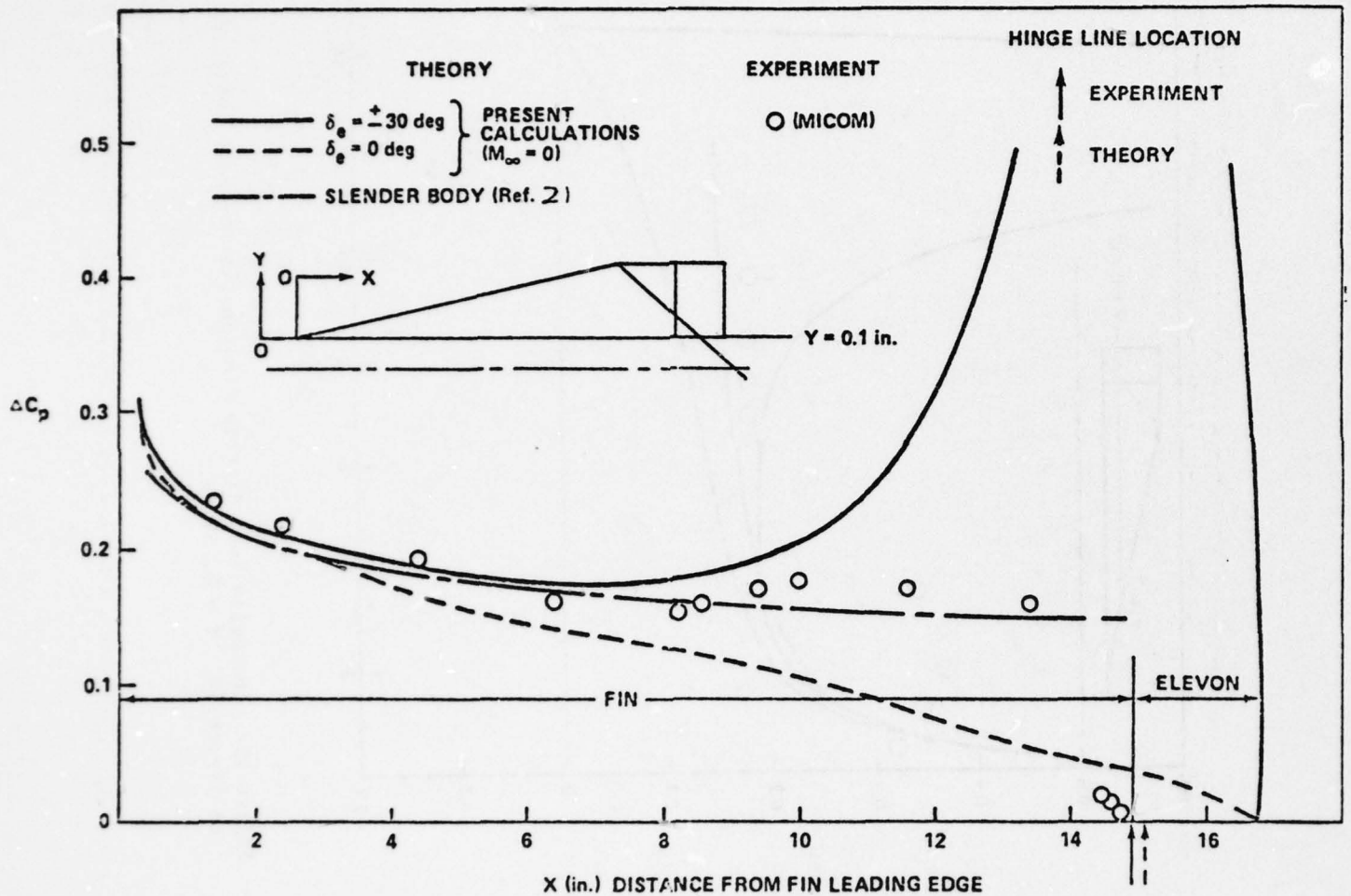

Figure 45b. Chordwise load distribution on fin ($M_\infty = 1.62$, $\alpha = 8.54°$, $\delta_e = \pm 30°$): Y = 0.1 in.

AD-A034 201 ARMY MISSILE RESEARCH DEVELOPMENT AND ENGINEERING LAB--ETC F/G 19/7
A STUDY OF VARIOUS SLENDER AND NON-SLENDER FIN-BODY COMBINATION--ETC(U)
NOV 76 N UCHIYAMA, J M WU

UNCLASSIFIED RD-CR-76-5 NL

2 OF 2
AD-A
034 201

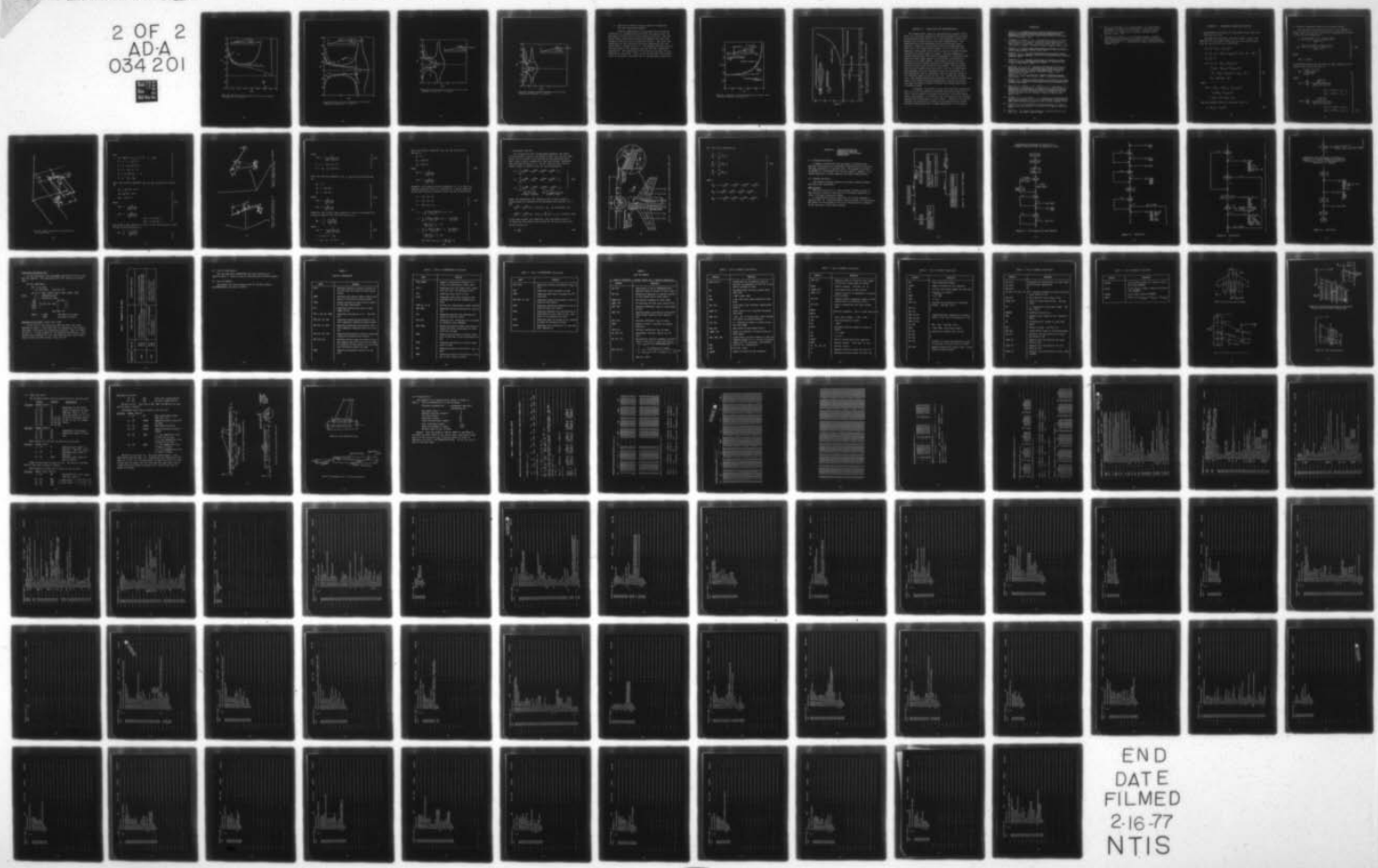

END
DATE
FILMED
2-16-77
NTIS

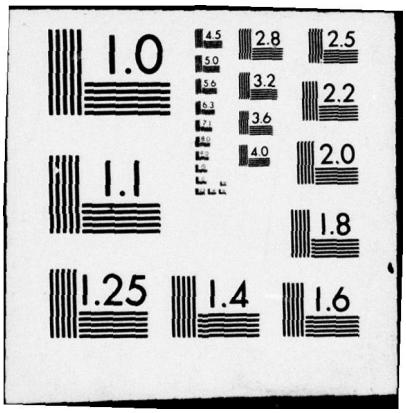
1.0
1.1
1.25
1.4
1.6
1.8
2.0
2.2
2.5
2.8
3.2
3.6
4.0
4.5
5.0
5.6
6.3
7.1

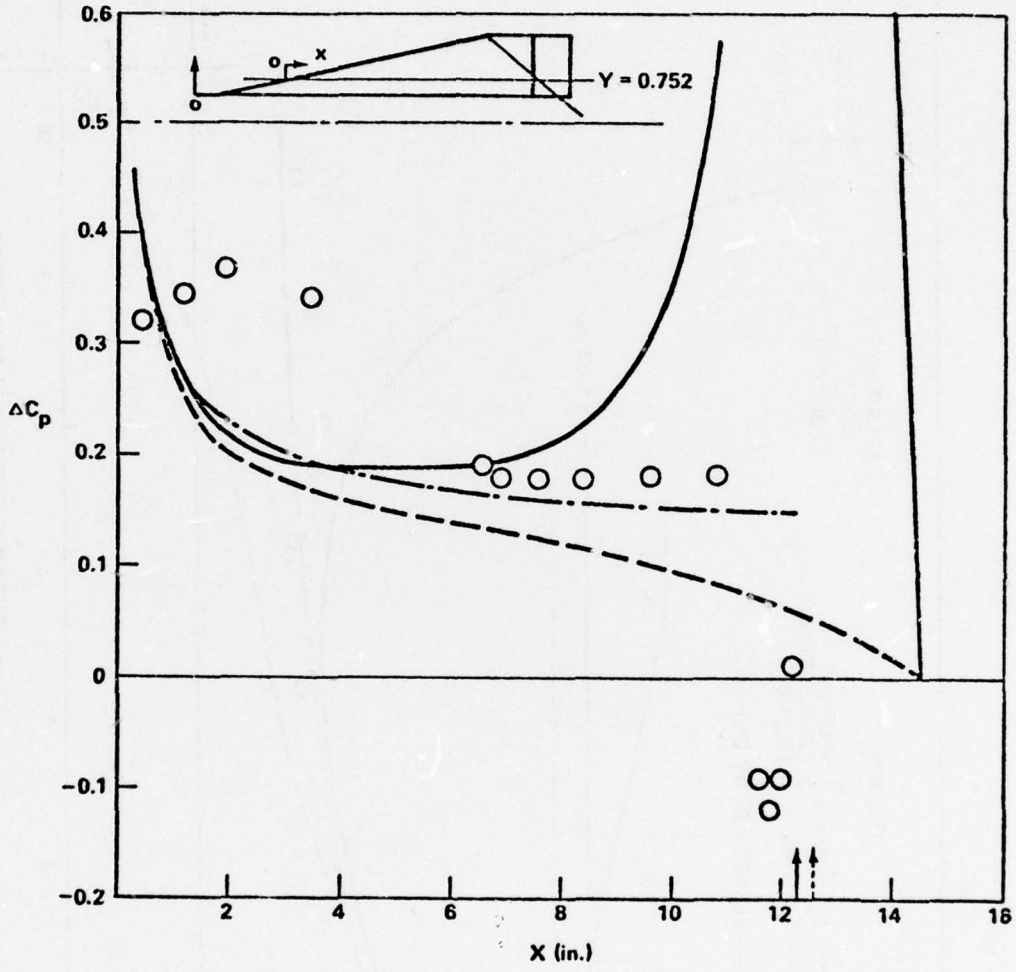

Figure 45c. Chordwise load distribution on fin for same conditions as Figure 69. Y = 0.752 in.

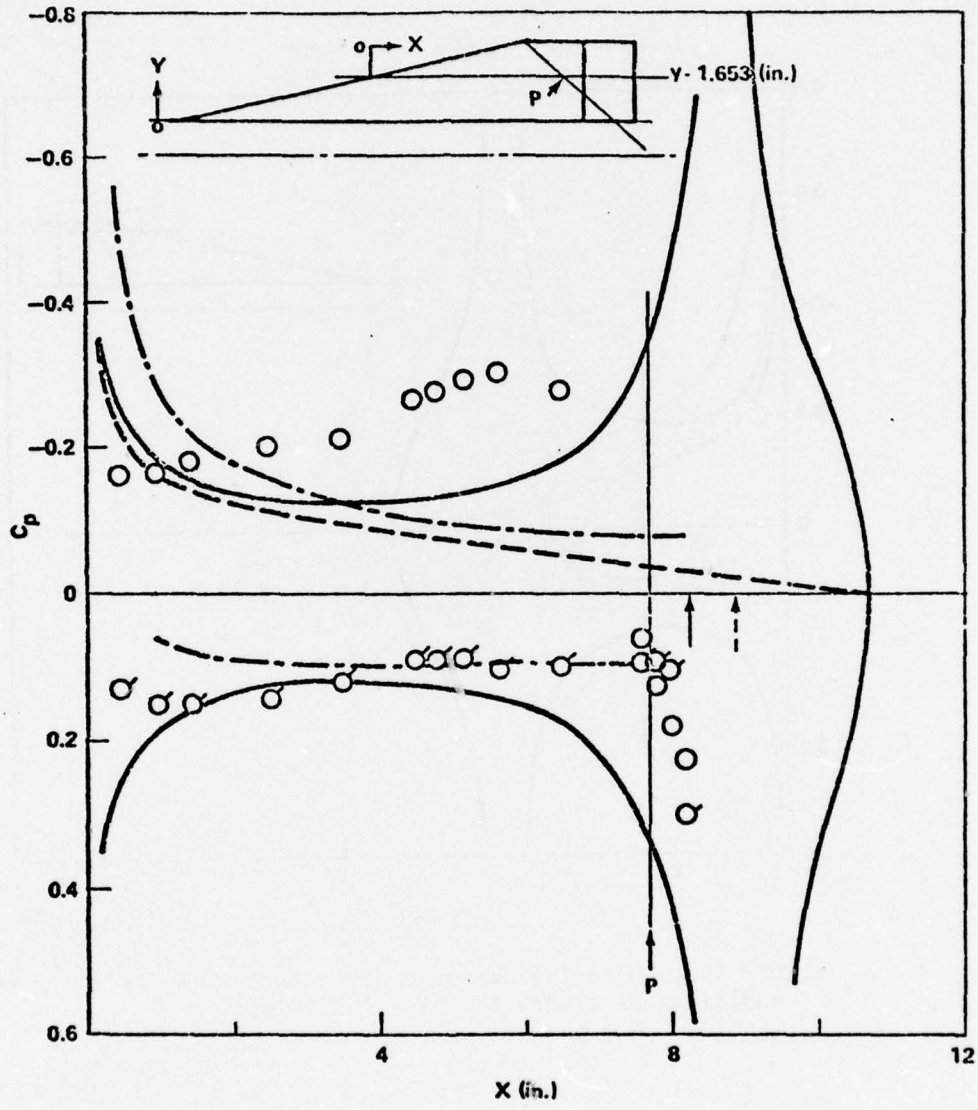

Figure 45d. Chordwise pressure distribution on fin for same conditions as Figure 69: Y = 1.653 in.

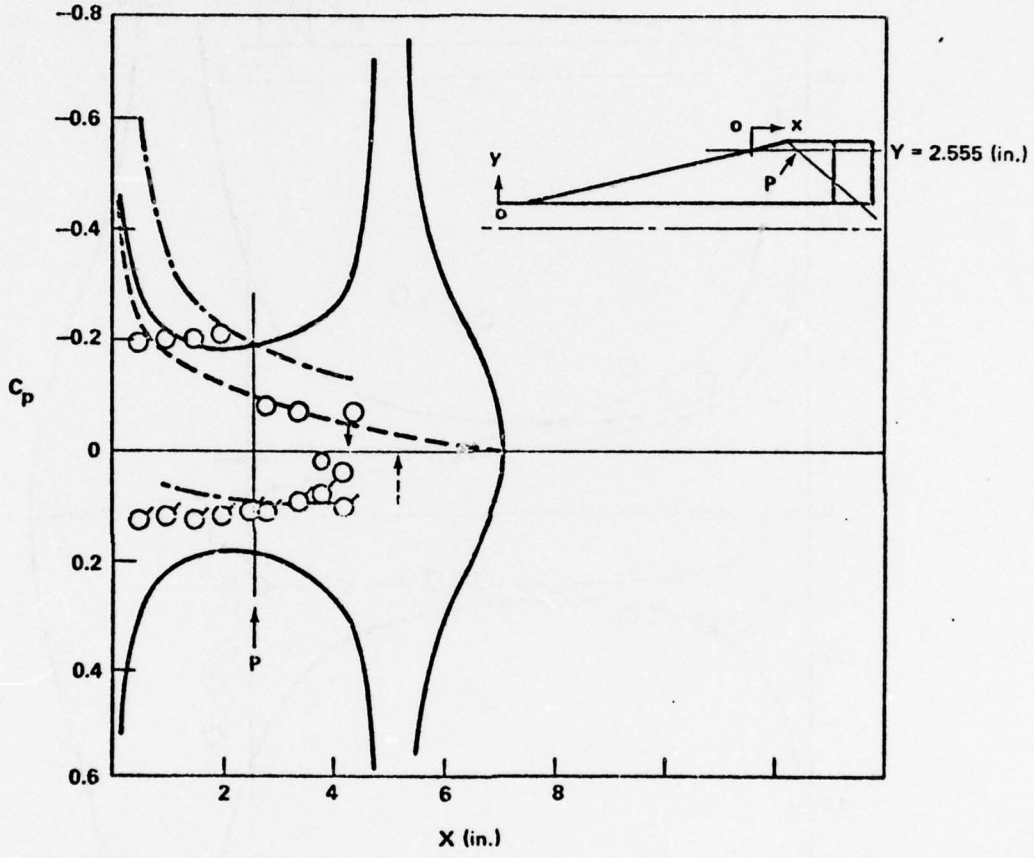

Figure 45e. Chordwise pressure distribution on fin for same conditions as Figure 69: Y = 2.555 in.

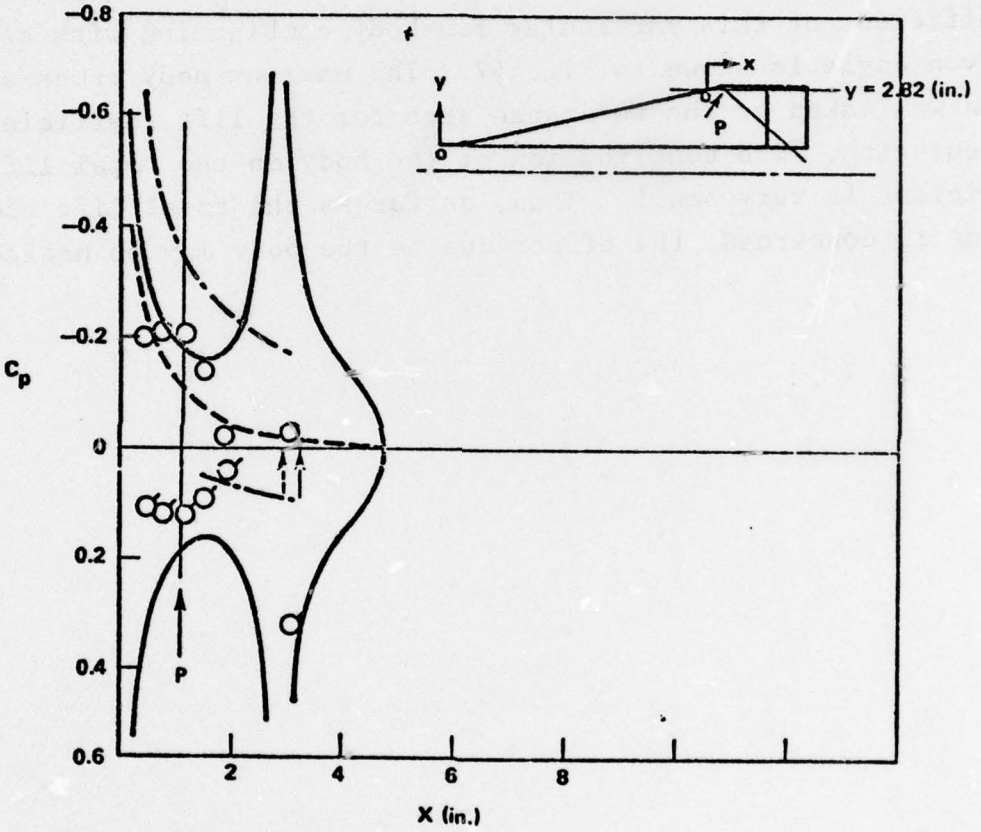

Figure 45f. Chordwise pressure distribution on fin for same conditions as Figure 69: Y = 2.82 in.

3. Variation of Surface Pressure and Lift Coefficient with Free Stream Mach Number.

Various compressibility corrections to the pressure coefficient of a sample point on the fin are shown in Fig. 46. The angle of attack of 8.5^{o} was assumed in this case. The computed results used Prandtl-Glauert and Kármán-Tsien rules and showed an over-correction as discussed earlier. The total lift coefficient of this particular fin-body combination with zero elevon angle is shown in Fig. 47. The maximum body cross-section area was taken as the reference area for the lift coefficient calculation. The contribution of the body on the total lift coefficient is very small. Thus, as far as the total lift coefficient is concerned, the effect due to the body may be neglected.

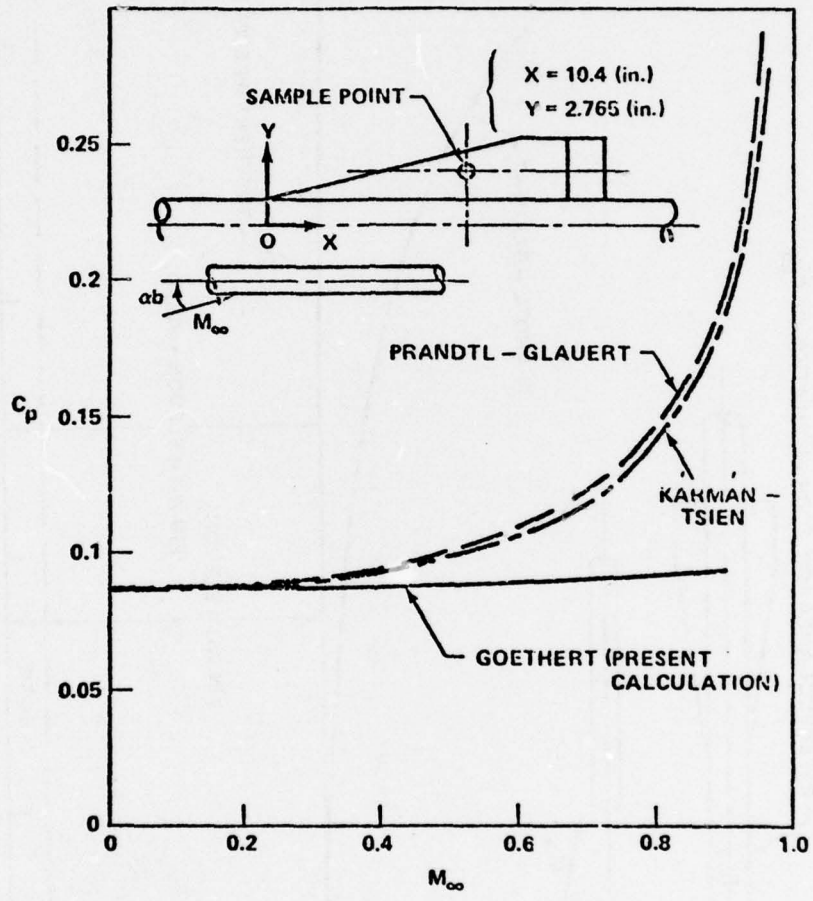

Figure 46. Comparison of compressibility effect of present result with other similarity rules (α_b = 8.5°).

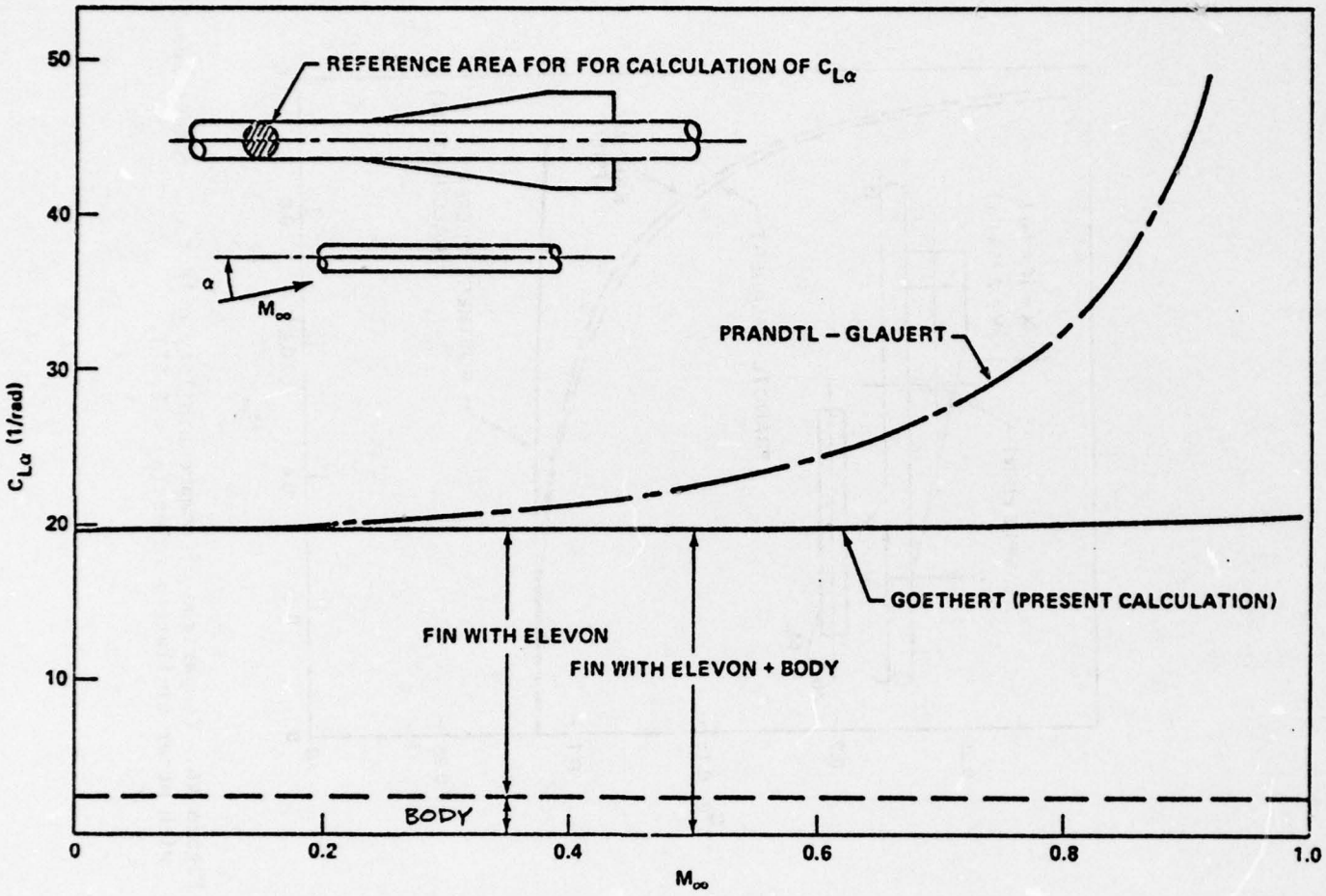

Figure 47. Variation of lift coefficient of fin-body combination with changing free-stream Mach number.

SECTION VII. CONCLUSIONS AND RECOMMENDATIONS.

The computational scheme for estimating the pressure distribution on a fin-body combination has been developed by the "Singularity Method" based on Ref. (1). The reasonable results were obtained over various kinds of fin-body configurations. The comparisons with the experimental data were generally good. Goethert's similarity rule predicted well the compressibility effect up to very high subsonic speed. This is not only for a moderately large aspect ratio fin but also to a slender fin-body combination at small angles of attack. The poor agreement of pressure distribution with the data appeared at a relatively high angle-of-attack (eight degrees in the present calculation) as reported in the other method. This seemed to be in the flow separation on the lifting surface due to high angles of attack, and thus further study on this will be needed. The calculated result by the slender-body theory (Ref. (2)) had a surprisingly good agreement with the experimental data for the slender fin-body combination even at supersonic speed as expected, except in the influence region of the fin tip, i.e., inside the tip Mach cone. The present analysis has coincided well with the slender-body theory, for slender fin-body configuration, and thus it may be said that the present analysis includes the slender-body theory at subsonic speed.

Although a flat plate fin case only has been investigated here, it is not too difficult to modify the present analysis so that it can be applied to include the cases of a fin with camber, twist, and thickness. Furthermore, the restriction of the straight leading and trailing edge is not so severe. Therefore, the present analysis can be applied to almost all the arbitrary plan formed fin-body combinations with a slight modification to the program.

REFERENCES

1. Koerner, H., Berechnung der Potential Theoretischen Strömung um Flügel-Rumpf-Kombinationen und Vergleich mit Messungen, Zeitschrift Für Flugwissenschaften, 20 Jahrgang, Heft 9, September, 1972.

2. Uchiyama, N. and Wu, J. M., "Inviscid Flow Analysis on Body of Revolution with Slender Cruciform Canted Delta Fins at Small Angle of Incidence," Technical Report RD-75-32, U. S. Army Missile Command, Redstone Arsenal, Alabama, March, 1975.

3. Koerner, H., Theoretische Parameteruntersuchungen an Flügel-Rumpf-Kombinationen, DLR-FB 72-63, 1972.

4. Lawrence, H. R., The Lift Distribution on Low Aspect Ratio Wings at Subsonic Speeds, Journal of The Aeronautical Sciences, October, 1951.

5. Woodward, F. A., Analysis and Design of Wing-Body Combinations at Subsonic and Supersonic Speeds, J. Aircraft, Vol. 5, No. 6, Nov.-Dec., 1968.

6. Woodward, F. A., et al., Analysis and Design of Supersonic Wing-Body Combinations, Including Flow Properties in the Near Field---Part I: Theory and Application, The Boeing Company, Renton, Washington, N67-34997, August, 1967. (Also NASA CR-73106)
LaRowe, E., et al. ---Part II: Digital Computer Program Description, N67-34994, August, 1967. (Also NASA CR-73107.)

7. Hedman, S. G., Vortex Lattice Method for Calculating of Quasi Steady State Loadings on Thin Elastic Wings in Subsonic Flow, FFA Rep. 105, 1966.

8. Manro, M. E., Tinoco, E. N., Bobbitt, P. J., and Rogers, J. T., Comparisons of Theoretical and Experimental Pressure Distributions on an Arrow-Wing Configuration at Transonic Speeds, Aerodynamic Analyses Requiring Advanced Computers, Part II, Langley Research Center, Hampton, Virginia, NASA Sp-347, March, 1975.

9. Chipman, R. R., and Rauch, F. J., Analytical and Experimental Study of the Effects of Wing-Body Aerodynamic Interaction on Space Shuttle Subsonic Flutter, NASA CR-2488, January, 1975.

10. Shapiro, A. H., The Dynamics and Thermodynamics of Compressible Fluid Flow, Vol. 1, The Ronald Press Company, New York, 1953.

11. Nielsen, J. N., Missile Aerodynamics, McGraw-Hill Book Company, Inc., New York, 1960, p. 211.

12. Wu, J. M., Moulden, T. H., and Uchiyama, N., "Aerodynamic Performance of Missile Configurations at Transonic Speeds Including the Effects of a Jet Plume," Technical Report RD-76-23, U. S. Army Missile Command, Redstone Arsenal, Alabama, March, 1976.

13. Uchiyama, N., and Wu, J. M., "A Further Study on Slender and Non-Slender Fin-Body Combinations of Missile Configurations with Emphasis on Low Supersonic Flow," Technical Report (in preparation), U. S. Army Missile Command, Redstone Arsenal, Alabama, 1977.

APPENDIX I. DETERMINING AERODYNAMIC MATRICES.

1. Determining the positions of a horseshoe vortex and a control point on a fin

By using the coordinates as shown in Figs. 2 and 3, the positions of a horseshoe vortex (x_v, y_v, z_v) a control point (x_D, y_D, z_D) on a fin can be written as:

$$
\begin{aligned}
y_v &= y_D = (e_{k,\ell} + e_{k,\ell+1})/2 \\
x_v &= a_k + c_k \cdot (3d_{k,m} + d_{k,m+1})/4 + (y_v - b_k) \cdot \tan\lambda \\
Z_v &= Z_D = 0 \\
x_D &= a_k + c_k \cdot (d_{k,m} + 3d_{k,m+1})/4 \\
&\quad + \{ c_{k+1} \cdot (d_{k+1,m} + 3d_{k+1,m+1})/4 \\
&\quad - c_k \cdot (d_{k,m} + 3d_{k,m+1})/4 + a_{k+1} - a_k \} \cdot \\
&\quad (y_v - b_k)/(b_{k+1} - b_k)
\end{aligned}
\qquad (21)
$$

where,

$$
\begin{aligned}
\tan\lambda = \{ & c_{k+1} \cdot (3d_{k+1,m} + d_{k+1,m+1})/4 \\
& - c_k (3d_{k,m} + d_{k,m+1})/4 \\
& + a_{k+1} - a_k \} / (b_{k+1} - b_k)
\end{aligned}
$$

The half spanwise width of a horseshoe vortex is,

$$h = (e_{k,\ell+1} - e_{k,\ell})/2 \qquad (22)$$

2. Velocity components induced by a horseshoe vortex

The vertically intercepted point $S(\xi, \beta\eta, \beta Z_v)$ between a bound vortex line and any control point $P(x_D, \beta y_D\ \beta Z_D)$ as shown in Fig. 48 can be written as:

$$\left.\begin{aligned} \xi &= \frac{x_v + x_D \tan^2 \mu + \beta \cdot (y_D - y_v) \tan \mu}{\tan^2 \mu + 1} \\ \beta\eta &= \frac{\beta y_D + \beta y_v \tan^2 \mu + (x_D - x_v) \tan \mu}{\tan^2 \mu + 1} \end{aligned}\right\} \quad (23)$$

where,

$$\tan \mu = \tan\lambda/\beta$$

By using Biot-Savart law, the velocity (W_B) induced at $\underline{P}$ by a bound vortex ξ can be written as:

$$\left.\begin{aligned} W_B &= \frac{\Gamma (\cos \gamma + \cos \phi)}{4\pi \sqrt{A^2 + Z^2}} \end{aligned}\right.$$

where

$$\cos \gamma = \frac{\overline{QS}}{\overline{QP}} = \frac{\pm \sqrt{B^2 + C^2}}{\sqrt{A^2 + B^2 + C^2 + Z^2}}$$

$$\cos \gamma > 0 \text{ for } \eta > y_v - h$$

$$\cos \gamma < 0 \text{ for } \eta < y_v - h$$

$$\cos \phi = \frac{\overline{RS}}{\overline{RP}} = \frac{\pm \sqrt{D^2 + E^2}}{\sqrt{A^2 + D^2 + E^2 + Z^2}}$$

$$\cos \phi < 0 \text{ for } \eta > y_v + h$$

$$\cos \phi > 0 \text{ for } \eta < y_v + h \quad (24)$$

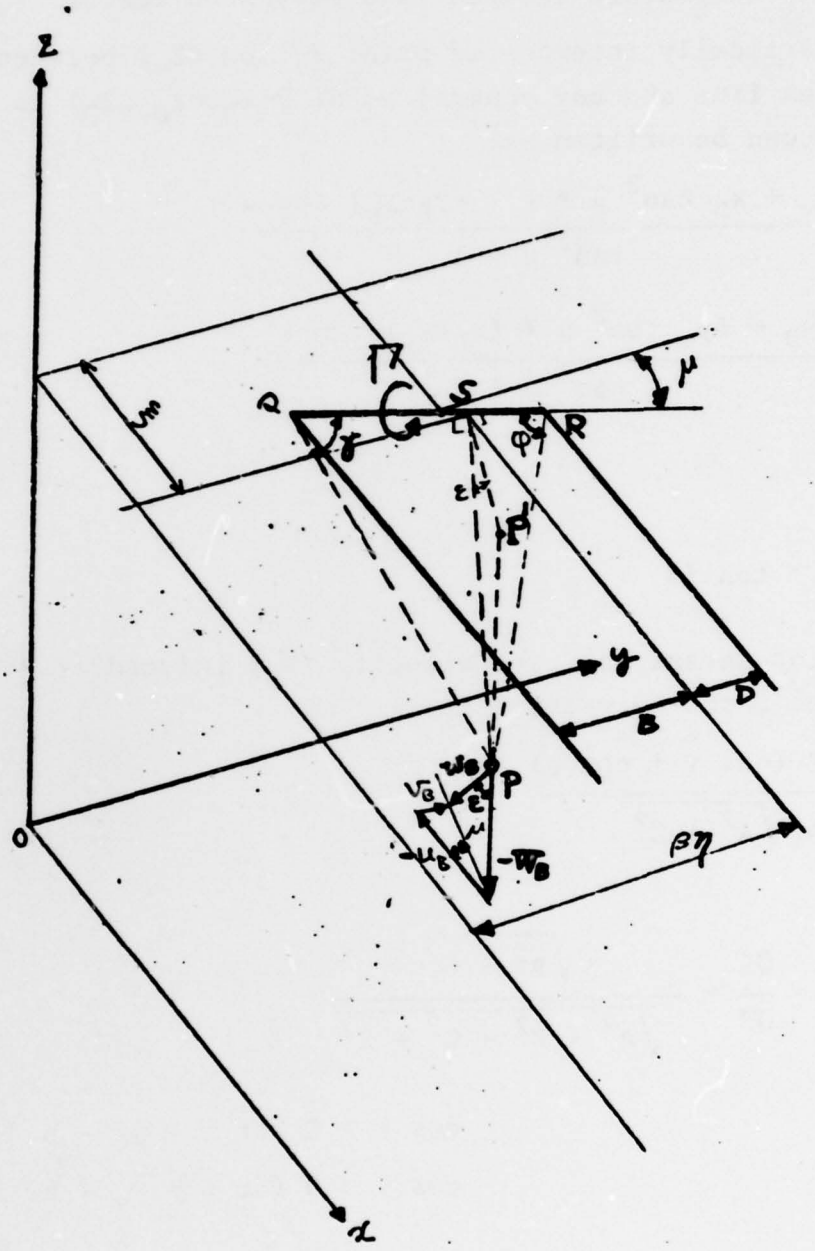

Figure 48. Induced velocity and its components due to a bound vortex.

and,

$$A^2 = (\overline{SP'})^2 = (x_D - \xi)^2 + \beta^2 \cdot (\eta - y_D)^2$$

$$B = \beta \cdot (\eta - y_v + h)$$

$$C = \xi - x_v + \beta h \tan \mu$$

$$D = \beta \cdot (y_v + h - \eta)$$

$$E = x_v + \beta h \tan \mu - \xi$$

$$Z = \beta \cdot (Z_v - Z_D)$$

thus, the velocity components (u_B, v_B, w_B) of W_B can be written as:

$$u_B = - W_B \sin \varepsilon \cos \mu$$

$$v_B = W_B \sin \varepsilon \sin \mu$$

$$w_B = - W_B \cos \varepsilon$$

where, (25)

$$\sin \varepsilon = \frac{Z}{\sqrt{A^2 + Z^2}}$$

$$\cos \varepsilon = \frac{\pm A}{\sqrt{A^2 + Z^2}}$$

$\cos \varepsilon > 0$ for $x_D > \xi$

$\cos \varepsilon < 0$ for $x_D < \xi$

The velocity (W_p) induced at P due to a port free vortex as shown in Fig. 49 can be written as:

$$W_p = \frac{\Gamma}{4\pi} \cdot \frac{1 + \cos k}{\sqrt{G^2 + Z^2}}$$

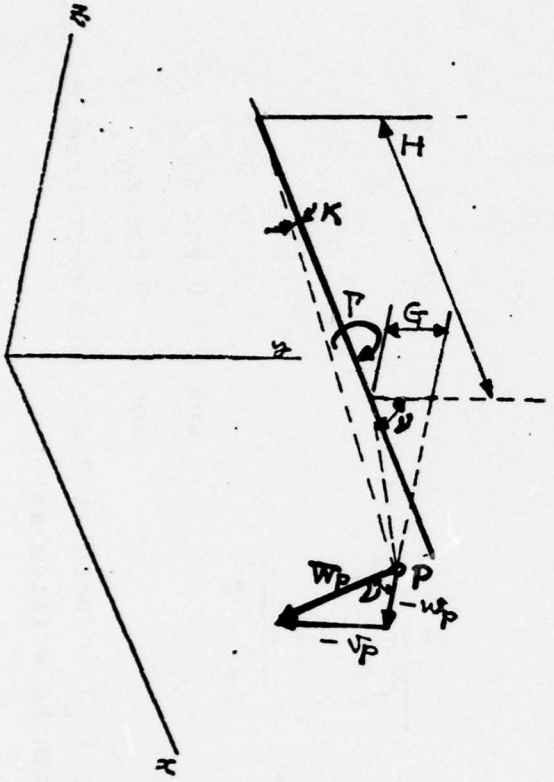

Figure 49. Induced velocity and its components due to a port free vortex.

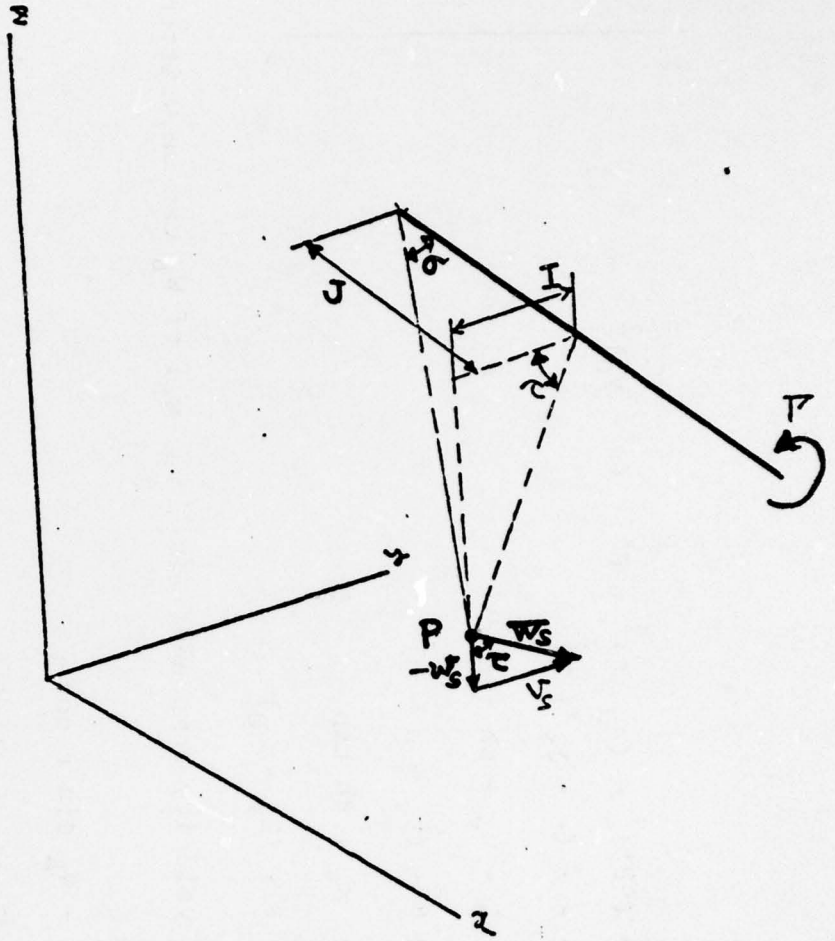

Figure 50. Induced velocity and its components due to a starboard free vortex.

where

$$\cos k = \frac{H}{\sqrt{G^2 + H^2 + Z^2}}$$

$$G = \beta \cdot (y_D - y_v + h)$$

$$H = x_D - x_v + \beta h \tan \mu \qquad (26)$$

thus, the velocity components (u_p, v_p, w_p) of W_p can be written as:

$$u_p = 0$$

$$v_p = - W_p \sin \nu$$

$$w_p = - W_p \cos \nu \qquad (27)$$

where,

$$\sin \nu = \frac{Z}{\sqrt{G^2 + Z^2}}$$

$$\cos \nu = \frac{G}{\sqrt{G^2 + Z^2}}$$

Similarly, the velocity (W_S) induced at P due to a starboard free vortex as shown in Fig. 50 can be written as:

$$W_S = \frac{\Gamma}{4\pi} \frac{1 + \cos \sigma}{\sqrt{I^2 + Z^2}}$$

where,

$$\cos \sigma = \frac{J}{\sqrt{I^2 + J^2 + Z^2}}$$

$$I = \beta (y_v + h - y_D)$$

$$J = x_D - x_v - \beta h \tan \mu \qquad (28)$$

thus, the velocity components (u_S, v_S, w_S) of W_S can be written as:

$$\left.\begin{aligned} u_S &= 0 \\ v_S &= W_S \sin\tau \\ w_S &= W_S \cos\tau \end{aligned}\right\} \qquad (29)$$

where,

$$\sin\tau = \frac{Z}{\sqrt{I^2 + Z^2}}$$

$$\cos\tau = \frac{I}{\sqrt{I^2 + Z^2}}$$

Therefore, the induced velocity components (u, v, w) due to a complete horseshoe vortex is considered as a linear summation of the three vortices mentioned above, and can be written as:

$$\left.\begin{aligned} u &= u_B + u_P + u_S \\ v &= v_B + v_P + v_S \\ w &= w_B + w_P + w_S \end{aligned}\right\} \qquad (30)$$

or,

$$\left.\begin{aligned} u &= -\frac{\Gamma}{4\pi}\frac{\cos\gamma + \cos\phi}{A^2 + Z^2} Z\cos\mu = P\Gamma \\ v &= \frac{\Gamma}{4\pi}\left[\frac{\cos\gamma + \cos\phi}{A^2 + Z^2}\sin\mu - \frac{1 + \cos k}{G^2 + Z^2}\right. \\ &\quad \left. + \frac{\cos\sigma + 1}{I^2 + Z^2}\right] Z = Q\Gamma \\ w &= \frac{\Gamma}{4\pi}\left[\mp\frac{\cos\gamma + \cos\phi}{A^2 + Z^2}\cdot A - \frac{1 + \cos k}{G^2 + Z^2} G\right. \\ &\quad \left. - \frac{\cos\sigma + 1}{I^2 + Z^2} I\right] = R\Gamma \end{aligned}\right\} \qquad (31)$$

The first term in w; $\begin{matrix} - \text{ for } x_D > \xi \\ + \text{ for } x_C < \xi \end{matrix}$

3. Aerodynamic Matrices.

For a planar fin-body configuration geometry, the effect of the horseshoe vortex on the opposite side's fin and the image vortex can be treated in the same way as that mentioned above. Thus, total velocity components at any control point induced by four horseshoe vortices (i.e., two on a pair of fins, and two inside a body) as shown in Fig. 51) can be written as:

$$\left.\begin{aligned} u_i &= \sum_{j=1}^{n} \left(P_{ij}^{(SS)} + P_{ij}^{(PS)} + P_{ij}'^{(SS)} + P_{ij}'^{(PS)}\right) \Gamma_j \\ v_i &= \sum_{j=1}^{n} \left(Q_{ij}^{(SS)} - Q_{ij}^{(PS)} - Q_{ij}'^{(SS)} + Q_{ij}'^{(PS)}\right) \Gamma_j \\ w_i &= \sum_{j=1}^{n} \left(\underbrace{R_{ij}^{(SS)} + R_{ij}^{(PS)}}_{\text{due to a pair of fins' vortices}} + \underbrace{R_{ij}'^{(SS)} - R_{ij}'^{(PS)}}_{\text{due to image vortices inside a body}}\right) \Gamma_j \end{aligned}\right\} \quad (32)$$

where, the superscript (SS) indicates that as well vortex as control point are situated on the starboard side (see Ref. (7)), and,

$P_{ij}^{(PS)} = P_{ij}^{(SS)}$ etc., with $y_D \equiv -y_D$, on the opposite fin

$P_{ij}'^{(PS)} = P_{ij}^{(SS)}$ etc., with $y \equiv \frac{a^2}{y}$ for $0 < y \leq a$, inside a body

It has been assumed, for simplicity, that the bound vortex of an image has the straight line instead of the actual curved line.

By the relation of,

$$\gamma = \frac{\Gamma}{bU_\infty} \quad , \quad (33)$$

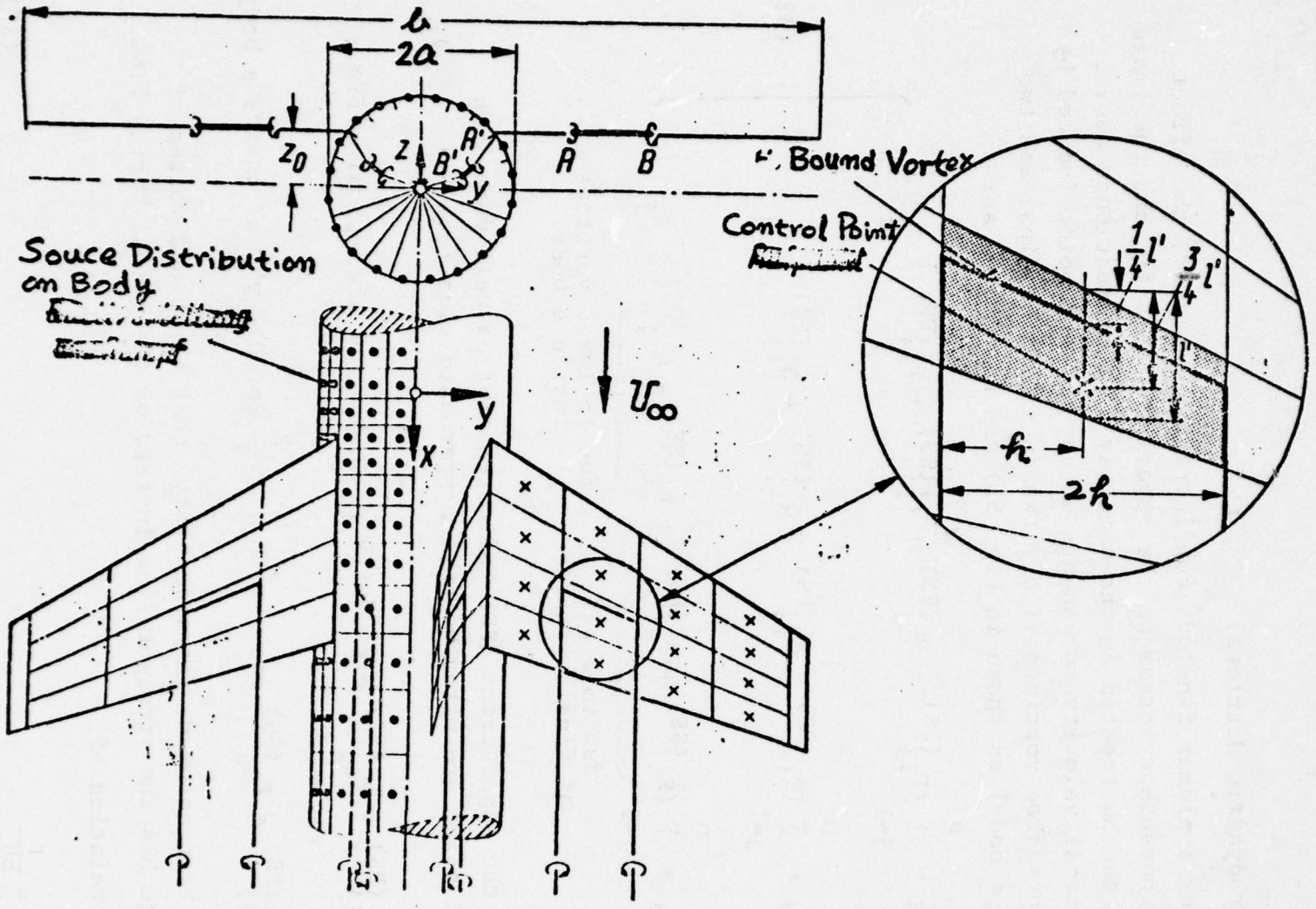

Figure 51. Illustration of wing-body combination with singularities (Refs. [1,3]).

Eq. (32) can be rewritten as:

$$\left.\begin{aligned} \frac{u_i}{U_\infty} &= \sum_{j=1}^{n} \bar{P}_{ij}\, \gamma_j \\ \frac{v_i}{U_\infty} &= \sum_{j=1}^{n} \bar{Q}_{ij}\, \gamma_j \\ \frac{w_i}{U_\infty} &= \sum_{j=1}^{n} \bar{R}_{ij}\, \gamma_j \end{aligned}\right\} \qquad (34)$$

where,

$$\left.\begin{aligned} \bar{P}_{ij} &= b\,\{\, P_{ij}^{(SS)} + P_{ij}^{(PS)} + P'^{(SS)}_{ij} + P'^{(PS)}_{ij} \,\} \\ \bar{Q}_{ij} &= b\,\{\, Q_{ij}^{(SS)} - Q_{ij}^{(PS)} - Q'^{(SS)}_{ij} + Q'^{(PS)}_{ij} \,\} \\ \bar{R}_{ij} &= b\,\{\, R_{ij}^{(SS)} + R_{ij}^{(PS)} + R'^{(SS)}_{ij} - R'^{(PS)}_{ij} \,\} \end{aligned}\right\}$$

APPENDIX 2. COMPUTER PROGRAM FOR DETERMINING PRESSURE DISTRIBUTION ON FIN-BODY COMBINATION

2.1 Program Description

A computer program has been developed to calculate the pressure distribution and aerodynamic characteristics of fin and fin-body combination in subsonic flow. The program is written in FORTRAN IV, and designed for IBM 360 computer, however, it is easily adaptable to other computers with minor modifications.

2.2 Program Structure

The computer program consists of one main overlay program and thirty-one subroutines.

Main Program

The brief outline of the Main program is shown in Fig. 52. The iteration scheme is used only for a fin-body combination to solve a fin-body interaction result.

A considerably detailed expression of the Main program is shown in Fig. 53. The Main program controls almost all subroutines. The effect of the horizontal fin on the vertical fin is computed in the rear part of this Main program.

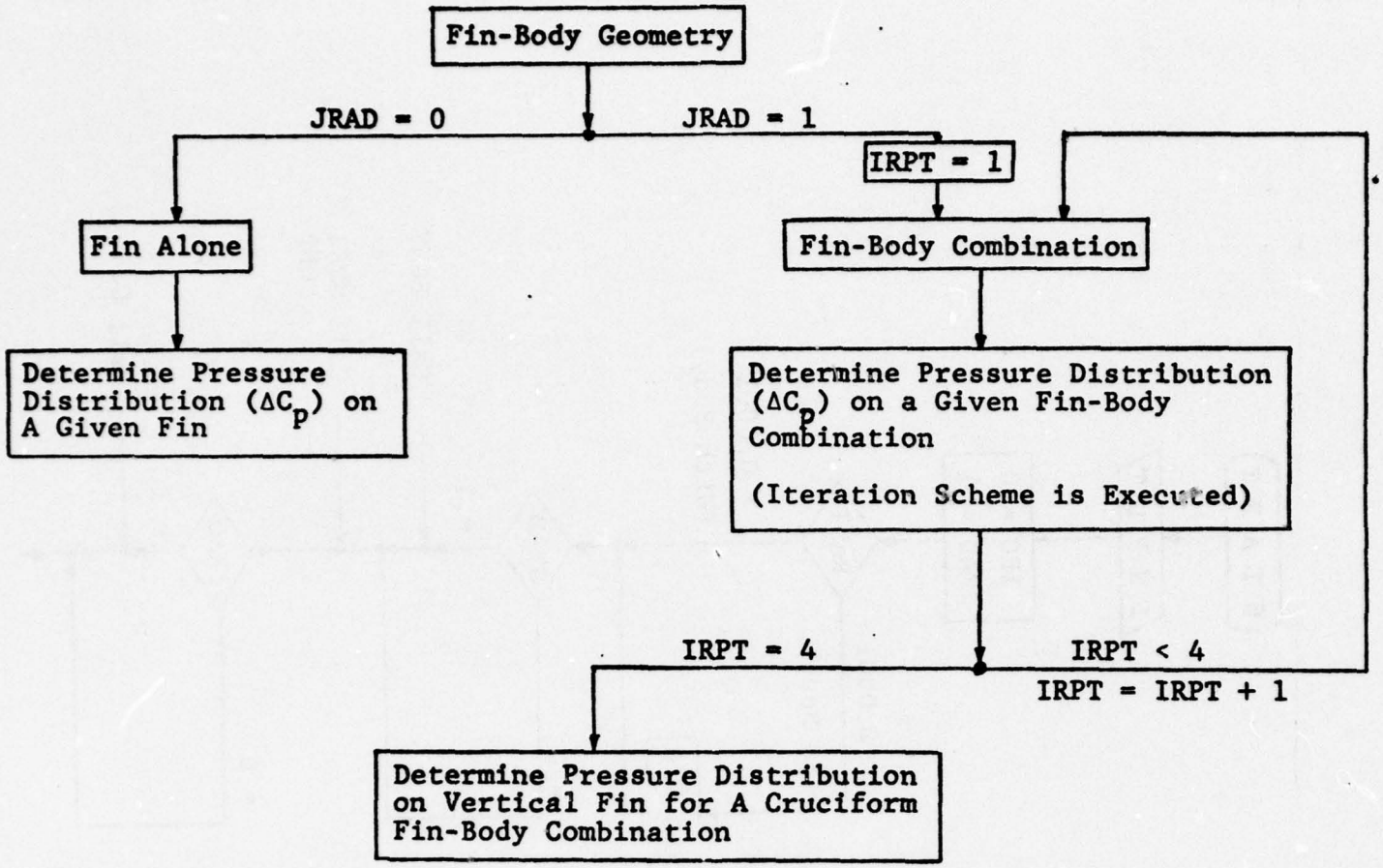

Figure 52. Outline of Main Program.

Aerodynamic Performance of Planar Fin or
Fin-Body Combination Must Be Computed at First.

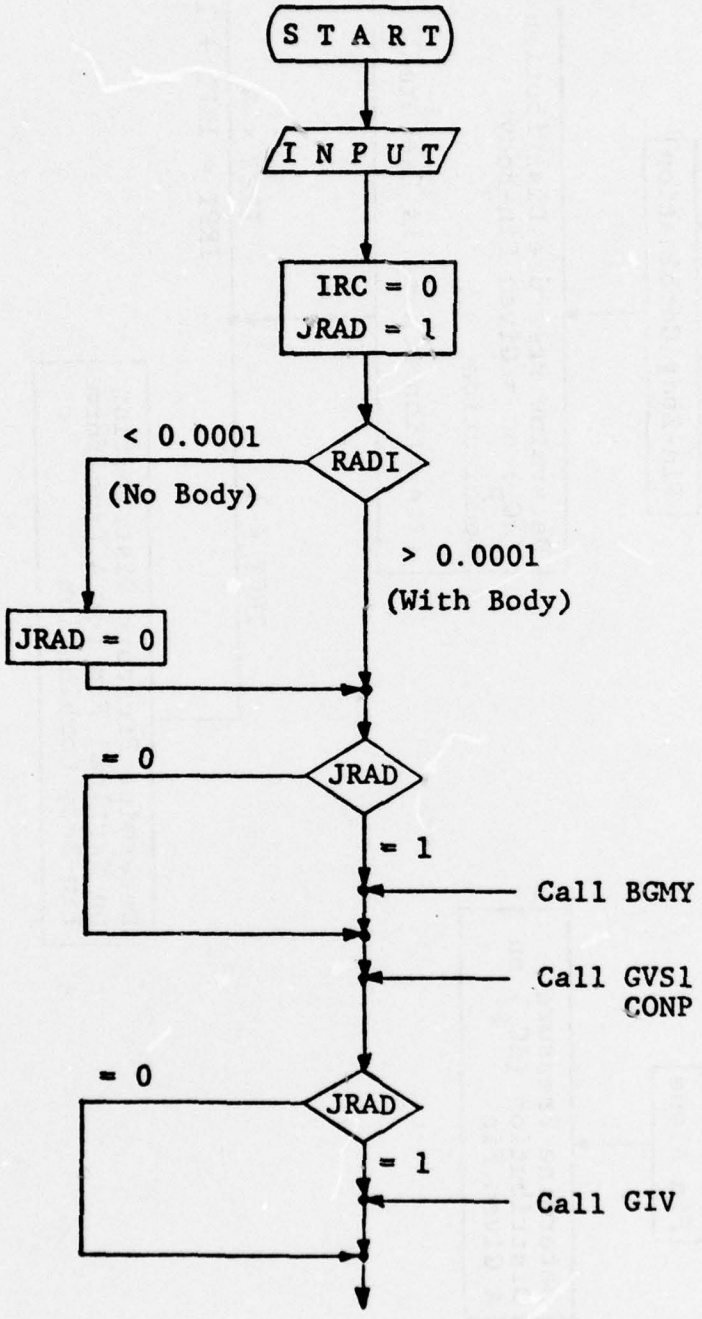

Figure 53. Flow Diagram for MAIN PROGRAM.

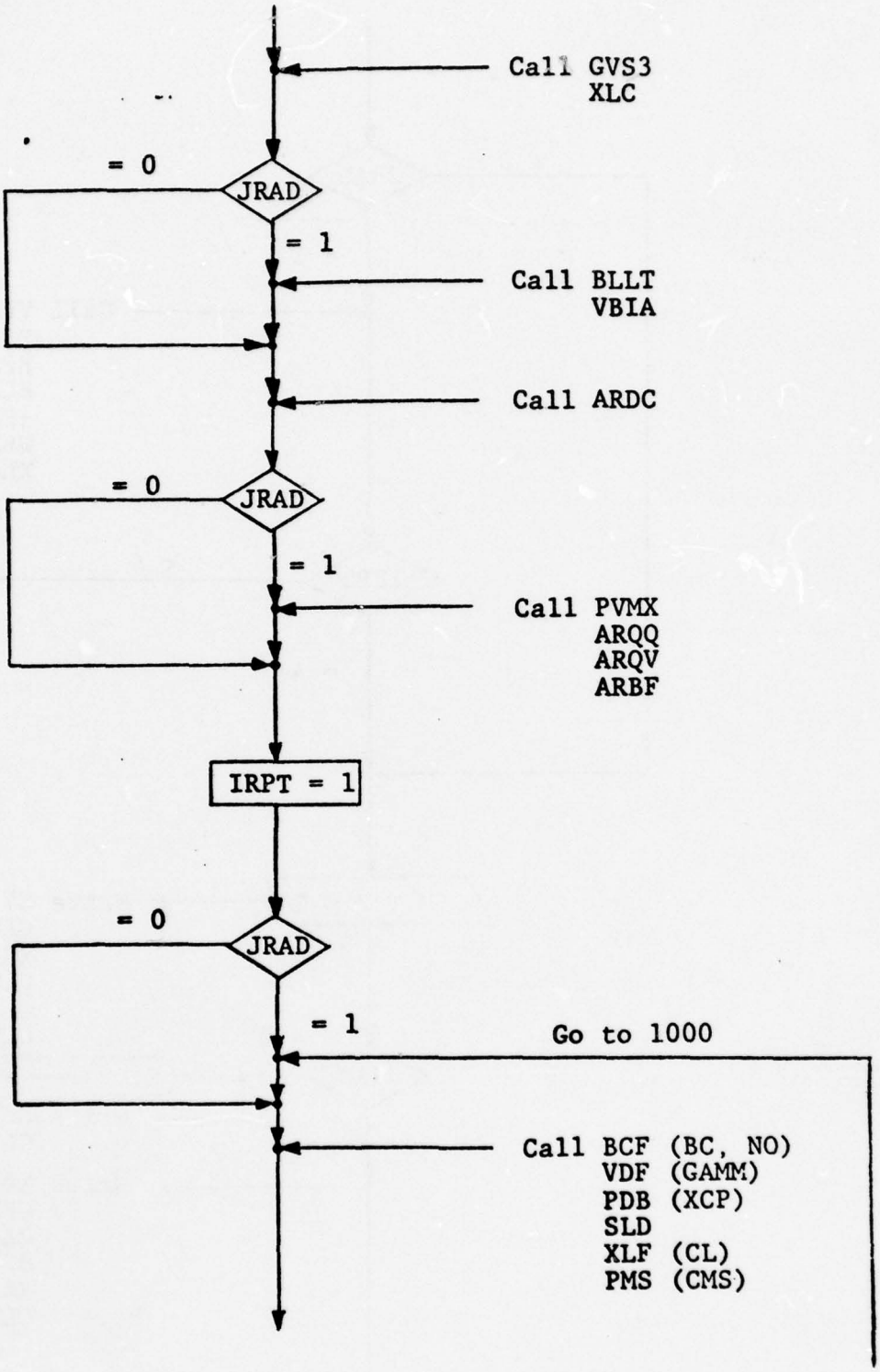

Figure 53. (Continued)

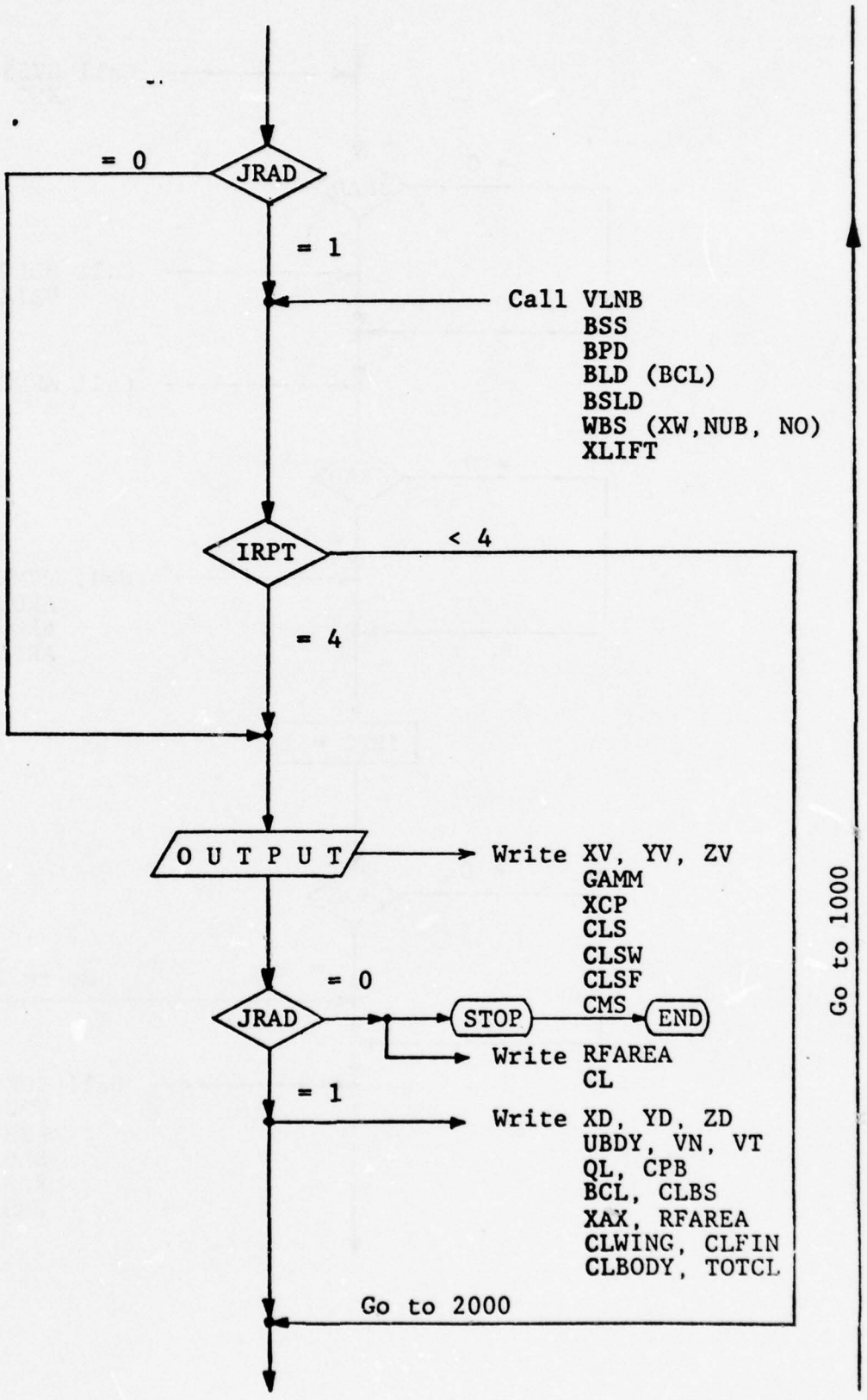

Figure 53. (Continued)

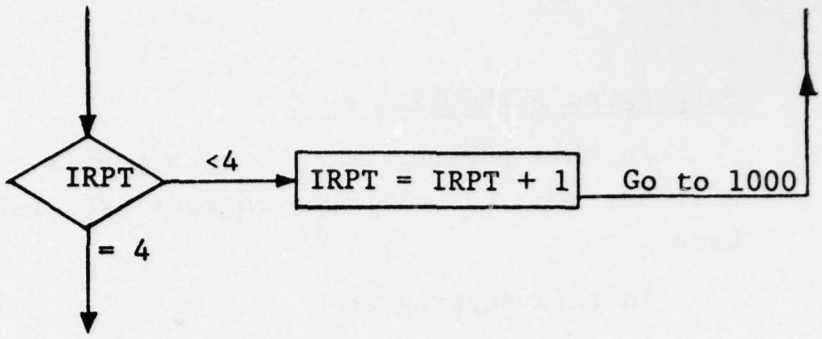

Computation for Aerodynamic Performance of Planar Fin or Fin-Body Combination Terminates. Subsequently, Effects of Horizontal Fin on Vertical Fin is Computed.

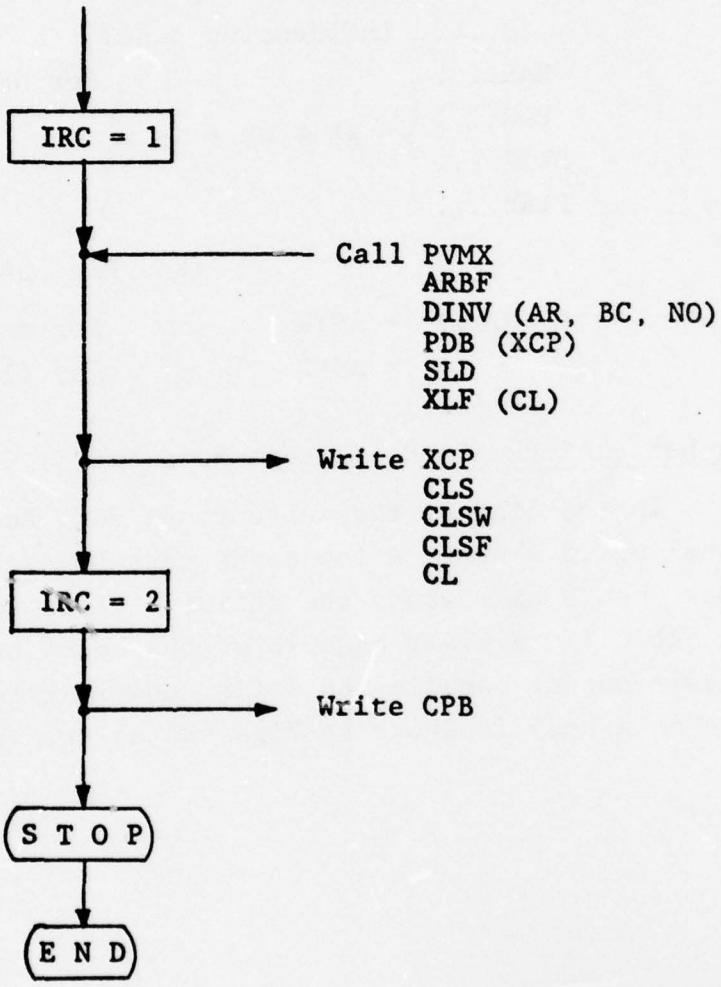

Figure 53. (Concluded)

Subprogram SUBROUTINE ARDC

In this subprogram, the aerodynamic matrices of a fin to fin will be computed. The subprograms PVB, PVP, and PVS are called here.

In this subprogram,

NN = 2, no body
= 4, with body (see Fig. 54)

AR (I,J) = SAR + ASYN * PAR + SIAR + ASYN * PIAR

where, I..... influenced panel
J..... influencing panel

SAR....
PAR....
SIAR....
PIAR.... } = WB + WP + WS { for NN = 1, = 2, = 3, = 4

(see Fig. 54)

ASYN.... = ASYW for main fin or wing
= ASYF for flap or elevon

Exchange of the Cards (except Data cards)

In the list of the subroutines BGMY and GVS1, the cosine paneling is shown. A few cards must be exchanged by the suitable ones when a user wants the equidistant paneling. They are shown in Table 1. A clear example of the spanwisely equidistant, chordwisely cosine paneling on a fin, and longitudinally cosine paneling on a body is shown in Figs. 28(a) and (b).

TABLE 1. EXCHANGE OF THE CARDS

SUBROUTINE	Line No.	Cosine Paneling	Equidistant Paneling
BGMY	0025	10 XN(J1+1)=XP+ABS(X1-XP)*SIN(AZ1*J1)	10 XN(J1+1) = XN(J1) + ABS(X1-XP)/NBF
	0029	20 XN(NBF+J2+1)=X1+ABS(X3-X1)*(1.-COS(AZ2*J2))/2	20 XN(NBF+J2+1)=XN(NBF+J2)+ABS(X3-X1)/NBM
	0034	30 XN(NB1+J3)=X3+ABS(XQ-X3)*(1.-COS(AZ3*J3))	30 XN(NB1+J3) = XN(NB1+J3-1)+ABS(XQ-X3)/NBB
GVS1	0017	YF(JC+1)=Y1 +(Y2-Y1)*(1.-COS(JC*PI/M))/2.	YF(JC+1)=Y1+(Y2-Y1)*JC/M
	0038	DK(K+1)=1.-COS(THW1*XK)	DK(K+1) = DK(K) + 1./N
	0056	DK(K+1)=1.-COS(THF1*XK)	DK(K+1) = DK(K) + 1./NFLP

2.3 List of Subprograms

All the subprogram SUBROUTINEs and their purposes are shown in Table 2. Most of them are controlled by the Main program.

2.4 List of Symbols

The symbols and their meanings used in the Main program and SUBROUTINEs are shown in Table 3.

TABLE 2

LISTS OF SUBPROGRAMS

NAME	PURPOSE
GVS 1	Defining location of control points on the fin, and half width of local bound vortex.
BGMY	Defining body control points (which also equals to location of body sources).
CONP	Naming location of total control points on fin-body combination.
GIV	Computing location and slope of body image vortex.
GVS 2 (SX, SY, TMU)	Computing interception at S. (See Fig. 48.)
PVB (UB, VB, WB)	Computing normalized perturbation velocity components induced by bound vortex.
PVP (UP, VP, WP)	Computing normalized perturbation velocity component induced by port free vortex.
PVS (US, VS, WS)	Computing perturbation velocity component induced by starboard free vortex.
BCF (XB, N3)	Defining initial angle of attack of fin, and induced angle of attack due to angle of incidence of body (when it is not zero) and distributed sources on body.
ARDC	Computing aerodynamic matrices of fin only.

Table 2. Lists of SUBPROGRAMS (Continued)

NAME	PURPOSE
VDF (GAMM)	Compute circulation strength (i.e., solve the simultaneous linear eqs.).
GVS 3	Computing local fin panel area, reference fin area, and reference chord.
XLC	Computing local chord of fin.
BLLT	Computing local chord length of fin provided that fin was extended into body.
DINV (D, E, N)	Solving the simultaneous linear equation.
PDB (XCP)	Computing pressure distribution (ΔC_p) on fin.
SLD	Computing spanwise lift distribution based on local fin chord.
XLF (CL)	Computing lift coefficient of fin based on reference area (RFAREA).
PMS (CMS)	Computing spanwise moment distribution around 25% local chord based on local chord CLL and XAX.
PVMX	Computing perturbation velocity component on body due to unit circulation of fin.
VLNB	Computing perturbation velocity components on body.
BPD	Computing pressure distribution (C_p) on body.
ARQQ	Computing pressure distribution on body due to unit source strength.

Table 2. Lists of SUBPROGRAMS (Continued)

NAME	PURPOSE
BLD (BCL)	Computing pressure distribution (ΔC_p) on body.
BSS	Computing source strength on body.
ARQV	Computing body source strength for m^{th} iteration.
WBS (XW, N1, N2)	Computing normalized downwash on fin induced by body source.
ARBF	Computing normalized downwash on fin induced by body unit source.
BSLD	Computing spanwise lift distribution on body based on local chord of fin, supposed to be extended into body.
VBIA	Computing angle of attack on fin induced by angle of incidence of body.
XLIFT	Computing lift coefficient of total fin-body combination.

TABLE 3

LIST OF SYMBOLS

*: Control parameter. Integer inside of ( ) denotes dimensions.

SYMBOLS	MEANINGS
BD (56)	(Equivalent to XB in SUBPROGRAM BCF.) Apparent angle of attack of local panel.
XW (56)	Normalized component of induced velocity on local panel due to body source.
GAMM (55)	Circulation strength of local panel
XREF (10)	X-coordinate for 25% local chord of fin.
XCP (55)	Pressure difference (ΔC_p) on local panel of fin.
CMS (10)	Spanwise moment distribution around 25% local chord, based on local chord of fin.
BCL (36)	Pressure difference (ΔC_p) on body.
RADI	Radius of body (= constant in present analysis).
CPB (72)	Pressure coefficient (C_p) on body.
AR (56, 56)	Aerodynamic influence matrix for fin only.
AQ (72, 72)	Perturbation velocity component (x-direction) on body due to body source ($(C_p)_B = -2(u + u_s)/\beta^2$, see SUBPROGRAM BPD).
ASV (72,72)	$= \frac{1}{2\pi} \frac{\left[1-\cos(\theta_\mu-\theta_\nu) \right] \beta a \Delta S_\nu}{\left[(x_\mu-x_\nu)^2 + \beta^2 \{ 1-\cos(\theta_\mu-\theta_\nu) \} a^2 \right]^{3/2}}$ (See Eq. (10).)

Table 3. List of Symbols (Continued)

SYMBOLS	MEANINGS
AFN (72,55)	Coefficient for determining induced velocity (w-component) on fin due to unit source strength on body.
MB	Circumferential division number along half body.
NB	= NBF + NBM + NBB.
NUB	= NB x MB; total panel numbers on half body.
PSA (55)	Local panel area (includes compressible effect).
BREF (5)	Local chord of fin, provided extending into body.
XDV (55)	= XG - SV; 1/2 local panel chord through its center in present analysis.
YVI (55)	Y - location of center of bound vortex for body image.
WHI (55)	Half width of body image vortex.
TLMDI (55)	Slope (or gradient) of bound vortex of body image.
NBF, NBM, NBB	Longitudinal division numbers on body for forward (ahead of L. E. of fin location), middle (at fin location), and backward (aft of it), respectively.
FDL	See Fig. 56(a).
BDL	See Fig. 56(a).
ALFAB	Angle of attack of body (degrees).

Table 3. List of Symbols (Continued)

SYMBOLS	MEANINGS
XBW (55)	Additive angle of attack of local panel of fin due to body angle of attack.
*JRAD	Control integer. See Figs. 52, 53.
AREAB (96)	Local panel area on body surface.
UBDY (72)	Induced velocity (u-component) at control point on body.
VN (72)	Induced velocity component normal to body surface due to circulation of fin.
QL (72)	Source strength per unit body surface area.
*ASYF *ASYW	} Control variables. See 2.2 Input Data Cards.
CLL (55)	Local chord length (= XC3 - XC1).
BCL	Load distribution on body.
M1	= MB/2.
NFLP	Chordwise division number for flap or elevon.
NT	= N + NFLP.
NW	= M x N.
AFLAP	Flap or elevon deflection (degrees).
*IRPT	Control integer. (See Figs. 52, 53).
X1, Y1...X6, Y6	See Fig. 55(a).
M	Spanwise division number for main fin.
N	Chordwise division number for main fin.

Table 3. - List of Symbols (Continued)

SYMBOLS	MEANINGS
XM	Free stream Mach number.
ALFAF	Angle of attack for fin (degrees).
NO	M x NT (total panel number for half fin).
PI	Constant (= 3.14159).
BETA	$= \sqrt{1 - M_\infty^2}$
SPN	(= Y 2)
XC1 (55)	Location in x-direction of intercept points. See Fig. 55(c).
XC2 (5)	
XC3 (5)	
ABU (72,55)	Induced velocity components at control point on fin, due to circulation of fin.
ABV (72,55)	
ABW (72,55)	
XL (10)	XC2 - XC1. See Fig. 55(c).
NTOT	= NO + NUB, total panel number.
XG (55)	Location of control point on fin.
YG (55)	
ZG (55)	
XS (72)	Location of source distribution on body (= location of control point on body).
TS (127)	Angular position for source (thus, control point) on body (radian).

Table 3. List of Symbols (Continued)

SYMBOLS	MEANINGS
XD (127) YD (127) ZD (127)	Location of control point of local panel of fin-body combination.
XV (55), YV (55), ZV (55)	Location of middle of bound vortex on local panel of fin.
WH (55)	Half width of local panel on fin.
TLMD (55)	Slope of local bound vortex. See Fig. 55(b).
YF	Y - location of local panel edges. See Fig. 55(b).
RFAREA	Reference area for C_L.
XAX	Maximum chord length of fin, reference chord.
DT	Circumferential length of local body panel.
*IRC	Control integer. See Fig. 53.
DX (96)	Longitudinal length of local body panel.
CLS (5)	Spanwise lift distribution for wing + fin based on CLL.
CLSW (5)	Spanwise lift distribution for wing, based on CLL.
CLSF (5)	Spanwise lift distribution for fin, based on CLL.
CLBS (5)	Spanwise lift distribution on body, based on BREF.

Table 3. List of Symbols (Continued)

SYMBOLS	MEANINGS
CLWING	C_L for wing or main fin, based on reference area (RFAREA)
CLFIN	C_L for flap or elevon, based on reference area (RFAREA).
CLBODY	C_L for body, based on RFAREA.
TOTCL	Total C_L $(= (C_L)_{wing} + (C_L)_{fin} + (C_L)_{body})$

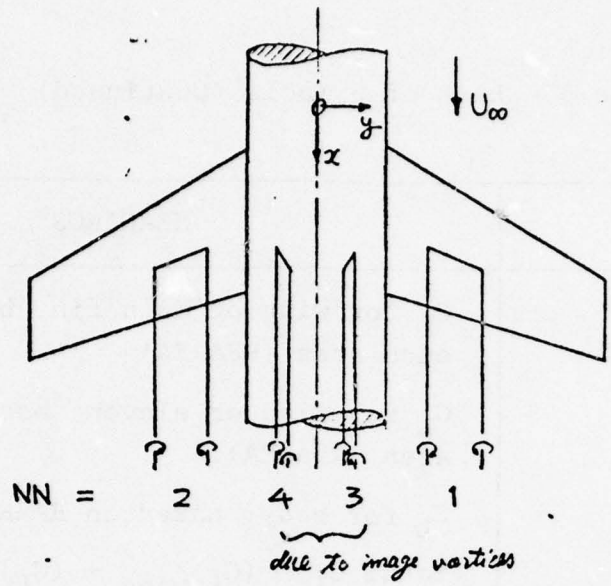

Figure 54. Fin vortices and its images.

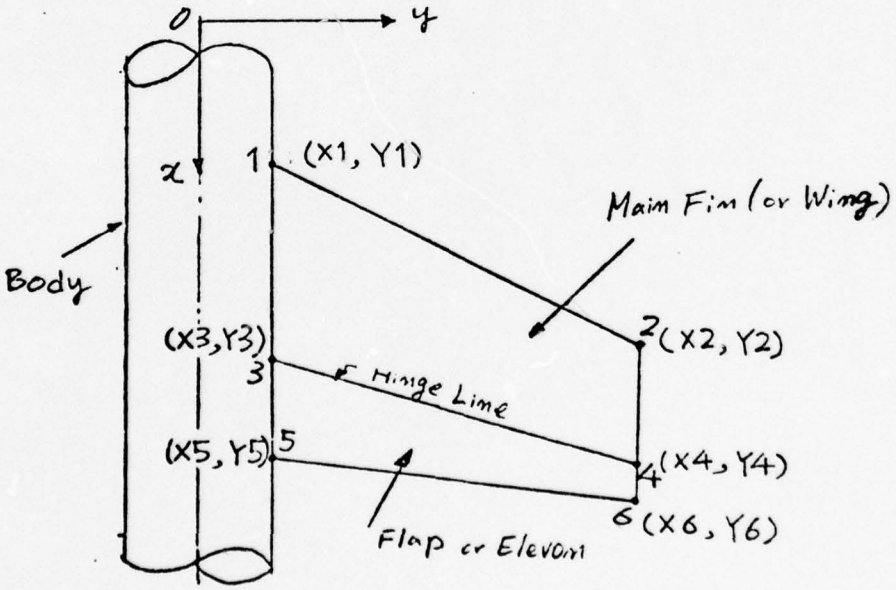

Figure 55a. Fin-body geometry coordinate input.

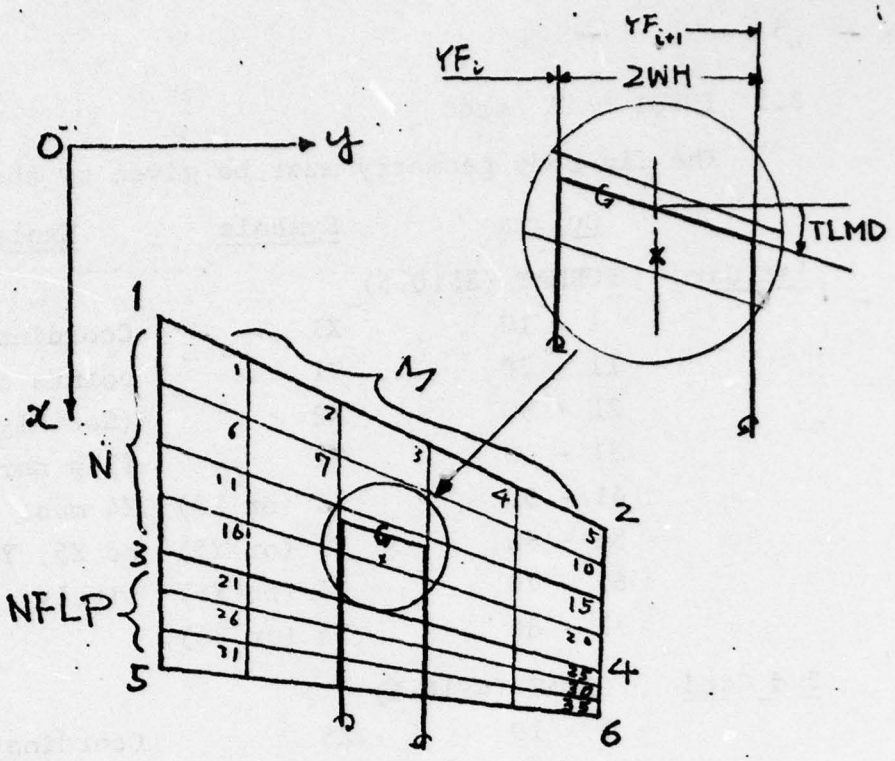

Figure 55b. Fin panel division number and named panels (the above figure shows total 35 panels case).

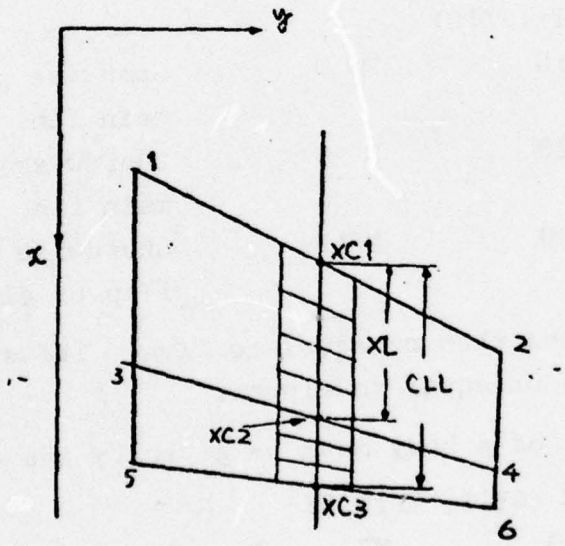

Figure 55c. Local chord definition.

2.5 INPUT DATA Cards

The fin-body geometry must be given by the 1st and 2nd cards.

	Column	Symbols	Explanation
1st Card	FORMAT (8F10.5)		
	1 - 10	X1	Coordinate of the corner points of main fin or wing. (See Fig. 55(a).) If no flap nor elevon, X3, Y3, X4, Y4 must be the same values as X5, Y5, X6, Y6, respectively.
	11 - 20	Y1	
	21 - 30	X2	
	31 - 40	Y2	
	41 - 50	X3 (or X5)	
	51 - 60	Y3 (or Y5)	
	61 - 70	X4 (or X6)	
	71 - 80	Y4 (or Y6)	
2nd Card	FORMAT (4F10.5)		
	1 - 10	X5	Coordinate of the corner points of a flap or an elevon.
	11 - 20	Y5	
	21 - 30	X6	
	31 - 40	Y6	

Panel number of a fin must be given by the 3rd card.

3rd Card	FORMAT (3I10)		
	1 - 10	M	Spanwise panel number of main fin. (See Fig. 55(b).)
	11 - 20	N	Chordwise panel number of main fin.
	21 - 30	NFLP	Chordwise panel number of flap or elevon.

M must be less than or equal to five. The sum of N and NFLP must be less than or equal to eleven.

Panel number of a body must be given by the 4th card.

4th Card	FORMAT (4I10, 2F10.5)		
	1 - 10	MB	Circumferential panel number. (See Fig. 56(a).)
	11 - 20	NBF	Longitudinal panel number for front part.
	21 - 30	NBM	Longitudinal panel number for middle part.
	31 - 40	NBB	Longitudinal panel number for aft part.

4th Card (Continued) --

41 - 50	FDL	Front part length/(X3-X1).
51 - 60	BDL	Aft part length/(X3-X1).

MB must be six. Total sum of NBF, NBM, and NBB must be less than or equal to twelve.

Aerodynamic Input must be given by the 5th card.

5th Card FORMAT (6F10.5)

1 - 10	XM	Free stream Mach number. (See Fig. 57.)
11 - 20	ALFAF	Angle-of-attack of main fin or wing.
21 - 30	ALFAB	Body Angle-of-attack.
31 - 40	AFLAP	Angle-of-attack of flap or elevon.
41 - 50	ASYW	= 1. for symmetrical flow of main fin or wing; = -1. for asymmetrical flow of main fin or wing.
51 - 60	ASYF	= 1. for symmetrical flow of flap or elevon. = -1. for asymmetrical flow of flap or elevon.

XM must be less than 1.0. Only when ALFAB equals to zero, ASYW and/or ASYF can take -1.0. Nonetheless that ASYW and/or ASYF equal to 1.0 or -1.0, the same amount of angle-of-attack of a pair of fins must be taken, thus the case that the right hand side of a pair of fins has angle-of-attack of 5^{o}, and the left has 3^{o}, cannot be allowed.

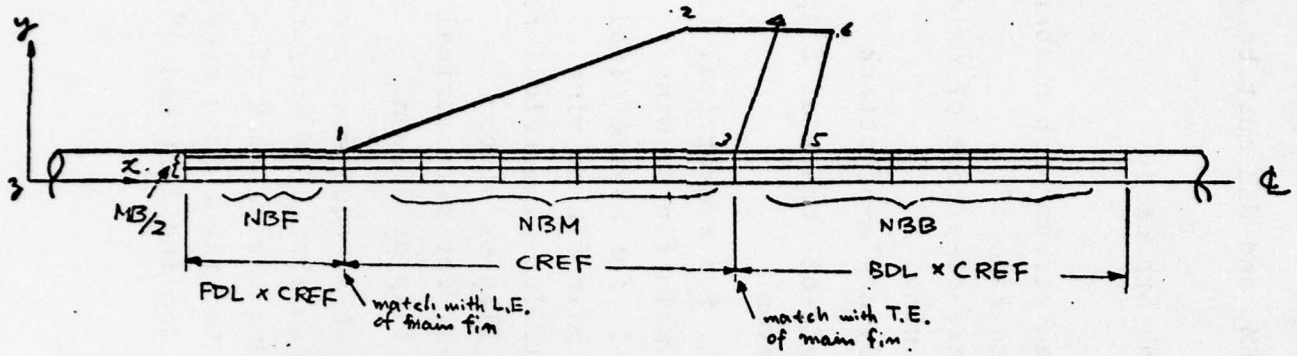

Figure 56a. Body paneling (for equidistance case).

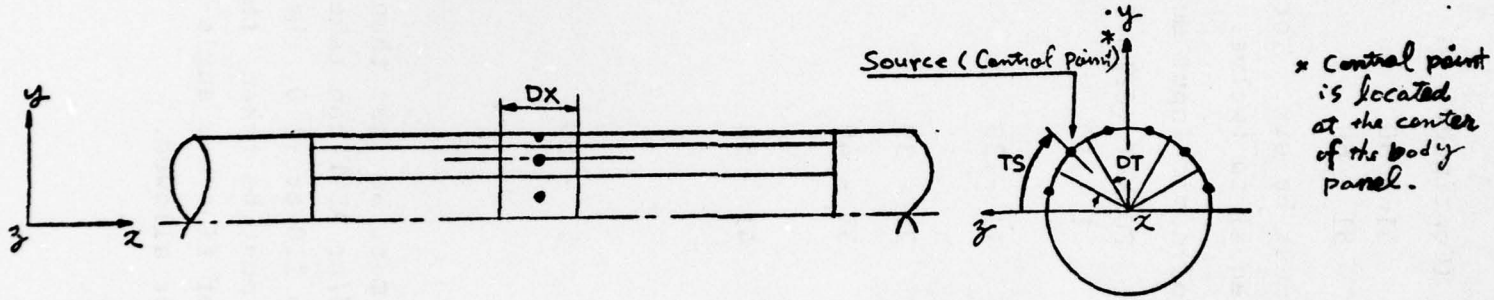

Figure 56b. Body paneling and body control point.

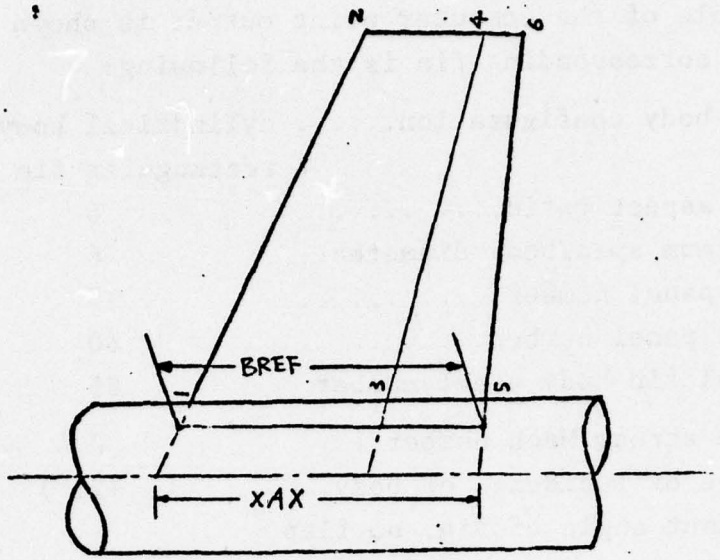

Figure 56c. Fin extended into body.

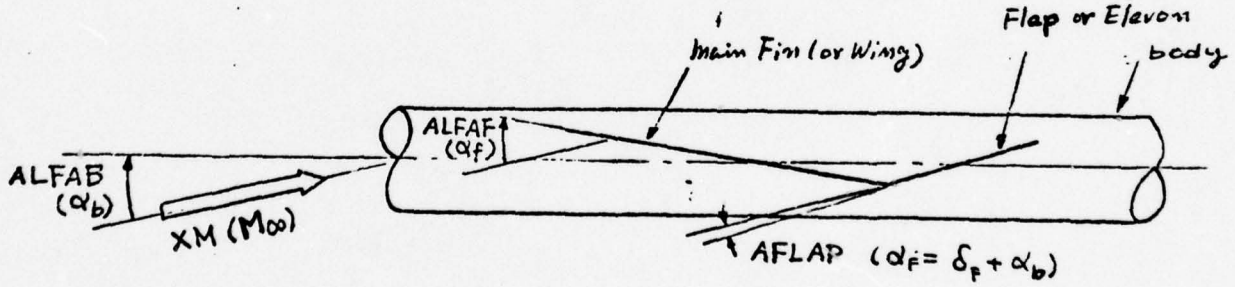

Figure 57. Aerodynamic input of fin-body combination

2.6 Program Output

One example of the computer print output is shown in Table 4. The corresponding fin is the following:

Fin-body configuration.....	cylindrical body with rectangular fin
Fin aspect ratio.....	6
Maximum span/body diameter..	6
Fin panel number.....	25
Body panel number.....	60
Total fin-body panel number.	85
Free stream Mach number.....	0.4
Angle of incidence of body..	+2(^{o})
No cant angle of fin, no flap	

Remark: Note that WING CL, FIN CL, BODY CL, and TOTAL CL in Output are half values of the correct ones, thus these values have to be multiplied by <u>two</u> to obtain correct CL based on reference area (also, see SUBROUTINE XLIFT). CL for fin only is also in the same thing.

TABLE 4. EXAMPLE OF COMPUTER OUTPUT

```
COMPUTATION FOR SURFACE PRESSURE DISTRIBUTION ON FIN-BODY COMBINATION AT SUBSONIC SPEEDS

FIN-BODY GEOMETRY ..........

   X1      Y1      X2      Y2      X3      Y3      X4      Y4      X5      Y5      X6      Y6
  0.0     0.500   0.0     3.000   1.000   0.500   1.000   3.000   1.000   0.500   1.000   3.000

FIN-BODY PANEL NUMBER .....

M =  5  N =  5  NFLP =  0  NW = 25  NO = 25

MB =  6  NBF =  3  NBM =  4  NBB =  3  NB = 10  NUB =  60
FDL =  0.50  BDL =  1.00     TOTAL PANEL =  85

MACH NO =  0.400  ANGLE OF INCIDENCE =  2.00 (DEG)  FIN ANGLE OF ATTACK =  2.00 (DEG)
FLAP ANGLE OF ATTACK =  2.00 (DEG)  FIN SYNMETRY =  1.00  FLAP SYNMETRY =  1.00

REFERENCE CHORD ..........

 ON BODY .....

                    1               2               3
 BREF(I) =  0.10000E 01     0.10000E 01     0.10000E 01

ON FIN .....

                    1               2               3               4               5
 XL(I)   =  0.10000E 01     0.10000E 01     0.10000E 01     0.10000E 01     0.10000E 01
 CLL(I)  =  0.10000E 01     0.10000E 01     0.10000E 01     0.10000E 01     0.10000E 01
 XC1(I)  =  0.0             0.0             0.0             0.0             0.0
 XC2(I)  =  0.10000E 01     0.10000E 01     0.10000E 01     0.10000E 01     0.10000E 01
 XC3(I)  =  0.10000E 01     0.10000E 01     0.10000E 01     0.10000E 01     0.10000E 01

ITERATION =  4
```

PRESSURE DISTRIBUTION ON PLANAR FIN .....

NO	XV	YV	ZV	XNR	YNR	GAMMA	XCP
1	0.12236E-01	0.61936E 00	0.0	0.12236E-01	0.20645E 00	0.37426E-02	0.10924E 01
2	0.12236E-01	0.10512E 01	0.0	0.12236E-01	0.35041E 00	0.33271E-02	0.97112E 00
3	0.12236E-01	0.17500E 01	0.0	0.12236E-01	0.58333E 00	0.29734E-02	0.86789E 00
4	0.12236E-01	0.24488E 01	0.0	0.12236E-01	0.81626E 00	0.25238E-02	0.73666E 00
5	0.12236E-01	0.28806E 01	0.0	0.12236E-01	0.96021E 00	0.18182E-02	0.53070E 00
6	0.84453E-01	0.61936E 00	0.0	0.84453E-01	0.20645E 00	0.41028E-02	0.41265E 00
7	0.84453E-01	0.10512E 01	0.0	0.84453E-01	0.35041E 00	0.38894E-02	0.38615E 00
8	0.84453E-01	0.17500E 01	0.0	0.84453E-01	0.58333E 00	0.34458E-02	0.34657E 00
9	0.84453E-01	0.24488E 01	0.0	0.84453E-01	0.81626E 00	0.28804E-02	0.28970E 00
10	0.84453E-01	0.28806E 01	0.0	0.84453E-01	0.96021E 00	0.19053E-02	0.19163E 00
11	0.24629E 00	0.61936E 00	0.0	0.24629E 00	0.20645E 00	0.32314E-02	0.20867E 00
12	0.24629E 00	0.10512E 01	0.0	0.24629E 00	0.35041E 00	0.32413E-02	0.20930E 00
13	0.24629E 00	0.17500E 01	0.0	0.24629E 00	0.58333E 00	0.29380E-02	0.18972E 00
14	0.24629E 00	0.24488E 01	0.0	0.24629E 00	0.81626E 00	0.23750E-02	0.15336E 00
15	0.24629E 00	0.28806E 01	0.0	0.24629E 00	0.96021E 00	0.13974E-02	0.90236E-01
16	0.48191E 00	0.61936E 00	0.0	0.48191E 00	0.20645E 00	0.23247E-02	0.11913E 00
17	0.48191E 00	0.10512E 01	0.0	0.48191E 00	0.35041E 00	0.23842E-02	0.12218E 00
18	0.48191E 00	0.17500E 01	0.0	0.48191E 00	0.58333E 00	0.21855E-02	0.11200E 00
19	0.48191E 00	0.24488E 01	0.0	0.48191E 00	0.81626E 00	0.16992E-02	0.87076E-01
20	0.48191E 00	0.28806E 01	0.0	0.48191E 00	0.96021E 00	0.95491E-03	0.48935E-01
21	0.76824E 00	0.61936E 00	0.0	0.76824E 00	0.20645E 00	0.13344E-02	0.61689E-01
22	0.76824E 00	0.10512E 01	0.0	0.76824E 00	0.35041E 00	0.13941E-02	0.64449E-01
23	0.76824E 00	0.17500E 01	0.0	0.76824E 00	0.58333E 00	0.12829E-02	0.59308E-01
24	0.76824E 00	0.24488E 01	0.0	0.76824E 00	0.81626E 00	0.97063E-03	0.44872E-01
25	0.76824E 00	0.28806E 01	0.0	0.76824E 00	0.96021E 00	0.54850E-03	0.25357E-01

SPANWISE LIFT AND MOMENT DISTRIBUTION .....

	1	2	3	4	5
CLS(I) =	0.21051E 00	0.20266E 00	0.18322E 00	0.14927E 00	0.94633E-01
CLSW(I) =	0.21051E 00	0.20266E 00	0.18322E 00	0.14927E 00	0.94633E-01
CLSF(I) =	0.0	0.0	0.0	0.0	0.0
CMS(I) =	-0.50055E-02	-0.23326E-02	-0.16661E-02	-0.26952E-02	-0.35314E-02

Reproduced from best available copy.

PRESSURE DISTRIBUTION ON BODY ••••••••••

NO	XD	YD	ZD	UBDY	VN	VT	QL	CPB
26	-0.37500E 00	0.12941E 00	0.48296E 00	0.10009E-01	0.85831E-02	-0.21149E-02	-0.15401E-01	-0.28372E-01
27	-0.37500E 00	0.35355E 00	0.35355E 00	0.96993E-02	0.85046E-02	-0.80122E-02	-0.15984E-01	-0.28005E-01
28	-0.37500E 00	0.48296E 00	0.12941E 00	0.51997E-02	0.46381E-02	-0.16680E-01	-0.92072E-02	-0.15564E-01
29	-0.37500E 00	0.48296E 00	-0.12941E 00	-0.51996E-02	-0.46380E-02	-0.16680E-01	0.92071E-02	0.15564E-01
30	-0.37500E 00	0.35355E 00	-0.35355E 00	-0.96993E-02	-0.85046E-02	-0.80123E-02	0.15984E-01	0.28005E-01
31	-0.37500E 00	0.12941E 00	-0.48296E 00	-0.10009E-01	-0.85831E-02	-0.21149E-02	0.15401E-01	0.28372E-01
32	-0.15849E 00	0.12941E 00	0.48296E 00	0.15468E-01	0.80508E-02	-0.14694E-02	-0.14110E-01	-0.32252E-01
33	-0.15849E 00	0.35355E 00	0.35355E 00	0.18411E-01	0.94835E-02	-0.75085E-02	-0.17683E-01	-0.40950E-01
34	-0.15849E 00	0.48296E 00	0.12941E 00	0.17453E-01	0.83412E-02	-0.28302E-01	-0.16749E-01	-0.42574E-01
35	-0.15849E 00	0.48296E 00	-0.12941E 00	-0.17453E-01	-0.83411E-02	-0.28303E-01	0.16749E-01	0.42574E-01
36	-0.15849E 00	0.35355E 00	-0.35355E 00	-0.18411E-01	-0.94835E-02	-0.75085E-02	0.17683E-01	0.40950E-01
37	-0.15849E 00	0.12941E 00	-0.48296E 00	-0.15468E-01	-0.80509E-02	-0.14694E-02	0.14110E-01	0.32252E-01
38	-0.33494E-01	0.12941E 00	0.48296E 00	0.18662E-01	0.60597E-02	-0.34533E-03	-0.10547E-01	-0.34006E-01
39	-0.33494E-01	0.35355E 00	0.35355E 00	0.24991E-01	0.75131E-02	-0.36780E-02	-0.13989E-01	-0.49672E-01
40	-0.33494E-01	0.48296E 00	0.12941E 00	0.45816E-01	0.95395E-02	-0.29323E-01	-0.19139E-01	-0.10415E 00
41	-0.33494E-01	0.48296E 00	-0.12941E 00	-0.45816E-01	-0.95395E-02	-0.29323E-01	0.19139E-01	0.10415E 00
42	-0.33494E-01	0.35355E 00	-0.35355E 00	-0.24991E-01	-0.75132E-02	-0.36780E-02	0.13989E-01	0.49672E-01
43	-0.33494E-01	0.12941E 00	-0.48296E 00	-0.18662E-01	-0.60597E-02	-0.34533E-03	0.10547E-01	0.34006E-01
44	0.38066E-01	0.12941E 00	0.48296E 00	0.20000E-01	0.43298E-02	0.55599E-03	-0.74660E-02	-0.29619E-01
45	0.38066E-01	0.35355E 00	0.35355E 00	0.27780E-01	0.51514E-02	0.94633E-04	-0.95323E-02	-0.46214E-01
46	0.38066E-01	0.48296E 00	0.12941E 00	0.62951E-01	0.51048E-02	-0.97593E-02	-0.10204E-01	-0.13082E 00
47	0.38066E-01	0.48296E 00	-0.12941E 00	-0.62952E-01	-0.51048E-02	-0.97594E-02	0.10204E-01	0.13082E 00
48	0.38066E-01	0.35355E 00	-0.35355E 00	-0.27780E-01	-0.51514E-02	0.94610E-04	0.95323E-02	0.46215E-01
49	0.38066E-01	0.12941E 00	-0.48296E 00	-0.20000E-01	-0.43298E-02	0.55600E-03	0.74660E-02	0.29619E-01
50	0.18451E 00	0.12941E 00	0.48296E 00	0.20892E-01	0.22249E-03	0.26448E-02	-0.60963E-04	-0.36517E-01
51	0.18451E 00	0.35355E 00	0.35355E 00	0.26694E-01	-0.50153E-03	0.88983E-02	0.12217E-02	-0.55985E-01
52	0.18451E 00	0.48296E 00	0.12941E 00	0.50302E-01	-0.25648E-02	0.25084E-01	0.53028E-02	-0.11293E 00
53	0.18451E 00	0.48296E 00	-0.12941E 00	-0.50302E-01	0.25648E-02	0.25084E-01	-0.53028E-02	0.11293E 00

54	0.18451E 00	0.35355E 00	-0.35355E 00	-0.28694E-01	0.50155E-03	0.88983E-02	-0.12217E-02	0.55985E-01
55	0.18451E 00	0.12941E 00	-0.48296E 00	-0.20892E-01	-0.22249E-03	0.26449E-02	0.60954E-04	0.36517E-01
56	0.45510E 00	0.12941E 00	0.48296E 00	0.17429E-01	-0.55169E-02	0.56840E-02	0.10124E-01	-0.33551E-01
57	0.45510E 00	0.35355E 00	0.35355E 00	0.21237E-01	-0.63250E-02	0.19251E-01	0.12191E-01	-0.44352E-01
58	0.45510E 00	0.48296E 00	0.12941E 00	0.29278E-01	-0.41329E-02	0.37880E-01	0.83853E-02	-0.67407E-01
59	0.45510E 00	0.48296E 00	-0.12941E 00	-0.29278E-01	0.41328E-02	0.37881E-01	-0.83852E-02	0.67408E-01
60	0.45510E 00	0.35355E 00	-0.35355E 00	-0.21237E-01	0.63250E-02	0.19251E-01	-0.12191E-01	0.44352E-01
61	0.45510E 00	0.12941E 00	-0.48296E 00	-0.17429E-01	0.55169E-02	0.56841E-02	-0.10124E-01	0.33551E-01
62	0.80866E 00	0.12941E 00	0.48296E 00	0.10614E-01	-0.77821E-02	0.73034E-02	0.14266E-01	-0.23002E-01
63	0.80866E 00	0.35355E 00	0.35355E 00	0.11376E-01	-0.75849E-02	0.23437E-01	0.14462E-01	-0.25599E-01
64	0.80866E 00	0.48296E 00	0.12941E 00	0.15766E-01	-0.47142E-02	0.44033E-01	0.95206E-02	-0.32320E-01
65	0.80866E 00	0.48296E 00	-0.12941E 00	-0.15766E-01	0.47142E-02	0.44033E-01	-0.95206E-02	0.32320E-01
66	0.80866E 00	0.35355E 00	-0.35355E 00	-0.11376E-01	0.75849E-02	0.23437E-01	-0.14462E-01	0.25599E-01
67	0.80866E 00	0.12941E 00	-0.48296E 00	-0.10614E-01	0.77821E-02	0.73035E-02	-0.14266E-01	0.23002E-01
68	0.10670E 01	0.12941E 00	0.48296E 00	0.65682E-02	-0.71850E-02	0.74206E-02	0.14056E-01	-0.17224E-01
69	0.10670E 01	0.35355E 00	0.35355E 00	0.60243E-02	-0.64725E-02	0.23112E-01	0.12935E-01	-0.16267E-01
70	0.10670E 01	0.48296E 00	0.12941E 00	0.31645E-02	-0.32060E-02	0.39467E-01	0.65702E-02	-0.87982E-02
71	0.10670E 01	0.48296E 00	-0.12941E 00	-0.31644E-02	0.32060E-02	0.39467E-01	-0.65701E-02	0.87981E-02
72	0.10670E 01	0.35355E 00	-0.35355E 00	-0.60243E-02	0.64725E-02	0.23112E-01	-0.12935E-01	0.16267E-01
73	0.10670E 01	0.12941E 00	-0.48296E 00	-0.65682E-02	0.71850E-02	0.74207E-02	-0.14056E-01	0.17224E-01
74	0.13170E 01	0.12941E 00	0.48296E 00	0.40922E-02	-0.59164E-02	0.71552E-02	0.11474E-01	-0.12849E-01
75	0.13170E 01	0.35355E 00	0.35355E 00	0.33790E-02	-0.49144E-02	0.21759E-01	0.97065E-02	-0.10671E-01
76	0.13170E 01	0.48296E 00	0.12941E 00	0.14309E-02	-0.20867E-02	0.35576E-01	0.42054E-02	-0.45456E-02
77	0.13170E 01	0.48296E 00	-0.12941E 00	-0.14308E-02	0.20867E-02	0.35576E-01	-0.42054E-02	0.45455E-02
78	0.13170E 01	0.35355E 00	-0.35355E 00	-0.33790E-02	0.49144E-02	0.21759E-01	-0.97065E-02	0.10671E-01
79	0.13170E 01	0.12941E 00	-0.48296E 00	-0.40922E-02	0.59164E-02	0.71553E-02	-0.11474E-01	0.12849E-01
80	0.17500E 01	0.12941E 00	0.48296E 00	0.20246E-02	-0.40373E-02	0.66695E-02	0.78626E-02	-0.82437E-02
81	0.17500E 01	0.35355E 00	0.35355E 00	0.15603E-02	-0.31336E-02	0.20025E-01	0.61627E-02	-0.62984E-02
82	0.17500E 01	0.48296E 00	0.12941E 00	0.60337E-03	-0.12206E-02	0.32404E-01	0.24246E-02	-0.24126E-02
83	0.17500E 01	0.48296E 00	-0.12941E 00	-0.60336E-03	0.12206E-02	0.32404E-01	-0.24245E-02	0.24126E-02
84	0.17500E 01	0.35355E 00	-0.35355E 00	-0.15603E-02	0.31336E-02	0.20025E-01	-0.61628E-02	0.62984E-02
85	0.17500E 01	0.12941E 00	-0.48296E 00	-0.20246E-02	0.40373E-02	0.66696E-02	-0.78626E-02	0.82437E-02

LOAD DISTRIBUTION ON BODY .....

1	0.56743E-01	2	0.56009E-01	3	0.31129E-01
4	0.64503E-01	5	0.81900E-01	6	0.85148E-01
7	0.68012E-01	8	0.99344E-01	9	0.20830E 00
10	0.59238E-01	11	0.92429E-01	12	0.26164E 00
13	0.73034E-01	14	0.11197E 00	15	0.22586E 00
16	0.67102E-01	17	0.88705E-01	18	0.13482E 00
19	0.46004E-01	20	0.51198E-01	21	0.64639E-01
22	0.34449E-01	23	0.32535E-01	24	0.17596E-01
25	0.25698E-01	26	0.21342E-01	27	0.90911E-02
28	0.16487E-01	29	0.12597E-01	30	0.48252E-02

SPANWISE LIFT DISTRIBUTION ON BODY .....

1	0.78256E-01	2	0.96747E-01	3	0.14851E 00.

MAX FIN CHORD = 1.000 REFERENCE AREA = 0.60000E 01

WING CL = 0.72392E-01 FIN CL = 0.0 BODY CL = 0.79603E-02

TOTAL CL = 0.80352E-01

PRESSURE DISTRIBUTION ON VERTICAL FIN .....

LOAD DISTRIBUTION ON VERTICAL FIN .....

NO	XCP	NO	XCP	NO	XCP	NO	XCP	NO	XCP
1	-0.48654E-02	2	-0.12267E-01	3	-0.99562E-02	4	-0.61927E-02	5	-0.36822E-02
6	-0.10294E-01	7	-0.78024E-02	8	-0.46928E-02	9	-0.27335E-02	10	-0.15389E-02
11	-0.14528E-01	12	-0.78556E-02	13	-0.35090E-02	14	-0.18359E-02	15	-0.96995E-03
16	-0.90121E-02	17	-0.69401E-02	18	-0.28508E-02	19	-0.13774E-02	20	-0.71187E-03
21	-0.67676E-02	22	-0.40359E-02	23	-0.18515E-02	24	-0.88402E-03	25	-0.46079E-03

SPANWISE LIFT DISTRIBUTION ON VERTICAL FIN .....

	1	2	3	4	5
CLS(I) =	-0.95180E-02	-0.66284E-02	-0.32970E-02	-0.17546E-02	-0.95422E-03
CLSW(I) =	-0.95180E-02	-0.66284E-02	-0.32970E-02	-0.17546E-02	-0.95422E-03
CLSF(I) =	0.0	0.0	0.0	0.0	0.0

LIFT COEFF. ON VERTICAL FIN CL = -0.17144E-02

PRESSURE DISTRIBUTION ON BODY INCLUDING VERTICAL FIN EFFECT .....

NO	CPB	NO	CPB	NO	CPB	NO	CPB	NO	CPB	NO	CPB
1	-0.28648E-01	2	-0.28564E-01	3	-0.16171E-01	4	0.16171E-01	5	0.28564E-01	6	0.28648E-01
7	-0.33031E-01	8	-0.42001E-01	9	-0.43528E-01	10	0.43528E-01	11	0.42001E-01	12	0.33031E-01
13	-0.35865E-01	14	-0.51168E-01	15	-0.10534E 00	16	0.10535E 00	17	0.51168E-01	18	0.35865E-01
19	-0.32598E-01	20	-0.47980E-01	21	-0.13215E 00	22	0.13215E 00	23	0.47980E-01	24	0.32598E-01
25	-0.41138E-01	26	-0.58172E-01	27	-0.11446E 00	28	0.11446E 00	29	0.58172E-01	30	0.41138E-01
31	-0.37786E-01	32	-0.46533E-01	33	-0.68968E-01	34	0.68968E-01	35	0.46533E-01	36	0.37786E-01
37	-0.25734E-01	38	-0.27008E-01	39	-0.33431E-01	40	0.33431E-01	41	0.27008E-01	42	0.25734E-01
43	-0.17665E-01	44	-0.16974E-01	45	-0.94928E-02	46	0.94927E-02	47	0.16974E-01	48	0.17665E-01
49	-0.13010E-01	50	-0.11029E-01	51	-0.49603E-02	52	0.49603E-02	53	0.11029E-01	54	0.13010E-01
55	-0.83002E-02	56	-0.64432E-02	57	-0.25989E-02	58	0.25989E-02	59	0.64432E-02	60	0.83001E-02

TABLE 5. LIST OF COMPUTER PROGRAM

Reproduced from best available copy.

```
FORTRAN IV G LEVEL  21                MAIN                DATE = 76132          14/11/16                PAGE 0001

                C     CALCULATION OF AERODYNAMIC PERFORMANCE OF FIN-BODY COMBINATION
0001                  DIMENSION BC(56),XW(56),GAMM(55),XREF(10),XCP(55),CMS(10),BCL(36)
0002                  COMMON /A1/RAD1/A2/CPB(72)/AR1/AR(56,56)/AR2/AQ(72,72)/AR3/ASV(72,
                     $72)/AR4/AFN(72,55)
0003                  COMMON /B1/MB,NB/B2/NUB/B3/PSA(55)/B4/BREF(5)/B6/XDV(55)/
                     $B7/YVI(55),WHI(55),TLMDI(55)/B11/NBF,NBM,NBB,FDL,BDL/BY1/ALFAB/BY2
                     $/ABW(55)/BY3/JRAD
0004                  COMMON /C1/BC/C2/AREAB(96)/C3/XW/C5/UBDY(72)/C6/VN(72)/C7/QL(72)/
                     $C9/VT(72)/CASEF/ASYF/CASEW/ASYW/CHORD/CLL(55)
0005                  COMMON /D1/BCL/D2/M1/FL1/NFLP/FL2/NT/FL3/NW/FL4/AFLAP/NAME/IRPT
0006                  COMMON /P1/X1,Y1,X2,Y2,X3,Y3,X4,Y4,X5,Y5,X6,Y6/P2/M,N/P3/XM,ALFAF/
                     $P4/NO/P5/PI/PC/BETA/P7/SPN/PT1/XC1(55),XC2(5),XC3(5)
0007                  COMMON /Q1/GAMM/Q2/XCP/QB/ABU(72,55),ABV(72,55),ABW(72,55)/R1/XL(
                     $10)/R3/XREF
0008                  COMMON /T1/NTOT/T2/XG(55),YG(55),ZG(55)/T3/XS(72),YS(72),ZS(72)/T4
                     $/TS(72)/T5/XD(127),YD(127),ZD(127)/T6/XV(55),YV(55),ZV(55),WH(55),
                     $TLMD(55)
0009                  COMMON /U1/YF(11)/U2/RFAREA,XAX/U3/DT/VL1/IRC/W1/DX(96)/W2/CLS(5),
                     $CLSW(5),CLSF(5)/W3/CLBS(5)/W4/CLWING,CLFIN,CLBODY,TOTCL
0010                  WRITE(6,900)
0011            900   FORMAT(//,3X,'COMPUTATION FOR SURFACE PRESSURE DISTRIBUTION ON FIN
                     $-BODY COMBINATION AT SUBSONIC SPEEDS',//)
0012                  PI=3.14159
                C     READING FIN-BODY GEOMETRY
0013                  READ(5,10) X1,Y1,X2,Y2,X3,Y3,X4,Y4,X5,Y5,X6,Y6
0014             10   FORMAT(8F10.5)
                C     READING DIVISION NUMBER
0015                  READ(5,15) M,N,NFLP
0016             15   FORMAT(3I10)
                C     READING BODY PANEL NUMBER
0017                  READ(5,17) MB,NBF,NBM,NBB,FDL,BDL
0018             17   FORMAT(4I10,2F10.5)
0019                  NW=M*N
0020                  NT=N+NFLP
0021                  NO=M*NT
0022                  NB=NBF+NBM+NBB
0023                  NUB=NB*MB
0024                  NTOT=NO+NUB
                C     READING AERODYNAMIC INPUT
0025                  READ(5,20) XM,ALFAF,ALFAB,AFLAP,ASYW,ASYF
0026             20   FORMAT(6F10.5)
0027                  WRITE(6,902)
0028            902   FORMAT(//,3X,'FIN-BODY GEOMETRY ..........',//)
0029                  WRITE(6,904)
0030            904   FORMAT(1H ,5X,'X1',6X,'Y1',6X,'X2',6X,'Y2',6X,'X3',6X,'Y3',6X,'X4'
                     $,6X,'Y4',6X,'X5',6X,'Y5',6X,'X6',6X,'Y6')
0031                  WRITE(6,906) X1,Y1,X2,Y2,X3,Y3,X4,Y4,X5,Y5,X6,Y6
0032            906   FORMAT(1HO,2X,12(F8.3))
0033                  WRITE(6,907)
0034            907   FORMAT(/,3X,'FIN-BODY PANEL NUMBER .....',/)
0035                  WRITE(6,908) M,N,NFLP,NW,NO
0036            908   FORMAT(1HO,2X,'M = ',I2,2X,'N = ',I2,2X,'NFLP = ',I2,2X,'NW = ',I2
```

```
     $,2X,'NO = ',I2)
0037      WRITE(6,910) MB,NBF,NBM,NBB,NB,NUB,FDL,BDL,NTOT
0038  910 FORMAT(1HO,2X,'MB = ',I2,2X,'NBF = ',I2,2X,'NBM = ',I2,2X,'NBB = '
     $,I2,2X,'NB = ',I2,2X,'NUB = ',I3/3X,'FDL = ',F5.2,2X,'BDL = ',F5.2
     $,5X,'TOTAL PANEL = ',I3)
0039      WRITE(6,912) XM,ALFAB,ALFAF,AFLAP,ASYW,ASYF
0040  912 FORMAT(1HO,2X,'MACH NO = ',F6.3,2X,'ANGLE OF INCIDENCE = ',F5.2,1X
     $,'(DEG)',2X,'FIN ANGLE OF ATTACK = ',F5.2,1X,'(DEG)'/3X,'FLAP ANGL
     $E OF ATTACK = ',F5.2,1X,'(DEG)',2X,'FIN SYNMETRY = ',F5.2,2X,'FLAP
     $ SYNMETRY = ',F5.2)
0041      BETA=SQRT(1.-XM**2)
0042      SPN=Y2
0043      M1=MB/2
0044      RADI=Y1
0045      IRC=0
0046      JRAD=1
0047      IF(RADI.LT.0.0001) JRAD=0
0048      IF(JRAD.EQ.0) GO TO 610
0049      CALL BGMY
0050  610 CALL GVS1
0051      CALL CONP
0052      WRITE(6,914)
0053  914 FORMAT(/,3X,'REFERENCE CHORD ..........',/)
0054      IF(JRAD.EQ.0) GO TO 612
0055      CALL GIV
0056  612 CALL GVS3
0057      CALL XLC
0058      IF(JRAD.EQ.0) GO TO 614
0059      CALL BLLT
0060      CALL VBIA
0061      WRITE(6,916)
0062  916 FORMAT(1H ,3X,'ON BODY .....',/)
0063      WRITE(6,917)
0064  917 FORMAT(1H ,18X,'1',13X,'2',13X,'3')
0065      WRITE(6,410) (BREF(I),I=1,M1)
0066  410 FORMAT(1H ,3X,'BREF(I) =  ',3(E12.5,2X))
0067  614 WRITE(6,918)
0068  918 FORMAT(/,3X,'ON FIN .....',/)
0069      WRITE(6,919)
0070  919 FORMAT(1H ,19X,'1',13X,'2',13X,'3',13X,'4',13X,'5')
0071      WRITE(6,400) (XL(JJ),JJ=1,M)
0072      WRITE(6,401) (CLL(JJ),JJ=1,M)
0073      WRITE(6,402) (XC1(JJ),JJ=1,M)
0074      WRITE(6,404) (XC2(JJ),JJ=1,M)
0075      WRITE(6,406) (XC3(JJ),JJ=1,M)
0076  400 FORMAT(1H ,3X,'XL(I)    =  ',5(E12.5,2X))
0077  401 FORMAT(1H ,3X,'CLL(I)   =  ',5(E12.5,2X))
0078  402 FORMAT(1H ,3X,'XC1(I)   =  ',5(E12.5,2X))
0079  404 FORMAT(1H ,3X,'XC2(I)   =  ',5(E12.5,2X))
0080  406 FORMAT(1H ,3X,'XC3(I)   =  ',5(E12.5,2X))
0081      CALL ARDC
0082      IF(JRAD.EQ.0) GO TO 616
```

```
0083            CALL PVMX
0084            CALL ARQQ
0085            CALL ARQV
0086            CALL ARBF
0087          616 IRPT=1
0088            IF(JRAD.EQ.0) GO TO 618
0089         1000 CONTINUE
0090          618 CALL BCF(BC,NO)
0091            CALL VDF(GAMM)
0092            CALL PDB(XCP)
0093            CALL SLD
0094            CALL XLF(CL)
0095            CALL PMS(CMS)
0096            IF(JRAD.EQ.0) GO TO 620
0097            CALL VLNB
0098            CALL BSS
0099            CALL BPD
0100            CALL BLD(BCL)
0101            CALL BSLD
0102            CALL WBS(XW,NUB,NO)
0103            CALL XLIFT
0104            IF(IRPT.LT.4) GO TO 2000
0105            WRITE(6,920) IRPT
0106          920 FORMAT(/,3X,'ITERATION = ',I2,/)
0107          620 WRITE(6,922)
0108          922 FORMAT(/,3X,'PRESSURE DISTRIBUTION ON PLANAR FIN ..........',/)
0109            WRITE(6,924)
0110          924 FORMAT(/,4X,'NO',6X,'XV',11X,'YV',11X,'ZV',11X,'XNR',10X,'YNR',10X
           $,'GAMMA',8X,'XCP',/)
0111            DO 312 IF=1,NO
0112            XNR=(XV(IF)-XC1(IF))/CLL(IF)
0113            YNR=YV(IF)/Y2
0114            WRITE(6,311) IF,XV(IF),YV(IF),ZV(IF),XNR,YNR,GAMM(IF),XCP(IF)
0115          311 FORMAT(1H ,I5,7(1X,E12.5))
0116          312 CONTINUE
0117            WRITE(6,926)
0118          926 FORMAT(/,3X,'SPANWISE LIFT AND MOMENT DISTRIBUTION ..........',/)
0119            WRITE(6,927)
0120          927 FORMAT(1HO,20X,'1',13X,'2',13X,'3',13X,'4',13X,'5')
0121            WRITE(6,500) (CLS(JX),JX=1,M)
0122            WRITE(6,502) (CLSW(JX),JX=1,M)
0123            WRITE(6,504) (CLSF(JX),JX=1,M)
0124            WRITE(6,506) (CMS(JX),JX=1,M)
0125          500 FORMAT(1HO,3X,'CLS(I)    =  ',5(E12.5,2X))
0126          502 FORMAT(1HO,3X,'CLSW(I)   =  ',5(E12.5,2X))
0127          504 FORMAT(1HO,3X,'CLSF(I)   =  ',5(E12.5,2X))
0128          506 FORMAT(1HO,3X,'CMS(I)    =  ',5(E12.5,2X))
0129            IF(JRAD.NE.0) GO TO 720
0130            WRITE(6,700) REAREA,CL
0131          700 FORMAT(/,2X,'FIN AREA = ',E12.5,5X,'LIFT COEFF. = ',E12.5,/)
0132            GO TO 622
0133          720 CONTINUE
```

```
      WRITE(6,928)
  928 FORMAT(/,3X,'PRESSURE DISTRIBUTION ON BODY ..........',/)
      WRITE(6,930)
  930 FORMAT(/,4X,'NO',6X,'XD',11X,'YD',11X,'ZD',11X,'UBDY',9X,'VN',11X,
     $'VT',11X,'QL',11X,'CPB',/)
      DO 850 I=1,NUB
      IB=I+NO
      WRITE(6,800) IB,XD(IB),YD(IB),ZD(IB),UBDY(I),VN(I),VT(I),QL(I),
     $CPB(I)
  800 FORMAT(1H ,I5,8(1X,E12.5))
  850 CONTINUE
      WRITE(6,932)
  932 FORMAT(/,3X,'LOAD DISTRIBUTION ON BODY ..........',/)
      DO 520 K1=1,NB
      K2=(K1-1)*M1+1
      K3=K1*M1
      WRITE(6,510) (IB,BCL(IB),IB=K2,K3)
  510 FORMAT(1H ,4(I10,2X,E12.5))
  520 CONTINUE
      WRITE(6,934)
  934 FORMAT(/,3X,'SPANWISE LIFT DISTRIBUTION ON BODY ..........',/)
      WRITE(6,550) ( IX,CLBS(IX) ,IX=1,M1)
      WRITE(6,954) ( IX,CLBS(IX) ,IX=1,M1)
  550 FORMAT(1H ,4(I10,2X,E12.5))
      WRITE(6,560) XAX,RFAREA,CLWING,CLFIN,CLBODY,TOTCL
  560 FORMAT(//,3X,'MAX FIN CHORD = ',F8.3,5X,'REFERENCE AREA = ',E12.5/
     $/3X,'WING CL = ',E12.5,2X,'FIN CL = ',E12.5,2X,'BODY CL = ',E12.5/
     $/3X,'TOTAL CL = ',E12.5//)
 2000 CONTINUE
      IF(IRPT.EQ.4) GO TO 1500
      IRPT=IRPT+1
      GO TO 1000
 1500 CONTINUE
C     COMPUTE AERODYNAMIC COEFFICIENT ON VERTICAL FIN
      WRITE(6,936)
  936 FORMAT(//,3X,'PRESSURE DISTRIBUTION ON VERTICAL FIN ..........',/)
      DO 60 I=1,NUB
      DO 60 J=1,NO
   60 ASV(I,J)=ABV(I,J)
      IRC=1
      DO 30 I=1,NO
      TF1=YD(I)
      TF2=ZD(I)
      YD(I)=TF2
   30 ZD(I)=TF1
      CALL PVMX
      CALL ARBF
      DO 34 I=1,NO
      SUM1=0.
      DO 32 J=1,NO
   32 SUM1=SUM1+ABV(I,J)*GAMM(J)
      SUM2=0.
```

```
0181            DO 33 J=1,NUB
0182         33 SUM2=SUM2+AFN(J,I)*QL(J)
0183         34 BC(I)=+(SUM1+SUM2)
0184            CALL DINV(AR,BC,NC)
0185            DO 36 I=1,NO
0186         36 GAMM(I)=BC(I)
0187            CALL PDB(XCP)
0188            CALL SLD
0189            CALL XLF(CL)
0190            WRITE(6,950)
0191            WRITE(6,951)
0192            DO 37 J=1,NT
0193            I1=(J-1)*M-1
0194            I2=I1+M-1
0195         37 WRITE(6,210) (I,XCP(I),I=I1,I2)
0196            WRITE(6,952)
0197            WRITE(6,953)
0198            WRITE(6,220) (CLS(I),I=1,M)
0199            WRITE(6,222) (CLSW(I),I=1,M)
0200            WRITE(6,224) (CLSF(I),I=1,M)
0201            WRITE(6,954) CL
0202        950 FORMAT(//,3X,'LOAD DISTRIBUTION ON VERTICAL FIN .....',/)
0203        951 FORMAT(1H ,5(3X,'NO',7X,'XCP',4X))
0204        210 FORMAT(1H ,5(I5,2X,E12.5))
0205        952 FORMAT(//,3X,'SPANWISE LIFT DISTRIBUTION ON VERTICAL FIN .....',/)
0206        953 FORMAT(1H0,20X,'1',13X,'2',13X,'3',13X,'4',13X,'5')
0207        220 FORMAT(1H0,3X,'CLS(I)   =  ',5(E12.5,2X))
0208        222 FORMAT(1H0,3X,'CLSW(I)  =  ',5(E12.5,2X))
0209        224 FORMAT(1H0,3X,'CLSF(I)  =  ',5(E12.5,2X))
0210        954 FORMAT(//,3X,'LIFT COEFF. ON VERTICAL FIN   CL =  ',E12.5,//)
0211            IRC=2
0212            WRITE(6,956)
0213        956 FORMAT(1H0,3X,'PRESSURE DISTRIBUTION ON BODY INCLUDING VERTICAL FI
                  $N EFFECT .....',/)
0214            WRITE(6,958)
0215        958 FORMAT(1H ,6(3X,'NO',6X,'CPB',4X))
0216            DO 40 I=1,NUB
0217            SUM1=0.
0218            DO 38 J=1,NO
0219         38 SUM1=SUM1+ASV(I,J)*GAMM(J)
0220         40 UBDY(I)=SUM1
0221            DO 50 NX=1,NB
0222            I1=MB*(NX-1)+1
0223            I2=I1+MB-1
0224            DO 45 MX=1,MB
0225            I=MB*(NX-1)+MX
0226            IX=I+M1
0227            L1=M1*(2*NX-1)+1
0228            IF(I.GE.L1) IX=I-M1
0229            ACPB=-2.*UBDY(IX)/BETA**2
0230         45 CPB(I)=CPB(I)+ACPB
0231         50 WRITE(6,240) (I,CPB(I),I=I1,I2)
```

```
0232          240 FORMAT(1H ,6(I5,1X,E12.5))
0233          622 CONTINUE
0234              STOP
0235              END
```

```
0001            SUBROUTINE BGMY
                C
                C       DEFINE SOURSE POSITION ON BODY
                C
0002            DIMENSION XN(17)
0003            COMMON /T3/XS(72),YS(72),ZS(72)
0004            COMMON /T4/TS(72)
0005            COMMON /C2/AREAB(96)
0006            COMMON /W1/DX(96)
0007            COMMON /P1/X1,Y1,X2,Y2,X3,Y3,X4,Y4,X5,Y5,X6,Y6
0008            COMMON /P4/NU
0009            COMMON /P5/PI
0010            COMMON /B1/MB,NB
0011            COMMON /B11/NBF,NBM,NBB,FDL,BDL
0012            COMMON /B2/NUB
0013            COMMON /A1/RADI
0014            COMMON /U3/DT
0015            DT=PI/MB
0016            C=1.
0017            NX=NBF-1
0018            NB1=NBF+NBM+1
0019            XP=X1-FDL*ABS(X3-X1)
0020            AZ1=PI/(2.*NBF)
0021            AZ2=PI*C/(2.*NBM)
0022            AZ3=PI/(2.*NBB)
0023            XN(1)=XP
0024            DO 10 J1=1,NX
0025         10 XN(J1+1)=XP+ABS(X1-XP)*SIN(AZ1*J1)
0026            XN(NBF+1)=X1
0027            NY=NBM-1
0028            DO 20 J2=1,NY
0029         20 XN(NBF+J2+1)=X1+ABS(X3-X1)*(1.-COS(AZ2*J2))/C
0030            XN(NB1)=X3
0031            NZ=NBB-1
0032            XQ=X3+BDL*ABS(X3-X1)
0033            DO 30 J3=1,NZ
0034         30 XN(NB1+J3)=X3+ABS(XQ-X3)*(1.-COS(AZ3*J3))
0035            XN(NB+1)=XQ
0036            DO 100 JJ=1,NB
0037            PP1=(XN(JJ)+XN(JJ+1))/2.
0038            PP2=ABS(XN(JJ+1)-XN(JJ))
0039            DO 100 JB=1,MB
0040            XS(JB+(JJ-1)*MB)=PP1
0041            DX(JB+(JJ-1)*MB)=PP2
0042        100 CONTINUE
0043            DO 120 I=1,NUB
0044        120 AREAB(I)=RADI*DT*DX(I)
0045            N1=NB-1
0046            DO 200 IB=1,MB
0047            TS(IB)=DT*(IB-.5)
0048            DO 150 JJ=1,N1
0049            TS(IB+JJ*MB)=TS(IB)
```

```
0050          150 CONTINUE
0051          200 CONTINUE
0052              DO 300 IB=1,NJB
0053              YS(IB)    =RADI*SIN(TS(IB))
0054              ZS(IB)    =RADI*COS(TS(IB))
0055          300 CONTINUE
0056              RETURN
0057              END
```

Reproduced from best available copy.


```
0001            SUBROUTINE GVS1
                C
                C   CONTROL POINT DEFFINITION
                C
0002            DIMENSION DK(15)
0003            COMMON /U1/YF(11)
0004            COMMON /T2/XG(55),YG(55),ZG(55)
0005            COMMON /T6/XV(55),YV(55),ZV(55),WH(55),TLMD(55)
0006            COMMON /P1/X1,Y1,X2,Y2,X3,Y3,X4,Y4,X5,Y5,X6,Y6
0007            COMMON /P2/M,N
0008            COMMON AP3/XM,ALFAF
0009            COMMON /P4/NO
0010            COMMON /P5/PI
0011            COMMON /FL1/NFLP
0012            COMMON /FL2/NT
0013            COMMON /FL3/NW
0014            NT1=NT-1
0015            YF(1)=Y1
0016            DO 20 JC=1,M
0017            YF(JC+1)=Y1     +(Y2-Y1)*(1.-COS(JC*PI/M))/2.
0018            YG(JC)=(YF(JC)+YF(JC+1))/2.
0019            WH(JC)=(YF(JC+1)-YF(JC))/2.
0020            DO 10 JJ=1,NT1
0021            YG(JC+JJ*M)=YG(JC)
0022            WH(JC+JJ*M)=WH(JC)
0023         10 CONTINUE
0024         20 CONTINUE
0025            DO 30 JJ=1,NO
0026            YV(JJ)=YG(JJ)
0027            ZG(JJ)=0.
0028            ZV(JJ)=0.
0029         30 CONTINUE
0030            THW=PI/N
0031            THW1=THW/2.
0032            N1=N-1
0033            N2=N+1
0034            DK(1)=0.
0035            DK(N2)=1.
0036            DO 37 K=1,N1
0037            XK=K
0038            DK(K+1)=1.-COS(THW1*XK)
0039         37 CONTINUE
                C   CONTROL POINT ON WING
0040            DO 50 K=1,N
0041            DO 40 J1=1,M
0042            J2=(K-1)*M+J1
0043            XG(J2)=X1+(X3-X1)*(DK(K)+3.*DK(K+1))/4.+((X4-X2)*(DK(K)+3.*DK(K+1)
               $)/4.-(X3-X1)*(DK(K)+3.*DK(K+1))/4.+X2-X1)*(YV(J1)-Y1)/(Y2-Y1)
0044            TLMD(J2)=((X4-X2)*(3.*DK(K)+DK(K+1))/4.-(X3-X1)*(3.*DK(K)+DK(K+1))
               $/4.+X2-X1)/(Y2-Y1)
0045            XV(J2)=X1+(X3-X1)*(3.*DK(K)+DK(K+1))/4.+(YV(J1)-Y1)*TLMD(J2)
0046         40 CONTINUE
```

```
0047            50 CONTINUE
0048               IF(NFLP.EQ.0) GO TO 80
0049               THF=PI/NFLP
0050               THF1=THF/2.
0051               N3=NFLP-1
0052               N4=NFLP+1
0053               DK(N4)=1.
0054               DO 60 K=1,N3
0055               XK=K
0056               DK(K+1)=1.-COS(THF1*XK)
0057            60 CONTINUE
                C     CONTROL POINT ON CONTROL FIN
0058               DO 70 K=1,NFLP
0059               DO 65 J1=1,M
0060               J2=(K-1)*M+J1
0061               XG(J2+NW)=X3+(X5-X3)*(DK(K)+3.*DK(K+1))/4.+((X6-X4)*(DK(K)+3.*DK(
                  $K+1))/4.-(X5-X3)*(DK(K)+3.*DK(K+1))/4.+X4-X3)*(YV(J1)-Y3)/(Y4-Y3)
0062               TLMD(J2+NW)=((X6-X4)*(3.*DK(K)+DK(K+1))/4.-(X5-X3)*(3.*DK(K)+DK(K+
                  $1))/4.+X4-X3)/(Y4-Y3)
0063               XV(J2+NW)=X3+(X5-X3)*(3.*DK(K)+DK(K+1))/4.+(YV(J1)-Y3)*TLMD(J2+NW)
0064            65 CONTINUE
0065            70 CONTINUE
0066            80 CONTINUE
0067               RETURN
0068               END
```

```
0001            SUBROUTINE CONP
                C
0002            COMMON /T2/XG(55),YG(55),ZG(55)
0003            COMMON /T3/XS(72),YS(72),ZS(72)
0004            COMMON /T5/XD(127),YD(127),ZD(127)
0005            COMMON /P4/NO
0006            COMMON /T1/NTOT
0007            COMMON /BY3/JRAD
0008            N1=NTOT
0009            IF(JRAD.EQ.0) N1=NO
0010            DO 10 JC=1,N1
0011            IF(JC.GT.NO) GO TO 5
0012            XD(JC)=XG(JC)
0013            YD(JC)=YG(JC)
0014            ZD(JC)=ZG(JC)
0015            GO TO 10
0016          5 XD(JC)=XS(JC-NO)
0017            YD(JC)=YS(JC-NO)
0018            ZD(JC)=ZS(JC-NO)
0019         10 CONTINUE
0020            RETURN
0021            END
```

```
0001          SUBROUTINE GIV
              C
0002          COMMON /B7/YVI(55),WHI(55),TLMDI(55)
0003          COMMON /T6/XV(55),YV(55),ZV(55),WH(55),TLMD(55)
0004          COMMON /P4/NO
0005          COMMON /A1/RADI
0006          DO 10 II=1,NO
0007          YVI(II)=RADI**2*(1./(YV(II)-WH(II))+1./(YV(II)+WH(II)))/2.
0008          WHI(II)=RADI**2*(1./(YV(II)-WH(II))-1./(YV(II)+WH(II)))/2.
0009          TLMDI(II)=TLMD(II)*WH(II)/WHI(II)
0010       10 CONTINUE
0011          RETURN
0012          END
```

```
0001            SUBROUTINE GVS3
                C
                C       COMPUTE PANEL SURFACE AREA
                C
0002            COMMON /B3/PSA(55)
0003            COMMON /B6/XDV(55)
0004            COMMON /T2/XG(55),YG(55),ZG(55)
0005            COMMON /T6/XV(55),YV(55),ZV(55),WH(55),TLMD(55)
0006            COMMON /P4/NO
0007            COMMON /P6/BETA
0008            COMMON /P1/X1,Y1,X2,Y2,X3,Y3,X4,Y4,X5,Y5,X6,Y6
0009            COMMON /U2/RFAREA,XAX
0010            XAX=X6-X1+Y1*(X2-X1)/(Y2-Y1)-Y6*(X6-X5)/(Y6-Y5)
0011            RFAREA=(XAX+X6-X2)*Y6
0012            DO 10 II=1,NO
0013            XDV(II)=XG(II)-XV(II)
0014            PSA(II)=4.*BETA*WH(II)*XDV(II)
0015         10 CONTINUE
0016            RETURN
0017            END
```

```
0001            SUBROUTINE XLC
                C
                C
                C       COMPUTE LOCAL CHORD LENGTH OF FIN
                C
0002            DIMENSION XREF(10),XREFF(5),XLF(5)
0003            COMMON /PT1/XC1(55),XC2(5),XC3(5)
0004            COMMON /R1/XL(10)
0005            COMMON /T2/XG(55),YG(55),ZG(55)
0006            COMMON /T6/XV(55),YV(55),ZV(55),WH(55),TLMD(55)
0007            COMMON /CHORD/CLL(55)
0008            COMMON /P1/X1,Y1,X2,Y2,X3,Y3,X4,Y4,X5,Y5,X6,Y6
0009            COMMON /P2/M,N
0010            COMMON /R3/XREF
0011            COMMON /FL2/NT
0012            N1=NT-1
0013            DO 10 JL=1,M
0014            XC1(JL)=X1+(X2-X1)*(YG(JL)-Y1)/(Y2-Y1)
0015            XC2(JL)=X3+(X4-X3)*(YG(JL)-Y3)/(Y4-Y3)
0016            XC3(JL)=X5+(X6-X5)*(YG(JL)-Y5)/(Y6-Y5)
0017            XL(JL)=XC2(JL)-XC1(JL)
0018            XLF(JL)=XC3(JL)-XC2(JL)
0019            XREF(JL)=XC1(JL)+XL(JL)/4.
0020            XREFF(JL)=XC2(JL)+XLF(JL)/4.
0021            CLL(JL)=XC3(JL)-XC1(JL)
0022            DO 5 J=1,N1
0023            I=JL+J*M
0024            XC1(I)=XC1(JL)
0025          5 CLL(I)=CLL(JL)
0026         10 CONTINUE
0027            RETURN
0028            END
```

```
FORTRAN IV G LEVEL  21                BLLT          DATE = 76114      10/33/50          PAGE 0001

0001                SUBROUTINE BLLT
                    C
0002                COMMON /B4/BREF(5)
0003                COMMON /T3/XS(72),YS(72),ZS(72)
0004                COMMON /D2/M1
0005                COMMON /P1/X1,Y1,X2,Y2,X3,Y3,X4,Y4,X5,Y5,X6,Y6
0006                DO 10 IB=1,M1
0007                B1=X1+(X2-X1)*(YS(IB)-Y1)/(Y2-Y1)
0008                B2=X6-(Y6-YS(IB))*(X6-X5)/(Y6-Y5)
0009             10 BREF(IB)=B2-B1
0010                RETURN
0011                END
```

```
0001            SUBROUTINE VBIA
                C
                C     VELOCITY ON FIN INDUCED BY BODY INCIDENCE ANGLE
                C
0002            COMMON /BY2/XBW(55)
0003            COMMON /T2/XG(55),YG(55),ZG(55)
0004            COMMON /BY1/ALFAB
0005            COMMON /P4/NO
0006            COMMON /A1/RADI
0007            COMMON /P5/PI
0008            ALB=ALFAB*PI/180.
0009            DO 10 J=1,NO
0010         10 XBW(J)=ALB*RADI**2/YG(J)**2
0011            RETURN
0012            END
```

```
0001          SUBROUTINE ARDC
              C
              C     COMPUTE AERODYNAMIC MATRIX
              C
0002          COMMON /AR1/AR(56,56)
0003          COMMON /T6/XV(55),YV(55),ZV(55),WH(55),TLMD(55)
0004          COMMON /B7/YVI(55),WHI(55),TLMDI(55)
0005          COMMON /TR1/TX,TY,TZ,TW,TM
0006          COMMON /B8/JS
0007          COMMON /P8/I,J
0008          COMMON /99/PSP
0009          COMMON /P4/NO
0010          COMMON /CASEW/ASYW
0011          COMMON /CASEF/ASYF
0012          COMMON /FL3/NW
0013          COMMON /BY3/JRAD
0014          NN=4
0015          IF(JRAD.EQ.0) NN=2
0016          DO 30 I=1,NO
0017          DO 20 J=1,NO
0018          IF(J.LE.NW) ASYN=ASYW
0019          IF(J.GT.NW) ASYN=ASYF
0020          TX=XV(J)
0021          TZ=ZV(J)
0022          DO 10 JS=1,NN
0023          IF(JS.LE.2) GO TO 15
0024          TY=YVI(J)
0025          TW=WHI(J)
0026          TM=TLMDI(J)
0027          GO TO 16
0028       15 TY=YV(J)
0029          TW=WH(J)
0030          TM=TLMD(J)
0031       16 CONTINUE
0032          IF(JS.EQ.1.OR.JS.EQ.3) PSP=1.
0033          IF(JS.EQ.2.OR.JS.EQ.4) PSP=-1.
0034          CALL PVB(UB,VB,WB)
0035          CALL PVP(UP,VP,WP)
0036          CALL PVS(US,VS,WS)
0037          XAR=WB+WP+WS
0038          IF(JS.EQ.1) SAR=XAR
0039          IF(JS.EQ.2) PAR=XAR
0040          IF(JS.EQ.3) SIAR=XAR
0041          IF(JS.EQ.4) PIAR=XAR
0042       10 CONTINUE
0043          IF(JRAD.NE.0) GO TO 50
0044          SIAR=0.
0045          PIAR=0.
0046       50 AR(I,J)=SAR+ASYN*PAR+SIAR+ASYN*PIAR
0047       20 CONTINUE
0048       30 CONTINUE
0049          RETURN
```

```
0050          END
```

```
FORTRAN IV G LEVEL  21                PVB              DATE = 76114      10/33/50          PAGE 0001

0001                  SUBROUTINE PVB(UB,VB,WB)
                C
                C     COMPUTE PERTURBATION VELOCITY COMPONENTS INDUCED BY BOUND VORTEX
                C
0002                  COMMON /T5/XD(127),YD(127),ZD(127)
0003                  COMMON /TR1/TX,TY,TZ,TW,TM
0004                  COMMON /P3/XM,ALFAF
0005                  COMMON /P5/PI
0006                  COMMON /P6/BETA
0007                  COMMON /P7/SPN
0008                  COMMON /P8/I,J
0009                  COMMON /P9/PSP
0010                  COMMON /B8/JS
0011                  CALL GVS2(SX,SY,TMU)
0012                  A=SQRT((XD(I)-SX)**2+BETA**2*(SY-PSP*YD(I))**2)
0013                  B=BETA*(SY-TY+TW)
0014                  C=SX-TX    +BETA*TW*TMU
0015                  D=BETA*(TY+TW-SY)
0016                  E=TX    +BETA*TW    *TMU-SX
0017                  Z=BETA*(TZ    -ZD(I))
0018                  AZ2=A**2+Z**2
0019                  BC2=B**2+C**2
0020                  DE2=D**2+E**2
0021                  CMU=1./SQRT(1.+TMU**2)
0022                  SMU=CMU*TMU
0023                  IF(SY.GT.TY-TW)        PP1=1.
0024                  IF(SY.LT.TY-TW)        PP1=-1.
0025                  CG=PP1*SQRT(BC2)/SQRT(AZ2+BC2)
0026                  IF(SY.GT.TY+TW)        PP2=-1.
0027                  IF(SY.LT.TY+TW)        PP2=1.
0028                  CF=PP2*SQRT(DE2)/SQRT(AZ2+DE2)
0029                  SCC=SPN*(CG+CF)/(2.*PI)
                C     COMPUTE INDUCED VELOCITY COMPONENTS FOR UNIT FREE STREAM VELOCITY AND
                C     UNIT VORTICITY STRENGTH
0030                  UB=-SCC*Z*CMU/AZ2
0031                  VB=SCC*Z*SMU/AZ2
0032                  IF(XD(I).GT.SX) PP3=-1.
0033                  IF(XD(I).LT.SX) PP3=1.
0034                  WB=PP3*SCC*A/AZ2
0035                  RETURN
0036                  END
```

Reproduced from best available copy.

```
0001          SUBROUTINE PVP(UP,VP,WP)
              C
              C     COMPUTE PERTURBATION VELOCITY COMPONENTS INDUCED BY PORT SIDE VORTEX
              C
0002          COMMON /T5/XD(127),YD(127),ZD(127)
0003          COMMON /TR1/TX,TY,TZ,TW,TM
0004          COMMON /P5/PI
0005          COMMON /P6/BETA
0006          COMMON /P7/SPN
0007          COMMON /P8/I,J
0008          COMMON /P9/PSP
0009          COMMON /B8/JS
0010          CALL GVS2(SX,SY,TMU)
0011          G=BETA*(PSP*YD(I)-TY+TW)
0012          Z=BETA*(TZ   -ZD(I))
0013          GZ2=G**2+Z**2
0014          XH=XD(I)-TX   +BETA*TW*TMU
0015          GZH2=GZ2+XH**2
0016          CK=XH/SQRT(GZH2)
0017          SCK=SPN*(1.+CK)/(2.*PI)
0018          UP=0.
0019          VP=-SCK*Z/GZ2
0020          WP=-SCK*G/GZ2
0021          RETURN
0022          END
```

```
0001            SUBROUTINE PVS(US,VS,WS)
                C
                C   COMPUTE PERTURBATION VELOCITY COMPONENTS INDUCED BY STARBORD SIDE VORTEX
                C
0002            COMMON /T5/XD(127),YD(127),ZD(127)
0003            COMMON /B8/JS
0004            COMMON /TR1/TX,TY,TZ,TW,TM
0005            COMMON /P5/PI
0006            COMMON /P6/BETA
0007            COMMON /P7/SPN
0008            COMMON /P8/I,J
0009            COMMON /P9/PSP
0010            CALL GVS2(SX,SY,TMU)
0011            XI=BETA*(TY+TW      -PSP*YD(I))
0012            Z=BETA*(TZ    -ZD(I))
0013            ZI2=Z**2+XI**2
0014            XJ=XD(I)-TX    -BETA*TW*TMU
0015            ZIJ2=ZI2+XJ**2
0016            CS=XJ/SQRT(ZIJ2)
0017            SCS=SPN*(1.+CS)/(2.*PI)
0018            US=0.
0019            VS=SCS*Z/ZI2
0020            WS=-SCS*XI/ZI2
0021            RETURN
0022            END
```

```
FORTRAN IV G LEVEL 21                GVS2              DATE = 76114      10/33/50              PAGE 0001

0001                  SUBROUTINE GVS2(SX,SY,TMU)
                      C
                      C     COMPUTE INTERCEPT POINT OF BOUND VORTEX
                      C
0002                  COMMON /T5/XD(127),YD(127),ZD(127)
0003                  COMMON /P3/XM,ALFAF
0004                  COMMON /P6/BETA
0005                  COMMON /P8/I,J
0006                  COMMON /P9/PSP
0007                  COMMON /B8/JS
0008                  COMMON /TR1/TX,TY,TZ,TW,TM
0009                  TMU=TM/BETA
0010                  SX=(TX    +XD(I)*TMU**2+BETA*(PSP*YD(I)-TY    )*TMU)/(1.+TMU**2)
0011                  SY=(BETA*(PSP*YD(I)+TY    *TMU**2)+(XD(I)-TX    )*TMU)/(1.+TMU**2)/
                     $BETA
0012                  RETURN
0013                  END
```

```
0001            SUBROUTINE PVMX
                C
0002            COMMON /Q8/ABU(72,55),ABV(72,55),ABW(72,55)
0003            COMMON /T6/XV(55),YV(55),ZV(55),WH(55),TLMD(55)
0004            COMMON /B7/YVI(55),WHI(55),TLMDI(55)
0005            COMMON /TR1/TX,TY,TZ,TW,TM
0006            COMMON /B8/JS
0007            COMMON /P4/NO
0008            COMMON /B2/NUB
0009            COMMON /P8/I,J
0010            COMMON /P9/PSP
0011            COMMON /CASEW/ASYW
0012            COMMON /CASEF/ASYF
0013            COMMON /FL3/NW
0014            COMMON /VL1/IRC
0015            N1=NUB
0016            IF(IRC.EQ.1) N1=NO
0017            DO 30 KK=1,N1
0018            I=NO+KK
0019            IF(IRC.EQ.1) I=KK
0020            DO 20 J=1,NO
0021            IF(J.LE.NW) ASYN=ASYW
0022            IF(J.GT.NW) ASYN=ASYF
0023            TX=XV(J)
0024            TZ=ZV(J)
0025            DO 10 JS=1,4
0026            IF(JS.LE.2) GO TO 15
0027            TY=YVI(J)
0028            TW=WHI(J)
0029            TM=TLMDI(J)
0030            GO TO 16
0031         15 TY=YV(J)
0032            TW=WH(J)
0033            TM=TLMD(J)
0034         16 CONTINUE
0035            IF(JS.EQ.1.OR.JS.EQ.3) PSP=1.
0036            IF(JS.EQ.2.OR.JS.EQ.4) PSP=-1.
0037            CALL PVB(UB,VB,WB)
0038            CALL PVP(UP,VP,WP)
0039            CALL PVS(US,VS,WS)
0040            RU=UB+UP+US
0041            RV=VB+VP+VS
0042            RW=WB+WP+WS
0043            IF(JS.EQ.1) GO TO 1
0044            IF(JS.EQ.2) GO TO 2
0045            IF(JS.EQ.3) GO TO 3
0046            IF(JS.EQ.4) GO TO 4
0047          1 SXU=RU
0048            SXV=RV
0049            SXW=RW
0050            GO TO 10
0051          2 PXU=RU
```

```
0052              PXV=RV
0053              PXW=RW
0054              GO TO 10
0055            3 SIXU=RU
0056              SIXV=RV
0057              SIXW=RW
0058              GO TO 10
0059            4 PIXU=RU
0060              PIXV=RV
0061              PIXW=RW
0062           10 CONTINUE
0063              ABU(KK,J)=SXU+ASYN*PXU+SIXU+ASYN*PIXU
0064              ABV(KK,J)=SXV-ASYN*PXV+SIXV-ASYN*PIXV
0065              ABW(KK,J)=SXW+ASYN*PXW+SIXW+ASYN*PIXW
0066           20 CONTINUE
0067           30 CONTINUE
0068              RETURN
0069              END
```

```
0001          SUBROUTINE ARQQ
              C
0002          COMMON /AR2/AQ(72,72)
0003          COMMON /T3/XS(72),YS(72),ZS(72)
0004          COMMON /C2/AREAB(96)
0005          COMMON /B2/NUB
0006          COMMON /P4/NO
0007          COMMON /P5/PI
0008          COMMON /P6/BETA
0009          DO 20 IB=1,NUB
0010          DO 20 JB=1,NUB
0011          DO 10 IS=1,2
0012          IF(IS.EQ.1) PSP=1.
0013          IF(IS.EQ.2) PSP=-1.
0014          IF(IB.EQ.JB.AND.IS.EQ.1) GO TO 5
0015          RHO=SQRT((XS(IB)-XS(JB))**2+BETA**2*((PSP*YS(IB)-YS(JB))**2+
             $(ZS(IB)-ZS(JB))**2))
0016          P=(XS(IB)-XS(JB))*BETA*AREAB(JB)/(4.*PI*RHO**3)
0017          IF(IS.EQ.1) P1=P
0018          IF(IS.EQ.2) P2=P
0019          GO TO 10
0020        5 P1=0.
0021       10 CONTINUE
0022          AQ(IB,JB)=P1+P2
0023       20 CONTINUE
0024          RETURN
0025          END
```

```
0001          SUBROUTINE AROV
              C
0002          COMMON /AR3/ASV(72,72)
0003          COMMON /T3/XS(72),YS(72),ZS(72)
0004          COMMON /T4/TS(72)
0005          COMMON /C2/AREAB(96)
0006          COMMON /B2/NUB
0007          COMMON /P4/NO
0008          COMMON /P5/PI
0009          COMMON /P6/BETA
0010          COMMON /A1/RADI
0011          DO 20 IB=1,NUB
0012          DO 20 JB=1,NUB
0013          DO 10 IS=1,2
0014          IF(IS.EQ.1) PSP=1.
0015          IF(IS.EQ.2) PSP=-1.
0016          IF(IB.EQ.JB.AND.IS.EQ.1) GO TO 5
0017          CIJ=1.-COS(PSP*TS(IB)-TS(JB))
0018          RHOB=SQRT((XS(IB)-XS(JB))**2+BETA**2*CIJ*RADI**2*2.)
0019          PC=CIJ*BETA**2*RADI*AREAB(JB)/(2.*PI*RHOB**3)
0020          IF(IS.EQ.1) PC1=PC
0021          IF(IS.EQ.2) PC2=PC
0022          GO TO 10
0023        5 PC1=0.
0024       10 CONTINUE
0025          ASV(IB,JB)=PC1+PC2
0026       20 CONTINUE
0027          RETURN
0028          END
```

```
FORTRAN IV G LEVEL  21                ARBF              DATE = 76114        10/33/50          PAGE 0001

0001          SUBROUTINE ARBF
              C
0002          COMMON /AR4/AFN(72,55)
0003          COMMON /T5/XD(127),YD(127),ZD(127)
0004          COMMON /C2/AREAB(96)
0005          COMMON /B2/NUB
0006          COMMON /P4/NO
0007          COMMON /P5/PI
0008          COMMON /P6/BETA
0009          DO 20 J=1,NO
0010          N1=NUB
0011          DO 20 I=1,N1
0012          IB=NO+I
0013          DO 10 IS=1,2
0014          IF(IS.EQ.1) PSP=1.
0015          IF(IS.EQ.2) PSP=-1.
0016          RHO=SQRT((XD(IB)-    XD(J))**2+BETA**2*((YD(IB)-PSP*YD(J))**2+(ZD(
             $IB)-    ZD(J))**2))
0017          PD=BETA**2*(ZD(J)-ZD(IB))*AREAB(I)/(4.*PI*RHO**3)
0018          IF(IS.EQ.1) PD1=PD
0019          IF(IS.EQ.2) PD2=PD
0020       10 CONTINUE
0021          AFN(I,J)=PD1+PD2
0022       20 CONTINUE
0023          RETURN
0024          END
```

```
0001          SUBROUTINE VDF(GAMM)
              C
              C     COMPUTE VORTEX DISTRIBUTION ON FIN
              C
0002          DIMENSION GAMM(55)
0003          DIMENSION XB(56)
0004          COMMON /AR1/AR(56,56)
0005          COMMON /C1/XB
0006          COMMON /P4/NO
0007          CALL DINV(AR,XB,NO)
0008          DO 10 I=1,NO
0009       10 GAMM(I)=XB(I)
0010          RETURN
0011          END
```

```
0001          SUBROUTINE BCF(XB,N3)
              C
              C     COMPUTE BOUNDARY CONDITION ON FIN
              C
0002          DIMENSION XB(56),XW(56),AL(56)
0003          COMMON /BY2/XBW(55)
0004          COMMON /C3/XW
0005          COMMON /NAME/IRPT
0006          COMMON /P3/XM,ALFAF
0007          COMMON /P5/PI
0008          COMMON /P6/BETA
0009          COMMON /BY3/JRAD
0010          COMMON /FL3/NW
0011          COMMON /FL4/AFLAP
0012          DO 5 I=1,N3
0013          IF(I.GT.NW) GO TO 2
0014          AL(I)=ALFAF*P°/180.
0015          GO TO 5
0016        2 AL(I)=AFLAP*PI/180.
0017        5 CONTINUE
0018          DO 10 II=1,N3
0019          IF(IRPT.EQ.1) XW(II)=0.
0020          IF(JRAD.EQ.0) XBW(II)=0.
0021          XB(II)=-BETA*(AL(II)+XBW(II))-XW(II)
0022       10 CONTINUE
0023          RETURN
0024          END
```

```
0001            SUBROUTINE DINV(D,E,N)
                C
0002            DIMENSION D(56,56),E(56),XL(56,56)
0003            NX=N+1
0004            DO 1 I=1,NX
0005            DO 1 J=1,NX
0006            XL(I,J)=0.
0007            XL(I,I)=1.
0008          1 CONTINUE
0009            DO 2 I=1,N
0010            IX=I+1
0011            XL(1,IX)=D(1,I)
0012          2 CONTINUE
0013            XL(2,1)=D(2,1)/XL(1,2)
0014            DO 7 J=2,N
0015            J1=J-1
0016            DO 4 K=J,N
0017            A=0.
0018            KX=K+1
0019            DO 3 I=1,J1
0020            A=A+XL(J,I)*XL(I,KX)
0021          3 CONTINUE
0022            XL(J,KX)=D(J,K)-A
0023          4 CONTINUE
0024            J2=J+1
0025            IF (J2-N) 8,8,9
0026          8 XL(J2,1)=D(J2,1)/XL(1,2)
0027            DO 6 K=2,J
0028            K1=K-1
0029            A=0.
0030            DO 5 I=1,K1
0031            A=A+XL(J2,I)*XL(I,K+1)
0032          5 CONTINUE
0033            XL(J2,K)=(D(J2,K)-A)/XL(K,K+1)
0034          6 CONTINUE
0035          7 CONTINUE
0036          9 CONTINUE
0037            DO 15 I=1,N
0038            IF(ABS(XL(I,I+1)).GE.0.0000001) GO TO 15
0039            WRITE(6,100)
0040            CALL EXIT
0041         15 CONTINUE
0042        100 FORMAT(//,3X,22HILL-CONDITIONED MATRIX,//)
0043            DO 10 I=2,N
0044            I1=I-1
0045            A=0.
0046            DO 11 J=1,I1
0047            A=A+XL(I,J)*E(J)
0048         11 CONTINUE
0049            E(I)=E(I)-A
0050         10 CONTINUE
0051            XL(NX,N)=E(N)/XL(N,N+1)
```

```
0052            N1=N-1
0053            DO 13 I=1,N1
0054            I1=N-I+1
0055            L=N-I
0056            A=0.
0057            DO 12 J=I1,N
0058            A=A+XL(L,J+1)*XL(NX,J)
0059         12 CONTINUE
0060            XL(NX,L)=(E(L)-A)/XL(L,L+1)
0061         13 CONTINUE
0062            DO 16 I=1,N
0063            E(I)=XL(NX,I)
0064         16 CONTINUE
0065            RETURN
0066            END
```


Reproduced from best available copy.

```
0001            SUBROUTINE PDB(XCP)
                C
                C       COMPUTE PRESSURE DISTRIBUTION ON FIN
                C
0002            DIMENSION XCP(55)
0003            DIMENSION GAMM(55)
0004            COMMON /B6/XOV(55)
0005            COMMON /P6/BETA
0006            COMMON /P7/SPN
0007            COMMON /P4/NO
0008            COMMON /Q1/GAMM
0009            DO 10 JJ=1,NO
0010            XCP(JJ)=2.*SPN*GAMM(JJ)/BETA**2/XOV(JJ)
0011          10 CONTINUE
0012            RETURN
0013            END
```

```
0001            SUBROUTINE SLD
                C
                C     COMPUTE SPANWISE LIFT DISTRIBUTION
                C
0002            DIMENSION GAMM(55)
0003            COMMON /W2/CLS(5),CLSW(5),CLSF(5)
0004            COMMON /CHORD/CLL(55)
0005            COMMON /P2/M,N
0006            COMMON /P6/BETA
0007            COMMON /P7/SPN
0008            COMMON /G1/GAMM
0009            COMMON /FL2/NT
0010            A1=4.*SPN/BETA**2
0011            DO 20 JC=1,M
0012            SUMW=0.
0013            SUMF=0.
0014            DO 10 JJ=1,NT
0015            JP=JC+(JJ-1)*M
0016            IF(JJ.GT.N) GO TO 5
0017            SUMW=SUMW+GAMM(JP)
0018            GO TO 10
0019          5 SUMF=SUMF+GAMM(JP)
0020         10 CONTINUE
0021            CLSW(JC)=A1*SUMW/CLL(JC)
0022            CLSF(JC)=A1*SUMF/CLL(JC)
0023            CLS(JC)=CLSW(JC)+CLSF(JC)
0024         20 CONTINUE
0025            RETURN
0026            END
```

```
FORTRAN IV G LEVEL 21                XLF          DATE = 76114      10/33/50      PAGE 0001
0001                SUBROUTINE XLF(CL)
                    C
                    C     COMPUTE LIFT COEFFICIENT OF FIN
                    C
0002                DIMENSION XCP(55)
0003                COMMON /B3/PSA(55)
0004                COMMON /P6/BETA
0005                COMMON /U2/RFAREA,XAX
0006                COMMON /P4/NO
0007                COMMON /Q2/ XCP
0008                SUM1=0.0
0009                DO 10 JX=1,NO
0010             10 SUM1=SUM1+PSA(JX)*XCP(JX)
0011                CL=SUM1/BETA/RFAREA
0012                RETURN
0013                END
```

```
0001          SUBROUTINE PMS(CMS)
              C
              C     COMPUTE SPANWISE MOMENT DISTRIBUTION
              C
0002          DIMENSION CMS(10)
0003          DIMENSION GAMM(55)
0004          DIMENSION XREF(10)
0005          COMMON /CHORD/CLL(55)
0006          COMMON /T6/XV(55),YV(55),ZV(55),WH(55),TLMD(55)
0007          COMMON /P2/M,N
0008          COMMON /FL2/NT
0009          COMMON /P6/BETA
0010          COMMON /P7/SPN
0011          COMMON /Q1/GAMM
0012          COMMON /R3/XREF
0013          COMMON /U2/RFAREA,XAX
0014          DO 10 JC=1,M
0015          SUM=0.
0016          DO 5 JJ=1,NT
0017          JP=JC+(JJ-1)*M
0018        5 SUM=SUM+GAMM(JP)*(XREF(JC)-XV(JP))
0019       10 CMS(JC)=-4.*SPN*SUM/CLL(JC)/XAX/BETA**2
0020          RETURN
0021          END
```

```
FORTRAN IV G LEVEL  21                VLNB            DATE = 76114      10/33/50          PAGE 0001

0001                  SUBROUTINE VLNB
                      C
0002                  DIMENSION GAMM(55)
0003                  COMMON /C5/UBDY(72)
0004                  COMMON /C6/VN(72)
0005                  COMMON /C9/VT(72)
0006                  COMMON /T4/TS(72)
0007                  COMMON /Q8/ABU(72,55),ABV(72,55),ABW(72,55)
0008                  COMMON /B2/NUB
0009                  COMMON /P4/NO
0010                  COMMON /Q1/GAMM
0011                  DO 20 I=1,NUB
0012                  SUM1=0.
0013                  SUM2=0.
0014                  SUM3=0.
0015                  DO 10 J=1,NO
0016                  SUM1=SUM1+ABU(I,J)*GAMM(J)
0017                  SUM2=SUM2+ABV(I,J)*GAMM(J)
0018                  SUM3=SUM3+ABW(I,J)*GAMM(J)
0019                10 CONTINUE
0020                  UBDY(I)=SUM1
0021                  VBDY=SUM2
0022                  WBDY=SUM3
0023                  SNS=SIN(TS(I))
0024                  CSS=COS(TS(I))
0025                  VN(I)=VBDY*SNS+WBDY*CSS
0026                  VT(I)=VBDY*CSS-WBDY*SNS
0027                20 CONTINUE
0028                  RETURN
0029                  END
```

```
0001            SUBROUTINE BSS
                C
                C     BODY SOURSE STRENGTH
                C
0002            DIMENSION SUM(72)
0003            COMMON /C7/QL(72)
0004            COMMON /C6/VN(72)
0005            COMMON /AR3/ASV(72,72)
0006            COMMON /B2/NUB
0007            COMMON /NAME/IRPT
0008            IF(IRPT.EQ.1) GO TO 15
0009            DO 10 I=1,NUB
0010            SUM(I)=0.
0011            DO 10 J=1,NUB
0012         10 SUM(I)=SUM(I)+ASV(I,J)*QL(J)
0013            GO TO 45
0014         15 DO 20 I=1,NUB
0015         20 SUM(I)=0.
0016         45 CONTINUE
0017            DO 50 I=1,NUB
0018         50 QL(I)=-2.*VN(I)-SUM(I)
0019            RETURN
0020            END
```

```
0001          SUBROUTINE BPD
              C
              C     BODY PRESSURE DISTRIBUTION
              C
0002          COMMON /AR2/AQ(72,72)
0003          COMMON /C7/QL(72)
0004          COMMON /A2/CPB(72)
0005          COMMON /C5/UBDY(72)
0006          COMMON /B2/NUB
0007          COMMON /P6/BETA
0008          DO 20 I=1,NUB
0009          SUM=0.
0010          DO 10 J=1,NUB
0011          SUM=SUM+AQ(I,J)*QL(J)
0012       10 CONTINUE
0013          CPB(I)=-2.*(UBDY(I)+SUM)/BETA**2
0014       20 CONTINUE
0015          RETURN
0016          END
```

```
0001          SUBROUTINE BLD(BCL)
              C
              C     BODY LIFT DISTRIBUTION
              C
0002          DIMENSION BCL(36)
0003          COMMON /A2/CPB(72)
0004          COMMON /B1/MB,NB
0005          COMMON /D2/M1
0006          DO 50 K1=1,NB
0007          DO 40 I1=1,M1
0008          BCL((K1-1)*M1+I1)=CPB(MB*K1-I1+1)-CPB((K1-1)*MB+I1)
0009       40 CONTINUE
0010       50 CONTINUE
0011          RETURN
0012          END
```

```
0001          SUBROUTINE BSLD
              C
              C     BODY SPANWISE LIFT DISTRIBUTION
              C
0002          DIMENSION BCL(36)
0003          COMMON /W3/CLBS(5)
0004          COMMON /B4/BREF(5)
0005          COMMON /W1/DX(96)
0006          COMMON /D1/BCL
0007          COMMON /D2/M1
0008          COMMON /B1/MB,NB
0009          DO 20 JJ=1,M1
0010          SUM=0.
0011          DO 10 KK=1,NB
0012          I=JJ+(KK-1)*M1
0013          SUM=SUM+BCL(I)*DX(I)
0014       10 CONTINUE
0015          CLBS(JJ)=SUM/BREF(JJ)
0016       20 CONTINUE
0017          RETURN
0018          END
```

```
0001          SUBROUTINE WBS(XW,N1,N2)
              C
              C     VELOCITY ON FIN INDUCED BY BODY SOURSE
              C
0002          DIMENSION XW(96)
0003          COMMON /C7/QL(72)
0004          COMMON /AR4/AFN(72,55)
0005          DO 20 J=1,N2
0006          SUM=0.
0007          DO 10 I=1,N1
0008          SUM=SUM+AFN(I,J)*QL(I)
0009       10 CONTINUE
0010          XW(J)=SUM
0011       20 CONTINUE
0012          RETURN
0013          END
```

```
0001          SUBROUTINE XLIFT
              C
              C     LIFT COEFFICIENT OF FIN-BODY COMBINATION
              C
0002          COMMON /W2/CLB(5),CLSW(5),CLSF(5)
0003          COMMON /CHORD/CLL(55)
0004          COMMON /U1/YF(11)
0005          COMMON /W3/CLBS(5)
0006          COMMON /B4/BREF(5)
0007          COMMON /W4/CLWING,CLFIN,CLBODY,TOTCL
0008          COMMON /D2/M1
0009          COMMON /P2/M,N
0010          COMMON /U3/DT
0011          COMMON /U2/RFAREA,XAX
0012          COMMON /A1/RADI
0013          SUMW=0.
0014          SUMF=0.
0015          DO 5 JF=1,M
0016          WD=YF(JF+1)-YF(JF)
0017          SUMW=SUMW+CLSW(JF)*CLL(JF)*WD
0018        5 SUMF=SUMF+CLSF(JF)*CLL(JF)*WD
0019          CLWING=SUMW/RFAREA
0020          CLFIN=SUMF/RFAREA
0021          SUMB=0.
0022          DO 10 JB=1,M1
0023       10 SUMB=SUMB+CLBS(JB)*BREF(JB)*COS(DT*(JB-0.5))
0024          CLBODY=DT*RADI*SUMB/RFAREA
0025          TOTCL=CLWING+CLFIN+CLBODY
0026          RETURN
0027          END
```